Universidade de Brasília – UnB

Instituto de Geociências – IG

Programa de Pós-Graduação em Geologia

Mélanges e Corpos Ofiolíticos do Grupo Araxá e sua Asociação com Terrenos Acrescionários

Matthew Thomas Brown

Tese de Doutorado N° 153

Orientador: Prof. Dr. Reinhardt Adolfo Fuck

Co-orientador: Prof. Dr. Elton Luiz Dantas

Brasília, DF,

15 de Março de 2019

“Mélanges e Corpos Ofiolíticos do Grupo Araxá e sua Asociação com Terrenos Acrescionários”

Banca Examinadora:

Prof. Leo Hartmann (UFRGS)
Prof. Elson Oliveira (UNICAMP)
Profª. Natalia Hauser (UnB)
Suplente: Profª. Maria Emilia Della Giustina (UnB)

Agradecimentos

I would like to thank my family (Aline, my wife, and my two beautiful children, Arthur and Helena), for putting up with me during this period. This work is dedicated to you guys.

To my parents and siblings, even though they were far away, they always sent their support.

A special thankyou is necessary for Maria Apericida, who directed me to converse with Marcio Pimentel. And of course, to Marcio, for letting me be a part of the Geochronology Family.

To my orientador, Professor Rienhart Aldofo Fuck, for his knowledge, help and patient, during this project.

To Elton, for his help and geological conversations, while trying to understand what is happening in the Brasília Belt.

Of course, I need to thank Eduardo. If I never met him, I would never had begun this crazy adventure, which shows no sign of ending.

Abstract

This study was conducted on the different rock assemblages of an ophiolitic mélange from the Araxá Group, Brasília Belt, in the area of Abadiânia. In order to have a discussion with the prospects of an ophiolitic mélange within the Araxá Group, this study first focuses on what is an ophiolite, then on the aspects and characterization of what is a mélange.

Ophiolites are pieces of oceanic lithosphere, which have been emplaced onto continental margins. Due to accretionary processes related to continental growth at ocean facing continental margins, ophiolitic assemblages are commonly found in orogenic belts. Mélanges are considered to be a mixture of rock assemblages, with a characteristic "block in matrix" appearance, and are the result of tectonic and/or sedimentary processes which mix different types of rocks together. The most common mélange forming environments are related to subduction zones. There are several different terms and classifications, which are related to types of mélanges and their tectonic environments. Ophiolitic mélange is a general term referring to a mélange that has incorporated an ophiolitic component.

The Brasília Belt is a Neoproterozoic orogenic belt formed during the Brasiliano-Pan-African Orogeny as part of the Tocantins Province, central Brazil. The belt includes a large sedimentary pile in its eastern portion, the Goiás Magmatic Arc on the western side, and the Goiás massif, an exotic continental fragment, comprising Archean granite-greenstone terrains, Paleoproterozoic granite-gneiss, Neoproterozoic layered complexes, and Proterozoic cover rocks, exposed between the magmatic arc and the metamorphic core in the central part of the belt, and the external zone farther north.

The Araxá Group is composed of metasedimentary rocks, which have been metamorphosed at greenschist and amphibolite facies, locally up to granulite facies. The ophiolitic mélange of the group is composed of large bodies to blocks of mafic and ultramafic rock assemblages representing pieces of oceanic lithosphere within a garnet-mica schist matrix. Quartzite and granites also occur as isolated bodies together with the ophiolitic assemblage. The purpose of this study is to use geochemical and geochronological methods (U-Pb and Lu-Hf on zircon grains, and Sm-Nd whole rock analysis) to investigate the different rock assemblages of the ophiolitic mélange, in order to better understand its evolution with respect to the Brasília Belt. The first article of this work is related to the ophiolitic assemblage of the mélange, with the goal of determining the environment in which it formed and its age of formation. The second article entails a provenance study of the other blocks found within the mélange and the encompassing schist matrix, with the goal of better understanding the origin of the blocks and depositional history of the mélange.

In the first article, body S9 was studied, due to its contact with a metamafic rock and well-developed metasomatic "black-wall" contact alteration zone. Samples of body S9 and the metamafic rocks were analyzed, as well as two micaschists in contact with the metamafic assemblage. The results from chemical analysis indicate that the metamafic assemblage has a MORB signature and was formed

in a back-arc environment. U/Pb analyses indicate a zircon age of crystallization of c. 800 Ma for the metamafic assemblage. The inner zone of the black-wall has a zircon age of c. 777 Ma, while the outer zone ranges in age from c. 800 to 760 Ma. ε_{Hf} values of selected zircon grains of the metamafic sample range from -21.67 to +13.66, with T_{DM} ages of 0.80–4.22 Ga, while the metaultramafic black-wall samples have highly depleted ε_{Hf} values ranging from +9.16 to +23.98, with T_{DM} model ages of 0.34–0.96 Ga. The studied micaschists have principal zircon population peaks of c. 790 to 890 Ma. ε_{Hf} ranges from -14.87 to +6.46 and T_{DM} ages of between 1.47 and 1.91 Ga for the studied micaschists. Metamafic and ultramafic rock assemblages all have positive ε_{Nd} values from +4.95 to +7.89, indicating a mantle signature. ε_{Nd} values for the micaschists are -8.31 and -8.16, and their T_{DM} values are 1.83 and 2.36 Ga, which indicate a continentally derived component. The results are interpreted as the ophiolitic component of the Araxá mélange formed in a back-arc basin environment, which formed at c. 800 Ma and lasted till c. 760 Ma, while the studied micaschists probably represent sediments deposited in the newly formed back-arc basin

In the second article, quartzite and granite samples were analyzed and compared with results from the garnet-mica schists of the Araxá Group. Quartz schists were derived from passive margin sequences and granite assemblages were derived from Paleoproterozoic basement, making these two rock assemblages the oldest components of the mélange. Samples of garnet-mica schists demonstrate that there are at least two different periods of sedimentation recorded in these rocks, the first occurring after the extensional event that formed the back-arc basin, and the second after a collisional event which occurred c. 670–650 Ma.

Geochemical and geochronological methods were helpful in unraveling the history of Precambrian mélanges recorded in the Araxá Group of the Neoproterozoic Brasília Belt. While not all the exact timings and events are known yet, it was determined that the ophiolitic assemblage was formed in a back-arc rift setting, where rifting lasted from ca. 800 to 760 Ma. Two periods of sedimentation occurred, one before 650 Ma, and one after 650 Ma. While the origin of the quartzite and granite bodies is known, it is not certain when they entered into the mélange, further studies may reveal this answer. Future studies in the Araxá Group should focus on geochemical analysis on the different mafic rocks and understanding their distribution, locating and dating other metasomatic rock assemblages from ultramafic bodies, determining the origin and distribution of the different exotic blocks and attempting to map the distribution of the two different periods of sedimentation in order to verify if there may be more.

Key Words: Brasília Belt, Ophiolite, Mélange, Araxá Group, Neoproterozoic

Resumo

Este estudo foi realizado nas melanges ofiolíticas do Grupo Araxá, Faixa Brasília, na região de Abadiânia. Com o propósito de discutir as perspectivas de uma mélange ofiolítica dentro do Grupo Araxá, este estudo enfoca, primeiramente, o que é um ofiolito e depois caracterizar os aspectos do que é uma melange.

Ofiolitos são fragmentos da litosfera oceânica preservados nas margens continentais durante o desenvolvimento do prisma acrescionário relacionado ao amalgamento de blocos, terrenos, bacias e arcos magmáticos que constituem os cinturões orogênicos. Melange é definida como uma assembleia de rochas com a característica de "bloco em matriz", resultado de processos tectônicos e sedimentares que misturam diferentes associações de rochas. Zonas de subducção são os principais ambientes formadores de melange. Existem vários termos e classificações diferentes relacionados as melange e seus ambientes tectônicos, mas melange ofiolítica obrigatoriamente implica em uma assembleia de rochas com fragmentos de crosta oceânica preservada.

A Faixa Brasília é um cinturão orogênico de idade neoproterozoica, formado durante a orogenia Brasiliano-Panafricana, que constitui a maior parte da Província do Tocantins, localizada na porção central do Brasil. A Faixa Brasília é composta por espessas sequencias sedimentares sua porção leste, Arco Magmático de Goiás no lado oeste, e o Maciço de Goiás. Este último um fragmento continental “exótico” compreendendo terrenos granito-greenstones arqueanos, complexos gnáissicos paleoproterozoicos, supracrustais e complexos acamados neoproterozoicos.

O Grupo Araxá é composto por rochas metassedimentares, que foram metamorfizadas em fácies xisto verde e anfibolito, localmente alguma porções chegam ao fácies granulito. A mélange ofiolítica Araxá é composta de corpos e blocos de assembleia mineral máfica e ultramáficas, litosfera oceânica, hospedados em granada-mica xistos. Lentes de quartzitos e corpos graníticos também ocorrem associados aos ofiolitos. O objetivo deste estudo foi a aplicação dos métodos geoquímico e geocronológicos (U-Pb e Lu-Hf em grãos de zircão e Sm-Nd em rocha total) para investigar as diferentes assembleias minerais da melange ofiolítica para entender sua importância na evolução na Faixa Brasília. O estudo foi dividido em dois artigos. O primeiro artigo determina o a geocronologia e o ambiente tectônico no qual foram gerados os Ofiolitos do Araxá. O segundo artigo apresenta as idades das proveniências dos sedimentos que contribuíram para história deposicional supracrustais que constituem o Grupo Araxá.

No primeiro artigo, corpo S9 foi estudado, devido ao seu contato com uma rocha metamáfica e sua zona de contato de alteração metasomatica bem desenvolvida de “black-wall.” Amostras de corpo S9 e as rochas metamáficas foram analisadas, também dois mica-xistos que estão em contato com as rochas metamáficas. Os resultados da análise química indicam que as metamáficas tem assinatura de MORB e foram geradas em um ambiente de back-arc. Análises U/Pb em zircão mostram idade de cristalização de

ca. 800 Ma para o protolito dessas metamáficas. O núcleo desses corpos máficos apresentam idade de 777 Ma, enquanto as suas bordas exibem idades entre 800 a 760 Ma. O ε_{Hf} dos zircões das rochas metamáficas variam de -21,67 a +13,66 com idades modelo TDM de 0,80 a 4,22 Ga. Por sua vez, os zircões das metaultramáficas apresentam ε_{Hf} de +9,16 a +23,98 com TDM entre 0,34 e 0,96 Ga. Os micaxistos têm populações principais de zircões em 790 e 890 Ma, os ε_{Hf} desses zircões variam de -14,87 a +6,46 e as idades TDM oscilam entre 1,47 e 1,91 Ga. Toda a associação de rochas máfica e ultramáficas têm valores positivos de εNd, entre +4,95 a +7,89, indicando fonte mantelíca. O εNd dos micaxistos são negativos, -8,31 a -8,16, indicando contribuições da crosta continental na fontes. Estes xistos apresentam idades modelo TDM entre 1,83 e 2,36 Ga. Os resultados permitem propor que Melange de Araxá foi formada em um ambiente de bacia de back-arc entre 800 e 760 Ma, enquanto os micaxistos representam os sedimentos depositados nesta bacia no mesmo intervalo de tempo.

No segundo artigo, amostras de quartzito e granito foram analisadas e comparadas com os resultados dos granada-micaxistos do Grupo Araxá. Xistos ricos em quartzo e granitos retrabalhados do embasamento Paleoproterozoico constituem as principais unidades das melange ofiolítica Araxá. Granada micaxisto indicam que há pelo menos dois períodos diferentes de sedimentação, o primeiro após o evento extensional durante o desenvolvimento da bacia de retro-arco, e o segundo após a colisão (ca. 670-650 Ma).

Métodos geoquímicos e geocronológicos foram úteis para desvendar a história das melanges pré-cambrianas registradas no Grupo Araxá, Faixa Brasília. Embora a evolução completa ainda não seja documentada, foi caracterizada a assembleia ofiolítica associada a instalação de bacias de retro-arco em ambiente de rifte (ca. 800 a 760 Ma). Dois períodos de sedimentação são registrados, um antes de 650 Ma e outro segundo após 650 Ma. Embora a origem das supracrustais e magmatismo alcalino e toleítico tenham sido reconhecidos, não é preciso o intervalo de tempo no qual foram amalgamados, também é necessário compreender melhor o ambiente de formação do protolito do ofiolitos.

Palavras-chave: Faixa de Brasília, Ofiolito, Mélange, Grupo Araxá, Neoproterozóico

Table of Contents

List of Figurers

List of Tables

Appendix

1. Theoretical Background

1.1 Introduction

The nature of the Araxá Group of the Neoproterozoic Brasília Belt, Tocantins Province, central Brazil, has been something of an enigma since its classification. It is composed mostly of metasedimentary rocks, thought to be pelitic sediments in origin, deposited in an arc related basin (Pimentel et al., 2011 Piuzana et al. 2003a). This group has been metamorphosed to greenschist and amphibolite facies, due to regional deformation (Fuck et al., 2017, and references therein). The presence of oceanic related volcanic rocks, ultramafic bodies and exotic blocks, such as marble, have led authors to classify parts of the Araxá group as an ophiolitic mélange (Drake Jr., 1980; Strieder & Nilson 1992 a, b, c). There are several types of mélanges in the literature and their formation is commonly attributed to subduction zones, in which they have been documented in several active and ancient volcanic arcs Cowen, 1985; Dilek and Furnes, 2014). Orogenic zones are common places where mélange formation occurs. Remnants of oceanic crust, called ophiolites can also be found in orogenic zones. These oceanic remnants are important in providing information on the chemistry of the oceanic crust and upper mantle. Their presence together with mélanges are characteristic in identifying and understanding ancient sutures and subduction zones (Coleman and Irwin, 1974).

The formation of the Neoproterozoic Brasilia Fold Belt represents the amalgamation of western Gondwana. Geochronological evidence demonstrates that the process of accretion of oceanic island-arc terrains, continental blocks and the final continental collision took place between roughly 900 Ma to 550 Ma (Pimentel et al. 1999, 2003; Laux et al. 2005; Marques et al., 2017). The ophiolitic mélange of the Araxá Group, along with the presence of granulite complexes associated with thrust belts, large shear zones and gravimetric anomalies, are considered indicators of collisional suture zones. Valuable information about the timing and formation of these suture zones and overall accretion of the Brasilia Belt may be preserved within this mélange.

This study began as an investigation of the ultramafic components of the Araxá Group ophiolitic mélange. With that in mind, samples of the ultramafic assemblage (serpentinite, chlorite schist and talc schist), were collected from the areas of Abadiânia, Morro Feio, Morro de Magnesia and Morro Dois Irmãos, Goiás, central Brazil. However, in order to fully understand one

component of a mélange, it is better to understand all of its components. Because of this, the study of samples of ultramafic rock assemblages should be accompanied by the analysis of associated mafic and metasedimentary components of the mélange. In the end, the ultramafic rocks and associated assemblages from the area of Abadiânia were selected, where an ultramafic body (S9) was found in contact with a mafic rock assemblage.

The focus of this study is to gain a better understanding of the nature of the Araxá Group mélanges. To this end, whole rock geochemistry was used together with geochronological methods Sm-Nd on whole rock samples and U-Pb and Lu-Hf on single zircon grains. The goal is to see if these methods can be used to discern the age of crystallization and provenance of the ophiolitic components and other mélange assemblages, and to try to determine the time interval of mélange activity and the type of mélange and its environment in which it formed.

1.2 Ophiolite

Ophiolites represent pieces of oceanic crust and mantle that have been tectonically emplaced onto continental margins. They are the remains of an oceanic basin that no longer exists (Gansser 1974), and valuable information can be preserved in these deposits. They contain a record of the evolution and destruction of oceanic lithosphere and are important for our understanding of the evolution of orogenic belts (Dilek 2006). Ophiolites are found as preserved, intact complexes with a predictable sequence, or as disseminated sequences in a subduction complex (Moore and Twist 2000).

The formal stratigraphic model of the ophiolite sequence is referred to as the Penrose model (Anonymous, 1972), which reflects the oceanic crust down to the transition with the upper mantle. Bottom up, this stratigraphic model includes: ultramafic harzburgite, with lesser amounts of lherzolite, dunite and chromite; cumulate dunite and wehrlite; coarse- to fine-grained gabbro, diorite and some plagiogranite; the next section consists of a sheeted dike complex that is composed of fine-grained mafic diabase, followed by extrusive volcanic rock, composed of pillow lava flows, dikes, sills and breccia, which could be formed as submarine eruptions; the ophiolite sequence is capped by pelagic sediments consisting of thinly bedded chert and limestone (fig 1.1).

Taken as formed at mid-ocean spreading centers, the ophiolite sequence was considered to have a layer-cake pseudo stratigraphy (Dilek and Eddy, 1992).

The Penrose model was mostly based on the Tethyan ophiolites; however, it became apparent that ophiolites are heterogenic compositionally, structurally and geochemically, and are not consistent with the model (Dilek et al, 2015; Furnes et al., 2015). The first geochemical approach to ophiolites determined an island-arc environment for the Troodos ophiolite (Miyashiro, (1973), and not mid-ocean spreading zones. Geochemical methods can be used to help determine the various environments in which ophiolites may form. Dilek and Furnes (2014) used geochemical data to create an ophiolite classification, separating their forming environments into subduction unrelated and subduction related setting (fig 1.2). Subduction unrelated ophiolites are separated into continental margin types, mid-ocean ridge types and plume types. Subduction related ophiolites are separated into suprasubduction zone types and volcanic arc types. The geochemical finger print of ophiolites is important, especially when ophiolites are dismembered and the full sequence is not present.

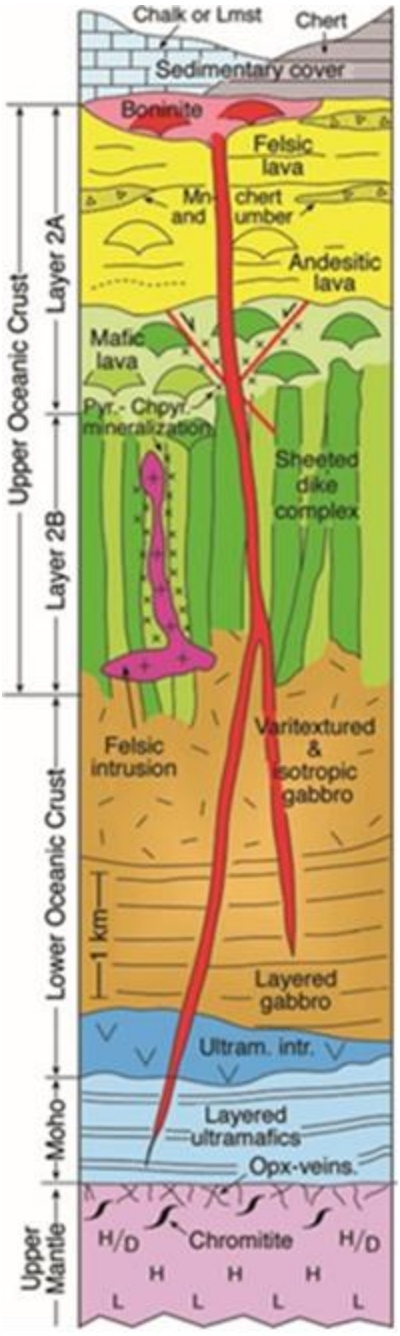

Figure 1.1 Schematic cross section of stylized ophiolitic sequence (Dilek & Furnes 2014).

The process of ophiolite emplacement on a continental margin was difficult to explain, with denser oceanic crust found on top of lighter continental crust. There are a few models that have been proposed to explain ophiolite emplacement, which is called obduction, but they all consider the subduction of

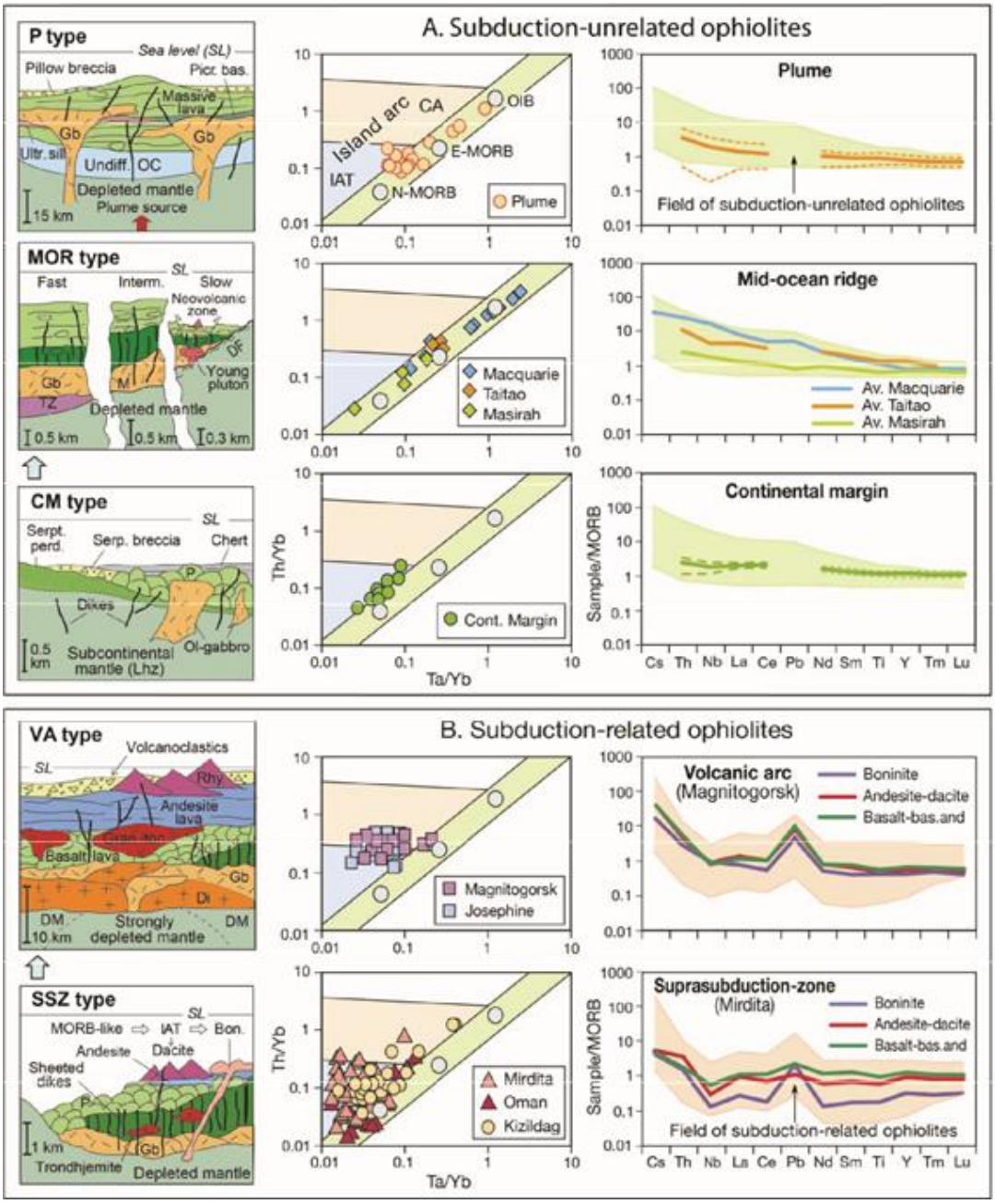

Figure 1.2. (LEFT COLUMN) Cross sections depicting the internal structure and lithological units of different ophiolite types. (CENTER AND RIGHT COLUMNS) Th/Yb– Ta/Yb and multi-element diagrams (modified from Dilek and Furnes 2011, and data sources therein) displaying the characteristic features of a selection of ophiolite types. Key to lettering: (A1) CM type = continental margin type; Lhz = lherzolite; Ol = olivine; P = pillow lava. (A2) DF = detachment fault; Gb = gabbro; M = Moho; MOR type = mid-ocean ridge type; TZ = transition zone. (A3) Gb = gabbro; P type = plume type; Picr. Bas = picritic basalt; Ultr. Sill = ultramafic sill; Undiff. OC = undifferentiated oceanic crust. (C1) Bon. = boninite; Gb = gabbro; IAT = island arc tholeiite; P = pillow lava; SSZ type = suprasubduction zone type. (C2) Di = diorite; DM = depleted mantle; Gb = gabbro; Gran/ton = granodiorite/tonalite; Rhy = rhyolite; VA type = volcanic arc type. (D1) and (D2) Bas. And = basaltic andesite (Dilek & Furnes 2014).

relatively new, hot oceanic crust. One model proposes that obduction occurs during continental or arc collision, where oceanic crust on a passive continental margin is emplaced during a collisional event. Another model suggests that an ophiolite is emplaced when a piece of the subducted oceanic plate detaches and is pushed onto the continental margin. Wakabayashi and Dilek (2003) developed a model to explain the emplacement of the Coastal Range Ophiolite of California, which involves an oceanic spreading ridge entering a subduction zone.

One of the problems encountered when studying ophiolites, is to be able to reliably date them. The mafic and ultramafic nature of these assemblages are poor in datable mineral. One of the only methods available for dating ophiolites is by dating associated plagiogranites. Recently, zircon grains collected from metasomatic assemblages related to serpentinites, have been utilized to date ophiolites (Dubińska et al., 2004; Li et al., 2013; Arena et al., 2017). Serpentinites are considered to be derived from the mantle section of ophiolites (Deschamps et al., 2013). Once the age/ages of metasomatic zircon grains are determined, the different pulses of serpentinization of ultramafic rock (ie. oceanic peridotite) can be related to the evolutional history of the ophiolitic body. This can be used later when trying to interpret the obduction of oceanic material onto continental crust and accretionary process related to continental growth. This idea was utilized by Arena et al. (2017), when describing the evolution of the Ibaré and Palma ophiolites, southern Brazil.

The presence of zircon grains in serpentinites and other ophiolitic bodies has been an enigma for some time. There are two schools of thought: 1. Grains may have formed within the mantle (Zheng et al., 2006); 2. They could be introduced into the serpentinite body through the process of subduction of continental derived sediments (Robinson et al., 2014). Work done by Belousova et al. (2015) suggests that they could be introduced during the emplacement of granite bodies.

The Sula-Dabie ultrahigh-pressure metamorphic belt in east-central China contains peridotite blocks or lenses which are interpreted as lithospheric mantle. Zheng et al. (2006) conducted a trace element study on zircon grains sampled from the peridotite. Visually the grains had a wide range of forms from subhedral to irregular to rounded. The trace elements had signatures that were similar to those of kimberlite or carbonatite. This led Zheng et al. (2006) to

conclude that the zircon grains formed within the peridotite from melts or fluids derived from the lithospheric mantle.

Examples of subduction related zircon grains, and other continental derived minerals, found in ultramafic rock assemblages was given by Robinson et al. (2014). Zircon grains were recovered from podiform chromitites collected from ophiolites located in Luobusa, Dongqiao and Oman. Grains from all ophiolites were subangular to well-rounded, with overgrowth and partial resorption patterns on grain boundaries. Rare earth element signatures of zircon grains were similar to those of continental derived sediments. The age of the zircon grains, determined by U-Pb analysis were older than the ophiolites in which they were found. Robinson et al. (2014) considered that these grains came from metasedimentary rocks that were subducted and introduced into the mantle wedge of the subduction zone, which later formed an ophiolite.

Another possibility for the occurrence of zircon grains in ultramafic rock was proposed by Belousova et al. (2015), comparing zircon grains collected from the Tumut ophiolitic complex to the neighboring Young granodiorite. U-Pb, Hf and O isotopes and single grain trace elements were analyzed for all samples collected. The majority of the grains from both the granodiorite and the ophiolitic complex were similar with none of the ophiolite grains showing oceanic-crust signatures. Belousova et al. (2015) speculated that the majority of zircon grains from the Tumut Ophiolite complex were derived from fluids related to the Young granodiorite, during its formation and emplacement. Zircon grains were either precipitated directly from these fluids and transported grains from the main magmatic event and inherited populations.

The evolution of accretionary orogenic belts involves the tectonic amalgamation of oceanic terranes (Dilek and Furnes, 2014). Because of this, ophiolites can commonly be found in orogenic zones. In Brazil, the majority of ophiolites are found in orogenic belts related to the Neoproterozoic Brasiliano-Pan-African Orogeny. These ophiolites represent the remains of Neoproterozoic oceans which were consumed (Suita et al., 2004). The oldest ophiolites are thought to be found in the Brasília Belt (ca. 0.9–0.85 Ga) and the youngest in the Ribeira and Dom Feliciano belts (ca. 0.7–0.6 Ga) (Alkmim et al., 2001; Suita et al., 2004). Recent work by Arena et al. (2016) dated an ophiolite from the São Gabriel terrane, in the Dom Feliciano belt, at ca. 923 Ma, indicating a much older age for the ophiolitic terrane.

1.3 Mélange

A mélange is a block in matrix, “chaotic” assemblage of rocks of different sizes and types, which can be found in many modern and ancient fore arc settings. The word mélange is French, and means mixture. The term mélange was first used in a geological context by Greenly (1919), who used it to describe the Precambrian “Gwna Group” of the Mona Complex. In his work on mélanges in California, Hsü (1968) termed mélanges as ”mappable bodies of deformed rocks characterized by the inclusion of native and exotic blocks, which may range up to several miles long, in a pervasively sheared, commonly pelitic matrix”.

The most common definition used in defining mélanges is block in matrix. Blocks are normally elongated, forming boudins, and are set in a sheared matrix (Fig. 1.3). Many of the chaotic mixtures of mélanges have diverse lithotypes and in irregularly folded matrixes. Blocks found within mélanges can range the entire spectrum of rock types, sedimentary, volcanic and metamorphic. The matrix of mélanges is normally composed of highly sheared shale or serpentine. This matrix forms scale type fragments, which when the matrix is shale, is sometimes called scaly clay, or *argile scagliose,* a term coined by Bailey and McCallien (1950, 1953) to define mélanges in the northern Apennines of Italy. Some definitions used to describe mélange fabrics as including stratal disruption, lenticular fabric, block-in-matrix and pervasive shearing (Cowen 1985).

Hsü (1968) definition stressed that mixing of the different rock assemblages in a mélange was tectonic in nature. However, various sedimentary processes are also capable of creating chaotic deposits. The most common environment in which a mélange forms, is an accretionary wedge in a subduction zone. In this environment, mélange formation is controlled by both sedimentary and tectonic processes. A review of the definition of a mélange reveals that there is no one straight forward definition of what a mélange is. In fact, there are several names and definitions given to mélanges. Some mélanges can be classified as different types of mélanges, an example being the ophiolitic mélange of Gansser (1974) and the serpentine

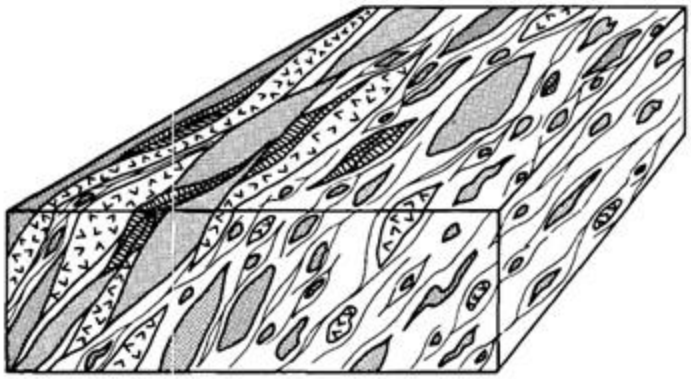

Figure 1.3. Three dimensional diagram showing basic mélange fabric, including elongated blocks in a sheared matrix (taken from Cowen, 1985).

mélange of Shervais (2011). Currently, mélange can be used to describe deposits from tectonic and sedimentary settings, even diapiric processes. Table 1.1 shows a classification system taken from Festa et al. (2010), which shows different mélange forming environments and possible mélange types.

Sedimentary Mélanges

The formation of several types of mélanges can be attributed to sedimentary processes. Mass wasting, gravity slumping and nappe erosion are just some of the processes that are capable of forming chaotic deposits. Cowen (1982) suggested that some mélanges could be the product of gravity deformation, caused by the spreading of sediments during flows in an oceanic trench. Wildflysch and olistostrome are two of the most common types of sedimentary related mélanges.

Flysch is a type of sequenced sedimentary rock deposited in a foreland basin, in a deep marine environment. When these sequences become disrupted, they can be considered a wildflysch, which is considered as a chaotic deposit with different degrees of stratal disruption (Festa et al., 2010). This name was given to chaotic deposits with exotic blocks from the Helvetic Nappe of the Habkern Valley by Kaufmann (1886), which was different from the normal well-bedded flysch succession.

Table 1.1. Table taken from Festa et al. (2010) showing different mélange forming environments, processes and their products.

Types of Mélanges	Geodynamic enviornment	Processes	Products
Related to:			
1. Extensional tectonics	Rifting	Gravitational	Mass-transport deposits (megabreccias, breccias, olistoliths, olistolith fields or swarm, debris avalanches, and flows, etc.)
2. Passive margins	Passive margins (after rifting)	Gravitational	Poorly sorted olistostromes (soft sediment deform.; progressive deformation from slumping to debris flows, to complete strata disruprion); slides
3. Strike-slip tectonics	Different types of collision	Tectonic	Broken formations; mélanges (exotic blocks were commonly recicled from other previously formed mélanges)
4. Subduction			
a. Mass-transport deposits at the wedge front	Subduction (at the front of the wedge)	Gravitational	Olistostromes and mass-transport deposits (debris flows and avalances, slumps, slides, etc.)
b. Broken fms. and tectonic mélanges	Subduction (at the base of the wedge)	Tectonic	Broken formations; mélanges? (exotic blocks were commonly recycled from other previously formed mélanges)
5. Collision	Different types of collision	Tectonic and gravitational	Broken formations; mélanges? (exotic blocks were commonly recycled from other previously formed
6. Intracontinental deformation			
a. Sub-nappe			
a1. Precursory olistostromes	At the base or front of intracontinental thrust sheets or	Gravitational	Olistostromes and mass-transport deposits (debris flows and avalanches, slumps, slides, etc.)
a2. Olistostromal carpet		Gravitational and tectonic	Mélanges (exotic blocks were commonly recycled from other previously formed sedimentary mélanges), broken formations
a3. Tectonic mélanges		Tectonic, gravitational	
b. Intra-nappe			
b1. Sedimentary	Within intracontinental thrust sheets or nappes	Gravitational	Olistostromes and mass-transport deposits (debris flows and avalanches, slumps, slides, etc.)
b2. Tectonic and/or tectono-sedim.		Tectonic, gravitational	Broken formations; mélanges? (exotic blocks were commonly recycled from other previously formed sedimentary mélanges)
c. Epi-nappe			
c1. Sedimentary	A top of intracontinental thrust sheets or nappes (e.g. piggy back, top thrust basins)	Gravitational	Olistostromes and mass-transport deposits (debris flows and avalanches, slumps, slides, etc.)
c2. Tectono-sedim.		Tectonic, gravitational	Broken formation, mélanges
c3. Diapiric		Diapiric	Mud diapirs and mud volcanoes

Olistostromes are another common type of sedimentary derived mélange. They were first described by Flores (1955), in Sicily, as sedimentary bodies with a chaotic, block-in-matrix fabric,

intercalated with well-bedded successions. These deposits can have blocks and clasts of one lithology embedded in a matrix of another. Olistostromes may contain mappable blocks of an individual rock type, which are called olistoliths (Moores and Twiss, 2000).

Both wildflysch and olistostromes are thought to be related to mass wasting, gravity flows in an oceanic trench environment. Mutti et al. (2009) explained how some of the exotic blocks found in these deposits can originate from the front of nappes in an oceanic environment, which would produce a mixture of sediments that include these exotic blocks. Elter and Trevisan (1973) called this kind of sedimentary mixing, precursory olistostromes. Aspects of wildflysch suggest formation from submarine slumping and sliding on a large scale, on a steep slope adjoining an actively rising ridge (Trümpy, 1960).

Tectonic Mélanges

Tectonic processes are a major driving force behind mélange formation. One of the first mélange forming environments discovered was in the accretionary prism in subduction zones (Cowen, 1985). While the mélange forming process is mainly driven by the subduction of oceanic lithosphere and the scraping of material from the lower plate onto the upper plate, sedimentary processes are also active, contributing to the mixing process (Figure 1.4). A mélange formed in a subduction zone can also turn into an olistostrome by mass wasting of the overriding nappes. This relationship caused a long debate as to whether "mélange" should be used to define only chaotic deposits related to tectonic environments or not. Some classic tectonic related mélanges are: coloured mélange, Iran (Gansser, 1955); broken formation, California (Hsü, 1968); obduction mélange, Himalayas (Gansser, 1974); tectonic mélange (Raymond, 1984).

One of the characteristics of a mélange caused by the tectonic process of subduction is the presence of high pressure-low temperature metamorphic grade rock. Blue schist, eclogite and amphibolite metamorphic facies are formed deep in subduction zones, blue schist relating to high

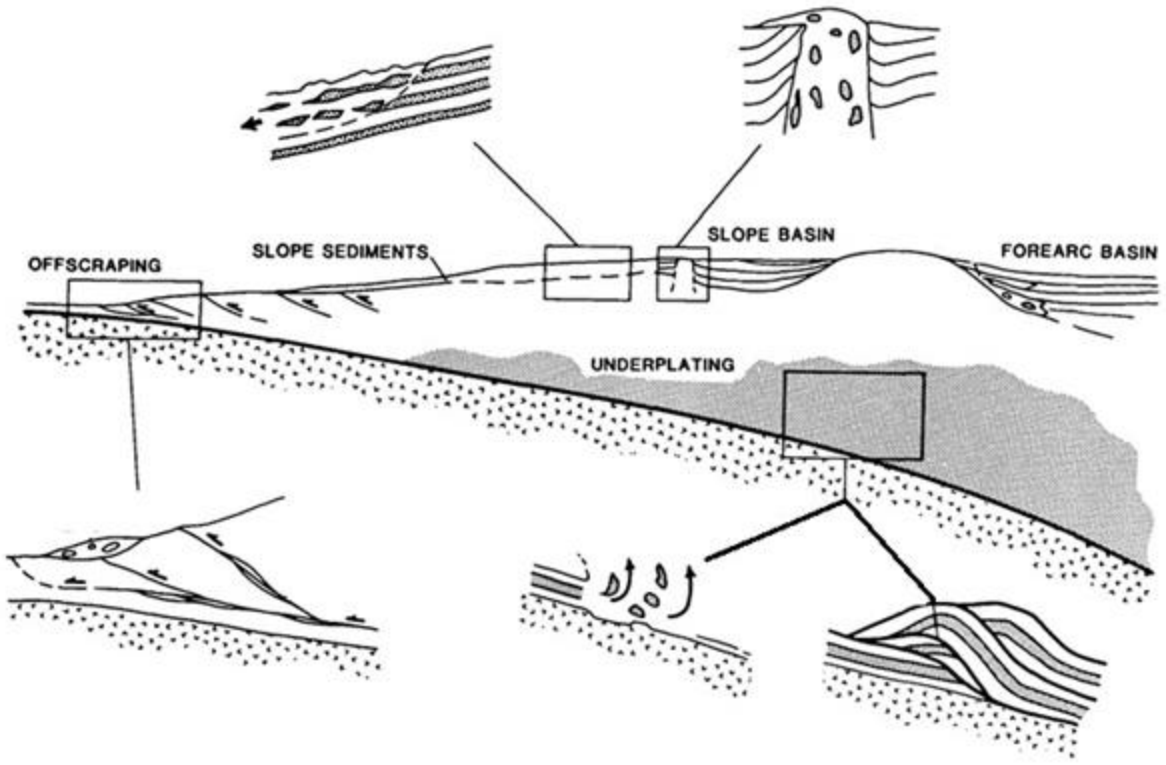

Figure 1.4. Schematic diagram of different possible mélange forming processes with the accretionary prism of a subduction zone (taken from Cowan 1985).

pressure zone within an accretionary wedge, while eclogite and amphibolite facies may represent upper mantle facies. The exhumation of these metamorphic rocks requires some kind of tectonic process. Cloos (1982) modeled a return-flow material path in mélanges and used this flow pattern to explain the mixture of different blocks within the Franciscan Complex. It may be possible that this process can pluck high grade rocks at depth and bring them to the surface.

Subduction is the most common and classical mélange forming environment. Both sedimentary and tectonic processes are at work in mélange formation. Sedimentary processes present in a subduction zone environment include deposits formed by mass transport, slumping and debris flows. These processes normally occur at the leading edge of the accretionary wedge. Mélanges caused by tectonic processes in a subduction zone display lithological and structural evidence for different degrees of mixing and deformation, depending on the rheology of the

rocks involved, superposition of different tectonic episodes, and different degrees of involvement in subduction processes.

Tectonic mélanges unrelated to subduction zones are associated with passive margins, extensional zones, continental collisional zones, strike-slip zones and intracontinental deformation. Mass transport, slumping, and/or olistolith formation are the primary types of mélanges formed by sedimentary processes in these environments, and they are the only types of mélange forming processes that occur in passive margins and extensional zones. In collisional, strike slip and intracontinental deformation zones, tectonic processes can form broken formations and remobilize older mélanges. It is important to note that mélanges formed in strike slip zones can have elongated blocks within them.

As stated above, a tectonic mélange is related to its tectonic environment. Different tectonic environments will produce different types of mélanges. There is a close relationship between mélange type and the geodynamic environment in which it was formed. However, these mélanges are a product of a combination of sedimentary and tectonic processes (Festa et al., 2010).

Analysis of individual components of mélanges can be used to gain information on the evolution of a mélange. As stated above, ophiolite formation and/or obduction can be determined by dating zircon grains from ophiolite related plagiogranites. Zircon grain populations can also be used to gain information on the provenance of sedimentary components of a mélange. Dangerfield et al. (2011) used the maximum age of sedimentation from a sandstone block recovered from the Ankara Mélange (Turkey) as the maximum age of mélange activity, and the maximum age of an overriding sedimentary unit as the maximum age of the end of mélange activity.

Ophiolitic Mélanges

The upper part of the Araxá Group has been associated with an ophiolitic mélange. The presence of ultramafic and mafic bodies was the major justification for Drake Jr. (1980) to characterize these areas of the Araxá Group as an ophiolitic mélange. Drake Jr. (1980) used the concept of Gansser (1974), when using the term ophiolitic mélange. Mélanges containing

ophiolitic components mixed with sedimentary and metamorphic rocks mark the boundary of suture zones (Coleman and Irwin, 1974).

According to Gansser (1974), an ophiolitic mélange is defined as an olistostromal and tectonic mixture of ophiolitic material and sediments of oceanic origin with exotic blocks, reflecting areas which have subsequently disappeared. The matrix of the mélange can be ophiolitic or sedimentary. Mélanges are sedimentary and tectonic mixtures; during emplacement, mass wasting events are common and are the cause of some of the mixing in ophiolitic mélanges. These mélanges can occur when the classical ophiolite suite is incomplete or missing and may outline geotectonic belts in the same way as an ophiolitic zone does (Gansser, 1974).

The occurrence of ophiolitic mélanges is restricted to areas that have ophiolitic belts and their formation and evolution is controlled by the area of their deposition. One of the main points behind the idea of the ophiolitic mélange is the close spatial and genetic relationship between mélanges containing ophiolitic assemblages and transported ophiolitic nappes. The formation of these mélanges is controlled by both tectonic and sedimentary processes. Tectonic aspects include subduction and collisional environments. This process is important in that it is needed for ophiolite emplacement (obduction). Sedimentary processes are also associated with ophiolite mélange formation. Mass wasting, in the form of olistostromes, is considered the main factor in depositing ophiolitic assemblages in the active mélange.

The classification and usage of the term “ophiolitic mélange” can cause confusion with the fact that several mélanges can be classified as an ophiolitic mélange, in the sense of Gansser (1974), but are defined as another type of mélange. One example is the Tehama-Colusa serpentine mélange of Northern California (Shervais et al., 2011). This mélange is composed of a serpentine matrix with a combination of sedimentary, high grade metamorphic and mafic to ultramafic blocks. Obduction mélanges (Gansser, 1974) are another example of a mélange that could harbor ophiolitic assemblages and can be referred to as an ophiolitic mélange. It could be that the definition of an ophiolitic mélange is too broad a term and may not be sufficient in mélange characterization.

1.4 Regional Geology

The Brasília Belt, located in central Brazil (fig 1.5), is a Neoproterozoic Brasiliano/Pan-African orogen resulting from the convergence and collision of three major continental blocks: the São Francisco-Congo, Amazonian and the Paranapanema. The eastern side of the Brasília Belt is composed of several sedimentary units (Paranoá, Canastra, Vazante, Araxá, Ibiá and Bambuí Groups), which form a fold and thrust belt, and were deposited on the western margin of the São Francisco craton. The Goiás Massif, an allochthonous block of Archean and Paleoproterozoic rocks, and the Anápolis–Itauçu granulite complex are located within the central part of the belt. The western margin of the Brasília Belt is bordered by the Neoproterozoic Goiás Magmatic Arc.

Sedimentary units of the fold and thrust belt are composed of several different groups, representing different deposition environments and were deposited on the western edge of the São Francisco craton. The sedimentary Paranoá, Canastra and Vazante groups are considered to have formed on a passive margin during the Mesoproterozoic (Dardenne, 2000; Pimentel et al., 2001, 2011, 2016; Rodrigues et al., 2010; Matteini et al., 2012). Studies on the provenance of these groups determined that the São Francisco craton was the sediment source (Pimentel et al., 2001, 2011; Rodrigues et al., 2010; Matteini et al., 2012). The Araxá and Ibiá groups are composed of various types of micaschists and micaceous quartzites, thought to be formed by pelitic and other deep marine sediments. Sm/Nd isotopic analyses on these groups show a bimodal nature, suggesting two sources for these sediments and U/Pb analyses on zircon grains demonstrated zircon populations related to the Goiás Magmatic arc. Authors have given an environment of foreland or back-arc basin for the deposition of these two groups. The Bambuí Group is composed of a thick pelitic and carbonatic sequence, which is thought to have formed in a foreland basin environment during the final stages of the Brasíla Belt evolution (Santos, 1998; Pimentel et al., 2001, 2011).

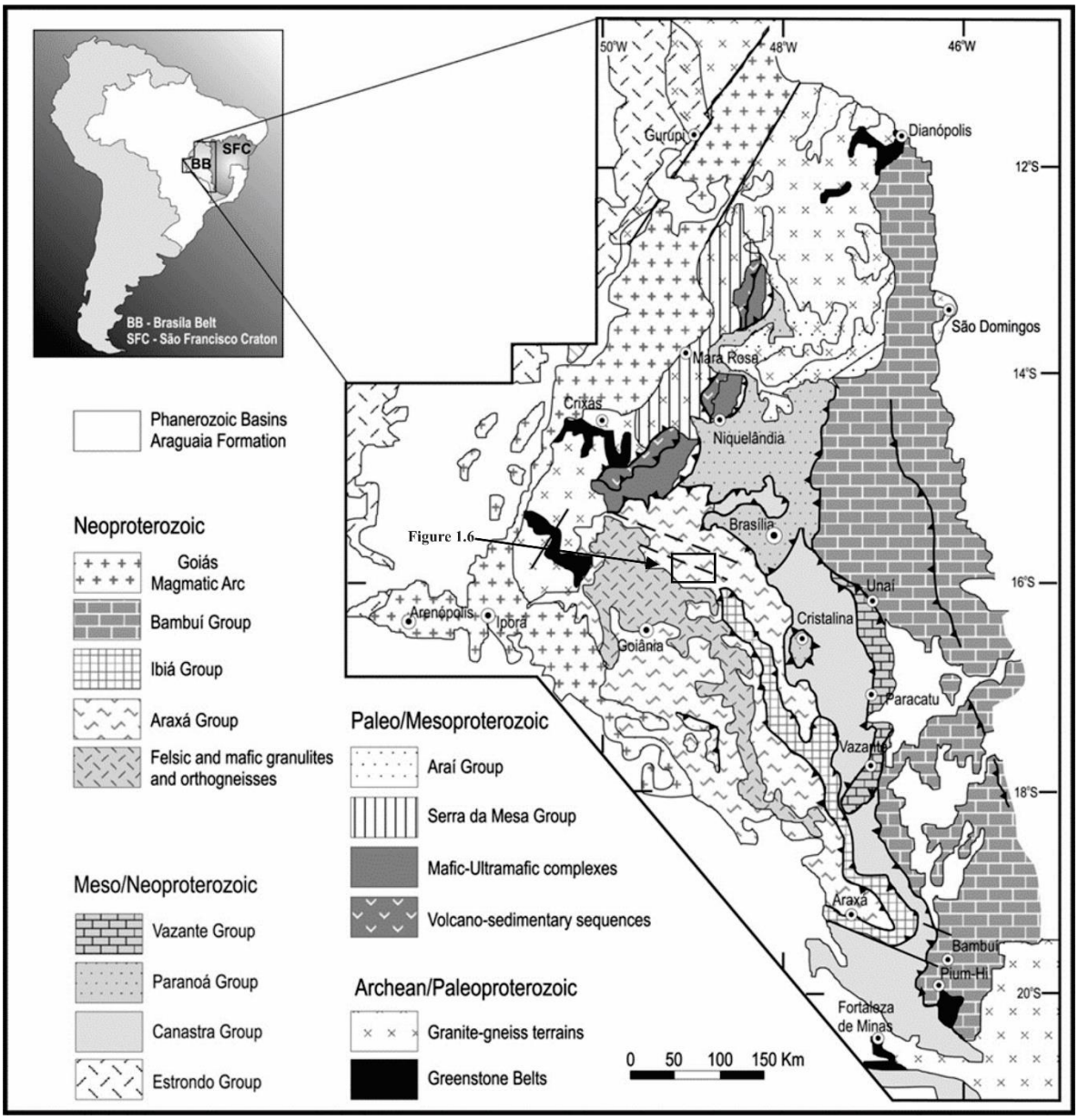

Figure 1.5. Simplified geological map of the Brasília Belt (modified from Dardenne 2000).

The Goiás Massif is considered an allochthonous microplate which was entrained within the Brasíla Belt, during its latest stages of orogenic evolution (Jost et al., 2013). It is composed of Archean TTG granite-gneiss complexes and greenstone belt terrains (Tassinari et al., 2006; Queiroz et al., 2008; Santos et al., 2008; Jost et al., 2010; Jost et al., 2013). Metaplutonic rocks from the complex were dated by U-Pb at 3.04 and 2.71 Ga (Pimentel et al., 2003). Some Neoproterozoic granite intrusions have been identified within the Goiás Massif and one was dated at 625 Ma, signaling that the massif had been emplaced before the intrusion (Pimentel et al., 2003).

East of the Goiás Massif are three large layered mafic-ultramafic complexes of Barro Alto, Niquelândia and Cana Brava. These three bodies are interpreted to have been a single structure, because of their geological and geochronological similarities, which was later disrupted during the evolution of the Brasília Belt (Ferreira Filho et al., 1998; Pimentel, 2016). The complexes are composed of two different magmatic systems, which are determined by petrological characteristics (Danni et al., 1982; Suita, 1996; Ferreira Filho et al., 1994; Ferreira Filho and Pimentel, 2000), with the three layered mafic intrusions on the east and layered amphibolite facies to the west. Some previous studies suggested that the two systems where formed during two different events, with the western intrusions forming in the Mesoproterozoic and the eastern units forming during the Neoproterozoic (Pimentel et al., 2004a, 2006). Recent work now supports the theory that the two units were formed during the same Neoproterozoic event (Correia et al. 2007, 2012; Rivalenti et al. 2008; Giovanardi et al. 2017). The magmatic event which created the intrusion is thought to have lasted from 800 to 770 Ma (Giovanardi et al., 2017), and is supported by U-Pb analysis on zircon grains from previous studies (Ferreira Filho et al., 1994, 2010; Suita et al., 1994; Pimentel et al., 2004a, 2006; Della Giustina et al., 2011; Correia et al., 2012; Giovanardi et al., 2015). The formation of the complexes is currently attributed to a back-arc extensional environment (Della Giustina et al., 2011; Giovanardi et al., 2017).

The western portion of the Brasília Belt consists of the Goiás volcanic arc. The Goiás Magmatic Arc is a Neoproterozoic juvenile arc located on the western edge of the Brasília Belt. The main magmatic terrains are separated by the Goiás Massif into two different arcs, known as the Mara Rosa arc in northern Goiás and southern Tocantins and the Arenópolis arc in

southwestern Goiás. Studies have shown that there were at least three episodes of volcanism related to the arc, comprising c. 930–770 Ma old calc-alkaline orthogneiss and remnants of volcano-sedimentary sequences, younger orthogneiss and supracrustals of continental arc affinity (750–600 Ma), as well as a number of late- to post-orogenic granite intrusions (560-520 Ma) (Pimentel et al. 1999, 2003; Laux et al. 2005; Marques et al., 2017). The majority of sediments found in the vicinity of the volcanic arcs yielded TDM model ages ranging from 1.20 to 0.93 Ga (Pimentel, 2001). Adakitic magmatic rocks in the magmatic arc were dated at ~540 Ma and were interpreted by Frasca et al. (2015) as evidence of arc delamination and the age of final suturing of the magmatic arc within the Brasília Belt.

The Araxá Group is a large metasedimentary rock group composed of various types of micaschists and micaceous quartzites. Similar to the Ibiá Group, the protolith is thought to be pelitic and other deep marine sediments deposited in a foreland or back-arc basin in a marine environment; however, some immature sequences have flyschoid characteristics (Lacerda Filho et al., 1989). The maximum age of deposition for these two groups is considered to be about 790 Ma, which was determined by U/Pb analysis of zircon grains collected from the Maratá volcanic-sedimentary unit (Pimentel et al., 1992). TDM model ages for the Araxá and Ibiá groups are 2.23 to 1.00 Ga and 2.47 to 1.16 Ga, respectively (Pimentel et al., 2001, 2011; Piuzana et al., 2003b; Rodrigues et al., 2010). The degree of metamorphism in the Araxá Group ranges from greenschist facies, and increases to the west to as high as granulite facies in some areas. There are series of low angle faults and nappes, causing tectonic overlapping of the Araxá Group, with vergence to the east, in direction of the São Francisco craton. The presence of mafic and ultramafic rocks within the Araxá Group is the principal reason to using the term of ophiolitic mélange for some parts of the rock group (Drake Jr., 1980).

There are several amphibolite bodies distributed throughout the Araxá Group, which have a Fe-enriched tholeiitic nature and show mid-ocean ridge tholeiitic or island-arc basalts affinity (Brod et al., 1992; Strieder and Nilson, 1992; Valeriano and Simões, 1997; Seer et al., 2001; Klein et al., 2008). REE and normalized trace elements diagrams demonstrated a T-MORB to E-MORB composition (Seer, 1999, 2000; Seer et al., 2001; Valeriano, 1992; Klein et al., 2008). Piuzana et al. (2003b) dated an amphibolite, located to the east of Goiânia, at 838±? Ma.

Three periods of igneous activity have affected the Araxá Group, similar to the Goiás Magmatic Arc, marked by numerous felsic igneous intrusions. The first episode occurred around 833 Ma, dated from granite in the southern portion of the Araxá Group and is thought to be related to oceanic arc magmatism (Seer and Moraes, 2013). The second episode occurred between 798 and 720 Ma (Pimentel et al., 2011; Klein et al., 2008; Seer and Moraes, 2013). Klein et al. (2008) hypothesized that an extensional event occurred during this time interval, which commenced at roughly 800 Ma and lasted until about 760 Ma. Evidence of this event was the presence of amphibolites with E-MORB signature, in association with granites and metarhyolites of the Maratá sequence, in south Goiás. The last episode occurred between 660 and 630 Ma (Pimentel et al., 2011; Klein et al., 2008; Seer and Moraes, 2013), and is regarded as the result of collision between the Amazonian and São Francisco cratons.

The Anápolis–Itauçu granulite complex (AIC) is composed of high-grade metamorphic rock assemblages, which were intruded by igneous rocks and is now considered as the high-grade metamorphic equivalent of the Araxá Group sequences. The presence of sapphirine in some rock assemblages of the AIC was suggested by Moraes et al. (2002) to be indicative of ultra-high-temperature metamorphism. The age of metamorphism for the complex was calculated to have occurred roughly between 664 and 630 Ma (Piuzana et al., 2003b; Baldwin et al., 2008). More recently, Della Giustina et al. (2011) hypothesized that there were two episodes of metamorphism, related to mafic magmatism that occurred in the AIC. The first occurred around 680-670 Ma and represents the ultra-high temperature metamorphic event, and the second occurred around 630 Ma and could be related to a post peak cooling of the ACI, and is consistent with metamorphism ages recorded in the Goiás arc and in Araxá rocks elsewhere.

1.5 Methods

Sampling

The study area is located about 15 km to the northwest of the town of Abadiânia, near the towns of Posse da Abadia and Planalmira (fig 1.). Access to the study area is found along roads GO-338, Abadiânia to Planamira, and high way 414, Anápolis to Planalmira. The targeted

mélange covers an area of about 550 km^2. To understand the nature of the ophiolitic mélange, samples of the individual components present in the mélange need to be studied. The mélange consists of bodies, and/or blocks, of mafic and ultramafic rocks, quartz schist and mylonitic

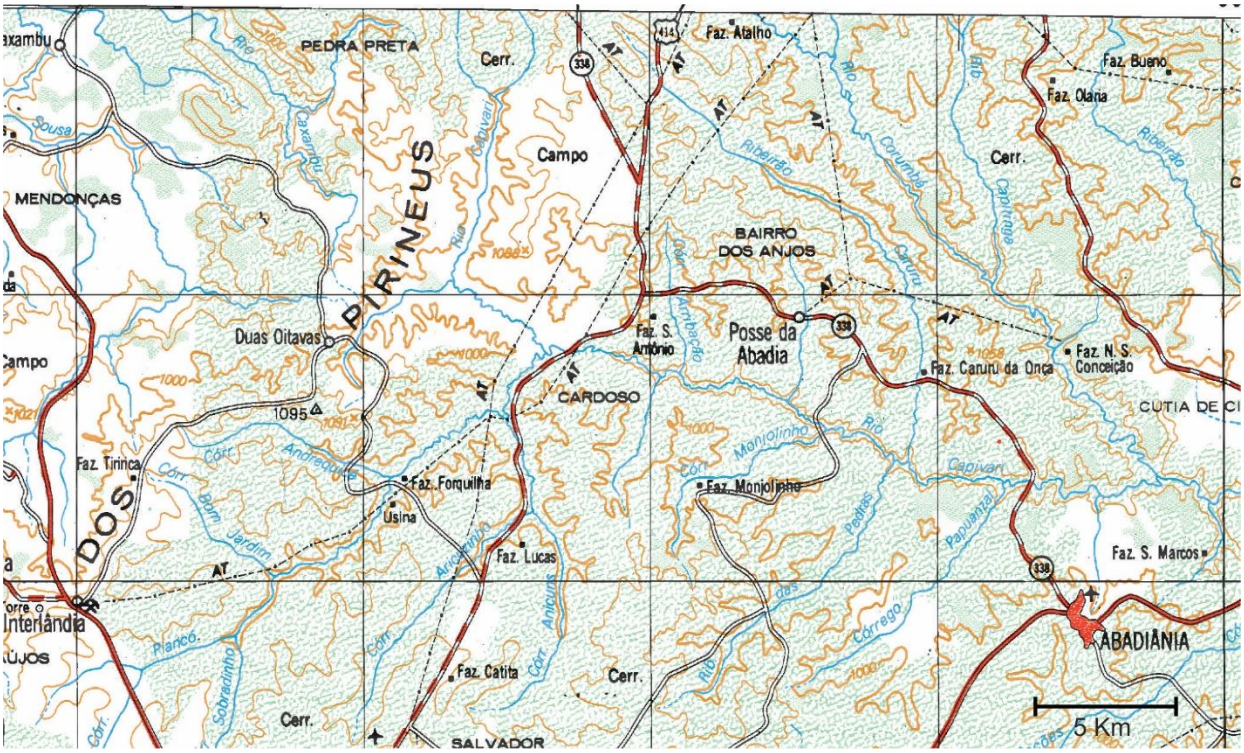

Figure 1.6. Map showing the general location of the study area, in relation to Abadiânia (IBGE, 1980).

granite. These blocks are bounded within a matrix of garnet-mica schist. Of special interest in the area, was ultramafic body S9, located near Posse da Abadia, which possesses a large metasomatic zone and is in contact with an amphibole schist. Figure (1.6) was taken in the field looking to the East at the metasomatic zone's contact with the amphibolite schist, the serpentinite core of S9 is located behind and to the right of the photographer. This metasomatic has the possibility of harboring zircon grains which could be used for dating the mélanges ophiolitic component. Another point of interest an outcrop of amphibole schist in the Corumba River, which was in contact with a plagioclase-mica schist (fig 1.7). Samples of the different blocks were collected (fig 1.5 B.), as well as the garnet-mica schist matrix.

Figure 1.7. A. Picture of amphibole-schist contact with metasomatic zone (samples aba-12 and aba-11). B. Example of serpentinite block from ultramafic body S9 (sample aba-10).

Figure 1.8. A. Picture of outcrop in the Corumbá River showing the contact between plagioclase-mica schist (on top) and amphibole schist (location of samples aba-ax-06, aba-ax-07, aba-ax-08 and aba-ax-10). B. Picture of granite from near the Padre Souza Creek (sample aba-ax-G3). C. Picture showing quartzite outcrop along BR 414 (collection point of sample aba-ax-05).

Petrology

The type of rock and mineral identification was determined by analysis with a translucent optical microscope. Samples also underwent X-ray diffraction analysis, in order to confirm the presence of different mineral assemblages. Samples were also investigated with a FEI Quanta 450 scanning electron microscope, in order to identify trace minerals and image zircon grains and confirm their presence in some samples.

Geochemistry

Geochemistry will be used on the metamafic assemblage of the ophiolitic component of the mélange. Samples are to be pulverized and sent to ASL Minerals in Goiânia, GO, for processing. Major elements were determined by x-ray fluorescence after glass disks were made with the samples by means of lithium borate fusion. Trace and rare earth elements were determined by ICP-MS/ ICP-AES, after preparation by lithium borate fusion.

Table 1.2. List of the collected samples and their localization.

Sample	Rock Type	S°	W°
Aba-001*	Chlorite Schist	16.08882°	48.82161°
Aba-004*	Serpentinite	16.08881°	48.82172°
Aba-005*	Chlorite Schist	16.08883°	48.8216°
Aba-006*	Tremolite Talc Schist	16.08918°	48.8219°
Aba-007*	Serpentinite	16.08882°	48.82178°
Aba-008*	Chlorite Schist	16.08883°	48.82159°
Aba-009*	Serpentinite	16.08864°	48.82141°
Aba-10*	Serpentinite	16.08882°	48.82179°
Aba-011*	Rodrigonite	16.8841°	48.82122°
Aba-012*	Epidote-amphibole schist	16.8841°	48.82122°
Aba-013	Quartzite	16.07845°	48.78988°
S9A*	chlorite schist	16.08882°	48.82161°
S9B*	chlorite schist	16.08881°	48.82162°
Aba-ax-02	Garnet-muscovite-biotite-schist	16.10553°	48.80067°
Aba-ax-03	Garnet-muscovite-biotite-schist	16.10094°	48.87049°
Aba-ax-05	Quartzite	16.12813°	48.89526°
Aba-ax-06**	Epidote-amphibole schist	16.08556°	48.73895°
Aba-ax-07**	Plagioclase-muscovite-biotite-schist	16.057°	48.73874°
Aba-ax-08**	Plagioclase-muscovite-biotite-schist	16.08546°	48.73924°
Aba-ax-10**	Chlorite-epidote-amphibole schist	16.08547°	48.73931°
Aba-ax-11	Garnet-muscovite-biotite-schist	16.09845°	48.95568°
Aba-ax-12	Garnet-muscovite-biotite-schist	16.072°	48.95193°
aba-ax-13	Epidote-amphibole schist	16.08789°	48.80895°
aba-ax-14	Epidote-amphibole schist	16.08625°	48.76616°
aba-ax-15**	Epidote-amphibole schist	16.08532°	48.73945°
Aba-ax-G2	Mylonite Granite	16.06245°	48.00417°
Aba-ax-G3	Mylonite Granite	16.06729°	48.00464°

* - smaples collected from ultramafic body S9

** - samples collected from within the Corumbá River

U-Pb

For the analysis of U-Pb method La-ICP-MS, zircon grains are extracted, by first processing in a rock crusher, producing chips roughly 3–5 cm in size, then processing in a Selfrag high voltage laboratory equipment, with a voltage of 130 kV and a frequency of 3 Hz.

Zircon grains are then concentrated using a pan to separate the heavy mineral fraction and a Franz was then used to remove the magnetic fraction. Zircon grains are next handpicked using a binocular microscope. Grains are mounted in epoxy mounts and polished to create a smooth surface. HNO_3 (ca. 2%) was used to clean the surface of the mounts. Backscatter electron images of the zircon grains are then taken with a FEI-Quanta 450 scanning electron microscope, working at 20 – 25 kV, at the University of Brasília, in order to characterize grain zonation.

All zircon grain analyses followed the analytical procedure described by Bühn et al. (2009) and are conducted at the Geochronology Laboratory at the University of Brasília. U-Pb La-ICP-MS method was conducted on a Thermo Finnigan Neptune MC-ICP-MS, coupled with a New Wave UP213 Nd: YAG laser (λ = 213 nm). Measurements consisted of point analyses. The laser was run with a 30 µm spot, with an energy of 4-5 mJ/cm^2 and a frequency of 10 Hz. Zircon standard GJ-1 (Jackson et al., 2004) was used as the primary standard, for mass bias and drift correction. During runs, 4 analyses are bracketed in between 2 standards and two blanks (Albarède et al., 2004). Results are also checked against the in-house standard 91500. Zircon ages are calculated using ISOPLOT v.3 (Ludwig, 2003), with isotopic ratio errors presented at the 1σ level.

Lu-Hf

The La-ICPMS Lu-Hf isotope method on single zircon grains is compared to results attained on crystals previously analyzed by U-Pb La-ICPMS method. Because of the relation between the Lu-Hf and the U-Pb methods, the two spot analyses need to be as close as possible in order to analyze the same areas of the individual zircon grains. A Thermo Finnigan Neptune MC-ICP-MS is utilized for these analyses, conducted at the Geochronology Laboratory at the University of Brasília, using the method described by Matteini et al. (2010). Before analyzing the zircon grains, the mass spectrometer is calibrated using a solution made from the SRM reference material JMC475. The laser ablation analyses were conducted using a New Wave UP213 Nd: YAG laser (λ = 213 nm), utilizing a spot of 40 µm and a frequency of 10 Hz. Results were compared to the GJ-1 zircon standard. Isotope ratios were translated to an Excel spreadsheet in order to calculate the values for ε_{Hf} ratios and Hf T_{DM} model ages.

Sm-Nd

Sm-Nd analyses are conducted at the Geochronology Laboratory at the University of Brasília, using the method described by Gioia & Pimentel (2000). Preparation for the Sm-Nd method analyses begins with whole rock samples being pulverized in a shatter box. 50 mg of sample are mixed with a $^{149}Sm/^{150}Nd$ spike solution and dissolved in Savillex capsules. Conventional cation exchange techniques are used to separate Sm and Nd from whole rock samples. Samples are evaporated onto Re filaments. Analyses are conducted on a Finnigan TRITON multi-collector mass spectrometer running in static mode. Uncertainties for the Sm/Nd and $^{143}Sm/^{144}Nd$ ratios are better than ±0.5% (2σ) and ±0.005%(2σ), respectively, and are based upon repeated analyses of international rock standards BHVO-1 and BCR-1. $^{143}Sm/^{144}Nd$ ratios are normalized to $^{146}Nd/^{144}Nd$ ratio of 0.7219 and the decay constant of 6.54×10^{12} was used. The T_{DM} model values were calculated using the method described by DePaolo (1981).

2. Isotopic age constraints and geochemical results of disseminated ophiolitic assemblage from Neoproterozoic mélange, Central Brazil

Matthew T. Brown[a*], Reinhardt A. Fuck[a], Elton L. Dantas[a]

[a]Laboratory of Geochronolgy, Institute of Geology, University of Brasília, Brasília, Federal District, 70910-900, Brazil

*Corresponding author. E-mail address: brownmt7@gmail.com

Abstract

The Neoproterozoic Brasília belt, central Brazil, formed during the amalgamation of West Gondwana, and contains a magmatic arc and a large metasedimentary pile. An ophiolitic mélange is contained within one of the metasedimentary units from the pile, and includes bodies of metamafic and ultramafic assemblages in a metasedimentary rock matrix. One of these metamafic bodies encompasses a serpentinite body, which displays a well-developed metasomatic "black-wall" alteration zone at its contact. Samples of metamafic, serpentinite and black-wall rocks were collected, as well as two garnet-mica schists in contact with the metamafic assemblage. The metamafic assemblage is composed of epidote-amphibole schist, chemical analysis of which indicates that its protolith was a tholeiitic basalt with a MORB signature that may have been formed in a back-arc environment. U-Pb analyses indicate an age of crystallization of c. 800 Ma for the protolith of the epidote-amphibole schist. The black-wall is mostly composed of chlorite schist, with the exception of an albite-hornblende fels at the contact with the epidote-amphibole schist. The black-wall has a range of ages from c. 800 to 760 Ma. ε_{Hf} values of selected zircon grains of the epidote-amphibole schist sample range from -21.67 to +13.66, with T_{DM} ages of 0.80–4.22 Ga, while the black-wall samples have highly depleted ε_{Hf}

values ranging from +9.16 to +23.98, with T_{DM} model ages of 0.34–0.96 Ga. The studied mica schists have zircon population peaks of c. 790 to 890 Ma. ε_{Hf} ranges from -14.87 to +6.46 and T_{DM} ages from 1.47 to 1.91 Ga. The epidote-amphibole schist, serpentinite and black-wall assemblages all have positive ε_{Nd} values from +4.95 to +7.89, indicating a mantle signature. ε_{Nd} values for the garnet-mica schists are -8.31 and -8.16, and their T_{DM} values are 1.83 and 2.36 Ga, which indicate a continentally derived components. The results suggest that the ophiolitic component of the Araxá mélange formed in a back-arc basin environment, which formed at c. 800 Ma and lasted till c. 760 Ma, while the studied schists probably represent sediments deposited in the newly formed back-arc basin.

Key Words: Brasília Belt, Neoproterozoic, Araxá Group, Ophiolite, Black-wall

2.1. Introduction

Ophiolites are considered as remnants of oceanic crust and upper mantle that have been tectonically emplaced onto continental margins (Dilek and Furnes, 2014). Ophiolitic rocks are important for understanding tectonic processes and crustal evolution. Precambrian ophiolites are the only available samples of oceanic crust from this time period (Furnes et al., 2015), and their study allows important insight into the evolution of continents, such as the break-up of Rodinia and the formation of Gondwana. However, dating ophiolites can be extremely difficult, due to the lack of datable minerals, normally depending on the presence of plagiogranite in order to reliably date an ophiolitic sequence (Samson et al., 2004; Dilek and Thy, 2006; Queiroga et al., 2007; Karaoglan et al., 2013; Rioux et al., 2013).

Recently, metasomatic zircon grains associated to metasomatic alteration zones related to serpentinization has been used to date ophiolite sequences (Dubińska and Wiewióra, 1999; Dubińska et al., 2004; Li et al., 2013; Liu et al., 2016; Arena et al., 2017). The metasomatic process causes a zonation comprising of a characteristic "black-wall", which consists mainly of chlorite, thought to be formed by the alteration of ultramafic rock, and a rock assemblage rich in Ca and Al mineral assemblages, such as rodingite, between the black-wall and some other associated rock type (Frost, 1975; O'Hanley, 1996; Dubińska et al. 2004). The dating of metasomatic zircon grains creates a new way to determine the age of ophiolite sequences and describe their evolutionary history (Liu et al., 2016; Arena et al., 2016; 2017), which helps in our understanding of the accretionary history of the continents.

The rifting of Rodinia caused opening of several ocean basins, which subsequently were closed during the amalgamation of Gondwana. The Goiás-Pharusian Ocean is another example of an ocean of considerable size, which opened after the rifting and breakup of Rodinia. The formation of West Gondwana created the Transbrasiliano-Kandi mega-shear zone and signals the closing of the Goiás-Pharusian Ocean. Several volcanic arcs associated with the closing are the result of the destruction of the Goiás-Pharusian oceanic crust, such as the Anti-Atlas range in Morocco, and the Goiás Magmatic Arc in central Brazil. Subduction within the Anti-Atlas range occurred roughly 760 – 600 Ma ago (Hefferan et al., 2000, 2014).The presence of several Neoproterozoic aged ophiolites found in several Pan-African and Brasiliano orogenic belts are evidence of this process (Stern, 1994; Patchett and Chase, 2002; Dilek and Ahmed 2003; Hefferan et al., 2000, 2014, Arena et al., 2016). In South America, the São Francisco craton has several occurrences of ophiolite assemblages located along its boundary and associated orogenic

belts (Strieder and Nilson, 1992; Pedrosa-Soares et al., 1998; Tassinari et al., 2001; Paixão et al., 2008; Caxito et al., 2014), which attest to the formation of West Gondwana.

The Goiás Magmatic Arc forms the western edge of the Brasília Belt and was shown to be active almost continuously from 930 to 630 Ma (Pimentel et al., 1999, 2003; Laux et al., 2005; Marques et al., 2017; Fuck et al., 2008, 2017).The Brasília Belt is a large Neoproterozoic orogen that formed on the western margin of the São Francisco Craton, contains large tectonically emplaced metasedimentary packages and a micro continental block. One of these metasedimentary packages hosts an ophiolitic mélange, which contains metamafic and metaltramafic bodies, dispersed in metasedimentary assemblages. The lack of geochemical and isotopic data, together with a lack of a definitive and complete stratigraphy, has left the nature of this ophiolitic mélange and its host metasedimentary unit an enigma.

The aim of this study is to examine the ophiolitic component of the mélange from the Araxá Group within the Brasília Belt, in the area near the town of Abadiânia. The intention is to gain insight into the formation environment and the age of the ophiolitic components. In order to determine the environment in which they formed, samples of mafic and ultramafic assemblages underwent whole rock geochemical and Sm-Nd isotopic analysis, while recovered zircon grains were analyzed by LA-ICP-MS for U-Pb and Lu-Hf isotopes, in order to constrain the age and nature of their formation.

2.2. Geological Background

2.2.1 Brasília Belt

The Brasília Belt (Fig. 2.1), located in central Brazil, is a Neoproterozoic Brasiliano/Pan-African orogen resulting from the convergence and collision of three major continental blocks: the São Francisco-Congo and Amazonian cratons and the Paranapanema block. The principal components of the belt comprise a large metasedimentary pile, a granulitic complex, the Goiás Massif, considered an allochthonous microplate, including three large layered mafic-ultramafic complexes and the Goiás Magmatic Arc (Pimentel et al., 2011; Fuck et al., 2017).

The metasedimentary pile is composed of several different sedimentary groups, which form a fold and thrust belt on the western margin of the São Francisco Craton. The main sedimentary groups are the Paranoá, Canastra, Vazante, Bambuí, Araxá and Ibiá groups. The Paranoá, Canastra and Vazante groups are considered to have formed on a passive margin at the end of the Mesoproterozoic and beginning of the Neoproterozoic (Dardenne, 2000; Pimentel et al., 2001, 2011, 2016; Rodrigues et al., 2011; Matteini et al., 2012; Fuck et al., 2017). Studies on the provenance of these groups determined that the São Francisco Craton was the main sediment source (Pimentel et al., 2001, 2011; Rodrigues et al., 2011; Matteini et al., 2012). The Araxá and Ibiá groups are composed of various types of micaschists and micaceous quartzites, thought to be formed of pelites and other deep marine sediments. Sm-Nd isotopic analysis on samples from these groups show a bimodal nature, suggesting two sources for these sediments, and U-Pb analysis on zircon grains demonstrated zircon populations related to the Goiás Magmatic Arc,

with peaks around 650 Ma (Pimentel et al., 2001, 2011; Piuzana et al., 2003b; Falci et al., 2018).

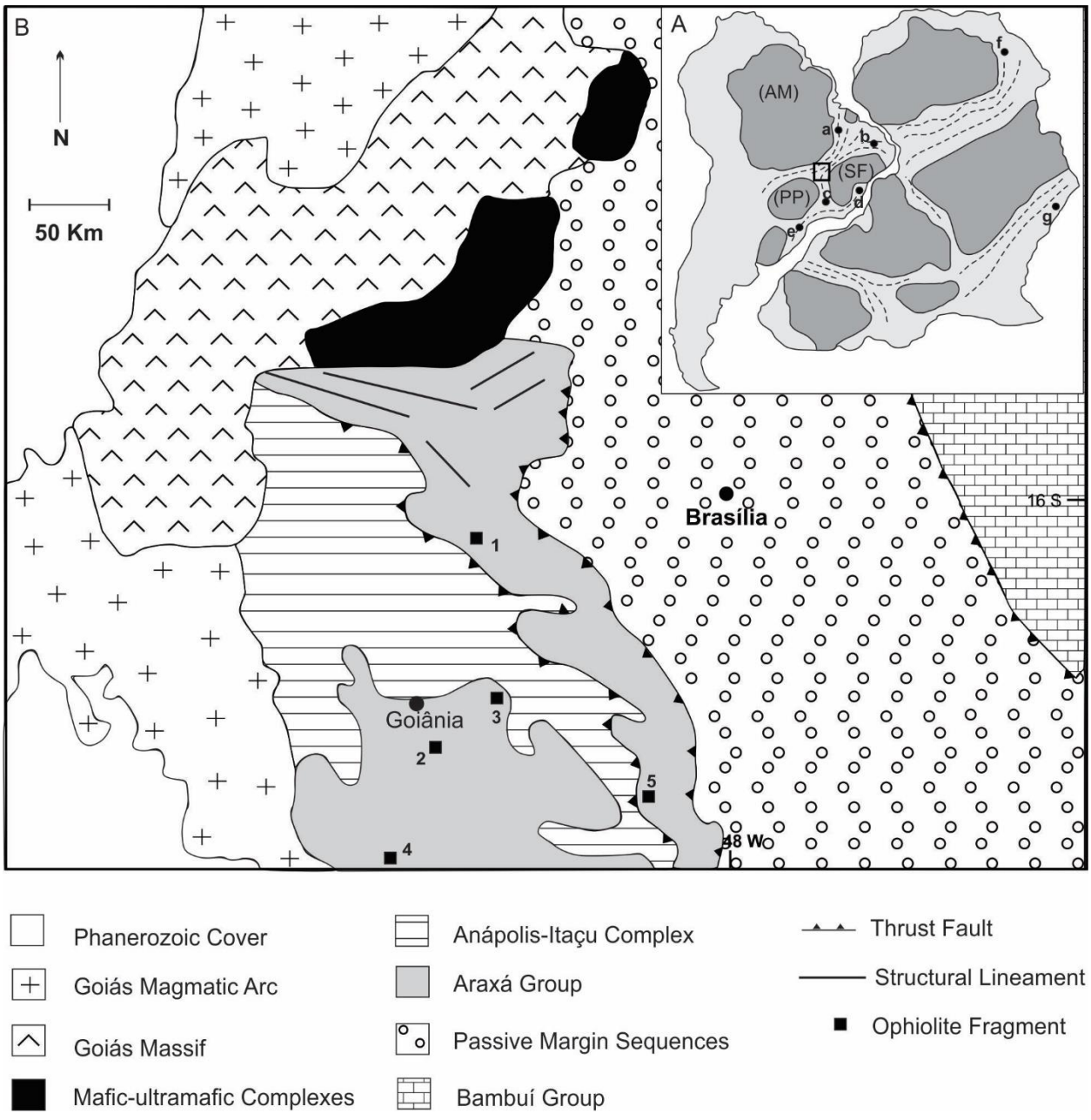

Figure 2.1. A. Crustal building blocks for the amalgamation of West Gondwana and locations of some documented ophiolites (A. Pedrosa-Soares et al. (1998), B. Caxito et al. (2014), C. Tassinari et al. (2001), D Paixão et al. (2008), E Arena et al. (2016), F. Hefferan et al. (2000), G. Dilek and Ahmed (2003). (AM - Amazonian Craton; SF – São Francisco Craton; PP – Paranapanema Craton). B. Simplified geological map of the Brasília Belt and the location of some registered ophiolites: 1 Abadiânia (Strieder & Nilson 1992a); 2. Morro Feio (Mello & Berbert 1969); 3. Bonfinópolis amphibolite (Piuzana et al., 2003b); 4 Mairipotaba and Cromínia (Navaro & Zanardo 2005); 5. Pires do Rio (Piauilino et al., 2019) (modified from Pimentel et al. 2004).

Authors have given an environment of foreland or back-arc basin for the deposition of these two groups (Pimentel et al 1999, 2011; Seer et al. 2001). The Bambuí Group is composed of a thick pelite and carbonate sequence, which is thought to have formed in a foreland basin environment during the final stages of the Brasíla Belt evolution (Pimentel et al., 2001, 2011).

The Anápolis–Itauçu granulite complex (AIC) is composed of high-grade metamorphic rock assemblages, which were intruded by igneous rocks, and is considered to be the metamorphic core of the Brasília Belt (Fuck et al., 2017). The age of metamorphism of the complex occurred roughly between 650 and 640 Ma (Piuzana et al., 2003b; Baldwin et al., 2008), and it has been shown that its rocks are at least in part the high-grade metamorphic equivalents of the Araxá Group sequences (Piuzana et al., 2003b).

The Goiás Massif, also known as the Goiás Archean Block (Pimentel, 2016), is considered an allochthonous microplate, which was entrained within the Brasília Belt during its latest stages of orogenic evolution (Jost et al., 2013). It is composed of Archean TTG granite-gneiss complexes and greenstone belt terrains (Tassinari et al., 2006; Queiroz et al., 2008; Santos et al., 2008; Jost et al., 2010, 2013). Metaplutonic rocks from the complex were dated by U-Pb at 3.04 and 2.71 Ga (Pimentel et al., 2003). Some Neoproterozoic granite intrusions have been identified within the massif, with one dated at 625 Ma, signaling that the massif had been emplaced before the intrusion (Pimentel et al., 2003).

The large layered mafic-ultramafic complexes of Barro Alto, Niquelândia and Cana Brava are located in the East of the Goiás Massif. These three bodies are interpreted to have been a single structure, which was later disrupted during the evolution of the Brasília Belt (Ferreira Filho et al., 1998; Pimentel, 2016). The complexes were formed during a Neoproterozoic event

thought to have persisted from 800 to 770 Ma (Giovanardi et al., 2017), which is supported by U-Pb analysis on zircon grains from previous studies (Ferreira Filho et al., 1994, 2010; Suita et al., 1994; Pimentel et al., 2004a, 2006; Della Giustina et al., 2011; Correia et al., 2012; Giovanardi et al., 2015). The formation of the complexes is currently attributed to a back-arc extensional environment (Della Giustina et al., 2011; Giovanardi et al., 2017).

The Neoproterozoic Goiás Magmatic Arc makes up the western portion of the Brasília Belt. The arc was active continuously from about 930 to 630 Ma and was formed by the subduction of the oceanic crust of the Goiás-Pharusian Ocean (Cordani et al., 2013). The arc is separated by the Goiás Massif into two different terrains, known as the Mara Rosa arc to the north and the Arenópolis arc to the south. Studies have indicated that there could have been at least three episodes of volcanism related to the arc, comprising c. 900–770 Ma old calc-alkaline orthogneiss and remnants of volcanic-sedimentary sequences, younger orthogneiss and supracrustals of continental arc affinity (750–630 Ma) related to a continental arc setting and continent-continent collisional setting, as well as a number of late- to post-orogenic granite intrusions 560-520 Ma (Pimentel et al., 1999, 2003; Laux et al., 2005; Marques et al., 2017). Adakitic magmatic rocks in the magmatic arc were dated at ~540 Ma and were interpreted by Frasca et al. (2015) as evidence of arc delamination and of the age of final suturing of the magmatic arc with the other rock units of the Brasilia Belt.

2.2 Araxá Sedimentary Sequence and Ophiolitic Mélange Assemblages

The Araxá Group is a large metasedimentary group composed of various types of micaschists and micaceous quartzites, thought to have been derived from pelitic and other deep marine sediments deposited in a foreland or back-arc basin in a marine environment. Some

immature sequences have flyschoid characteristics (Lacerda Filho et al., 1989). In the southern portion of the Brasília Belt, the Araxá Group is considered to have been deposited in a passive margin environment with a maximum age of sedimentation between 1.0 and 0.9 Ga (Valeriano et al., 2004). Sm-Nd T_{DM} model ages for the Araxá are 2.23 to 1.00 Ga (Pimentel et al., 2001, 2011; Piuzana et al., 2003; Rodrigues et al., 2010). An important feature is the presence of serpentinite and amphibolite bodies within the Araxá Group. The association of mafic and ultramafic assemblages, and discontinuous bodies of marble, disseminated in metasedimentary rocks was interpreted as an ophiolitic mélange by Drake Jr. (1980). In the sense of Gansser (1974), ophiolitic mélange is defined as an olistostromal and tectonic mixture of ophiolitic material and sediments of oceanic origin with exotic blocks. Metamafic bodies have a Fe-enriched tholeiitic nature and show mid-ocean ridge tholeiitic or island-arc basalt affinity (Brod et al., 1992; Strieder and Nilson, 1992a; Valeriano and Simões, 1997; Seer et al., 2001; Klein et al., 2008; Piauilino et al., 2019). REE and normalized trace elements diagrams demonstrated a T-MORB to E-MORB composition (Seer, 1999; Seer and Dardenne, 2000; Seer et al., 2001; Valeriano, 1992; Klein et al., 2008; Piauilino et al., 2019).

There are several igneous rock bodies located in the Araxá Group, which have been dated, including those of mafic affinity described above, but also numerous felsic igneous rock bodies as well. Piuzana et al. (2003b) dated an amphibolite (Bonfinópolis amphibolite), thought to be a piece of oceanic crust, located to the east of Goiânia, at ca. 838 Ma, which is similar to the age of a granite in the southern portion of the Araxá Group (833 Ma), thought tobe a rift-related intrusion (Seer and Moraes, 2013). The Maratá Sequence is a volcanic-sedimentary unit, located near the town of Catalão, which has metarhyolite interlayered with schists of the Araxá Group, dated at ca. 790 Ma, considered as the minimum age of deposition of the Araxá Group

(Pimentel et al., 1992). Granites are present in the general area of the Maratá sequence, and further south in the Araxá Group, which have been dated between 798 and 720 Ma (Klein et al., 2008; Pimentel et al., 2011; Seer and Moraes, 2013). Klein et al. (2008) hypothesized that an extensional event occurred during this time interval, which commenced at roughly 800 Ma and lasted until about 760 Ma. Evidence of this event was the association of amphibolites with E-MORB signature, together with granites and metarhyolites of the Maratá sequence, in south Goiás. Younger granitic rocks have been dated at ca. 660 and 630 Ma (Pimentel et al., 2011; Klein et al., 2008; Seer and Moraes, 2013), regarded as the collision between the Amazonian and São Francisco cratons.

The degree of metamorphism in the Araxá Group increases westwards from greenschist facies to as high as granulite facies in some areas. A series of low angle faults and nappes cause tectonic overlapping of the Araxá Group, with vergence to the east, toward the São Francisco Craton (Pimentel, 2016; Fuck et al., 2017). The southern portion of the Araxá Group represents a tectonic mixture of sedimentary units deposited in different tectonic environments and during different time periods, which were later tectonically juxtaposed through nappe stacking (Falci et al., 2018).

2.3 The Study Area

The study area is located roughly 80 km to the west of Brasília, near the towns of Posse de Abadia and Planalmira (Fig 2.2). The rock assemblages of the Araxá Group in this area are composed of garnet-muscovite-biotite-quartz schist and muscovite-quartz schist, epidote-amphibole schist and ultramafic rock assemblages. This area was categorized as an ophiolitic mélange by Strieder (1989), because of the combination of rock types. Felsic rocks in the form of

mylonitic granite are also present in the area, considered to be part of the basement of the Brasília Belt (Berbert et al., 1970). Fresh outcrops are scarce in the study area, with most outcrops being highly altered, and higher elevation capped with laterite.

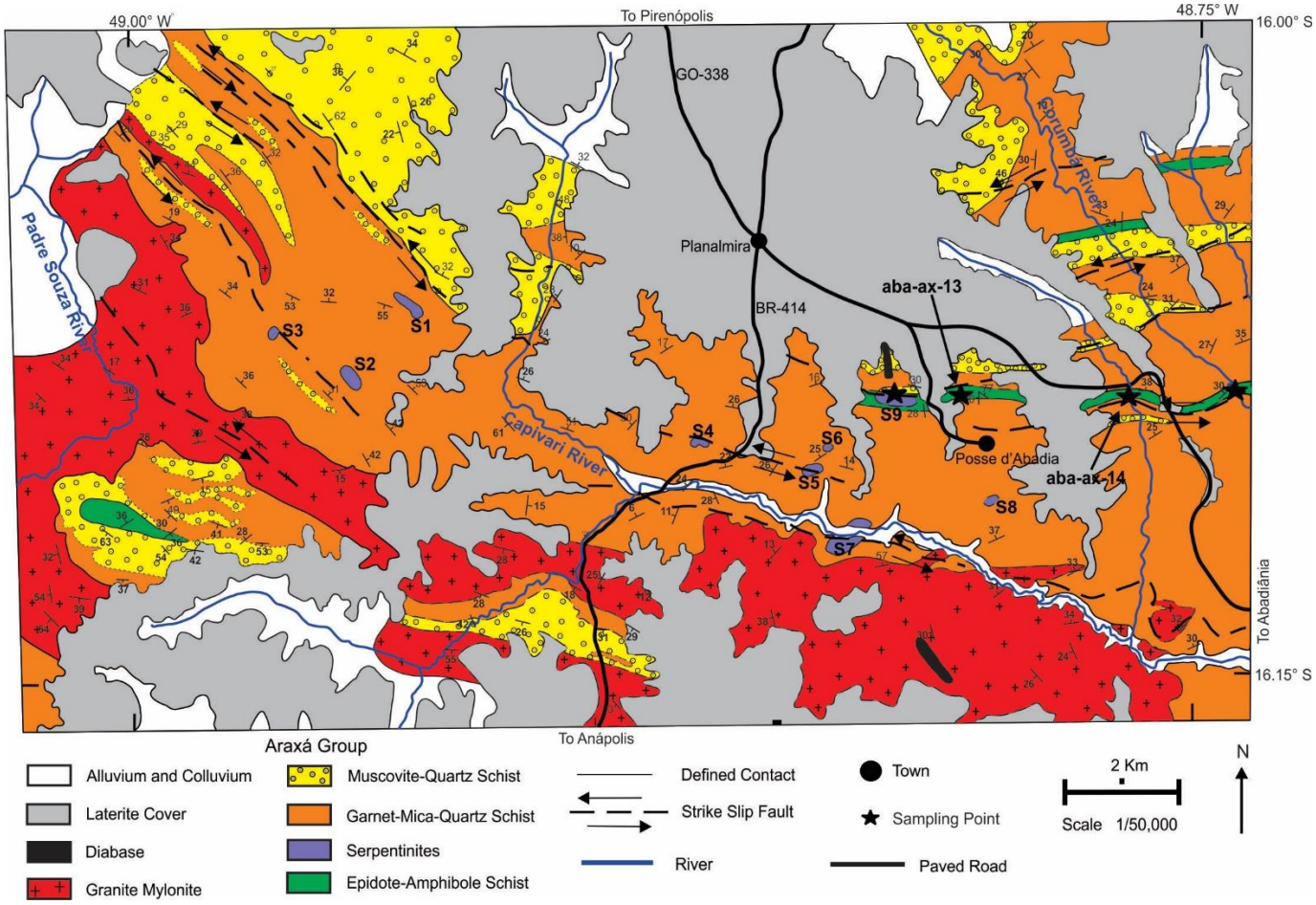

Figure 2.2. Geological map of the study area, showing the main components of the ophiolitic mélange in the area of Abadiânia (after Strieder, 1989). The main ophiolite components comprise four epidote-amphibole schist bodies (green) and nine ultramafic bodies denoted S1, S2 …S9. Ultramafic body S9 and its encompassing epidote-amphibole schist were targeted in this study.

There are four main metamafic bodies in the study area (Fig 2.2), which are dispersed in garnet-mica-quartz schist host rock. These metamafic rock assemblages are composed mainly of amphibole and epidote, and are referred to as epidote-amphibole schists, due to the varying amounts of amphibole and epidote, with end members containing mostly one or the other mineral.

The epidote-amphibole schists occur as elongate bodies that trend along the regional deformation of NW-EW direction. The geochemical signature of these rocks shows that they have Fe-enriched tholeiitic nature, which demonstrates a regional mid-ocean ridge tholeiitic or island-arc basalt affinity (Strieder and Nilson, 1992c). These results are similar to those of other metamafic rocks, which have been studied in other parts of the Araxá Group (Brod et al., 1992; Seer et al 2001). Some of the amphibole-epidote schist outcrops are associated to muscovite-plagioclase-quartz schist, which was considered by Strieder (1989) to be evidence of plagiogranite.

In the study area, Strieder (1989) mapped 9 ultramafic bodies, denoted S1, S2 … S9, included in the Araxá Group. They are small elongated bodies, composed of serpentinite, (Berbert et al., 1970; Strieder & Nilson, 1992a, c), and are concentrically zoned with talc and chlorite schist at the boundaries and serpentinite at the core (Mello & Berbert, 1969). The presence of podiform chromite has been confirmed from some of the ultramafic bodies (Berbert et al., 1970; Strieder & Nilson, 1992a, b). The highly aluminous nature of the chromite indicates that the serpentinites were formed from a residual harzburgite protolith (Strieder & Nilson, 1992 a, b). Metasomatism caused by serpentinization created a concentric border of talc and chlorite schist (black-wall alteration) with the surrounding host rock. Chlorite schist can be fine- to coarse-grained, has light to dark green color and may contain porphyroblasts of large euhedral magnetite crystals. Talc schist can be fine- to coarse-grained, white to greenish in color.

2.3. Methods

2.3.1 Sampling

A total of three field trips were taken and a total of 19 samples were collected (appendix 2.1). Attention was given to the large amphibole-epidote schist body (Fig 2.2), which encompasses ultramafic body S9. The epidote-amphibole schist strikes east-west and is about 12 km long and about 500 m wide. Sampling revealed a large black-wall along the border between ultramafic body S9 and the encompassing epidote-amphibole schist, indicating metasomatic processes that took place along the contact of these two rock units. Body S9 consists of a serpentinite core, with outcrops of the black-wall in the form of massive chlorite schist on the western and southern borders, and the presence of talc-actinolite schist on the western border. The black-wall is continuous on the eastern side of S9, where it makes contact with an outcrop of amphibole-epidote schist; unfortunately, the structure has been dismembered by the creation of a small reservoir. Twelve samples were collected from ultramafic body S9, four of serpentinite, seven from the metasomatic alteration zone, and one sample of epidote-amphibole schist (Fig 2.2). Systematic sampling of the main epidote-amphibole schist body exposed along the Corumbá River revealed a variety of well-preserved rocks and their contacts. Five samples were collected from outcrops in the Corumbá River, three samples of epidote-amphibole schist and two samples of muscovite-quartz schist. Two more samples of epidote-amphibole schist were collected at different outcrops along the GO-338 road, in between ultramafic body S9 and the outcrops in the Corumbá River (Fig. 2.2). Figure 2.3 shows examples from the field of some of the collected samples.

2.3.2 Petrography

The type of rock and mineral identification was determined by thinsection analysis with a

Figure 2.3. A. Road cut exposing the contact between the metamafic (epidote-amphibole schist), and the outer zone of the metasomatic alteration zone of ultramafic body S9. B. chlorite schist from black-wall, with large porphyroblasts of magnetite. C. Chlorite schist, inter-grown with amphibole. D. Serpentinite block within the central region of body S9. E. Fresh epidote-amphibole schist (aba-ax-06) outcropping in the Corumbá river.

translucent optical microscope. In order to confirm the presence of different mineral assemblages, eight samples underwent X-ray diffraction analysis at the X-Ray Laboratory of the Geoscience Institute, Universidade de Brasília.

An investigation was also conducted on some selected samples with a FEI Quanta 450 scanning electron microscope, using backscatter electron imaging, working at 20 – 25 kV, at Universidade de Brasília. Electron diffraction spectrometry (EDS) was conducted with an Ametek model APOLLO X EDAX detector with TEAM software, in order to identify trace minerals and image and confirm the presence of zircon grains in the samples.

2.3.3 Geochemistry

Six amphibole-epidote schist samples (aba-12, aba-ax-06, aba-ax-10, aba-ax-13, aba-ax-14 and aba-ax-15) were selected for geochemical analysis. Samples were pulverized and sent to ASL Minerals in Goiânia, Goiás, for processing. Major elements were determined by X-ray fluorescence after glass disks were made with the samples by means of lithium borate fusion. Trace and rare earth elements were determined by ICP-MS/ ICP-AES, after preparation by acid digestion.

2.3.4 U-Pb (LA-ICPMS)

Eight samples were selected for U-Pb LA-ICPMS analysis in zircon grains: one epidote-amphibole schist (aba-ax-06), 5 samples from the black-wall (aba-06, aba-08, aba-11, S9A and S9B) and two metasedimentary rock samples (aba-ax-07 and aba-ax-08). In order to extract zircon grains, samples were first processed in a rock crusher, producing chips roughly 3–5 cm in size. Samples were then processed in a Selfrag high voltage laboratory equipment, with a voltage

of 130 kV and a frequency of 3 Hz. Zircon grains were concentrated using a pan to separate the heavy mineral fraction and a Franz was then used to remove the magnetic fraction. Zircon grains were handpicked using a binocular microscope. Grains were mounted in epoxy mounts and polished to create a smooth surface. HNO_3 (ca. 2%) was used to clean the surface of the mounts. Backscatter electron images of the zircon grains were taken with a FEI-Quanta 450 scanning electron microscope, working at 20 – 25 kV, at the University of Brasília, in order to characterize grain zonation.

All zircon grain analyses followed the analytical procedure described by Bühn et al. (2009) and were conducted at the Geochronology Laboratory at the University of Brasília. U-Pb La-ICP-MS analyses were conducted on a Thermo Finnigan Neptune MC-ICP-MS, coupled with a New Wave UP213 Nd: YAG laser ($\lambda = 213$ nm). Measurements consisted of point analyses. The U-Pb analyses on zircon grains were carried out using the standard-sample bracketing method (Albarède et al., 2004), using the GJ-1 standard zircon (Jackson et al., 2004) as the primary standard, for mass bias and drift correction.

The tuned masses were ^{238}U, ^{207}Pb, ^{206}Pb, ^{204}Pb and ^{202}Hg. The integration time was 1 second and the ablation time was 40 seconds for all isotopes. A 30 µm spot size was used and the laser setting had an energy of 4-5 mJ/cm^2 and a frequency of 10 Hz. Two to four unknown grains were analyzed between GJ-1 analyses. $^{206}Pb/^{207}Pb$ and $^{206}Pb/^{238}U$ ratios were time corrected. On smaller grains of zircon (~50 µm), single-spot laser-induced fractionation of the $^{206}Pb/^{238}U$ ratio was corrected using the linear regression method (Kosler et al., 2002). Results were checked against an unknown reference material, which during these analyses was zircon standard 91500 (Wiedenbecket al. 1995, 2004), with an average age value of 1068±18 (MSWD

= 0.95). Raw data were processed using an Excel sheet with the aid of "Chronus" software (Oliveira, 2015). Zircon ages were calculated using ISOPLOT v.3 (Ludwig, 2003), with isotopic ratio errors presented at the 1σ level.

2.3.5 Lu-Hf

The Lu-Hf isotope method on single zircon grains is compared to results attained on crystals previously analyzed by the U-Pb method. Seven samples were selected for the analysis: one epidote-amphibole schist (aba-ax-06), four samples from the black-wall (aba-08, aba-11, S9A and S9B) and two metasedimentary rock samples (aba-ax-07 and aba-ax-08). A Thermo Finnigan Neptune MC-ICP-MS was utilized for these analyses, conducted at the Geochronology Laboratory at the University of Brasília, using the method described by Matteini et al. (2010). The laser ablation analyses were conducted using a New Wave UP213 Nd: YAG laser (λ = 213 nm), utilizing a spot of 40 μm and a frequency of 10 Hz. The measured spots were analyzed in areas of the same age of individual zircon grains.

The Hf values are calculated using the decay constant $\lambda = 1.865 \times 10^{-11}$, proposed by Scherer et al. (2001). The values of $^{176}Lu/^{177}Hf = 0.0384$ and $^{176}Hf/^{177}Hf = 0.282772$ were used for the depleted mantle (Chauvel and Blichert-Toft, 2001), and $^{176}Lu/^{177}Hf = 0.0113$ for average crust (Taylor and McLennan, 1985; Wedepohl, 1995). Before analyzing the zircon grains, the mass spectrometer is calibrated using a solution made from the SRM reference material JMC475. During analyses various measurements of the GJ-1 zircon standard were conducted.

2.3.6 Sm-Nd

A total of 16 samples were analyzed by whole rock Sm-Nd isotopic analysis: six epidote-amphibole schists (aba-12, aba-ax-06, aba-ax-10, aba-ax-13, aba-ax-14 and aba-ax-15), two serpentinites (aba-07 and aba-10), six samples of black-wall (aba-01, aba-05, aba-06, aba-08, aba-11 and S9A) and two metasedimentary rock samples (aba-ax-07 and aba-ax-08). Sm-Nd analyses were conducted at the Geochronology Laboratory at the University of Brasília, using the method described by Gioia & Pimentel (2000). Preparation for the Sm-Nd method analyses begins with whole rock samples being pulverized in a shatter box. 50 mg of sample were mixed with a $^{149}Sm/^{150}Nd$ spike solution and dissolved in Savillex capsules. Conventional cation exchange techniques were used to separate Sm and Nd from whole rock samples. Samples were evaporated onto Re filaments. Analyses were conducted on a Finnigan TRITON multi-collector mass spectrometer running in static mode. Uncertainties for the Sm/Nd and $^{143}Sm/^{144}Nd$ ratios are better than ±0.5% (2σ) and ±0.005% (2σ), respectively, and were based upon repeated analyses of international rock standards BHVO-2, with $^{147}Sm/^{144}Nd=0.1491$ and $^{143}Nd/^{144}Nd = 0.512993 \pm 0.000006$. $^{143}Sm/^{144}Nd$ ratios were normalized to $^{146}Nd/^{144}Nd$ ratio of 0.7219 and the decay constant of 6.54×10^{12} was used. The T_{DM} model values were calculated using the method described by DePaolo (1981).

2.4 Results

2.4.1 Petrography

2.4.1.1 Epidote-Amphibole Schists

Six samples of epidote-amphibole schist were collected from the study area (aba-12, aba-ax-06, aba-ax-10, aba-ax-13, aba-ax-14 and aba-ax-15). The generic term "epidote-amphibole schist" is used to describe rocks which were derived from a protolith of mafic composition, and the mineralogy is composed mainly of epidote and actinolite (more than 80%). Due to the low amount of albite in the samples (ca.5%), the protolith of these samples is most likely a tholeiitic basalt.

Granular epidote and coarse-grained actinolite have a nematoblastic to granoblastic texture and form milimetric banding in this rock, which alternates with bands of mostly quartz and some albite. Some samples are fine-grained and were more affected by regional deformation causing the rocks to be crenulated, folded and subject to recrystallization in the form of mylonite epidote schist.

The presence of chlorite, quartz and epidote indicates metamorphism at greenschist facies conditions. Evidence of metamorphism is also supported by injected and folded quartz and calcite veins in some of the samples, along with rotated amphibole porphyroblasts displaying epidote and quartz inclusions. Figures 2.4A, B show thin section images, which best represent the epidote-amphibole schists within the study area.

2.4.1.2 Serpentinites

The serpentinites occur in the form of less than 1 km long elongate bodies, and their location is controlled by regional structures. The serpentinite at Abadiânia was collected from the interior of ultramafic body S9 and is represented by four samples (aba-04, aba-07, aba-09 and aba-10). All primary minerals are completely serpentinized, with pseudomorphs of olivine and

pyroxene remaining, suggesting a dunite to harzburgite protolith for these rocks. The most common texture is very fine-grained texture, referred to as bladed-mat after Maltman (1978). The other common form found in the samples is ribbon-type serpentine (Maltman, 1978), which has

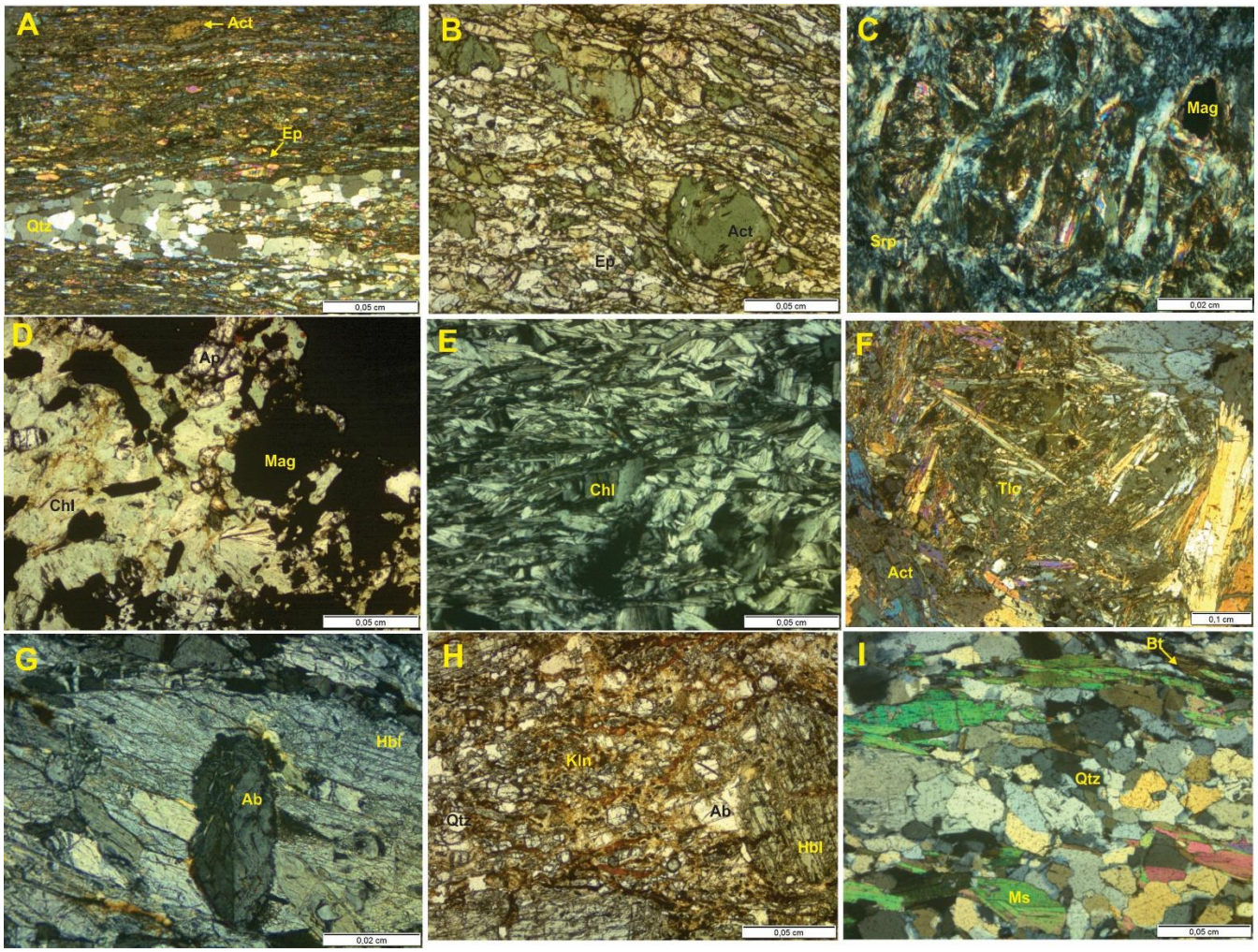

Figure 2.4. A. Sample of epidote-amphibole schist (aba-ax-06), showing a fine-grained matrix of actinolite and a quartz vein, probably introduced during later metamorphism. B. Epidote-amphibole schist, with large actinolite porphyroblasts, dispersed in a matrix of smaller epidote and actinolite grains (aba-12). C. Typical serpentinite sample, showing fine-grained cross bladed mat texture, with olivine pseudomorphs and magnetite grains (aba-07). D. Black wall sample (aba-01), showing grains of apatite and magnetite in a matrix of chlorite. E . Chlorite grains showing a penetrative texture and some oriented mineral platelets (aba-ax-05). F. Actinolite-talc schist, with large grains of actinolite in a talc matrix (aba-06). G. Large albite crystal intergrown with hornblende (aba-11). H Grains of albite and hornblende undergoing alteration, with some quartz in a matrix of kaolinite (aba-11). I. Muscovite-quartz schist, defined by bands of quartz and muscovite, and some biotite. Ab-albite, Act-actinolite, Bt-biotite, Chl-chlorite, Ep-Epidote, Hbl-hornblend, Kln-kaolinite, Ms-Muscovite, Qtz-quartz, Srp-serpentinte, Tlc-talc.

the form of long blades of antigorite. Magnetite occurs as nodules and aggregate bands within serpentine layers, and is associated as stringers, which are oriented along foliation. Carbonate and talc were also observed to truncate the serpentine and demonstrate corrosion borders along the schistosity, which could indicate the circulation of fluids related to metasomatism. Figure 2.4C, shows a typical example of serpentinite from the study area.

2.4.1.3 Black-wall

The metasomatic alteration zone of ultramafic body S9 is a zone of about 50 meters composed of chlorite, chlorite + magnetite and chlorite + magnetite + amphibole. This zone is interpreted as a metasomatic black-wall sequence, which has been well documented in ophiolite sequences around the world (Coleman, 1967; Frost 1975; Dubińska et al., 1999; Arena et al., 2017). Seven samples were collected from the black-wall of ultramafic body S9: aba-01, aba-05, aba-06, aba-08, aba-11, S9A and S9B. X-ray diffraction was conducted on a few selected samples (aba-01, aba-06, aba-11, S9A and S9B), in order to complement petrographic analysis and help with mineral identification. The majority of the rock samples (aba-01, aba-05, aba-08, S9A and S9B) are chlorite schists, with clinochlore being the main type of chlorite in the rocks. The chlorite schist presents penetrative lepidoblastic texture, with oriented mineral platelets (Fig 2.4E). Some chlorite crystals are interlacing, demonstrating chlorite recrystallization. The chlorite schists are composed of 50% to 90% chlorite. Magnetite is a common phase in this sequence; magnetite crystals are porphyroblastic, commonly containing inclusions of chlorite (Fig 2.4D). Magnetite sometimes is associated with regional banding, in between chlorite layers. Porphyroblastic apatite

grains were observed in two samples of chlorite schist (aba-01 and aba-08), and are also observed in chlorite schists from the black-wall in southern Brazil (Arena et al., 2017). One sample of chlorite schist (S9A) contains diablastic crystals of amphibole, identified as magnesiohornblende by X-ray diffraction, within a chlorite matrix. This sample does not contain magnetite, indicating a change in the mineral phases of the chlorite schist, probably related to fluid composition during the metasomatic process.

Sample aba-06 is composed mainly of diablastic crystals of actinolite, with some endoblastic talc crystals (Fig 2.4F). Chlorite is also present in this sample, formed by alteration.

Sample aba-11, collected at the contact with the epidote-amphibole schist, is considered as a metarodingite, in the sense of Frost (1975). It is the transition zone between the black-wall and the metamafic epidote-amphibole schist. This sample is composed of diablastic to poikiloblastic crystals of albite and magnesiohornblende, with some endoblastic crystals of quartz. This sample also has a brecciated texture, which could indicate the circulation of fluids during metasomatism. There are also alteration minerals present in the sample, including kaolinite, goethite and saponite. These minerals represent secondary alteration of primary minerals in the sample, which probably took place after the main metasomatic event. Sample aba-11 is referred to here as an albite-hornblende fels, but may be interpreted as some form of metarodingite. Figures 2.4G, H show characteristic examples from the black-wall.

SEM analysis was conducted on black-wall samples aba-01, aba-08, S9A and S9B, in order to determine the presence and association of zircon crystals in the black-wall rocks. This is important to determine if the present zircon crystals are related to the metasomatic mineral assemblages or if they were incorporated from another source. If zircon grains are related to the

metasomatic mineral assemblage, then they probably formed together, meaning that an acquired age collected from these samples would represent the age of metasomatism and of the formation of the black-wall.

Large to small zircon crystals can be found within chlorite crystal boundaries or within magnetite in samples aba-01, aba-08 and S9A (Fig. 2.5A, B, D). Some smaller zircon crystals can also be observed forming small clusters along chlorite grain boundaries. Irregular shaped grains of monazite and xenotime were also observed along chlorite grain boundaries in samples aba-01 and aba-08, which may indicate some of the fluids during metasomatism were rich in REEs. In sample S9B, zircon grains are also associated with a titanium oxide, as determined by EDS (Fig 2.5C), which may be amorphous since no titanium related minerals were detected by X-ray diffraction in this sample. This oxide looks brownish to opaque in translucent light, but shows a network structure in back scattered images.

A zircon crystal was observed in sample S9B, which appeared to contain chlorite inclusions, hosted within a magnetite porphyroblast. EDS mapping indicates that the zircon inclusions and the chlorite ground mass have similar intensities of Mg and Al, while Fe and Zr are restricted almost exclusively to the magnetite and zircon crystals, respectively. These results demonstrate that the inclusions and the groundmass are similar in composition and that the inclusions maybe crystals of chlorite (Fig. 2.6). This would signify that chlorite and zircon were in equilibrium and indicates that the zircon and chlorite in the black-wall formed during the same metasomatic event.

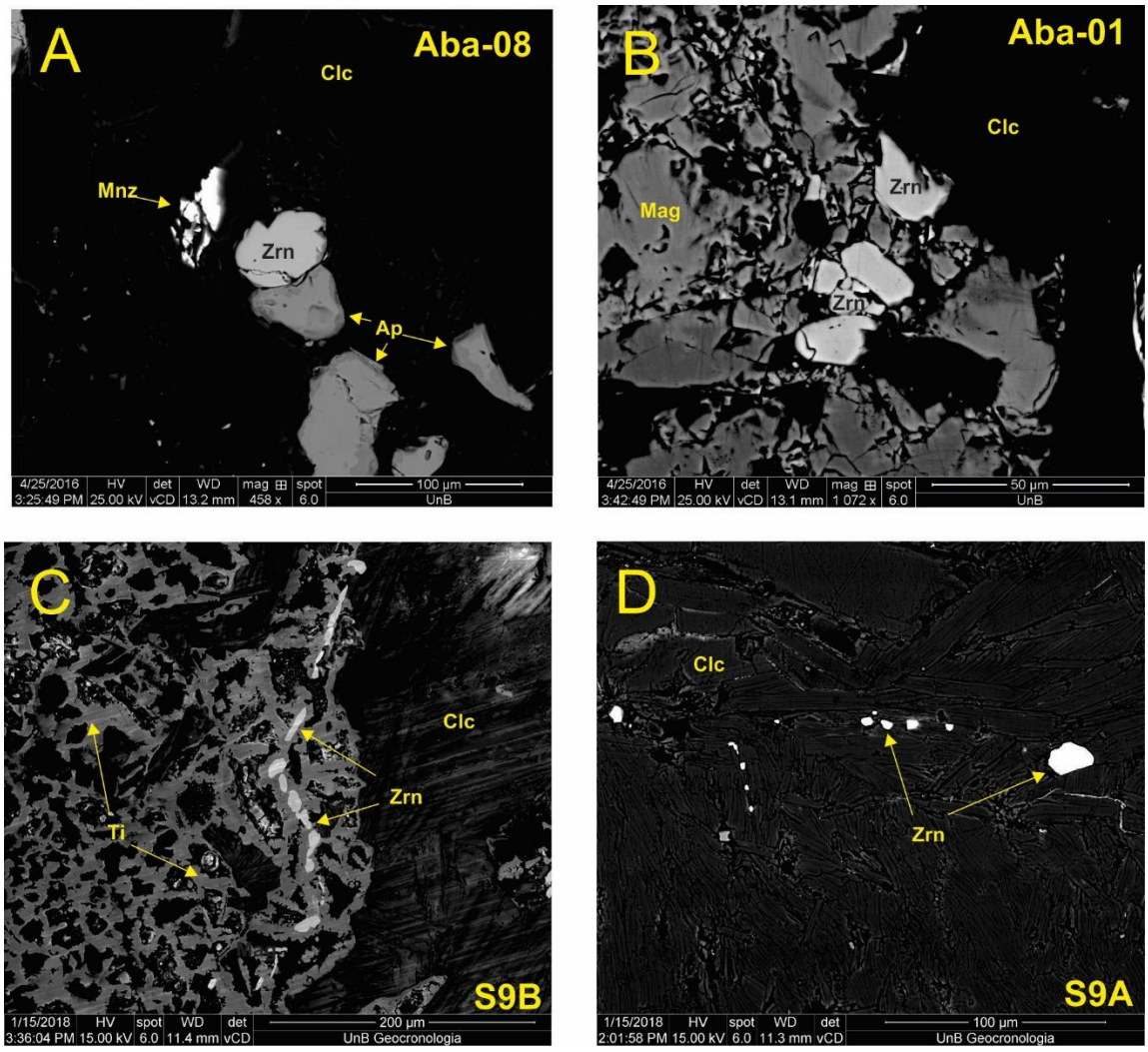

Figure 2.5. Electron backscatter images of A. Zircon, monazite and apatite grains in sample aba-08. B. Group of zircon grains associated with a magnetite grain in sample aba-01. C. Trail of zircon grains, which formed within an amorphous titanium oxide in sample S9B. D. Zircon grains which formed along chlorite grain boundaries, sample S9A. Ap-apatite, Chl-chlorite, Mag-magnetite, Mz-monazite, Ti-amorphous titanium, Zrn-zircon.

2.4.1.4 Muscovite-Quartz Schist

The mafic and ultramafic bodies present in the ophiolitic mélange are hosted in metasedimentary rocks, which are composed of mica-quartz schist, with or without garnet (Strieder, 1989). The

contact between the epidote-amphibole schist and the hosting metasedimentary rocks is exposed in the Corumbá River. Two samples were collected from this area (aba-ax-07 and aba-ax-08) for comparison with the ophiolite assemblages. Aba-ax-07 was collected on the southeastern side of the epidote-amphibole schist outcrop, where the two rock units share a tectonic contact. This sample is composed mostly of muscovite and quartz and is referred to as muscovite-quartz schist. Some biotite is also present, but is undergoing alteration to chlorite. The schistosity is defined by the muscovite crystals, and there are alternating bands rich in quartz and muscovite + biotite (Fig 2.4H). Sample aba-ax-08 was collected from the western side of the outcrop, where it forms a thin strip on top of the epidote-amphibole schist. This sample is similar to aba-ax-07, composed mostly of muscovite and quartz, with the muscovite defining foliation. The sample has alternating quartz rich and muscovite + biotite rich bands.

2.4.2 Geochemistry

Geochemistry results are shown in appendix 2.2. The epidote-amphibole schist samples are representative of pieces of oceanic crust, however alteration transformed these rocks into epidote-amphibole schist and no primary minerals remain. Post-depositional tectonothermal events can modify the primary geochemical signatures of the studied rocks (Rosing et al., 1993; Gruau et al., 1996; Rose et al., 1996; Frei et al., 2002; Polat and Hofmann, 2003). In order to determine whether the studied samples underwent chemical alteration, criteria used by Polat and Hofmann (2003) were used.

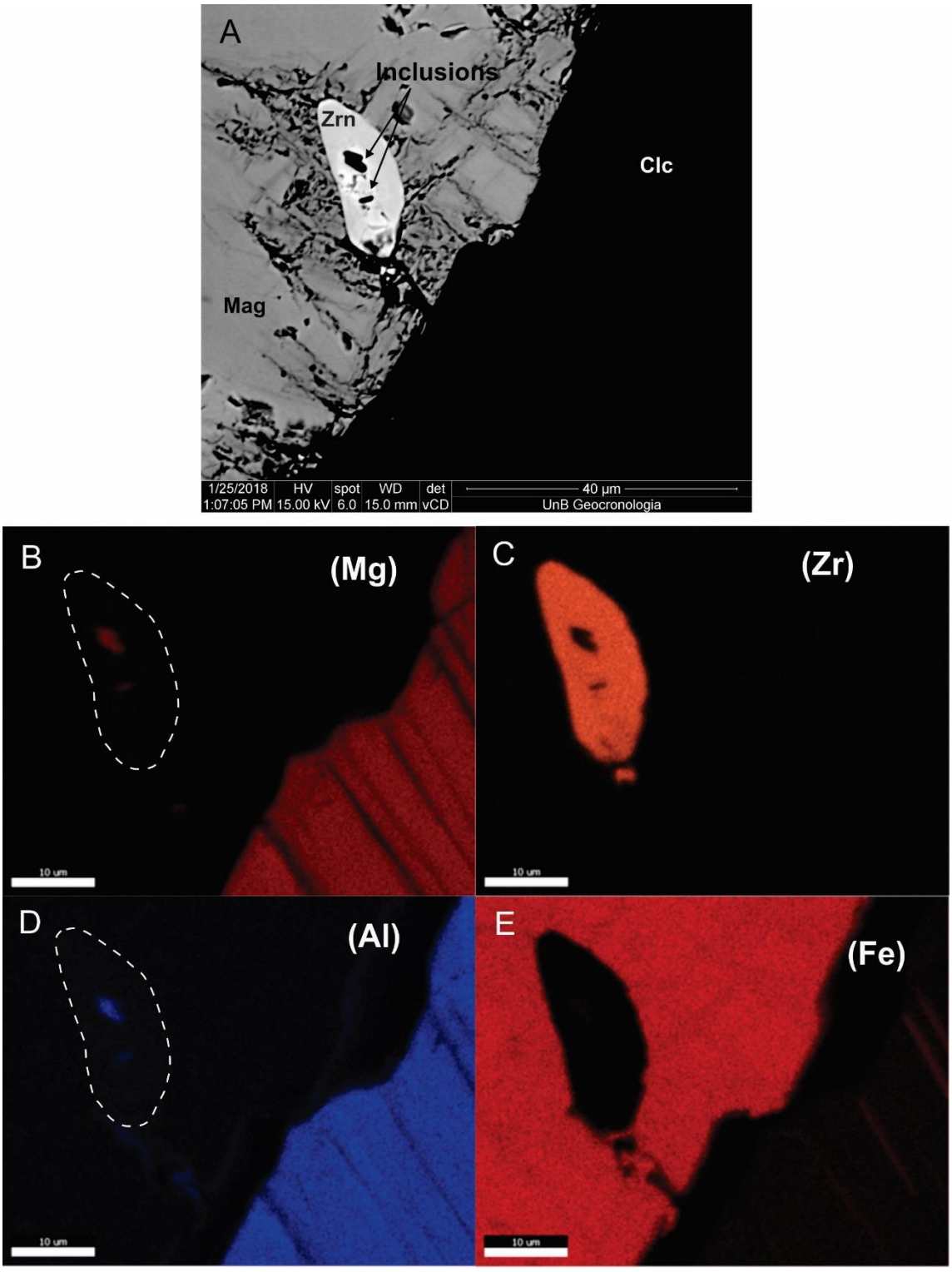

Figure 2.6. A. Electron backscatter image of zircon grain with inclusions that are probably of chlorite. B EDS map of imaged zircon grain, showing the distribution of Magnesium, C-Zirconium, D-Aluminum and E-Iron.

These include: (1) the existence of significant carbonate and silica (quartz) enrichment (>2%); (2) samples with high LOI (>6 wt.%) were considered as variably altered; (3) the degree of correlation with Zr, on binary diagrams; elements having a correlation coefficient (R) <0.75 were considered as mobile; and (4) the presence of large Ce anomalies on primitive mantle-normalized diagrams; samples possessing Ce/Ce∗ ratios greater than 1.1 and less than 0.9 were designated to be variably altered.

All the samples of epidote-amphibole schist display similar values of MgO (6.43 – 8.71 wt%), Al_2O_3 (14.20 – 16.85), CaO (1.05 – 1.85 wt%) and TiO_2 (0.78 – 1.10 wt%). Samples aba-12, aba-ax-06, aba-ax-10, aba-ax-13 and aba-ax-14 have similar chemical compositions, with SiO_2 (48.10 – 50.90 wt%), Fe_2O_3 (9.60 – 11.35 wt%), CaO (11.35 – 15.90 wt%) and all the samples have LOI values less than 6 wt%. Sample aba-ax-15 deviates from the other samples with SiO_2 value of 44.60 wt%, Fe_2O_3 value of 8.72 wt%, CaO of 15.90 wt% and LOI of 6.42wt%. This deviation of sample aba-ax-15 is caused by the presence of carbonate veins within the sample location. Si, Al, Na, Ca, Rb, K, Sr, Ba, Ca, Mn, Nb, and Sm do not correlate well with Zr. On the other hand, Ti, Y, LREE (minus Sm) and the HREE (minus Tm) show strong correlation with Zr (Fig. 2.7). The Ce/Ce∗ ratios for all the samples do not go beyond what is considered to be altered. These results indicate that these samples were not significantly affected by chemical alteration.

Chondrite-normalized REE concentrations are shown in figure 2.8A and have a curve similar to NMORB. Samples are slightly depleted in LREE (La/Sm_{CN} = 0.51 – 0.72) and HREE show slight negative to positive fractionation (Gd/Yb_{CN} = 0.91 – 1.17). Most samples exhibit a

small negative Eu anomaly (Eu/Eu* = 0.85 – 0.97). NMORB-normalized trace elements concentrations are shown in figure 2.8B. There is an increase in large-ion lithophile elements (LILE), with major peaks associated with Cs, Rb, and Ba. Two samples have elevated contents of Pb, while the other four are below the level of detection.

All samples plot within the tholeiitic basalt field of Irvine and Baragar (1971) (Fig 2.9A) When plotted on the Zr/Ti–Nb/Y diagram of Floyd and Winchester (1975), the samples demonstrate that the protoliths of the epidote-amphibole schists are basaltic in nature (Fig. 2.9B). When plotted on the Nb/Y–Th/Yb diagram of Pearce (2008), the samples have a cluster of three near the NMORB, while the other three samples have very low Th values and plot below and outside the range of oceanic basalts (Fig. 2.9C). The TiO_2/Yb–Nb/Yb diagram of Pearce (2008) shows that the magma of the basaltic protolith of the epidote-amphibole schists was created from mantle melting at shallow depth (Fig. 2.9D).

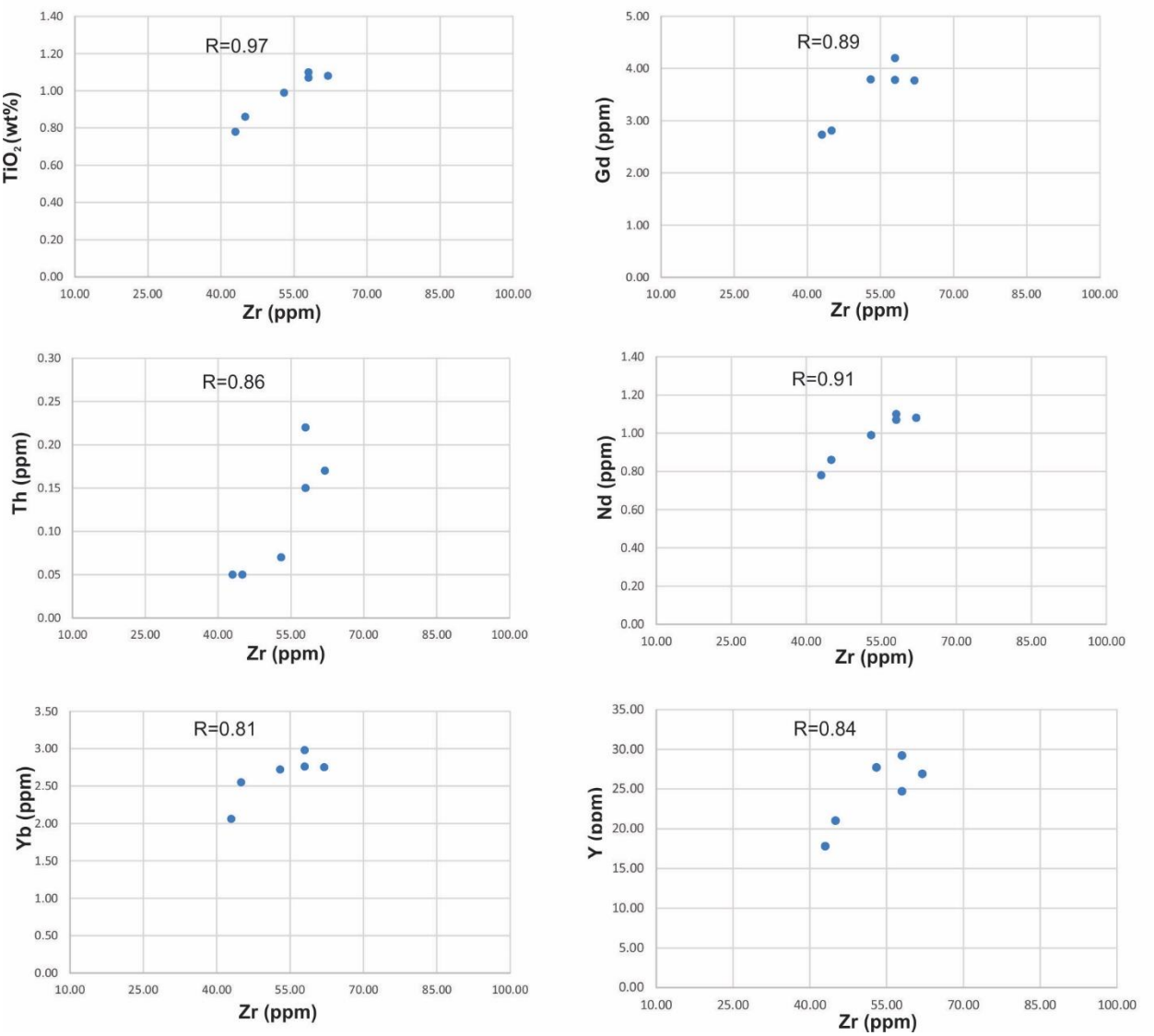

Figure 2.7. Zr vs. selected element variation diagrams. Various REE, Th and Ti have a strong correlation with Zr, indicating that they were not significantly disturbed during post metamorphic alteration. R: correlation coefficient.

2.4.3 U-Pb

Eight samples (aba-06, aba-08, aba-11, S9A, S9B, aba-ax-06, aba-ax-07 and aba-ax-08) were processed. 5 samples (aba-06, aba-08, aba-11, S9A, S9B) representing the black-wall, and two representing the metasedimentary rocks in contact with the epidote-amphibole schist in the

Corumbá River were also selected for U-Pb analysis. Results for all U-Pb analyses are shown in appendix 2.3.

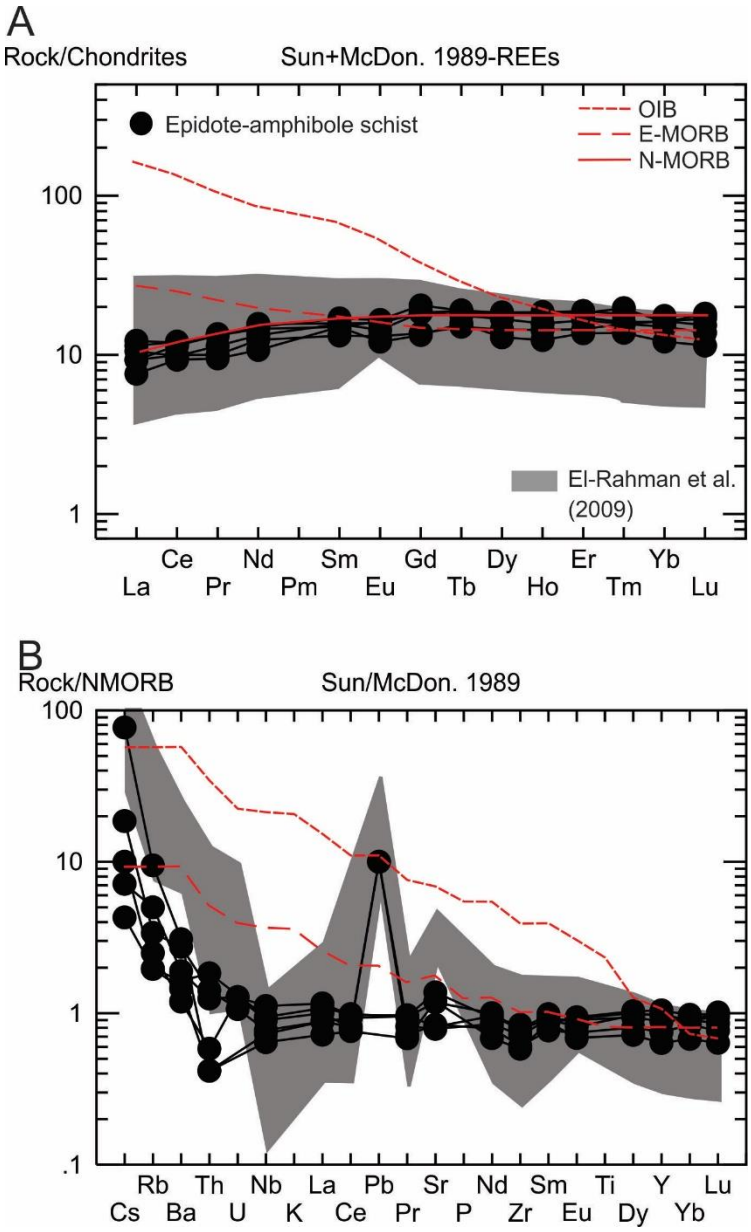

Figure 2.8. . A. Graph showing chondritic normalized REEs for samples of epidote-amphibole schists (black circles) compared to values of NMORB of Sun and McDonald (1989). B. Graph showing NMORB normalized trace element concentrations of epidote-amphibole schists, compared to EMORB and IAB. Values are from Sun and McDonald (1989). Shaded area is the range of gabbro values from the Wadi Ghadir ophiolite (El-Rahman et al., 2009).

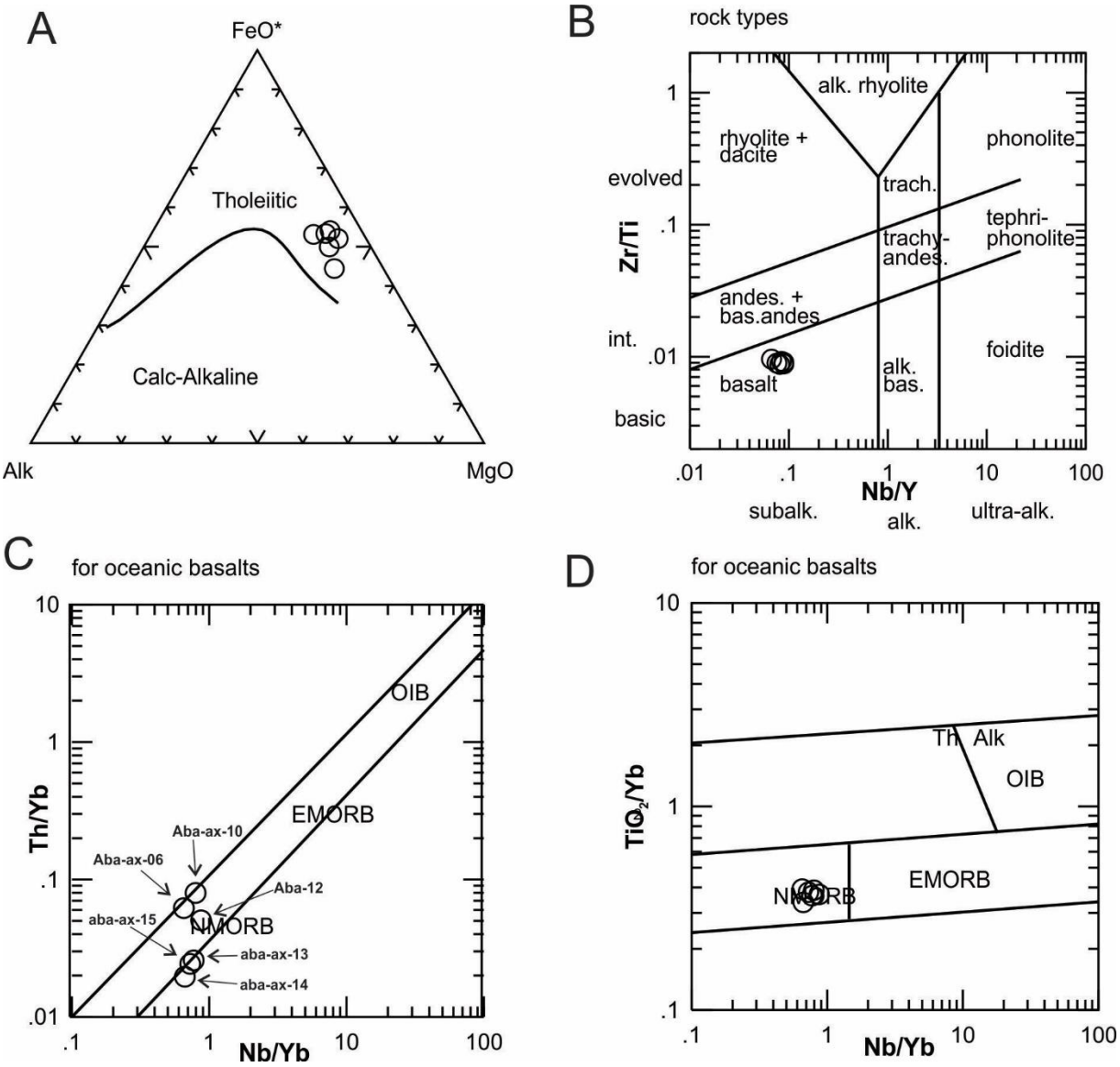

Figure 2.9. A. AMF diagram of Irvine and Baragar (1971) demonstrating the Tholeiitic affinity of the epidote-amphibole schists. Proxies for the epidote-amphibole schists (B: Zr/Ti–Nb/Y; C: Th/Yb–Nb/Yb; D: TiO2/Yb–Nb/Yb) for rock classification and tectonic setting. After Pearce (2008).

2.4.3.1 Epidote-Amphibole Schist

Of the six collected samples of epidote-amphibole schist, only sample aba-ax-06 yielded 31 zircon grains. Under a hand lens, the grains are euhedral to subhedral, transparent, with some

grains showing a brownish heu. When viewed by electron backscatter imaging, some grains have a faint magmatic zoning, while others are fractured and have metamorphic borders. Some grains were observed to have a porous metamorphic texture as described by Hay and Dempster (2009), which may demonstrate that the grains underwent metamorphism at greenschist facies. This same texture can also be caused by metasomatism (Pelleter et al., 2007) (fig. 2.10). 11 zircon grains yielded a Discordia with a lower intercept of 225±250 Ma and an upper intercept of 800±14 Ma (MSWD=1.4), while the remainder of the grains have Mesoproterozoic and older ages. The upper intercept age of 800±14 Ma is considered to be the crystallization age of the epidote-amphibole schist protolith, while the older populations of zircon grains are interpreted as inherited.

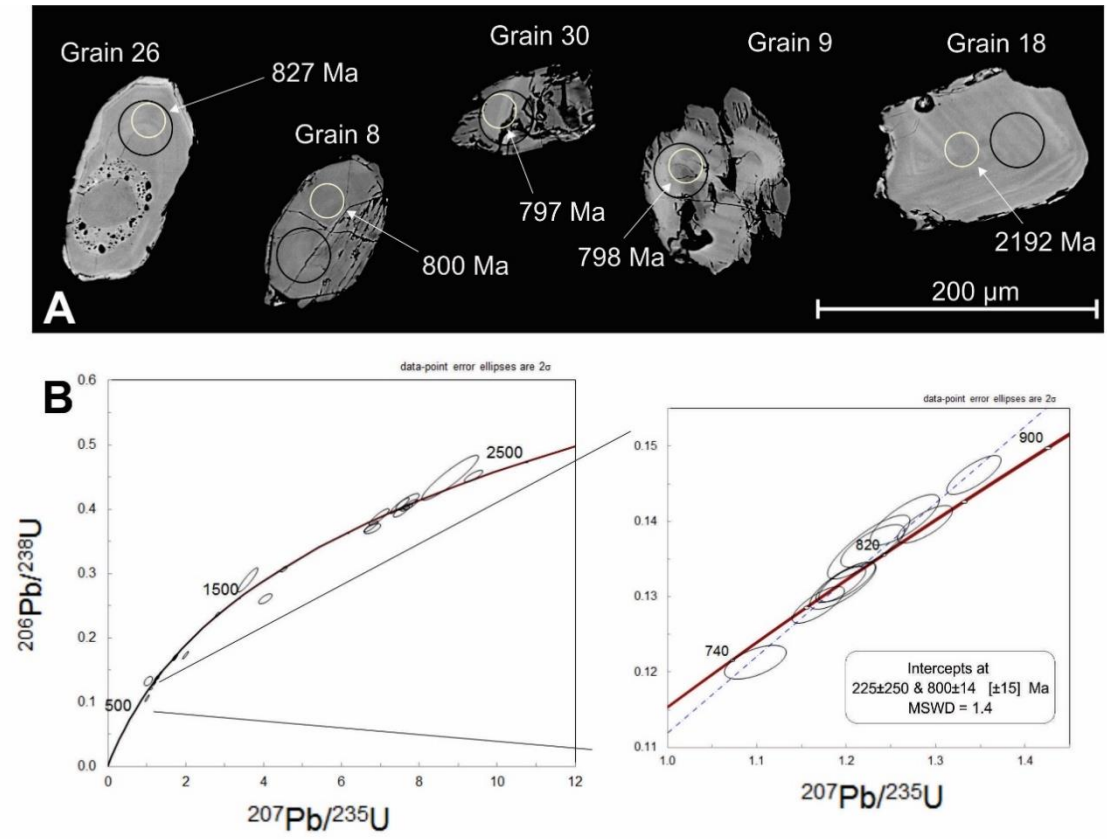

Figure 2.10. A. Image showing examples of zircon grains taken from epidote-amphibole schist aba-ax-06; white circles indicate the spot area for U/Pb analysis with the measured age for each spot. Black circles represent the location of the Lu/Hf. B. Results of U/Pb analysis and calculated Discordia graph for sample aba-ax-06.

2.4.3.2 Black-wall

2.4.3.2.1 S9A

57 zircon grains were analyzed in this sample. Grains are transparent, subhedral and vary from 50 µm to more than 200 µm. Backscattered imaging shows that the grains have a faint magmatic zonation or none at all. Some grains are fractured, while others have a porous texture with small inclusions of xenotime, similar to those described by Hay and Dempster (2009) and Pelleter et al. (2007) (Fig. 2.11 A). 36 zircon grains yielded concordant ages ranging from 790 to

745 Ma. Two average concordia ages were calculated for this sample, at 775.9±2.3 Ma (MSWD = 1.7, N = 28) and 756.7±4.7 Ma (MSWD=1.1, N=8) (Fig 2.12 A).

2.4.3.2.2 S9B

70 zircon grains were analyzed from sample S9B. Grains vary in size, from 50 µm to more than 100 µm, and are subhedral. Backscattered analysis of the grains revealed some faint magmatic zoning and alteration borders. This sample also exhibits some zircon grains with fractured or porous texture and the presence of inclusions (Fig. 2.11B). 49 grains yielded concordant ages, which have a range of ages spanning 816 to 750 Ma. Three average concordia ages, 763.4±7.5 Ma (MSWD=6.8, N=8), 780.5±8.3 Ma (MSWD=4.5, N=3) and 793.3±4.6 Ma (MSWD=1.7, N=17) were obtained (Fig 2.12 B).

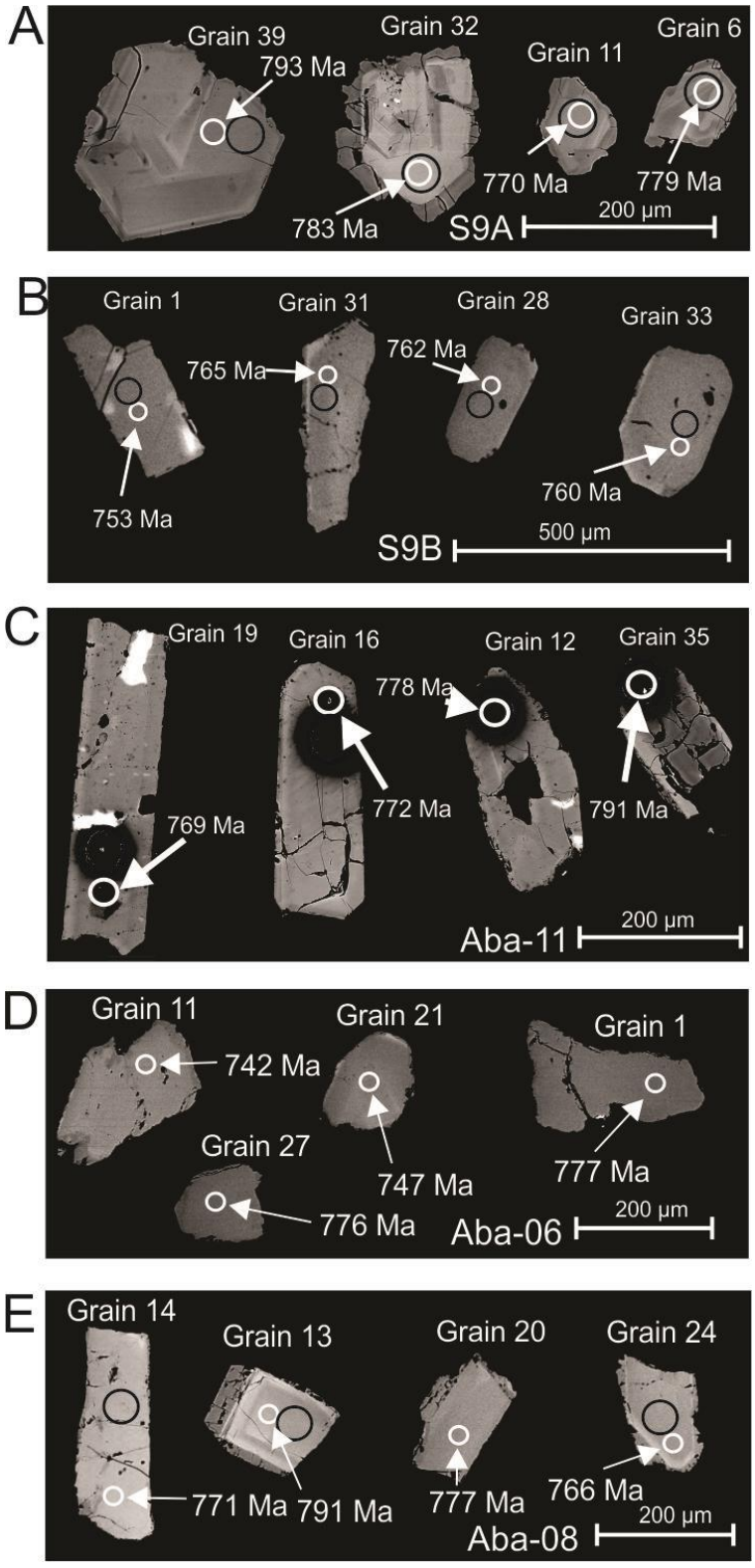

Figure 2.11. Examples of zircon grains in electron backscatter images for samples from the black-wall: A. Sample S9B, B. S9A, C. aba-11, D. aba-06, E. aba-08.

2.4.3.2.3 Aba-011

38 zircon grains were analyzed from sample Aba-011. The grains are subhedral and vary from 50 µm to more than 100 µm in size. Some grains have magmatic zonation, while other grains have homogeneous interiors, with faint borders (Fig. 2.11C). Thirteen grains yielded

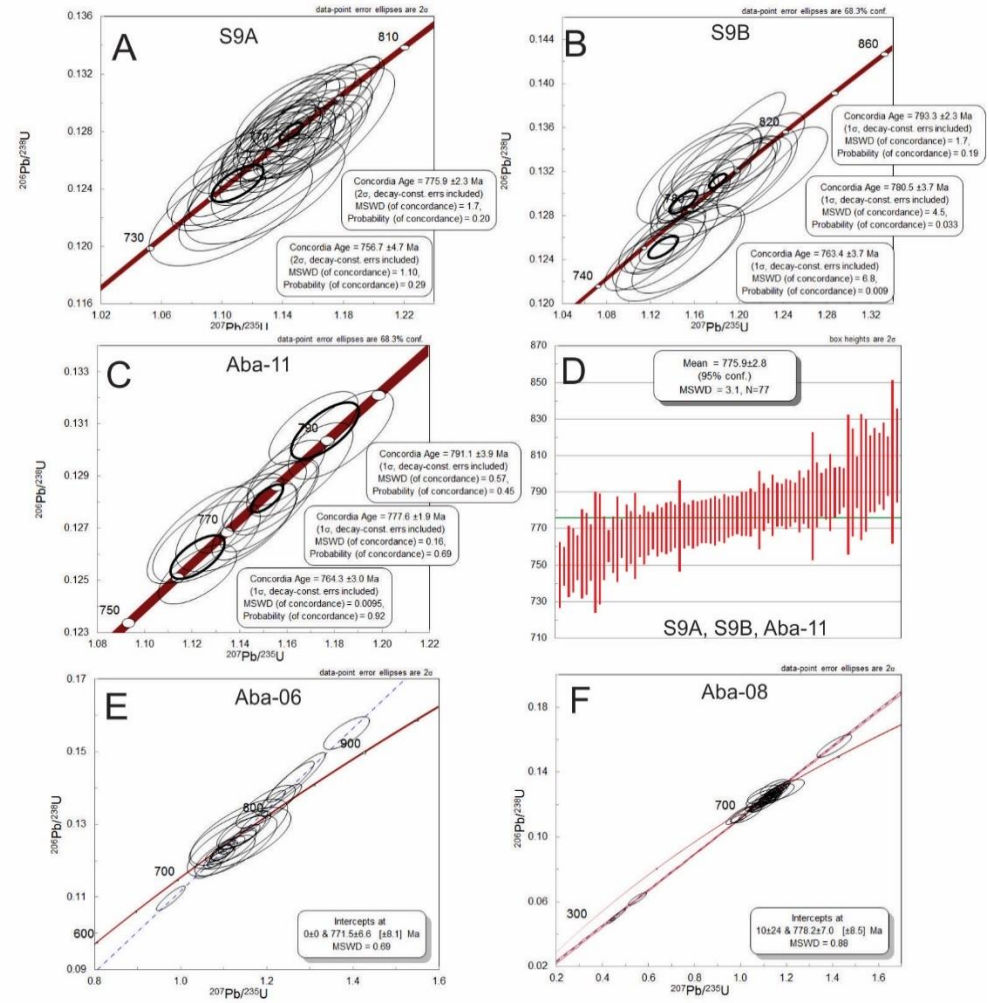

Figure 2.12. Concordia diagrams for samples A. S9A; B. S9B: C. aba-11. D Weighted mean ages of zircon grains from samples S9A, S9B and aba-11, showing the average age from the three samples. Discordia diagrams for samples E. sample aba-06, F. aba-08.

concordant ages, ranging from 793 to 761 Ma, with three average concordia ages of 791.1±7.8 Ma (MSWD=0.57, N=2), 777.6±3.9 Ma (MSWD=0.16, N=8) and 764.3±6.1 Ma (MSWD=0.0095, N=3) (Fig 2.12 C).

2.4.3.2.4 Aba-06

This sample had 45 zircon grains recovered. Grains are subhedral and have a clear to yellowish color. Grains range in size from 50 µm to more than 100 µm. Backscattered images show magmatic zonation in some grains, to a more homogeneous interior. Some of the grains are fractured while a few have a porous appearance with micro-inclusions (Fig. 2.11 D). 26 zircon grains yielded a discordia age of 771.5±6.6 Ma (MSWD=0.69, N=26), calculated from analyzed zircon grains (Fig. 2.12 E).

2.4.3.2.5 Aba-08

54 zircon grains were recovered from this sample. Grains are clear to yellowish in color, prismatic to subhedral and have faint magmatic zoning, with metamorphic rims. Some grains are fractured, and have a porous metamorphic texture. Grains range in size from 50 µm to more than 100 µm (Fig. 2.11 E). 37 zircon grains yielded a discordia age with an upper intercept of 778.2±7 Ma (MSWD=0.88, N=37), which is considered to be the age of crystallization of this sample (Fig. 2.12 F).

2.4.3.3 Metasedimentary rocks

2.4.3.3.1 Aba-ax-07

57 grains were analyzed. The majority of the grains are euhedral to subhedral, while a few of the grains are anhedral. Grains show magmatic zonation, and several of them are fractured (Fig. 2.13 A). A graph of the population density reveals that the majority, ca. 84%, of the grains are Neoproterozoic in age, with the main peaks at 790 and 886.5 Ma (Fig. 2.13 C, D). There is another, smaller population of zircon grains of Mesoproterozoic age and older.

2.4.3.3.2 Aba-ax-08

60 grains were analyzed. Zircon grains from this sample are similar to those of aba-ax-07. Grains are euhedral to subhedral and have magmatic zonation. Several grains are also fractured and a few grains have porous texture (Fig 2.13B). 43 zircon grains were used to make a population density graph, which shows that the majority, 81%, of the grains are Neoproterozoic in age, with the principal peak at 795.6 Ma (Fig. 2.13 E and F). This sample also contains a small population of zircon grains of Mesoproterozoic age and older.

2.4.4 Lu-Hf

Lu-Hf analyses were conducted on selected zircon grains from 7 samples. Results are shown in appendix 2.4. Samples aba-08, aba-11, S9A and S9B all have very positive ε_{Hf} (+9.16 to +23.98) with T_{DM} model ages of 0.96–0.34 Ga. The positive ε_{Hf} (t) values obtained in this study indicate that these zircon populations have a highly depleted Hf isotopic composition,

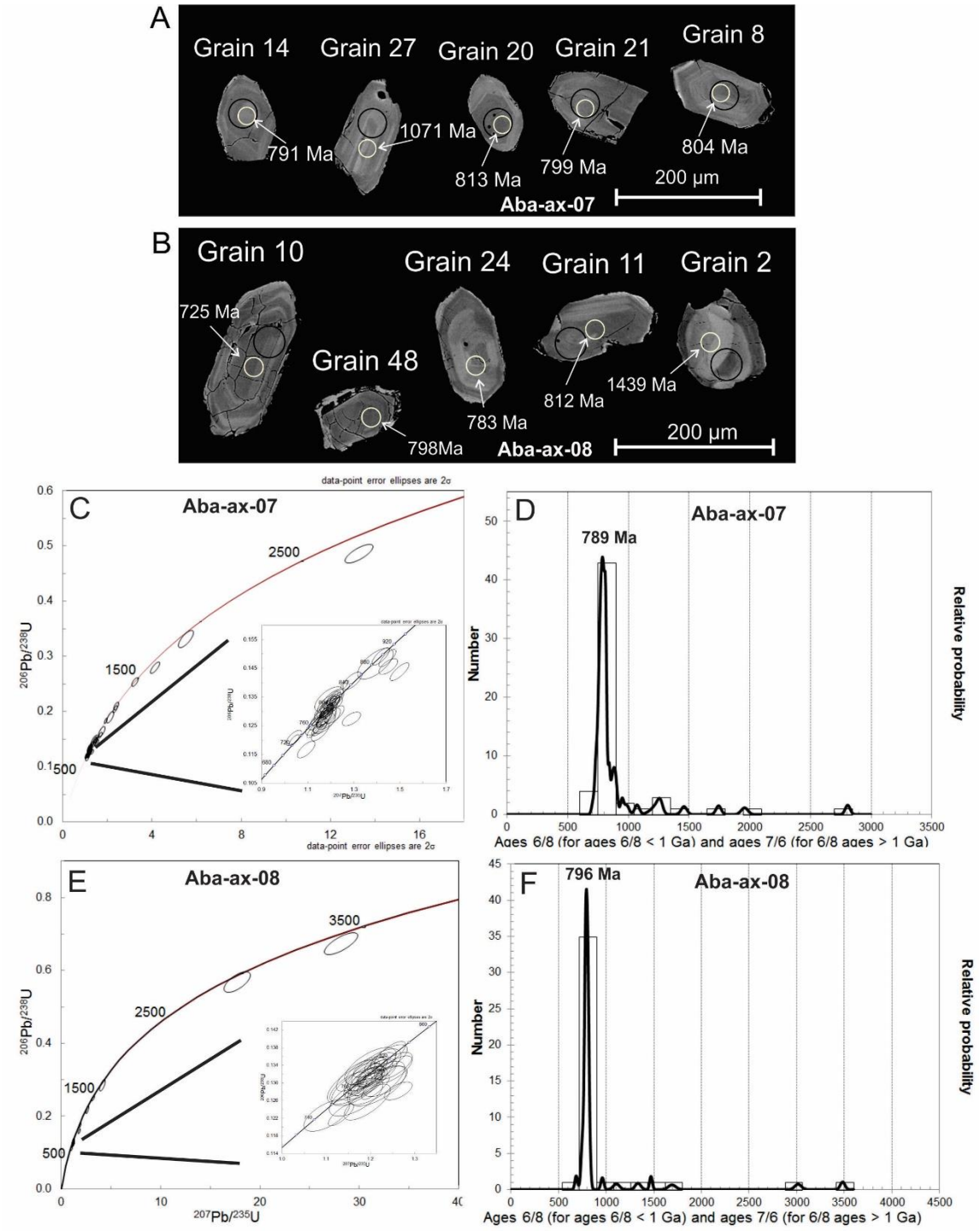

Figure 2.13. Electron backscatter images of zircon grains from samples A. aba-ax-07; B. aba-ax-08. C. Concordia diagram for sample aba-ax-07, inset shows youngest population. D. Probability density plot showing the distribution of the different zircon populations in sample aba-ax-07. E. Concordia diagram for sample Aba-ax-07, inset shows youngest population. F. Probability density plot showing the distribution of the different zircon populations in sample aba-ax-08.

similar to results obtained by Liu et al. (2016). Sample aba-ax-06 has a spread of ε_{Hf} values ranging from -21.67 to +13.66, with T_{DM} ages between 4.22 and 0.80 Ga. Samples aba-ax-07 and 08 have similar values, with positive to negative ε_{Hf} ranging from -14.87 to +6.46 and T_{DM} ages of 1.9 and 1.47 Ga. Figure 2.14 shows the distribution of ε_{Hf} values versus their ages as determined by U-Pb analysis.

2.4.5 Sm-Nd

Six samples of epidote-amphibole schist, five samples from the black-wall, two serpentinites and two metasedimentary rocks underwent analysis for Sm/Nd. Results for Sm-Nd are shown in appendix 2.5. For ε_{Nd}, the value for (T) varied by rock type. Sample aba-ax-06 had the value of 800 Ma used for T, which led to ε_{Nd} (800) values ranging from +6.48 to +7.69. These values demonstrate a mantle signature, indicating the source of these rocks. The value of 756.7 Ma is used as T to determine the ε_{Nd} value for the chlorite schists and serpentinites, because it is the latest concordant age for all the black-wall related metasomatites in this study and should represent the last period of metamorphism affecting these rock assemblages and the serpentinite core of ultramafic body S9. The chlorite schists collected from around the serpentinite mass have ε_{Nd} (756.7) values ranging from +4.95 to +7.89, while the serpentinites have even more depleted values at +11.11 and +8.01. These values demonstrate a mantle signature, indicating that the chlorite schist formed from a protolith that had a very strong mantle component, while the serpentinite also demonstrated its mantle signature. The value 638 Ma was given to T to calculate ε_{Nd}, because this was the age of a tonalite, which Piuzana et al. (2003b) estimated to be the minimum age of deposition for the original sediments of the Araxá Group. The distribution

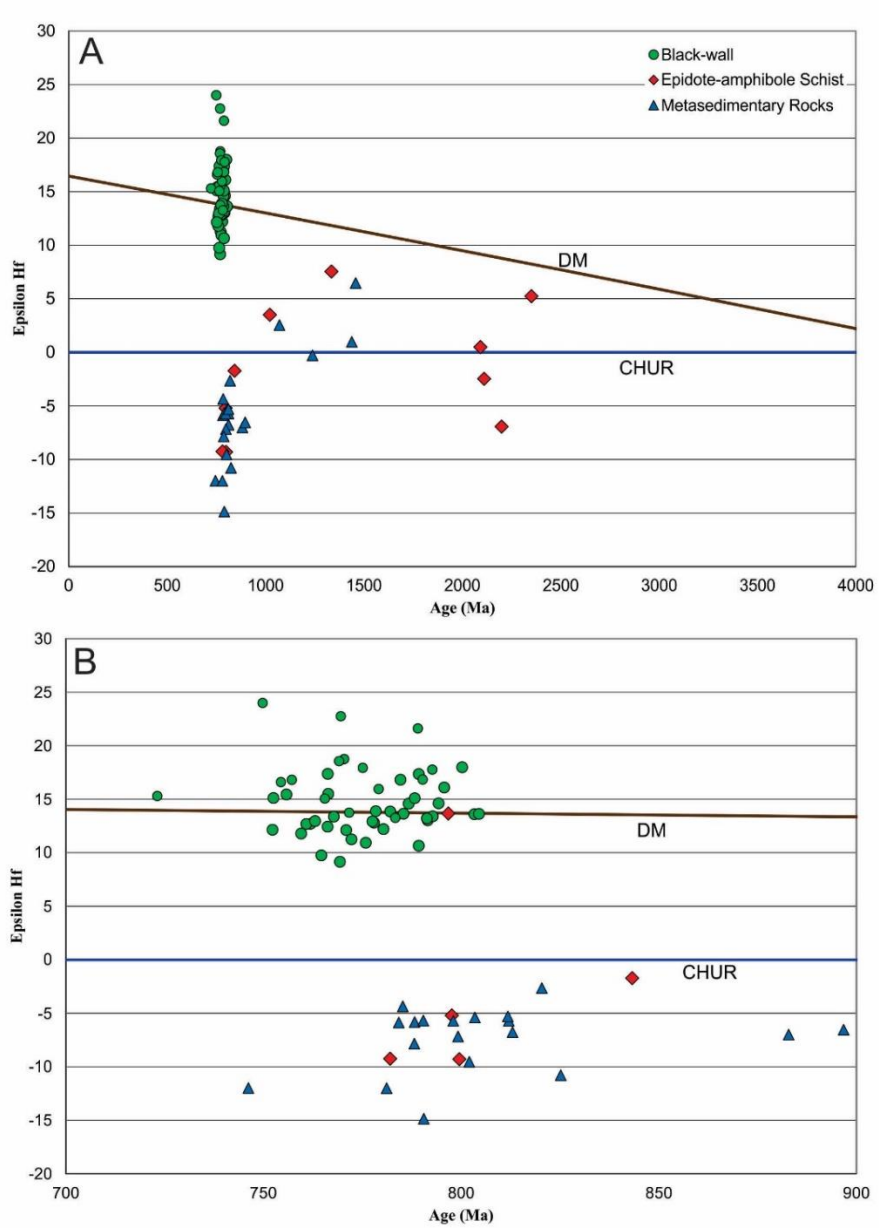

Figure 2.14. Graphs showing the distribution of: A. ƐHf of zircon grains over their age. Metasomatic zircon grains have extremely positive values, indicating their Hf-depleted nature. B. Close up view of the youngest zircon grains from A.

of values for ε_{Nd} are shown in figure 2.15. Schists aba-ax-07 and aba-ax 08 have ε_{Nd} (638) equal to -8.31 and -8.16,and T_{DM} values of 1.83 and 2.36 Ga, respectively. These values demonstrate

that there is a crustal component within these metasedimentary rocks, which was most likely derived from the São Francisco Craton.

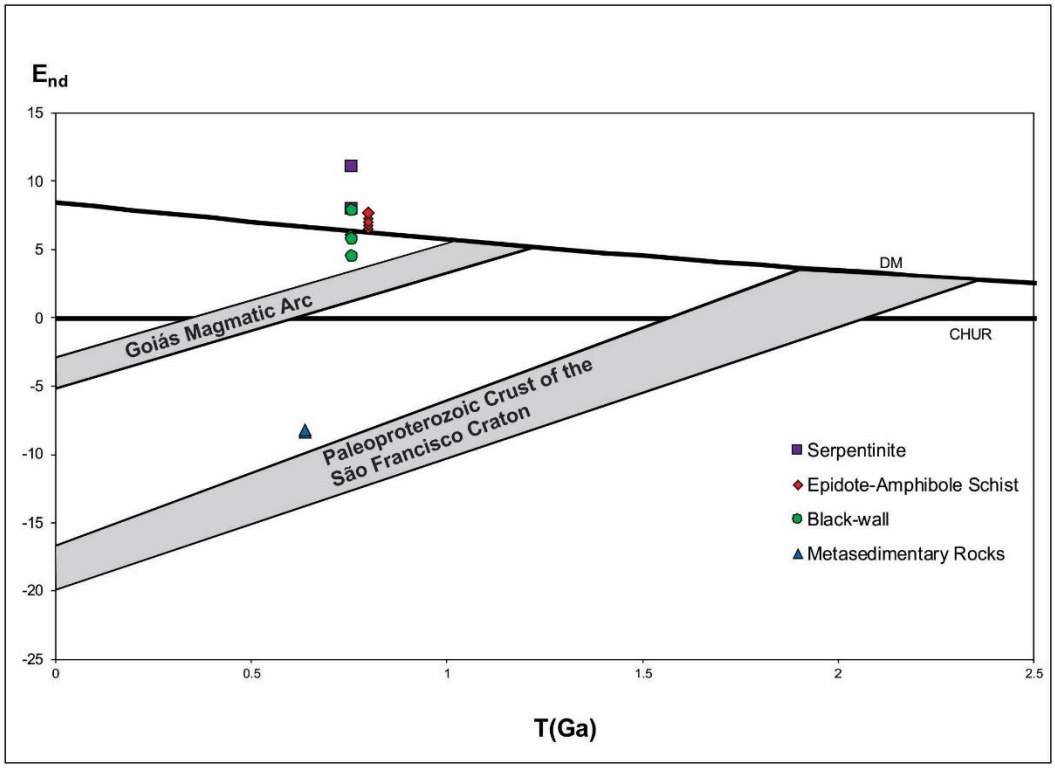

Figure 2.15. Graph showing the results for ƐNd of sampled serpentinites, epidote-amphibole schist, metasomatic rocks (chlorite schists) and metasedimentary rocks. Values for Goiás Magmatic Arc and São Francisco Craton are from Pimentel et al. (2001).

2.5 Discussion

2.5.1 Ophiolite Environment

The tectonics of the Neoproterozoic can be characterized by a reorganization of the continents, with the breakup of Rodinia, which later on lead to the formation of Gondwana. During this process, large ocean basins were opened and subsequently closed. The Mozambique Ocean, considered to have been a large global ocean and compared in size to the present Pacific Ocean (Stern, 1994), is an example of one of these ocean basins, which was closed during the collision between West and East Gondwana, forming the East African Orogen. Ophiolites from the Arabian-Nubian Shield are considered as remnants of oceanic crust from the Mozambique Ocean (Stern, 1994). The various ophiolites from the Arabian-Nubian Shield range in age from 870 to 627 Ma and record the processes of rift-drift, sea-floor spreading and collisional tectonics, with older ophiolites related to oceanic crust formed in a SSZ environment and younger ophiolites related to collisional events in a continental subduction zone setting (Dilek and Ahmed, 2003).

The Goiás–Pharusian Ocean was another substantially large ocean, which closed during the formation of West Gondwana, producing the Transbrasiliano-Kandi mega-shear zone (Cordani et al., 2013). Destruction of Goiás-Pharusian oceanic crust through subduction created volcanic arcs, such as the Goiás Magmatic arc, central Brazil and the Anti-Atlas, Morocco. The Goiás Magmatic Arc was active from ~930 to 630 Ma (Pimentel et al., 1992, 2011; Laux et al., 2005), while the Anti-Atlas was active from 778 to 615 Ma (Hefferan et al., 2000). Ophiolites found within suture zones related to the amalgamation of West Gondwana, such as the Monte Orebe metabasalts from the Borborema Province (Caxito et al., 2014), the Quatipuru of the Araguaia belt (Paixão et al., 2008) and ophiolite fragments from the Brasília belt (Brod et al., 1992; Piauilino et al., 2019), attest to the presence of the oceanic basin that was destroyed during this orogenic process.

Our results indicate that the studied epidote-amphibole schists have chondrite normalized REE values similar to a MORB signature. Using the classification diagram of Floyd and Winchester (1975) (Fig. 2.9 B), a basaltic composition is indicated for the protolith of the epidote-amphibole schists. The Nb/Yb vs Th/Yb diagram by Pearce (2008) was used to gain information on the tectonic setting of the protolith of the epidote-amphibole schist. Samples plot within or just below the mantle array of NMORB (Fig.2. 9 C). On the TiO_2/Yb vs Th/TiO_2 graph by Pearce (2008), the samples plot within the N-MORB zone, related to shallow melting of the mantle source (Fig. 2.9 D). This shows that the ophiolites in the study area are similar to mid-ocean ridge types. Positive ε_{Nd} (800) values (6.48 to 7.69) also indicate N-MORB generated magma and show a definite mantle signature. The study indicates that the protolith of the epidote-amphibole schist formed at a mid-ocean ridge, which according to Stern et al. (2012), would have been very difficult to be preserved.

The age of ca. 800 Ma for epidote-amphibole schist sample aba-ax-06 is interpreted as the age of crystallization of its basaltic protolith. However, the presence of a small population of older cratonic derived zircon indicates that the mantle source, the magma derived of which later became the epidote-amphibole schists, may have been contaminated with cratonic material. This is supported by negative to positive ε_{Hf} (-21.67 to +13.66) values for the recovered zircon grains, indicating the presence of older recycled crust, mixed with juvenile crust. Zircon grains may have been introduced into the upper mantle by subduction, as suggested by Robinson et al. (2015).

A study of chromite grains collected from other podiform chromite-bearing serpentinite bodies, using electron micro-probe analyses was conducted by Strieder and Nilson (1992b). Several samples yielded chromite, which was altered by metamorphism, however Strieder and Nilson (1992b) state that some of the serpentinite bodies (bodies S1, S4 and S7) contained

preserved primary chromite. When the primary chromite from serpentinites are plotted on the Cr# vs. Mg# taken from Stern et al. (2012), they mostly plot in the range of abyssal peridotite, close to the back-arc field of Ohara et al. (2002), with one plotting within it (Fig 2.16). The same holds true when the data are plotted on the Cr# vs TiO_2 graph. The data also plot close to the fore-arc field chrome spinel compositions, but still the majority of the data plot in the abyssal to back-arc peridotite fields.

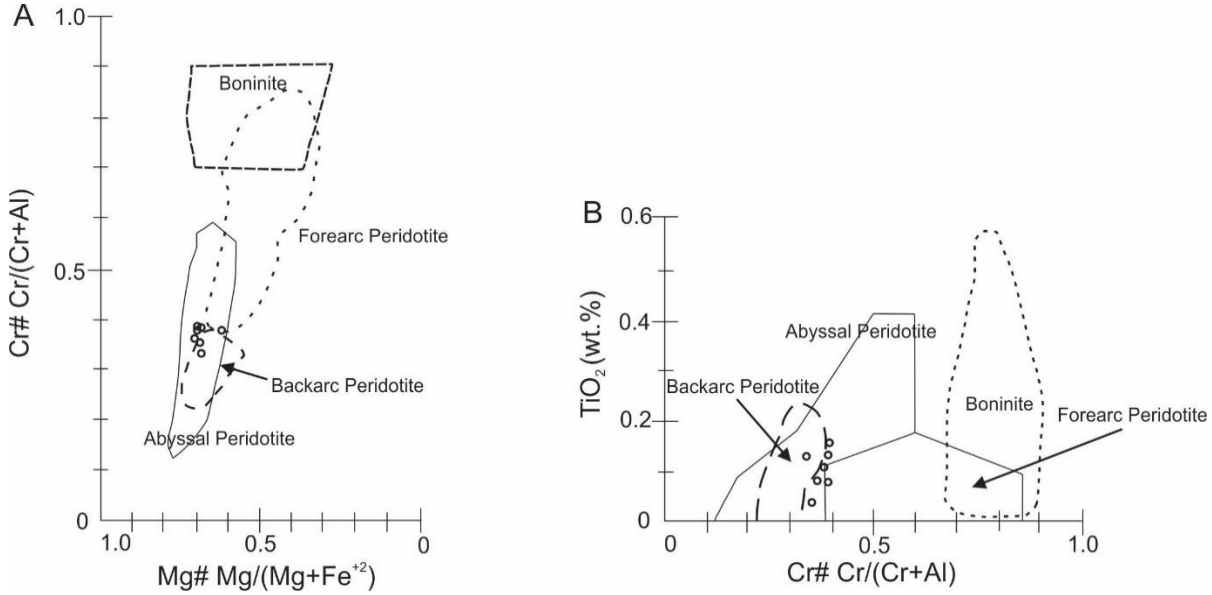

Figure 2.16. A. Diagram showing the composition of podiform chromites Cr# versus Mg# with data taken from Strieder and Nilson (1992b), modified from Dick and Bullen (1984) and including the composition of back-arc basin from Ohara et al. (2002). B. Cr# versus TiO2, of chromites, after Tamura and Arai (2006), with back-arc basin zone taken from Ohara et al. (2002).

The results from this study were compared with the results from two different studies from El-Rahman et al. (2009), selected because the ophiolites are considered Neoproterozoic back-arc remnants, and from Sinton et al. (2003), selected because the study was on modern back-arc

volcanics. Normalized N-MORB trace element plots are very similar to the region delineated by gabbros of the Wadi Ghadir ophiolite (El-Rahman et al. 2009). These gabbros display enrichment in elements like Cs, Rb, Ba, Pb, and negative Nb values and were interpreted to have formed in a back-arc environment. When compared to the Manus Back-Arc Basin, Papua-New Guinea, a modern day back-arc rift zone, the epidote-amphibole schists also fit in the interval of back-arc basalts, as determined by Sinton et al. (2003). The enrichment of some mobile elements was attributed to elements concentrated in the mantle wedge from the subduction zone, which mixed in the magma chamber of the Manus Back-arc rift (Sinton et al., 2003).

The presented data indicate that the protolith of the epidote-amphibole schist has a tholeiitic affinity. REE and trace element values are similar to N-MORB values, with some similarities with basalt formed in a back-arc ridge setting, ca. 800 Ma. The presence of oceanic crust formation during this time period has been reported by Caxito et al. (2014) and Piauilino et al. (2019), at ca. 820 Ma. Taken together, these data demonstrate evidence of an ocean basin that developed along the margin of the São Francisco Craton. The data presented by Piauilino et al. (2019), indicate that the ophiolites have an E-MORB affinity, which may indicate the beginning a rifting event. The data presented in this study could be a continuation of rifting, in which the magmas generated have N-MORB affinity, but is still being influenced by enrichment from a subduction zone mantle wedge.

2.5.2 Black-wall

The fluid interaction between serpentinizing ultramafic bodies and rocks in contact with them can form metasomatic alteration zones along the contact (Childester, 1962; Coleman, 1967). The metasomatic zone closest to the ultramafic rock is normally a chlorite rich zone, referred to as

black-wall, formed by the metasomatic addition of aluminum to the serpentinite or its peridotite protolith (Chidester, 1962; Frost 1975). The majority of the descriptions of metasomatic zoning between ultramafic and other rocks are of reaction zones around a mafic inclusion within the peridotite (Coleman, 1967; Frost, 1975). According to Frost (1975), mafic hornfels inclusions in contact with peridotite, at the Happy Go Lucky Pass, formed an outer black-wall zone, composed principally of chlorite, and an inner 'metarodingite zone' composed of various calcium-aluminum silicates. This kind of metasomatic zoning was also described by Coleman (1967), at several localities along the Western Coast of the United States, when a mafic rock was in contact with an ultramafic rock. However, Coleman (1967) also noted that metasomatic alteration zones can occur also along the contacts of ultramafic bodies with other rock types.

The ultramafic body S9, in Abadiânia, central Brazil, formed an extensive metasomatic alteration zone along the contact with its hosting epidote-amphibole schist. While the nature of the contact is not preserved, it is assumed that they were tectonically conjoined before the metasomatism began. Geochemical analysis indicates that the protolith of the epidote-amphibole schist has a tholeiitic composition. The metasomatic alteration zone consists of an extensive black-wall formed principally of chlorite schist, which encompasses ultramafic body S9, and has an albite-hornblende fels at the contact with the epidote-amphibole schist host rock. The black-wall composes the inner zone of the metasomatic alteration zone of the ultramafic body, and is composed mainly of chlorite schist, magnetite-chlorite schist, talc-actinolite-chlorite schist and hornblende-chlorite schist. Since the black-wall is formed from the metasomatism of serpentine, the variations in the mineral composition of the chlorite schist may be caused by a variation in the fluids which caused the alteration. The outer zone is represented by an albite-hornblende fels (aba-11), which is composed of albite, magnesiohornblende, quartz and clay minerals. Ca, taken from

the mafic rock assemblage, reacts with Al-rich fluids to form calcium-aluminum silicate mineral assemblages (Frost, 1975). While the outer zone in the study area does not have the same mineral composition (ie. grossular, diopside and clinozoisite), it does fit the overall pattern of metasomatic alteration zones described in the literature (Coleman 1967). It is possible that these minerals did exist at one time in the outer zone of the metasomatic alteration zone, but later metamorphic events and or weathering may have transformed them into the observed clay minerals. Samples S9A and aba-11 are part of the inner and outer zones, respectively, however, they share a common mineral phase of magnesio hornblende. It is possible that S9A represents the beginning of a transition phase of the black-wall inner zone to the outer zone. Unfortunately, the construction of a small dam disrupted the rock sequence and the relation of the contact between the inner and outer zones could not be determined (Fig. 2.17).

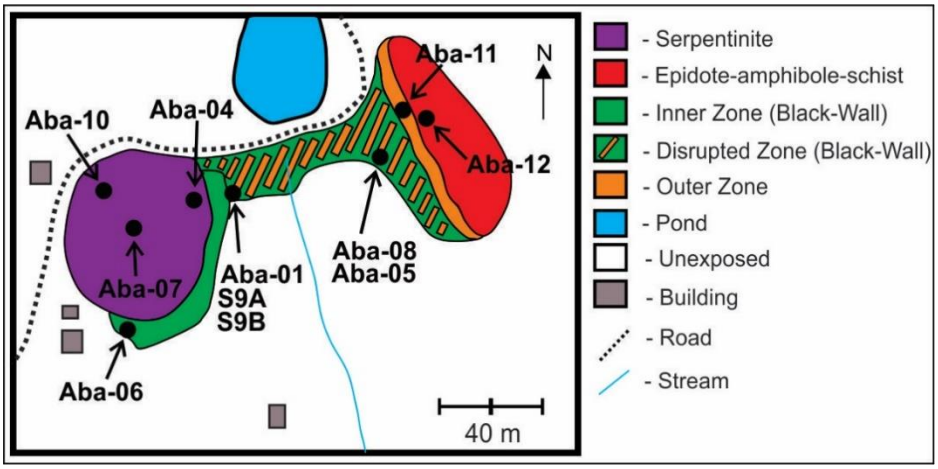

Figure 2.17. Diagram showing the observed black-wall zonation of ultramafic body S9 and its contact with an epidote-amphibole schist.

Dubińska et al. (2004) determined that metasomatic zircon may be used to date the timing of serpentinization of an ultramafic body. A study done by Arena et al. (2017) determined that the Ibaré and Palma ophiolites of southern Brazil record four different periods of serpentinization, by dating metasomatic zircon grains. Normally, mafic and ultramafic rocks are poor in Zr and do not form zircon minerals. The transference of Zr into the black-wall may have come from an external source and associated black-wall related protolith (Dubińska et al., 2004). The formation of zircon crystals in the black-wall could have been facilitated by the crystallization of chlorite, which could lower the pH of the normally highly alkaline fluids produced during serpentinization, or Zr may be mobilized by CO_2-rich fluids (Neal and Stangler, 1985; Saccocia et al., 1994). The process of subduction generates a wide range of element rich fluids (Deschamps, 2013), which could have been the source of the metasomatic fluids that created the alteration zone in the study area. The presence of what may be chlorite inclusions within zircon grains analyzed in this study would indicate that the zircon grains are cogenetic with the metasomatic assemblages, an indicator demonstrated by Dubińska et al. (2004).

The ages calculated from this study demonstrate two different age groups. Samples aba-06 and aba-08 have discodia ages of 772±6 and 778±7 Ma, respectively. Samples aba-11, S9A and S9B have a span of ages ranging from ca. 800 to 756 Ma, with an average age of 775.9±2.8 Ma (Fig. 2.12 D). These data suggest that the ultramafic body S9 was undergoing serpentinization for about 44 Ma. When put together, the age determined from the epidote-amphibole schist (sample aba-ax-06) and the age of the metasomatic zircon grains, models can be created to describe the evolution of these ophiolite assemblages. The age of 800±14 Ma (amphibole-epidote schist sample aba-ax-06) indicates the formation of the ophiolite assemblage. Metasomatic zircon grains dated from the black-wall show ages ranging from 793±2 to 756±5 Ma, interpreted as an extended

period of serpentinization, which spans 37±7 Ma years. These results can be interpreted to indicate that a back-arc rift formed at ca. 800 Ma and rifting continued for roughly 37 Ma. Another interpretation could be that the protolith of the epidote-amphibole schist formed and was quickly emplaced with the serpentine in a subduction zone and was under the influence of the subduction zone for roughly 40 Ma.

2.5.3 Metasedimentary rocks

Metasedimentary rock samples aba-ax-07 and aba-ax-08 represent units of the metamorphosed sedimentary units of the Araxá Group. The negative ε_{Nd} (638 Ma) values (-8.31 and -8.16) suggest that the majority of the material that formed the metasedimentary rocks in this study were derived from older sources, such as the São Francisco Craton. Results of U-Pb analysis on zircon grains obtained for these samples and the presence of two distinct zircon populations show that they are actually metasedimentary rocks. The first population is composed of large prismatic zircon grains, with magmatic zoning, which have Neoproterozoic ages that span from roughly 900 to 700 Ma. The second, smaller population, consists of Mesoproterozoic and older zircon grains, and represents a contribution of sediments from an older source, such as the passive margin of the São Francisco Craton. The mostly positive ε_{Hf} (t) values for the smaller Mesoproterozoic zircon grains indicate that they were formed in a juvenile setting. The negative ε_{Hf}(t) and older T_{DM} values indicate that the younger zircon population represents reworked Meso- to Paleoproterozoic crustal material.

The Neoproterozoic aged zircon grains in the metasedimentary rocks are most likely related to an arc setting with the recycling of older crust, and the ε_{Hf}(t) values are similar to those

from S-type granites (Villaros et al., 2012). A study conducted by Matteini et al. (2010) on rocks from the Mara Rosa arc demonstrated that two orthogneisses had a large population of Neoproterozoic aged zircon grains, with the youngest ages being 792±8 and 811±7 Ma, with similar negative ε_{Hf} (t) values. Another likely source for the Neoproterozoic zircon population in samples aba-ax-07 and 08 could be the Maratá Sequence. This sequence was dated by Pimentel et al. (1992) at ca. 790 Ma. Recently, Sabaraense (2016) conducted Lu/Hf analyses on zircon from the sequence and determined that the ε_{Hf} (t) values were all negative, with T_{DM} values indicating reworking of Meso- to Paleoproterozoic crust. Sabaraense (2016) also conducted analysis on two schists from the Araxá Group. Results of U-Pb on zircon show similar population peaks at 805 and 799 Ma, with zircon grains showing negative ε_{Hf} (t) values as well.

Samples aba-ax-07 and 08 represent sediments that were deposited in a fore-arc or back-arc environment. Another study on metasedimentary rocks of the Araxá Group conducted in a nearby area was done by Piuzana et al. (2003a). Only one metasedimentary rock was dated by U-Pb on zircon grains, and the results demonstrated that the sample had a younger zircon population than the ones from this study. ε_{Nd} values for the schists studied by Piuzana et al. (2003a) demonstrated two distinct groups, one with negative ε_{Nd} (T) values and another with positive values. Schists that have negative ε_{Nd} (T) values may represent the first depositional period that took place in the back-arc basin, while positive ε_{Nd} (T) values represent a later period with a different sedimentary regime and a different source.

2.5.4 The Brasília Belt

The evolutional history of the Brasília Belt begins with a passive margin on the western side of the São Francisco Craton at the end of the Mesoproterozoic. Consumption of the Goiás-Pharusian oceanic crust began at about 930 Ma, as indicated by the presence of arc related igneous rocks of ocean island arc affinity within the Goiás Magmatic Arc (Pimentel et al., 1992, 1999; Junges et al., 2003; Laux et al., 2005; Matteini et al., 2010). Oceanic arc related volcanism continued until about 770 Ma, when the volcanic arc affinity changed to continental related at about 750 Ma and continued until roughly 630 Ma.

This study reveals evidence that, beginning at 800 Ma, a back-arc rift system formed during the evolution of the Goiás Magmatic Arc, between it and the São Francisco Craton, which lasted till ~756 Ma. Evidence exists of magmatic activity in other areas of the Araxá Group during the same time interval dated in this study (e.g. 800, 790, 775 and 720 Ma) (Pimentel et al., 1992; Klein et al., 2008; Seer and Moraes, 2013). Igneous rocks aged 800 to 663 Ma are present in the area of Catalão, south of the study area (Pimentel et al., 1992, 2011; Klein et al., 2008). The combination of granite and metarhyolite, associated with amphibolites with an EMORB signature, led Klein et al. (2008) to speculate of an extensional event on the western edge of the São Francisco Craton, which lasted from 800 to 720 Ma.

The formation of a back-arc rift may have led to the opening of a small oceanic basin, which would have been the depocenter for the sediments which would become the Araxá Group metasedimentary rocks. A large portion would have come from the São Francisco Craton, and apparently from magmatic rocks that are present in the Araxá Group. Magmatic assemblages, including S-type granites with similar ages as those reported in this study (Klein et al., 2008; Seer and Moraes, 2013), could be another major source of sediments that entered into the back-arc

basin. Deposition could have begun with a sedimentation regime similar to that, which is represented by the schists from this study, consisting of a large amount of distal sediments derived from the São Francisco Craton (small zircon population and negative ε_{Nd}) and arc derived detrital sediments. A change in sedimentary regime is represented by a sample from Piuzana et al. (2003b), which has a larger amount of arc-derived juvenile material, younger zircon populations and positive ε_{Nd} value. This can be interpreted to coincide with the beginning of continental arc magmatism and the beginning of collisional events ending with the formation of Western Gondwana. Continental collisions could have destroyed original rift sequences through sequence disruption and nappe formation, and redistributed the pieces throughout the Araxá Group. This is the same idea that Falci et al. (2018) use to explain the distribution of sequences in the southern portion of the Araxá Group.

With the data collected in this study, a model describing the evolution of the ophiolites from Abadiânia can be created. Evidence of volcanism within the Araxá Group beginning at about 830 Ma (Seer et al. 2013), suggests magmatic activity occurring on the western margin of the São Francisco Craton. This magmatism may be related to an arc that was recycling older continentaly-derived material or crust, as is indicated by the negative ε_{Hf} values from the metasedimentary rocks in this study (Fig. 2.14 B). Similar ε_{Hf} values were obtained by Sabaraense (2016) for the Maratá Sequence. At roughly 800 Ma, this arc, referred to herein as the Maratá Arc, experienced slab rollback, which initiated an extensional event, opening a back-arc basin. Rifting continued for about 40 Ma. Sediments, represented by the studied metasedimentary rocks, were deposited in the back-arc basin. The metasedimentary rocks indicate that the Maratá Arc was active until about 780 Ma, at which time evidence of its activity is no longer recorded in the studied metasedimentary rocks. Between ca. 650 and 630 Ma, the Maratá Arc collided with the western edge of the São

Francisco Craton, an event which could have formed the Anápolis–Itauçu Granulite Complex. Later sedimentation formed the metasedimentary rocks reported by Piuzana et al. (2003a), indicating a younger zircon population, which is thought to have been derived from younger arc rocks and possibly from the Anápolis–Itauçu Granulite Complex.

2.6 Conclusions

- Chemical analyses of the epidote-amphibole schists in the area of Abadiânia, Goiás, central Brazil, indicate that they have a MORB composition interpreted to have formed in a back-arc environment at ~800 Ma.

- U-Pb analyses of zircon grains, recovered from the metasomatic alteration zone of ultramafic body S9, yielded ages of ~793±2 to 756±5 Ma. This suggests that there are roughly 37±7 Ma of serpentinization recorded in the black-wall. This age range is interpreted to be related to the duration of back-arc rifting, or subduction to collisional activity in this area of the Brasilia Belt.

- Quartz-mica schists, which are tectonically emplaced into epidote-amphibole schist outcrops, are metasedimentary rocks which may represent the first sedimentary deposits to enter the back-arc basin. Ages between 830 and 780 Ma and negative ε_{Nd} values indicate that the sediments had a large contribution from the Maratá Arc, which was reworking older continentally derived components.

- The initiation of the back-arc rift can be related to a slab rollback of the Maratá Arc, which moved from producing recycled volcanic material, to more juvenile, c. 650 Ma.

Acknowledgements

The author would like to acknowledge the Brazilian National Council for Scientific and Technological Development (CNPq) for the doctoral scholarship. The aurtor also acknowledges the Instituto Nacional de Ciência e Tecnologiastudos Tectonicos and CAPES for finacial support. Reinhardt A. Fuck and Elton L. Dantas acknowledge CNPq research fellowships.

2.7 Appendix

Appendix 2.1. Major (wt%) and trace elements (ppm), analyzed epidote-amphibole schist.

Sample	Aba-012	ABA-AX-06	ABA-AX-10	Aba-ax-13	Aba-ax-14	Aba-ax-15
SiO2	49.7	48.1	50.6	49.5	50.9	44.6
Al2O3	14.2	16.85	16.05	14.45	14.75	14.8
Fe2O3	11.15	11.25	11.35	11.1	9.6	8.72
CaO	11.6	13.85	12.25	12.45	11.35	15.9
MgO	8.06	7.3	6.9	7.21	8.71	6.43
Na2O	1.05	1.4	1.95	1.17	1.94	1.35
K2O	0.14	0.17	0.18	0.11	0.16	0.09
Cr2O3	0.07	0.06	0.04	0.03	0.05	0.04
TiO2	1.1	1.08	1.07	0.99	0.86	0.78
MnO	0.18	0.17	0.17	0.17	0.17	0.17
P2O5	0.05	0.07	0.09	0.07	0.05	0.04
SrO	<0.01	0.01	0.01	0.01	0.01	0.02
BaO	<0.01	<0.01	<0.01	<0.01	<0.01	<0.01
LOI	3.04	1.89	1.62	2.21	1.61	6.47
Total	100.34	>102.00	>102.00	99.47	100.16	99.41
Trace elements (ppm)						
Li	20	20	20	20	30	20
Sc	42	44	43	43	40	38
V	293	282	268	333	292	238
Cr	470	380	240	230	380	300
Co	86	74	87	76	77	66
Ni	156	74	69	86	123	97
Cu	40	62	75	78	78	90
Zn	87	93	78	84	75	54
Gd	4.2	3.77	3.78	3.79	2.81	2.73
Rb	2.8	1.9	1.1	1.4	5.3	1.1
Sr	73.2	123.5	106	70.9	75.4	108
Y	29.2	26.9	24.7	27.7	21	17.8
Zr	58	62	58	53	45	43
Nd	7	6.8	7.3	6.2	5.8	5
Cs	0.05	0.13	0.07	<0.01	0.54	0.03
Ba	11.9	17.3	10.3	7.5	19.4	9.2
La	2.9	2.2	2.7	2.5	2.2	1.8
Ce	7.3	7	7.4	6	6.1	5.7
Pr	1.28	1.26	1.25	1.08	0.95	0.9
Nb	2.6	1.8	2.2	2.1	1.7	1.5
Sm	2.59	2.29	2.41	2.39	2.02	2.29

Eu	0.96	0.94	0.92	0.83	0.76	0.7
Gd	4.2	3.77	3.78	3.79	2.81	2.73
Tb	0.71	0.71	0.66	0.7	0.56	0.59
Dy	4.69	4.57	4.27	4.41	3.66	3.27
Ho	1.05	1.03	0.89	1.05	0.81	0.7
Er	3.12	2.84	2.72	3.03	2.4	2.26
Yb	2.98	2.75	2.76	2.72	2.55	2.06
Lu	0.45	0.43	0.39	0.46	0.35	0.29
Hf	1.6	1.9	1.7	1.3	1.2	1.1
Ta	0.3	0.3	0.2	0.6	0.7	0.6
Pb	<2	<2	<2	3	3	<2
Th	0.15	0.17	0.22	0.07	0.05	0.05
U	0.06	0.05	<0.05	0.06	<0.05	<0.05

Appendix 2.2. Summary of results of U/Pb LA-ICPMS data.

Sample S9A											Aperant Ages						
Zircon	Th/U	$^{206}Pb/^{204}Pb$	1σ%	$^{207}Pb/^{206}Pb$	1σ %	$^{207}Pb/^{235}U$	1σ %	$^{206}Pb/^{238}U$	1σ %	Rho	$^{207}Pb/^{206}Pb$	2σ abs	$^{206}Pb/^{238}U$	2σ abs	$^{207}Pb/^{235}U$	2σ abs	Conc %
004-ZR2	0.53301	114853.59	14.76	0.06526	0.39	1.17354	1.05	0.13042	0.90	0.86	782.61	16.48	790.26	13.39	788.30	11.48	-0.98
005-ZR3	0.58108	58124.59	21.45	0.06500	0.67	1.16702	1.10	0.13020	0.79	0.72	774.36	27.87	789.03	11.78	785.25	11.99	-1.90
008-ZR6	0.24286	20865.88	25.04	0.06567	0.77	1.16339	1.23	0.12847	0.88	0.71	795.98	32.32	779.14	12.85	783.55	13.35	2.12
080-ZR63	0.41773	85710.26	71.82	0.06511	1.06	1.15993	1.39	0.12920	0.81	0.58	777.78	44.39	783.32	11.96	781.92	15.07	-0.71
009-ZR7	1.07195	80290.16	22.98	0.06586	0.74	1.15915	1.16	0.12763	0.81	0.70	802.06	30.98	774.34	11.82	781.55	12.61	3.46
054-ZR41	0.76259	30029.10	15.03	0.06532	0.78	1.15909	1.68	0.12870	1.44	0.86	784.54	32.48	780.42	21.20	781.53	18.24	0.53
059-ZR46	0.08092	25991.89	29.03	0.06577	0.87	1.15806	1.33	0.12769	0.93	0.70	799.20	36.35	774.65	13.58	781.04	14.42	3.07
069-ZR54	0.38118	27161.51	18.84	0.06466	0.88	1.15547	1.28	0.12959	0.85	0.66	763.40	36.87	785.52	12.50	779.83	13.84	-2.90
003-ZR1	0.45893	38215.70	19.59	0.06572	0.66	1.15458	1.13	0.12741	0.83	0.74	797.48	27.62	773.05	12.13	779.40	12.22	3.06
044-ZR33	0.86310	113497.48	15.57	0.06480	0.37	1.15453	0.94	0.12921	0.78	0.83	767.92	15.59	783.33	11.44	779.38	10.17	-2.01
026-ZR20	0.39830	5842.20	16.40	0.06575	1.24	1.15322	2.14	0.12720	1.71	0.80	798.49	51.65	771.85	24.81	778.76	23.18	3.34
048-ZR37	0.40511	28264.94	17.69	0.06493	0.64	1.14919	1.10	0.12835	0.82	0.74	772.10	26.89	778.46	11.97	776.86	11.94	-0.82
075-ZR58	2.33989	45821.72	16.03	0.06451	0.73	1.14901	1.39	0.12918	1.12	0.81	758.29	30.80	783.17	16.56	776.78	15.06	-3.28
040-ZR32N	0.04644	109002.72	26.61	0.06484	0.58	1.14481	1.02	0.12805	0.76	0.74	769.01	24.49	776.74	11.06	774.79	11.07	-1.01
063-ZR48	0.77649	45296.27	13.51	0.06408	0.80	1.14302	1.22	0.12935	0.85	0.70	744.41	33.51	784.16	12.59	773.94	13.22	-5.34
010-ZR8	0.56562	53142.35	29.90	0.06564	0.68	1.14260	1.10	0.12624	0.78	0.71	794.86	28.58	766.39	11.32	773.74	11.92	3.58
019-ZR15	1.27188	41333.39	16.56	0.06513	0.75	1.14198	1.16	0.12717	0.81	0.70	778.41	31.20	771.68	11.78	773.45	12.54	0.86
076-ZR59	0.53386	24023.19	13.89	0.06494	1.11	1.14044	1.48	0.12736	0.90	0.61	772.41	46.32	772.77	13.13	772.72	15.91	-0.05
037-ZR29	0.64556	76205.72	12.78	0.06403	0.48	1.13891	1.07	0.12899	0.88	0.82	742.64	20.33	782.12	12.90	771.99	11.50	-5.32
016-ZR12	0.48619	41271.02	15.31	0.06518	0.55	1.13888	0.95	0.12672	0.68	0.72	780.11	23.20	769.12	9.90	771.98	10.29	1.41
025-ZR19	0.24966	89494.52	14.08	0.06412	0.55	1.13773	0.93	0.12868	0.66	0.71	745.55	23.03	780.35	9.71	771.43	10.07	-4.67
017-ZR13	0.37850	33814.69	17.85	0.06456	0.66	1.13736	1.09	0.12777	0.78	0.72	759.92	27.65	775.12	11.46	771.25	11.74	-2.00
013-ZR9	0.35364	33105.26	17.33	0.06526	0.80	1.13471	1.33	0.12609	0.99	0.75	782.86	33.35	765.52	14.33	770.00	14.27	2.22
064-ZR49	0.28341	12421.73	14.15	0.06504	0.96	1.13288	1.51	0.12632	1.10	0.73	775.59	40.10	766.84	15.90	769.12	16.18	1.13
068-ZR53	0.50177	70322.29	26.78	0.06455	0.76	1.13236	1.21	0.12722	0.86	0.71	759.66	32.10	772.00	12.51	768.88	13.00	-1.63
015-ZR11	0.29036	43633.71	15.59	0.06459	0.67	1.13062	1.23	0.12694	0.96	0.78	761.09	28.03	770.39	13.92	768.05	13.17	-1.22
024-ZR18	0.49749	32521.96	19.58	0.06423	0.63	1.13058	1.11	0.12766	0.83	0.75	749.09	26.39	774.50	12.18	768.03	11.90	-3.39
030-ZR24	0.54494	34463.69	18.30	0.06436	0.73	1.12531	1.17	0.12680	0.84	0.71	753.54	30.76	769.57	12.16	765.52	12.57	-2.13
057-ZR44	0.46585	6258.51	17.82	0.06570	1.28	1.12819	2.05	0.12453	1.57	0.76	796.84	53.09	756.60	22.35	766.89	22.00	5.05
036-ZR28	0.46066	7588.82	14.57	0.06600	1.42	1.12785	1.91	0.12393	1.22	0.64	806.44	59.00	753.12	17.31	766.73	20.45	6.61
039-ZR31	0.48403	13334.19	12.92	0.06515	1.01	1.11962	1.52	0.12463	1.06	0.70	779.15	42.28	757.17	15.20	762.79	16.19	2.82
074-ZR57	1.14936	44562.45	15.45	0.06442	0.74	1.11385	1.35	0.12540	1.06	0.79	755.36	31.19	761.56	15.23	760.03	14.36	-0.82
023-ZR17	0.81697	43651.26	16.21	0.06401	0.81	1.11219	1.15	0.12600	0.73	0.63	742.05	34.22	765.02	10.52	759.23	12.30	-3.10
055-ZR42	0.39809	10442.92	15.47	0.06544	1.49	1.10547	1.99	0.12252	1.27	0.64	788.41	61.97	745.03	17.85	755.99	21.14	5.50
028-ZR22	0.17150	17728.52	18.37	0.06436	1.06	1.10171	1.42	0.12415	0.86	0.61	753.34	44.57	754.41	12.21	754.18	15.01	-0.14
029-ZR23	0.53197	14814.46	19.11	0.06453	0.81	1.09747	1.15	0.12335	0.73	0.63	758.91	33.96	749.80	10.32	752.13	12.19	1.20

Sample S9B											Aperant Ages						
Zircon	Th/U	$^{206}Pb/^{204}Pb$	1σ%	$^{207}Pb/^{206}Pb$	1σ %	$^{207}Pb/^{235}U$	1σ %	$^{206}Pb/^{238}U$	1σ %	Rho	$^{207}Pb/^{206}Pb$	2σ abs	$^{206}Pb/^{238}U$	2σ abs	$^{207}Pb/^{235}U$	2σ abs	Conc %
047-Zir34	0.51184	63250.11	15.76	0.06426	0.71	1.15413	1.28	0.13025	0.92	0.72025	750.28	33.77	789.27	13.64	779.19	13.83	-5.20
026-Zir18	0.33230	30723.48	17.94	0.06459	1.41	1.15402	1.59	0.12956	1.13	0.71209	761.16	44.17	785.38	16.76	779.14	17.25	-3.18
006-Zir51	0.54884	113209.05	14.28	0.06467	2.17	1.14444	1.09	0.12834	0.81	0.74649	763.55	26.18	778.40	11.93	774.61	11.78	-1.94
065-Zir48	0.42557	23747.41	18.35	0.06663	0.99	1.14541	3.29	0.12467	2.32	0.70536	826.28	94.62	757.36	33.12	775.07	35.36	8.34
009-Zir53	0.35725	23681.86	19.78	0.06698	1.87	1.15417	2.94	0.12497	2.11	0.71805	837.05	82.64	759.12	30.17	779.21	31.71	9.31
029-Zir21	0.36692	50792.22	31.21	0.06570	0.82	1.12798	2.50	0.12452	1.70	0.68001	796.68	74.24	756.52	24.20	766.79	26.69	5.04
029-Zir67	0.40450	32852.58	18.77	0.06561	2.11	1.14189	2.30	0.12622	1.62	0.70476	793.98	65.97	766.24	23.40	773.40	24.75	3.49
044-Zir31	0.24689	33054.00	28.94	0.06510	1.64	1.13047	2.31	0.12593	1.62	0.70028	777.64	66.79	764.61	23.28	767.98	24.71	1.68
004-Zir01	0.36465	22974.79	20.47	0.06505	1.24	1.11063	1.93	0.12381	1.37	0.70934	776.04	54.57	752.48	19.43	758.48	20.51	3.04
046-Zir33	0.36710	42668.18	13.82	0.06541	2.66	1.12778	1.84	0.12504	1.21	0.65800	787.50	55.46	759.52	17.31	766.69	19.68	3.55
025-Zir17	0.33760	31226.29	17.73	0.06557	0.91	1.13945	1.73	0.12603	1.26	0.72897	792.61	46.79	765.17	18.17	772.25	18.61	3.46
023-Zir63	0.38540	18709.99	18.41	0.06760	1.92	1.23060	2.70	0.13203	2.04	0.75458	856.22	71.17	799.41	30.61	814.61	30.04	6.63
034-Zir70	0.54577	37168.52	20.54	0.06595	1.15	1.21831	2.24	0.13396	1.68	0.74804	804.89	59.78	810.44	25.52	809.00	24.86	-0.69
058-Zir43	0.62465	33283.10	22.89	0.06588	0.96	1.20551	1.79	0.13271	1.29	0.72116	802.46	49.06	803.31	19.44	803.13	19.73	-0.11
055-Zir40	0.39054	63860.26	15.42	0.06571	1.18	1.20428	1.49	0.13292	1.07	0.72064	797.07	40.07	804.48	16.19	802.56	16.43	-0.93
026-Zir64	0.40796	42859.11	20.56	0.06593	1.44	1.20156	1.84	0.13217	1.39	0.75609	804.11	47.63	800.24	20.93	801.31	20.29	0.48
033-Zir69	0.45953	36936.16	17.13	0.06613	1.73	1.19765	2.77	0.13134	1.97	0.71001	810.53	79.24	795.49	29.45	799.50	30.47	1.86
016-Zir58	0.47177	70361.52	18.45	0.06552	1.12	1.18694	1.35	0.13138	0.93	0.68671	791.11	37.94	795.71	13.88	794.54	14.84	-0.58
054-Zir39	0.32301	15107.55	21.96	0.06561	1.33	1.18652	3.71	0.13116	2.56	0.69072	793.84	109.55	794.47	38.26	794.35	40.49	-0.08
027-Zir65	0.63953	50621.54	23.94	0.06444	1.31	1.18456	3.22	0.13332	2.95	0.91522	755.99	52.10	806.77	44.66	793.43	35.18	-6.72
057-Zir42	0.30899	26735.22	16.08	0.06437	1.61	1.17980	2.30	0.13291	1.57	0.68232	753.94	68.40	804.46	23.68	791.22	25.09	-6.70
004-Zir49	0.37091	27358.93	15.93	0.06561	1.59	1.17677	3.18	0.13007	2.35	0.74006	794.06	87.11	788.24	34.87	789.81	34.61	0.73
021-Zir61	0.60091	86545.94	14.39	0.06547	1.79	1.17512	1.49	0.13016	1.19	0.79795	789.57	34.12	788.79	17.63	789.04	16.27	0.10
033-Zir23	0.27439	27984.86	19.35	0.06407	2.01	1.17077	2.44	0.13253	1.52	0.62424	743.81	78.10	802.27	22.96	787.01	26.55	-7.86
007-Zir04	0.41066	47977.02	18.23	0.06513	2.30	1.16575	1.50	0.12980	1.07	0.70968	778.68	41.37	786.70	15.77	784.66	16.34	-1.03
050-Zir37	0.37103	24002.16	15.98	0.06400	0.62	1.16376	3.18	0.13188	2.29	0.72069	741.54	90.59	798.57	34.37	783.72	34.43	-7.69
015-Zir57	0.31195	26539.93	16.14	0.06454	1.05	1.16038	2.02	0.13038	1.40	0.69482	759.47	58.73	790.04	20.87	782.13	21.93	-4.02
014-Zir56	0.38456	100111.19	27.07	0.06486	0.80	1.15766	1.08	0.12944	0.72	0.66945	769.88	29.89	784.64	10.70	780.86	11.76	-1.92

Sample aba-11											Aperant Ages						
Zircon	Th/U	$^{206}Pb/^{204}Pb$	1σ%	$^{207}Pb/^{206}Pb$	1σ %	$^{207}Pb/^{235}U$	1σ %	$^{206}Pb/^{238}U$	1σ %	Rho	$^{207}Pb/^{206}Pb$	2σ abs	$^{206}Pb/^{238}U$	2σ abs	$^{207}Pb/^{235}U$	2σ abs	Conc %
024-Zir15	0.45669	42885.48	18.42	0.06456	0.98	1.12607	1.33	0.12648	0.82	0.61	760.19	41.20	767.78	11.84	765.88	14.28	-1.00
033-Zir19	1.04366	74706.64	11.68	0.06428	0.82	1.12354	1.32	0.12675	0.97	0.73	751.00	34.46	769.30	14.06	764.67	14.17	-2.44
023-Zir14	0.77379	74338.33	19.54	0.06497	0.67	1.12225	0.98	0.12526	0.61	0.62	773.44	28.14	760.79	8.68	764.05	10.47	1.64
034-Zir20	0.94949	74904.96	13.65	0.06494	1.08	1.13866	1.48	0.12716	0.94	0.63	772.41	45.12	771.64	13.60	771.87	15.90	0.10
011-Zir06	0.88161	42019.34	18.85	0.06538	0.79	1.16546	1.27	0.12928	0.92	0.73	786.59	32.87	783.73	13.55	784.52	13.78	0.36
039-Zir23	0.93313	140893.90	14.49	0.06536	0.67	1.15263	1.20	0.12789	0.91	0.77	785.90	28.18	775.84	13.37	778.48	12.95	1.28
030-Zir18	1.71440	90319.41	22.47	0.06479	0.64	1.13988	1.09	0.12760	0.79	0.73	767.41	27.05	774.15	11.53	772.45	11.71	-0.88
028-Zir16	1.70232	109518.43	16.70	0.06533	0.61	1.14649	1.04	0.12726	0.76	0.73	785.08	25.33	772.23	11.07	775.58	11.26	1.64
029-Zir17	1.09870	108414.50	16.34	0.06532	0.62	1.15465	1.03	0.12819	0.74	0.72	784.75	25.93	777.53	10.85	779.44	11.23	0.92
021-Zir12	0.89362	93412.74	27.21	0.06505	0.64	1.15050	1.02	0.12826	0.70	0.69	776.00	26.67	777.94	10.26	777.48	11.01	-0.25
010-Zir05	0.36135	135600.14	16.15	0.06512	0.56	1.15971	0.93	0.12914	0.65	0.69	778.37	23.39	782.97	9.52	781.82	10.13	-0.59
004-Zir1	0.40149	35074.52	21.13	0.06381	0.93	1.17541	1.47	0.13358	1.08	0.73	735.48	39.22	808.25	16.38	789.17	16.10	-9.89
006-Zir3	0.79433	90731.82	33.68	0.06517	0.54	1.24778	0.95	0.13885	0.69	0.73	779.82	22.66	838.18	10.88	822.40	10.72	-7.48
009-Zir04	0.82351	165776.14	22.97	0.06445	0.54	1.17471	0.95	0.13219	0.69	0.73	756.31	22.56	800.35	10.41	788.85	10.40	-5.82
018-Zir11	2.30021	222091.38	26.13	0.06509	0.47	1.23022	0.91	0.13706	0.68	0.75	777.36	19.91	828.01	10.57	814.44	10.16	-6.52
057-Zir35	0.51054	87969.68	16.38	0.06567	0.80	1.18267	1.24	0.13060	0.86	0.70	795.88	33.56	791.32	12.85	792.55	13.57	0.57
012-Zir07	0.84196	183556.10	18.04	0.06491	0.69	1.17127	1.06	0.13086	0.71	0.67	771.44	28.73	792.77	10.63	787.24	11.53	-2.76
046-Zir28	0.60116	19209.37	11.72	0.06703	3.29	1.10487	4.69	0.11955	3.32	0.71	838.56	134.00	727.96	45.69	755.70	49.39	13.19
016-Zir09	0.56168	13580.53	14.81	0.06494	3.32	1.14589	4.61	0.12796	3.18	0.69	772.46	136.78	776.23	46.36	775.30	49.39	-0.49
005-Zir2	0.29262	10163.03	21.26	0.06457	2.76	1.13463	4.02	0.12744	2.89	0.72	760.20	114.45	773.27	42.10	769.96	42.92	-1.72
035-Zir21	0.54330	12342.68	19.12	0.07217	2.94	1.27665	3.87	0.12829	2.49	0.64	990.64	117.53	778.12	36.41	835.36	43.63	21.45
022-Zir13	0.54571	24646.24	17.67	0.06418	2.38	1.11388	3.29	0.12587	2.24	0.68	747.52	99.10	764.25	32.21	760.04	34.89	-2.24
040-Zir24	0.57455	19695.13	14.10	0.06714	2.24	1.14141	3.21	0.12329	2.26	0.71	842.14	91.96	749.46	31.95	773.18	34.40	11.01
048-Zir30	1.20031	28443.00	15.87	0.06674	1.85	1.15468	2.82	0.12548	2.10	0.74	829.55	76.24	762.02	30.08	779.45	30.46	8.14
054-Zir34	0.64396	33973.55	13.00	0.06644	1.51	1.17444	2.38	0.12819	1.80	0.76	820.32	62.60	777.54	26.34	788.72	25.95	5.22
042-Zir26	0.69484	22173.04	19.63	0.06620	1.49	1.14269	2.32	0.12518	1.74	0.75	812.64	61.71	760.33	24.99	773.78	25.01	6.44
017-Zir10	0.54866	23437.48	22.24	0.06680	1.58	1.13604	2.30	0.12334	1.63	0.71	831.41	65.28	749.77	23.07	770.63	24.72	9.82
045-Zir27	0.57883	38850.11	13.70	0.06573	1.51	1.12045	2.10	0.12361	1.41	0.67	797.93	62.49	751.33	20.04	763.19	22.40	5.84
015-Zir08	0.53049	54398.68	16.02	0.06542	0.96	1.16599	1.85	0.12925	1.53	0.83	787.91	40.07	783.60	22.63	784.76	20.10	0.55

Sample aba-06																	
Zircon	Th/U	$^{206}Pb/^{204}Pb$	1σ%	$^{207}Pb/^{206}Pb$	1σ %	$^{207}Pb/^{235}U$	1σ %	$^{206}Pb/^{238}U$	1σ %	Rho	Aperant Ages						Conc %
											$^{207}Pb/^{206}Pb$	2σ abs	$^{206}Pb/^{238}U$	2σ abs	$^{207}Pb/^{235}U$	2σ abs	
004-ZR01	0.34925	16356.99	15.34	0.06431	2.82	1.13531	4.07	0.12803	2.92	0.72	751.74	116.72	776.64	42.64	770.28	43.50	-3.31
019-ZR14	1.09343	80029.85	23.36	0.06421	0.66	1.25572	1.79	0.14183	1.62	0.91	748.44	27.82	855.02	25.91	825.98	20.11	-14.24
014-ZR09	0.30307	115328.20	19.12	0.06456	0.50	0.97658	1.41	0.10970	1.26	0.90	759.96	21.14	671.03	16.03	691.85	14.05	11.70
054-ZR40	0.33575	31490.09	16.59	0.06437	1.46	1.19813	2.34	0.13499	1.80	0.77	753.67	60.95	816.29	27.51	799.72	25.77	-8.31
013-ZR08	0.27071	250771.57	15.95	0.06438	0.45	1.20853	1.16	0.13614	1.00	0.86	754.12	18.83	822.78	15.45	804.52	12.82	-9.11
015-ZR10	0.55535	280931.96	19.21	0.06454	0.34	1.10467	0.81	0.12413	0.64	0.79	759.27	14.13	754.31	9.12	755.61	8.65	0.65
009-ZR06	0.24386	133256.06	19.55	0.06445	0.79	1.26393	2.37	0.14222	2.21	0.93	756.46	33.17	857.20	35.38	829.67	26.73	-13.32
056-ZR42	0.44437	32242.05	19.60	0.06463	1.43	1.14689	2.24	0.12869	1.68	0.75	762.29	59.90	780.41	24.61	775.78	24.12	-2.38
026-ZR19	0.66979	164356.68	23.00	0.06470	0.52	1.09376	0.92	0.12259	0.66	0.72	764.71	21.70	745.46	9.28	750.33	9.69	2.52
016-ZR11	0.44362	82418.45	23.18	0.06474	0.82	1.08968	1.20	0.12207	0.79	0.66	765.81	34.22	742.47	11.12	748.35	12.64	3.05
036-ZR27	0.38718	48354.96	23.44	0.06478	1.21	1.14246	1.97	0.12790	1.51	0.77	767.12	50.67	775.89	22.01	773.68	21.21	-1.14
027-ZR20	0.34166	119117.71	24.98	0.06465	0.96	1.38527	1.57	0.15539	1.19	0.76	762.97	40.20	931.12	20.59	882.68	18.45	-22.04
028-ZR21	0.42214	89054.39	20.32	0.06500	0.57	1.10124	1.16	0.12287	0.94	0.81	774.29	23.73	747.06	13.21	753.95	12.26	3.52
057-ZR43	0.80455	308806.04	21.76	0.06497	0.43	1.17137	1.09	0.13074	0.93	0.85	773.50	18.16	792.10	13.91	787.29	11.95	-2.40
018-ZR13	0.48326	317502.22	13.83	0.06506	0.54	1.09938	1.00	0.12254	0.75	0.75	776.30	22.84	745.19	10.55	753.05	10.59	4.01
008-ZR05	0.36986	139335.62	48.79	0.06512	0.60	1.08088	1.07	0.12037	0.81	0.75	778.30	25.15	732.68	11.15	744.06	11.26	5.86
030-ZR23	0.47125	108361.42	23.00	0.06522	0.69	1.11884	1.13	0.12442	0.81	0.72	781.30	28.91	755.94	11.55	762.42	12.05	3.25
043-ZR31	0.34933	10907.01	18.20	0.06528	3.22	1.13725	4.25	0.12635	2.75	0.65	783.26	132.41	766.99	39.77	771.20	45.44	2.08
017-ZR12	0.43484	13366.62	18.92	0.06540	2.59	1.11977	3.82	0.12417	2.78	0.73	787.25	106.98	754.52	39.47	762.87	40.52	4.16
038-ZR29	0.54916	140033.98	30.58	0.06550	0.67	1.09391	1.19	0.12113	0.91	0.76	790.29	28.01	737.04	12.61	750.40	12.54	6.74
049-ZR37	0.32365	68478.62	31.53	0.06542	0.70	1.23401	1.56	0.13679	1.35	0.86	787.93	29.16	826.50	20.88	816.17	17.44	-4.90
058-ZR44	1.23929	116485.05	21.39	0.06550	0.69	1.15269	1.14	0.12763	0.83	0.73	790.35	28.75	774.34	12.16	778.51	12.39	2.03
007-ZR04	0.37049	88797.08	23.39	0.06559	0.68	1.06443	1.15	0.11768	0.84	0.73	793.44	28.59	717.22	11.44	736.00	11.98	9.61
059-ZR45	0.39925	53183.80	19.53	0.06557	0.71	1.14453	1.13	0.12659	0.80	0.71	792.67	29.74	768.37	11.56	774.66	12.23	3.07
045-ZR33	0.41230	37747.88	15.49	0.06565	1.20	1.12140	1.98	0.12388	1.54	0.78	795.15	49.75	752.87	21.80	763.64	21.16	5.32
037-ZR28	0.30328	22047.08	17.56	0.06581	1.76	1.10261	2.61	0.12151	1.89	0.72	800.28	72.82	739.25	26.36	754.61	27.57	7.63

Sample aba-08																	
Zircon	Th/U	$^{206}Pb/^{204}Pb$	1σ%	$^{207}Pb/^{206}Pb$	1σ %	$^{207}Pb/^{235}U$	1σ %	$^{206}Pb/^{238}U$	1σ %	Rho	Aperant Ages						Conc %
											$^{207}Pb/^{206}Pb$	2σ abs	$^{206}Pb/^{238}U$	2σ abs	$^{207}Pb/^{235}U$	2σ abs	
030-Zir23	0.46050	123112.04	0.02	0.06471	878.77	1.11931	87.86	0.12545	567.30	0.72	764.80	23.87	761.85	10.22	762.64	10.52	0.38
044-Zir32	0.53950	95704.47	0.03	0.06474	998.35	1.10554	89.51	0.12384	525.98	0.66	765.97	27.12	752.61	9.25	756.03	10.52	1.74
025-Zir18	0.49548	101336.37	0.01	0.06519	976.90	1.11687	95.30	0.12425	618.18	0.72	780.42	26.66	754.98	10.94	761.48	11.37	3.26
065-Zir49	1.28223	140032.01	0.01	0.06478	768.20	1.05904	100.82	0.11855	732.96	0.81	767.36	20.90	722.22	11.87	733.35	11.12	5.88
039-Zir30	0.83821	116068.76	0.02	0.06566	1235.02	1.14134	97.42	0.12606	526.99	0.60	795.65	33.82	765.32	9.58	773.15	12.00	3.81
035-Zir26	0.55154	145584.83	0.02	0.06496	1260.25	1.15272	97.11	0.12868	518.64	0.60	773.16	34.27	780.35	9.81	778.53	12.14	-0.93
018-Zir13	0.62374	91202.77	0.02	0.06535	1126.43	1.17727	98.28	0.13064	621.62	0.70	785.71	30.77	791.52	12.09	790.04	12.67	-0.74
053-Zir39	0.49970	101899.54	0.03	0.06487	1165.77	1.06947	110.19	0.11956	689.47	0.70	770.12	31.68	728.04	11.35	738.48	12.33	5.46
016-Zir11	0.61278	95979.32	0.02	0.06597	1216.23	1.12812	106.92	0.12402	661.93	0.68	805.28	33.41	753.68	11.67	766.86	12.94	6.41
054-Zir40	0.56311	59498.32	0.03	0.06587	1087.72	1.07665	114.51	0.11854	786.52	0.76	802.21	29.87	722.15	12.73	742.00	12.94	9.98
019-Zir14	0.72258	197610.25	0.02	0.06470	1205.89	1.13319	109.62	0.12703	702.82	0.72	764.46	32.71	770.87	12.97	769.27	13.36	-0.84
033-Zir24	0.32488	58735.18	0.03	0.06529	1381.28	1.13622	111.90	0.12621	646.52	0.64	783.70	37.66	766.18	11.78	770.71	13.69	2.24
046-Zir34	0.53254	38342.27	0.06	0.06573	1299.22	1.09763	117.10	0.12111	731.88	0.69	797.65	35.60	736.96	12.34	752.20	13.61	7.61
027-Zir20	0.92419	73868.69	0.02	0.06599	1151.51	1.16630	113.47	0.12817	794.41	0.77	806.18	31.65	777.40	14.90	784.91	14.42	3.57
034-Zir25	0.41022	95249.38	0.03	0.06520	970.79	1.17879	112.64	0.13112	844.11	0.83	780.69	26.49	794.27	16.53	790.75	14.54	-1.74
036-Zir27	0.53639	83354.14	0.02	0.06516	1121.29	1.15880	114.65	0.12898	811.00	0.79	779.44	30.57	782.02	15.40	781.39	14.43	-0.33
026-Zir19	0.13130	78529.19	0.01	0.06439	1461.81	0.99232	138.48	0.11177	832.20	0.68	754.41	39.48	683.00	12.05	699.91	13.85	9.47
029-Zir22	0.38175	68651.46	0.02	0.06565	1336.63	1.12303	123.79	0.12406	816.18	0.73	795.20	36.59	753.89	14.40	764.43	14.88	5.20
045-Zir33	0.30912	34030.34	0.06	0.06492	1627.71	1.10012	133.51	0.12289	773.35	0.65	771.85	44.17	747.16	13.40	753.41	15.56	3.20
038-Zir29	1.44402	240330.55	0.01	0.06506	793.46	1.02969	148.65	0.11478	1213.14	0.91	776.17	21.64	700.47	18.47	718.77	15.71	9.75
043-Zir31	0.41214	50691.77	0.07	0.06520	1676.96	1.14671	135.21	0.12754	811.48	0.67	780.92	45.63	773.81	15.08	775.69	16.75	0.91
028-Zir21	0.26674	45036.45	0.03	0.06440	1782.68	1.16279	144.26	0.13095	890.14	0.69	754.70	48.09	793.27	17.39	783.26	18.23	-5.11
024-Zir17	0.12695	70760.89	0.03	0.06484	1434.64	0.43583	410.64	0.04875	3043.00	0.83	769.12	38.93	306.82	8.89	367.31	11.00	60.11
007-Zir04	0.55017	73388.14	0.02	0.06549	1506.51	1.12097	161.75	0.12413	1188.58	0.81	790.15	41.14	754.30	20.99	763.44	19.37	4.54
050-Zir38	0.76730	31325.30	0.06	0.06451	2126.14	1.07136	185.37	0.12045	1152.14	0.70	758.31	57.34	733.13	19.22	739.41	20.75	3.32
069-Zir53	0.47080	28059.69	0.06	0.06358	2311.67	1.14611	187.77	0.13073	1168.53	0.71	727.72	61.71	792.01	22.75	775.40	23.21	-8.83
063-Zir47	0.33974	44042.85	0.06	0.06526	1683.24	1.40817	154.39	0.15649	1175.27	0.85	782.64	45.82	937.26	32.05	892.39	25.65	-19.76
004-Zir01	0.75172	84461.68	0.02	0.06324	1690.65	0.99025	226.86	0.11355	1709.00	0.86	716.42	45.09	693.35	25.49	698.85	22.57	3.22
008-Zir05	0.49123	42937.56	0.03	0.06508	2355.91	1.11268	212.29	0.12398	1418.11	0.74	777.07	63.84	753.44	24.98	759.46	25.11	3.04
068-Zir52	0.37678	127192.54	0.06	0.06607	1885.58	1.10498	216.81	0.12128	1659.30	0.84	808.74	51.71	737.92	28.03	755.76	25.38	8.76
049-Zir37	2.54544	36362.57	0.05	0.06497	2694.20	1.02369	259.73	0.11427	1721.13	0.74	773.31	72.82	697.50	25.98	715.77	27.13	9.80
015-Zir10	0.25016	21835.55	0.07	0.06330	3098.55	1.10364	245.23	0.12644	1445.53	0.68	718.33	82.20	767.54	26.42	755.11	28.63	-6.85
056-Zir42	0.32841	24845.61	0.07	0.06616	2725.64	1.15672	236.09	0.12679	1590.82	0.74	811.47	74.54	769.54	29.23	780.41	29.53	5.17
020-Zir15	0.51958	26892.48	0.07	0.06680	3024.20	1.19101	244.57	0.12930	1597.46	0.71	831.59	83.12	783.87	30.45	796.43	31.90	5.74
055-Zir41	0.33842	23055.67	0.06	0.06428	3470.75	1.10263	264.32	0.12439	1477.71	0.63	750.99	92.85	755.79	26.19	754.62	30.80	-0.64
005-Zir02	0.15707	151953.56	0.02	0.06446	2140.80	0.55117	531.20	0.06201	4121.08	0.87	756.79	57.70	387.83	19.22	445.76	21.02	48.75
014-Zir09	0.60106	76490.49	0.04	0.06497	1311.75	0.46733	631.53	0.05217	5369.90	0.95	773.35	35.66	327.80	17.89	389.34	19.00	57.61

Sample aba-ax-07												Aperant Ages						
Zircon	Th/U	$^{206}Pb/^{204}Pb$	1σ%	$^{207}Pb/^{206}Pb$	1σ %	$^{207}Pb/^{235}U$	1σ %	$^{206}Pb/^{238}U$	1σ %	Rho	$^{207}Pb/^{206}Pb$	2σ abs	$^{206}Pb/^{238}U$	2σ abs	$^{207}Pb/^{235}U$	2σ abs	Conc %
067-ZR47	0.39924	91742.55	16.22	0.19758	1.24	13.27758	1.95	0.48734	1.46	0.75	2806.35	40.31	2559.16	61.39	2699.59	36.49	8.81
061-ZR44	0.18711	64008.27	17.26	0.12005	1.59	5.50537	2.46	0.33258	1.85	0.75	1956.96	56.11	1850.86	59.25	1901.43	41.87	5.42
075-ZR53	0.32162	145676.33	10.24	0.10667	1.18	4.12377	2.00	0.28037	1.57	0.79	1743.23	43.05	1593.22	44.30	1659.03	32.46	8.60
079-ZR57	0.37098	64315.23	11.06	0.09156	1.25	3.21221	1.80	0.25443	1.24	0.69	1458.26	47.20	1461.28	32.27	1460.11	27.64	-0.21
009-ZR6	0.20391	36526.21	17.00	0.08174	1.56	2.37494	2.10	0.21072	1.37	0.65	1239.20	60.40	1232.65	30.66	1235.09	29.86	0.53
046-ZR31	0.19935	610113.94	90.90	0.08271	1.04	2.33334	1.70	0.20459	1.29	0.76	1262.43	40.37	1199.91	28.14	1222.50	23.96	4.95
060-ZR43	0.25654	25105.52	18.95	0.08027	2.24	2.11012	3.23	0.19064	2.29	0.71	1203.63	86.94	1124.86	47.24	1152.12	43.96	6.54
039-ZR27	0.18493	84875.82	13.86	0.07511	0.98	1.90963	1.60	0.18439	1.21	0.76	1071.37	39.19	1090.91	24.29	1084.46	21.25	-1.82
020-ZR15	0.37977	27351.65	15.26	0.07615	2.29	1.73321	3.20	0.16505	2.20	0.69	1099.12	90.26	984.80	40.10	1020.94	40.74	10.40
040-ZR28	0.10897	60387.14	14.72	0.07618	1.48	1.66397	2.11	0.15841	1.46	0.69	1099.72	58.59	947.95	25.77	994.89	26.62	13.80
032-ZR22	0.35952	64030.38	15.40	0.06881	1.33	1.41614	2.15	0.14925	1.64	0.76	893.06	54.54	896.77	27.44	895.74	25.38	-0.42
058-ZR41	0.05244	56150.17	13.47	0.07051	1.27	1.44500	2.13	0.14862	1.67	0.78	943.32	51.48	893.20	27.77	907.80	25.35	5.31
008-ZR5	0.27120	13204.89	15.41	0.06883	3.41	1.39302	4.57	0.14677	3.02	0.66	893.64	137.56	882.85	49.81	885.98	53.32	1.21
016-ZR11	0.11380	37284.15	22.90	0.07212	1.71	1.44878	2.33	0.14569	1.53	0.66	989.20	68.96	876.78	25.08	909.37	27.78	11.37
036-ZR24	0.13332	53607.23	17.00	0.07548	1.30	1.49835	2.23	0.14395	1.77	0.79	1081.44	51.91	866.98	28.64	929.72	26.95	19.83
062-ZR45	0.08725	27946.31	19.07	0.06662	1.87	1.29343	2.59	0.14081	1.75	0.68	825.81	76.96	849.23	27.88	842.82	29.43	-2.84
028-ZR18	0.68132	123173.39	18.35	0.06550	0.65	1.25908	1.16	0.13940	0.89	0.76	790.52	27.32	841.27	13.98	827.50	13.11	-6.42
027-ZR17	0.20716	102019.41	18.01	0.06508	0.65	1.21573	1.19	0.13547	0.92	0.78	777.01	27.17	818.99	14.19	807.82	13.19	-5.40
004-ZR1	0.17750	59137.86	21.12	0.06511	1.36	1.21149	2.02	0.13494	1.45	0.72	777.87	56.60	815.99	22.28	805.88	22.40	-4.90
017-ZR12	0.13374	49614.17	22.47	0.06576	1.10	1.21931	1.79	0.13446	1.36	0.76	798.85	45.71	813.26	20.73	809.46	19.82	-1.80
030-ZR20	0.52562	17730.83	16.91	0.06530	2.37	1.21034	3.20	0.13441	2.12	0.66	784.15	97.99	812.98	32.38	805.35	35.30	-3.68
015-ZR10	0.33254	21300.44	17.46	0.06432	3.27	1.19155	4.23	0.13435	2.65	0.63	752.14	135.22	812.64	40.43	796.68	46.15	-8.04
026-ZR16	0.18942	102840.58	23.05	0.06549	0.71	1.21239	1.10	0.13425	0.76	0.68	790.16	29.84	812.08	11.52	806.29	12.24	-2.77
029-ZR19	0.15185	92519.83	18.41	0.06497	0.91	1.19977	1.41	0.13392	1.02	0.72	773.38	37.92	810.19	15.54	800.48	15.61	-4.76
007-ZR4	0.17499	42723.99	20.06	0.06520	1.32	1.19739	1.92	0.13318	1.34	0.70	780.91	54.85	805.97	20.35	799.38	21.11	-3.21
037-ZR25	0.07772	54830.68	11.47	0.06572	1.50	1.20524	2.23	0.13300	1.61	0.72	797.41	62.37	804.96	24.37	803.00	24.65	-0.95
013-ZR8	0.10201	56129.84	17.14	0.06613	1.33	1.21051	1.93	0.13274	1.34	0.70	810.64	55.19	803.48	20.30	805.43	21.32	0.88
014-ZR9	0.07857	26902.03	13.50	0.06501	2.45	1.18975	3.23	0.13272	2.07	0.64	774.65	101.23	803.37	31.26	795.84	35.29	-3.71
066-ZR46	0.08807	44140.00	14.83	0.06655	1.60	1.21590	2.30	0.13249	1.61	0.70	823.87	66.12	802.06	24.22	807.90	25.45	2.65
057-ZR40	0.12927	29784.18	13.76	0.06530	1.47	1.18942	2.20	0.13210	1.59	0.72	783.99	61.21	799.82	23.90	795.69	24.11	-2.02
031-ZR21	0.10510	55387.28	13.72	0.06489	1.41	1.18092	1.94	0.13199	1.28	0.66	770.62	58.74	799.21	19.22	791.74	21.21	-3.71
059-ZR42	0.06186	37087.15	16.08	0.06616	1.64	1.19186	2.36	0.13064	1.65	0.70	811.51	67.76	791.53	24.59	796.82	25.85	2.46
019-ZR14	0.10787	30852.90	16.98	0.06530	1.86	1.17472	2.52	0.13047	1.66	0.66	783.86	77.33	790.56	24.65	788.85	27.47	-0.85
082-ZR60	0.07734	49435.74	9.74	0.06494	1.97	1.16808	2.80	0.13045	1.96	0.70	772.30	81.68	790.44	29.13	785.75	30.41	-2.35
069-ZR49	0.10332	47897.36	14.64	0.06586	1.39	1.18124	2.03	0.13006	1.44	0.71	802.05	57.65	788.23	21.34	791.89	22.25	1.72
047-ZR32	0.14060	109357.54	12.73	0.06586	1.08	1.17957	1.63	0.12990	1.17	0.71	801.79	44.92	787.27	17.26	791.11	17.85	1.81
042-ZR30	0.09837	45797.46	18.09	0.06601	1.58	1.18071	2.18	0.12973	1.46	0.67	806.54	65.30	786.31	21.66	791.65	23.86	2.51
081-ZR59	0.33197	31125.95	11.28	0.06552	2.12	1.16870	2.91	0.12936	1.96	0.67	791.03	87.76	784.22	28.96	786.04	31.64	0.86
070-ZR50	0.11103	24316.84	16.55	0.06827	2.09	1.21445	2.89	0.12900	1.96	0.68	876.90	85.29	782.15	28.78	807.23	31.88	10.81
071-ZR51	0.07150	33994.43	14.74	0.06691	1.83	1.18487	2.66	0.12842	1.90	0.71	835.07	75.34	778.83	27.84	793.58	29.12	6.73
035-ZR23	0.14672	56641.89	18.02	0.06489	1.32	1.14263	2.07	0.12769	1.55	0.75	770.87	55.09	774.70	22.56	773.76	22.26	-0.50
078-ZR56	0.23945	22836.57	15.61	0.06760	2.65	1.18978	3.59	0.12764	2.39	0.67	856.35	108.30	774.38	34.82	795.86	39.23	9.57
010-ZR7	0.16105	37142.60	11.95	0.06704	2.21	1.17937	2.97	0.12757	1.95	0.66	839.16	90.58	773.99	28.42	791.02	32.36	7.77
006-ZR3	0.11677	5849.27	33.00	0.07334	1.99	1.28921	2.54	0.12748	1.54	0.61	1023.43	79.46	773.46	22.39	840.95	28.85	24.42
018-ZR13	0.07519	37101.97	15.21	0.06679	1.46	1.17386	2.37	0.12747	1.82	0.77	831.10	60.44	773.40	26.56	788.45	25.80	6.94
048-ZR33	0.12929	39099.82	16.64	0.06662	1.45	1.17086	2.12	0.12745	1.51	0.71	826.02	59.85	773.31	21.98	787.05	23.13	6.38
041-ZR29	0.29656	49079.34	15.67	0.06659	1.31	1.16588	2.06	0.12698	1.55	0.75	824.83	54.25	770.62	22.50	784.71	22.43	6.57
050-ZR35	0.08739	52504.05	13.05	0.06526	1.64	1.13625	2.38	0.12626	1.67	0.71	782.83	68.30	766.51	24.18	770.73	25.50	2.08
072-ZR52	0.08519	24395.24	18.86	0.06749	2.42	1.17076	3.34	0.12580	2.27	0.68	852.94	99.01	763.88	32.60	787.00	36.22	10.44
056-ZR39	0.07964	54522.92	17.83	0.06701	1.50	1.15623	2.24	0.12512	1.62	0.72	838.22	61.83	759.99	23.20	780.18	24.23	9.33
080-ZR58	0.11385	28827.39	14.28	0.06578	2.27	1.13466	3.17	0.12509	2.19	0.69	799.51	93.52	759.77	31.33	769.97	33.95	4.97
049-ZR34	0.06967	30623.71	15.06	0.06717	1.54	1.14947	2.28	0.12410	1.64	0.72	843.08	63.43	754.14	23.25	776.99	24.57	10.55
076-ZR54	0.25005	74049.62	30.42	0.06606	1.27	1.12666	2.26	0.12368	1.84	0.81	808.42	52.70	751.70	26.06	766.16	24.22	7.02
077-ZR55	0.08559	53512.44	29.87	0.06805	1.79	1.15365	2.73	0.12295	2.03	0.74	870.02	73.41	747.51	28.65	778.96	29.53	14.08
038-ZR26	0.23627	31861.25	20.03	0.06238	1.91	1.03969	2.68	0.12087	1.85	0.69	687.12	80.28	735.59	25.68	723.76	27.56	-7.05
005-ZR2	0.08212	65792.31	16.66	0.06289	1.07	1.04241	1.70	0.12020	1.26	0.74	704.52	45.31	731.74	17.41	725.11	17.49	-3.86
052-ZR37	0.10077	59906.89	40.49	0.06787	2.02	1.09338	2.91	0.11683	2.06	0.71	864.67	82.76	712.28	27.72	750.15	30.62	17.62

Sample aba-ax-08												Aperant Ages						
Zircon	Th/U	$^{206}Pb/^{204}Pb$	1σ%	$^{207}Pb/^{206}Pb$	1σ %	$^{207}Pb/^{235}U$	1σ %	$^{206}Pb/^{238}U$	1σ %	Rho	$^{207}Pb/^{206}Pb$	2σ abs	$^{206}Pb/^{238}U$	2σ abs	$^{207}Pb/^{235}U$	2σ abs	Conc %
044-ZR31	0.31280	96250.01	15.50	0.30220	1.60	28.12983	2.46	0.67506	1.82	0.74	3481.53	49.17	3325.37	94.37	3423.63	47.59	4.49
075-ZR53	0.08581	102221.21	12.66	0.22462	2.23	17.66412	3.02	0.57032	2.01	0.66	3014.07	70.73	2909.14	93.76	2971.62	57.32	3.48
081-ZR59	0.34609	49390.19	15.77	0.10370	2.21	4.09579	3.12	0.28643	2.17	0.70	1691.38	80.44	1623.68	62.16	1653.46	50.30	4.00
005-ZR2	0.04280	271164.89	15.10	0.09214	0.76	3.17690	1.43	0.25004	1.16	0.81	1470.30	28.56	1438.70	29.91	1451.56	22.03	2.15
067-ZR47	0.52399	90186.32	8.21	0.08582	1.53	2.59335	2.54	0.21915	1.99	0.78	1334.09	58.68	1277.40	46.14	1298.76	36.92	4.25
058-ZR41	0.40269	41437.22	12.77	0.07647	1.69	1.86763	2.40	0.17711	1.66	0.69	1107.53	66.85	1051.16	32.10	1069.69	31.45	5.09
049-ZR36	0.12663	47327.80	13.84	0.08091	1.80	1.79154	2.56	0.16058	1.77	0.69	1219.20	70.01	960.02	31.62	1042.39	33.04	21.26
015-ZR10	0.11174	31014.31	15.12	0.06604	1.51	1.24367	2.31	0.13657	1.71	0.74	807.76	62.47	825.21	26.43	820.54	25.82	-2.16
010-ZR7	0.14099	29817.51	17.09	0.06631	2.05	1.24105	2.74	0.13572	1.77	0.65	816.32	84.68	820.42	27.27	819.36	30.56	-0.50
020-ZR15	0.12376	59204.11	17.22	0.06585	1.82	1.22113	2.35	0.13448	1.44	0.61	801.74	75.21	813.35	21.97	810.29	26.04	-1.45
016-ZR11	0.11722	92142.90	15.14	0.06572	1.07	1.21614	1.59	0.13421	1.12	0.70	797.35	44.65	811.82	17.08	808.01	17.69	-1.81
039-ZR29	0.41241	31803.01	43.25	0.06500	2.99	1.19949	3.97	0.13384	2.59	0.65	774.20	123.22	809.72	39.30	800.35	43.48	-4.59
061-ZR44	0.22247	26459.85	18.60	0.06779	2.06	1.25099	2.81	0.13383	1.88	0.67	862.21	84.17	809.66	28.62	823.85	31.49	6.10
070-ZR50	0.09799	36671.63	11.82	0.06588	2.72	1.21265	3.78	0.13349	2.59	0.69	802.51	111.95	807.77	39.29	806.41	41.59	-0.66
018-ZR13	0.18971	36955.75	21.11	0.06473	1.54	1.19003	2.02	0.13334	1.26	0.62	765.41	64.24	806.88	19.03	795.98	22.18	-5.42
009-ZR6	0.13589	33347.22	15.83	0.06823	1.91	1.25170	2.74	0.13304	1.93	0.70	875.63	77.98	805.17	29.12	824.17	30.65	8.05
024-ZR16	0.10957	24902.01	12.09	0.06489	2.21	1.18802	2.97	0.13277	1.95	0.66	770.87	91.56	803.63	29.47	795.04	32.48	-4.25
047-ZR34	0.11697	24995.20	16.57	0.06659	2.20	1.21463	2.98	0.13228	1.98	0.66	825.06	90.38	800.84	29.84	807.31	32.96	2.94
037-ZR27	0.12382	35398.24	15.01	0.06629	2.00	1.20872	2.78	0.13223	1.89	0.68	815.55	82.41	800.60	28.46	804.60	30.62	1.83
019-ZR14	0.08512	50792.86	12.82	0.06611	1.50	1.20131	2.04	0.13178	1.33	0.65	809.96	62.29	797.99	19.90	801.19	22.48	1.48
068-ZR48	0.14633	41887.18	10.09	0.06543	2.15	1.18838	3.33	0.13173	2.52	0.76	788.06	88.84	797.71	37.69	795.21	36.36	-1.22
056-ZR39	0.14112	28589.00	11.81	0.06423	2.06	1.16616	3.03	0.13167	2.20	0.72	749.20	85.68	797.39	32.92	784.85	32.88	-6.43
038-ZR28	0.10050	48588.78	14.62	0.06549	1.85	1.18579	2.69	0.13132	1.92	0.71	790.01	76.54	795.37	28.63	794.00	29.38	-0.68
007-ZR4	0.06931	58772.27	14.73	0.06643	1.12	1.19964	1.78	0.13096	1.33	0.75	820.10	46.34	793.31	19.88	800.42	19.60	3.27
029-ZR21	0.12235	45927.52	14.85	0.06572	1.46	1.18645	2.28	0.13093	1.72	0.75	797.40	60.42	793.16	25.64	794.31	25.00	0.53
048-ZR35	0.31184	21894.20	13.54	0.06857	2.47	1.23290	3.29	0.13039	2.15	0.65	885.97	100.43	790.07	31.87	815.66	36.58	10.82
013-ZR8	0.16904	69222.13	16.97	0.06684	1.24	1.20108	2.14	0.13031	1.70	0.80	832.92	51.11	789.63	25.26	801.09	23.52	5.20
050-ZR37	0.10821	20371.38	17.79	0.06628	2.43	1.18857	3.37	0.13005	2.31	0.69	815.21	99.82	788.15	34.20	795.30	36.82	3.32
069-ZR49	0.18466	25210.00	9.35	0.06764	3.04	1.21272	4.35	0.13001	3.09	0.71	857.69	123.83	787.95	45.79	806.44	47.89	8.13
079-ZR57	0.32324	12605.12	12.25	0.06506	3.30	1.16555	4.45	0.12992	2.97	0.67	776.34	135.83	787.40	43.90	784.56	48.09	-1.42
060-ZR43	0.11696	38348.02	14.30	0.06661	1.83	1.19128	2.46	0.12970	1.60	0.65	825.59	75.42	786.16	23.72	796.55	26.99	4.78
028-ZR20	0.08731	44822.47	16.70	0.06585	1.22	1.17620	1.89	0.12954	1.39	0.74	801.57	50.68	785.24	20.61	789.54	20.63	2.04
082-ZR60	0.19817	17054.00	16.25	0.06820	3.18	1.21617	4.30	0.12932	2.87	0.67	874.66	129.11	783.99	42.35	808.02	47.41	10.37
036-ZR26	0.16579	25671.64	19.23	0.06447	1.96	1.14812	2.90	0.12915	2.11	0.73	757.04	81.47	783.03	31.02	776.35	31.21	-3.43
076-ZR54	0.18318	33653.43	20.60	0.06561	2.90	1.16817	3.96	0.12912	2.68	0.68	794.00	119.26	782.84	39.46	785.79	42.93	1.40
034-ZR24	0.19921	55818.72	18.24	0.06806	1.15	1.21140	2.14	0.12907	1.76	0.82	870.51	47.31	782.58	25.95	805.84	23.63	10.10
006-ZR3	0.15336	64811.48	13.48	0.06571	1.05	1.16720	1.72	0.12882	1.30	0.76	797.13	43.85	781.13	19.15	785.34	18.68	2.01
026-ZR18	0.57514	2191.69	9.41	0.07141	1.53	1.26249	2.04	0.12821	1.29	0.63	969.24	61.97	777.65	18.91	829.03	22.98	19.77
071-ZR51	0.13526	23208.66	9.63	0.06673	3.23	1.16688	4.27	0.12682	2.76	0.65	829.32	132.03	769.68	40.03	785.18	46.16	7.19
059-ZR42	0.32095	18546.11	11.04	0.06880	2.42	1.19222	3.59	0.12568	2.63	0.73	892.62	98.32	763.17	37.82	796.99	39.30	14.50
035-ZR25	0.06617	44158.04	19.37	0.06692	1.22	1.13347	2.09	0.12284	1.65	0.79	835.24	50.47	746.87	23.28	769.41	22.40	10.58
072-ZR52	0.25702	43937.85	16.92	0.06506	2.94	1.10091	3.82	0.12271	2.40	0.63	776.31	121.37	746.17	33.82	753.79	40.21	3.88
025-ZR17	0.73016	5891.46	41.80	0.06417	3.55	0.99273	4.15	0.11219	2.12	0.51	747.38	146.63	685.43	27.48	700.11	41.56	8.29

Appendix 2.3. Summary of in situ Lu/Hf data.

	Age					$^{176}Hf/^{177}Hf$		εHf	T_{DM}
sample	(Ma)	$^{176}Hf/^{177}Hf$	±2SE	$^{176}Lu/^{177}Hf$	±2SE	(t)	±2SE	(t)	(Ga)
aba-08									
zir 13	792	0.282676	0.000029	0.001596	0.000078	0.282653	0.839541	13.03	0.82
zir 14	771	0.282657	0.000031	0.001191	0.000039	0.282640	0.597475	12.13	0.84
zir 23	762	0.282679	0.000036	0.001176	0.000063	0.282662	0.857754	12.71	0.81
zir 24	766	0.282672	0.000029	0.001387	0.000014	0.282652	0.314835	12.43	0.82
zir 25	794	0.282747	0.000056	0.003451	0.000097	0.282696	0.716923	14.62	0.76
zir 26	780	0.282667	0.000042	0.002031	0.000024	0.282637	0.297481	12.22	0.84
zir 27	782	0.282766	0.000058	0.005747	0.000090	0.282682	0.491239	13.85	0.78
zir 41	756	0.282763	0.000073	0.001347	0.000140	0.282744	2.158641	15.45	0.69
aba-ax-06									
zir 1	2112	0.281383	0.000039	0.000462	0.000004	0.281364	0.036413	-2.47	2.55
zir 8	800	0.282042	0.000035	0.001677	0.000069	0.282017	0.530052	-9.30	1.71
zir 29	2200	0.281203	0.000045	0.000524	0.000002	0.281181	0.071770	-6.93	2.79
zir 25	2352	0.281480	0.000052	0.001238	0.000007	0.281424	0.064749	5.24	2.47
zir 22	2093	0.281496	0.000043	0.000888	0.000016	0.281460	0.013953	0.49	2.42
zir 21	1023	0.282278	0.000054	0.002183	0.000030	0.282236	0.151627	3.49	1.40
zir 17	1335	0.282186	0.000042	0.001425	0.000006	0.282150	0.111843	7.54	1.50
zir 18	2198	0.281496	0.000044	0.017383	0.000155	0.280768	0.331518	-21.67	4.22
zir 30	797	0.282684	0.000040	0.001151	0.000044	0.282667	0.772480	13.66	0.80
zir 13	843	0.282229	0.000043	0.001649	0.000070	0.282203	0.096608	-1.72	1.45
zir 9	798	0.282163	0.000041	0.001967	0.000057	0.282134	0.222770	-5.21	1.56
zir 3	782	0.282049	0.000036	0.001329	0.000062	0.282030	0.570243	-9.26	1.69
aba-11									
zir 7	793	0.282694	0.000050	0.002102	0.000015	0.282663	0.275172	13.41	0.81
zir 12	778	0.282683	0.000046	0.001945	0.000065	0.282655	0.596507	12.80	0.82
zir 16	772	0.282662	0.000060	0.003274	0.000122	0.282615	0.583077	11.25	0.88
zir 15	768	0.282708	0.000041	0.002108	0.000005	0.282678	0.241428	13.38	0.79
zir 14	761	0.282689	0.000037	0.001891	0.000023	0.282662	0.299843	12.68	0.81
zir 17	778	0.282699	0.000081	0.002770	0.000063	0.282659	0.476201	12.93	0.81
zir 19	769	0.282596	0.000076	0.002646	0.000152	0.282558	0.697682	9.16	0.96
zir 23	776	0.282650	0.000061	0.003169	0.000041	0.282604	0.331617	10.94	0.89
zir 35	791	0.282672	0.000046	0.000964	0.000013	0.282658	0.395216	13.21	0.81
S9B									
zir 34	789	0.282816	0.000067	0.002672	0.000178	0.282776	1.458012	17.36	0.64
zir 43	803	0.282695	0.000038	0.002243	0.000017	0.282661	0.436882	13.60	0.81
zir 40	804	0.282718	0.000043	0.003747	0.000067	0.282661	0.519871	13.63	0.81
zir 1	752	0.282755	0.000035	0.001298	0.000060	0.282736	1.093810	15.11	0.70
zir 4	787	0.282747	0.000042	0.003170	0.000201	0.282700	1.220770	14.59	0.75
zir 31	765	0.282607	0.000040	0.002042	0.000034	0.282577	0.462607	9.75	0.93
zir 33	760	0.282660	0.000033	0.001546	0.000093	0.282638	0.982479	11.80	0.84
zir 34	789	0.282629	0.000040	0.002848	0.000051	0.282587	0.375296	10.66	0.92
zir 18	785	0.282702	0.000034	0.001898	0.000011	0.282674	0.371775	13.64	0.79
zir 35	763	0.282681	0.000032	0.000854	0.000043	0.282669	0.952249	12.95	0.80
zir 49	788	0.282741	0.000045	0.001855	0.000036	0.282713	0.964292	15.11	0.73
zir 51	778	0.282726	0.000046	0.002813	0.000201	0.282685	1.208028	13.89	0.77
zir 58	796	0.282776	0.000030	0.002597	0.000028	0.282737	0.453995	16.11	0.70
zir 56	785	0.282805	0.000035	0.002781	0.000020	0.282764	0.354145	16.82	0.66
zir 54	752	0.282692	0.000048	0.002771	0.000136	0.282653	0.796369	12.15	0.82
zir 62	766	0.282774	0.000030	0.002511	0.000087	0.282738	0.810493	15.50	0.70
zir 64	800	0.282828	0.000055	0.002728	0.000035	0.282787	0.704872	17.98	0.62
zir 67	766	0.282830	0.000044	0.002719	0.000026	0.282791	0.700207	17.37	0.62

	Age					$^{176}Hf/^{177}Hf$		εHf	T_{DM}
sample	(Ma)	$^{176}Hf/^{177}Hf$	±2SE	$^{176}Lu/^{177}Hf$	±2SE	(t)	±2SE	(t)	(Ga)
S9A									
zir 2	790	0.282802	0.000044	0.002735	0.000046	0.282761	0.572454	16.84	0.66
zir 3	789	0.282930	0.000024	0.002279	0.000101	0.282897	1.284430	21.62	0.47
zir 5	723	0.282797	0.000036	0.002695	0.000027	0.282760	0.696584	15.30	0.67
zir 6	779	0.282751	0.000023	0.000561	0.000021	0.282743	0.858632	15.96	0.69
zir 9	766	0.282748	0.000039	0.001530	0.000032	0.282726	0.599584	15.05	0.72
zir 11	770	0.282861	0.000035	0.002312	0.000011	0.282828	0.427837	18.75	0.57
zir 12	769	0.282867	0.000030	0.003064	0.000040	0.282823	0.480261	18.56	0.57
zir 13	775	0.282827	0.000054	0.001765	0.000091	0.282801	1.190391	17.93	0.61
zir 22	754	0.282798	0.000045	0.001455	0.000057	0.282777	0.917519	16.59	0.65
zir 23	750	0.283010	0.000069	0.001520	0.000056	0.282989	1.215755	23.99	0.34
zir 24	770	0.282990	0.000039	0.003424	0.000076	0.282941	0.864614	22.75	0.39
zir 15	772	0.282724	0.000036	0.002706	0.000012	0.282685	0.271310	13.73	0.77
zir 33	783	0.282683	0.000041	0.001287	0.000015	0.282664	0.349554	13.25	0.80
zir 31	757	0.282827	0.000035	0.003203	0.000010	0.282781	0.391971	16.80	0.63
zir 39	793	0.282822	0.000045	0.002473	0.000006	0.282785	0.358903	17.76	0.63
aba-ax-07									
zir 8	803	0.282151	0.000040	0.001722	0.000025	0.282125	0.217066	-5.41	1.57
zir 16	812	0.282139	0.000041	0.001907	0.000080	0.282110	0.321103	-5.72	1.59
zir 14	791	0.281887	0.000038	0.001423	0.000045	0.281866	0.932513	-14.87	1.92
zir 6	1239	0.282013	0.000035	0.000978	0.000004	0.281990	0.015286	-0.29	1.72
zir 5	883	0.282050	0.000039	0.001285	0.000051	0.282029	0.677451	-7.02	1.69
zir 27	1071	0.282196	0.000037	0.000905	0.000017	0.282178	0.142095	2.55	1.47
zir 20	813	0.282100	0.000041	0.001304	0.000022	0.282080	0.385369	-6.77	1.62
zir 21	799	0.282098	0.000038	0.001364	0.000026	0.282077	0.308620	-7.18	1.62
zir 22	897	0.282050	0.000058	0.000981	0.000007	0.282033	0.247128	-6.54	1.67
zir 46	802	0.282030	0.000037	0.001434	0.000039	0.282009	0.549629	-9.54	1.72
zir 49	788	0.282144	0.000040	0.001494	0.000019	0.282122	0.233509	-5.83	1.56
zir 57	1458	0.282102	0.000052	0.002242	0.000004	0.282040	0.221882	6.46	1.66
zir 59	784	0.282144	0.000029	0.001349	0.000019	0.282124	0.298952	-5.87	1.56
zir 60	790	0.282146	0.000044	0.001461	0.000014	0.282125	0.263650	-5.70	1.56
zir 53	3014	0.281670	0.000044	0.000730	0.000016	0.281628	1.296494	28.05	2.18
aba-ax-08									
zir 52	746	0.281993	0.000050	0.001275	0.000033	0.281975	0.857295	-11.99	1.76
zir 37	788	0.282101	0.000037	0.002433	0.000073	0.282065	0.578156	-7.85	1.67
zir 14	798	0.282142	0.000051	0.001510	0.000025	0.282119	0.236529	-5.72	1.57
zir 11	812	0.282149	0.000038	0.001772	0.000035	0.282122	0.217461	-5.31	1.57
zir 20	785	0.282195	0.000041	0.001975	0.000050	0.282166	0.224815	-4.36	1.51
zir 10	825	0.282008	0.000061	0.003185	0.000206	0.281959	1.044312	-10.79	1.84
zir 7	820	0.282232	0.000051	0.002653	0.000072	0.282191	0.160712	-2.65	1.49
zir 2	1439	0.281922	0.000040	0.000886	0.000009	0.281897	0.030194	0.97	1.84
zir 3	781	0.281983	0.000038	0.002093	0.000064	0.281952	0.661605	-12.01	1.82

Appendix 2.4 Summary of whole rock Sm/Nd data.

sample	Sm(ppm)	Nd(ppm)	147Sm/144Nd	143Nd/144Nd	T (Ma)	εNd (T)	TDM
aba-001	41.220	123.748	0.2014	0.512966+/-2	756.7	+ 5.95	-
aba-006	0.424	1.283	0.1996	0.513056+/-14	756.7	+ 7.89	-
aba-008	9.597	27.562	0.2105	0.513005+/-3	756.7	+ 5.83	-
aba-011	1.448	4.188	0.2090	0.512994+/-5	756.7	+ 5.77	-
S9A	1.070	2.971	0.2177	0.512977+/-18	756.7	+ 4.59	-
aba-012	2.864	7.910	0.2189	0.513148+/-4	800	+ 7.70	-
aba-ax-06	2.721	7.415	0.2218	0.513157+/-13	800	+ 7.57	2.18
aba-ax-07	9.219	46.241	0.1205	0.511894+/-16	638	- 8.31	1.83
aba-ax-08	5.221	20.995	0.1503	0.512080+/-14	638	- 8.16	2.36
aba-ax-10	2.578	7.315	0.2130	0.513055+/-13	800	+ 6.48	3.19
aba-ax-13	1.875	5.159	0.2197	0.513131+/-16	800	+ 7.27	2.24
aba-ax-14	2.046	5.485	0.2255	0.513134+/-7	800	+ 6.75	1.24
aba-ax-15	1.649	4.469	0.2231	0.513133+/-12	800	+ 6.97	1.57

Provenance of Neoproterozoic Ophiolitic Mélange sediments in the Brasilia Belt, central Brazil

Matthew T. Brown[a*], Reinhardt A. Fuck[a], Elton L. Dantas[a]

[a]Laboratory of Geochronolgy, Institute of Geology, University of Brasília, Brasília, Federal District, 70910-900, Brazil

*Corresponding author. E-mail address: brownmt7@gmail.com

Abstract

Mélanges are a chaotic mixture of different rock assemblages that can be associated with orogenic belts and suture zones. The Brasília Belt is a Neoproterozoic orogenic belt in central Brazil, which contains a poorly understood ophiolitic mélange. In order to better understand the sedimentation that was associated with this mélange, isotopic U-Pb and Lu-Hf analyses on single zircon grains, and Sm-Nd on whole rock samples was conducted on mélange metasedimentary rock (garnet-mica-quartz schists and quartzites) and basement (mylonitic granites) assemblages. The quartzite samples have a maximum age of deposition of about 930 Ma, while their negative ε_{Nd} (T) values and T_{DM}, -7.78 to -11.57 and 1.70 to 2.07 Ga, are similar to other metasedimentary rock units interpreted to have formed in a passive margin environment. ε_{Hf} and Hf T_{DM} model values from the quartzite samples range from -12.72 to 8.99 and 2.56 to 1.36 Ga, respectively. The mylonitic granite has an age of ~ 2.1 Ga, ε_{Hf} values ranging from -0.97 to 2.18, and T_{DM} model values ranging from 2.38 and 2.53 Ga, indicating that it was derived from Juvenile Paleoproterozoic basement. Results of the garnet-mica schists reveal that they represent two different rock units, defined by two different periods of sedimentation. The first group of garnet-mica schist has a maximum age of deposition of 672 Ma and ε_{Nd} (T) values and T_{DM} -7.90 to -7.62 and 1.82 to 1.88 Ga, respectively. ε_{Hf} and T_{DM} model values range from -23.50 to 11.69 and 3.23 to 1.45 Ga, respectively, and indicate the presence of similar zircon populations as the passive margin sequence and basement zircon population; there is also a contribution of a younger zircon population derived from older reworked crustal material. The second group is marked by a maximum age of deposition of 616 Ma and ε_{Nd} (T) values and T_{DM} ranging from 0.61 to 0.22 and 1.16 to 1.25 Ga, respectively. ε_{Hf} and T_{DM} model values range from -8.24 to 16.04 and 2.97 to 0.79 Ga, respectively. These results also indicate the presence of passive margin and basement zircon populations, but the younger zircon populations are derived from juvenile sources. The depositional periods of the garnet-mica schists occurred between roughly 800 to 650 Ma and 650 to 600 Ma, and indicate that changes in the tectonic environment present in the Brasília Belt created different depositional environments and basins, which opened, closed and were later dismembered. The quartzites, mylonitic granites and ophiolites most likely represent blocks which were introduced into the mélange by sedimentation or tectonic processes.

Key Words: Mélange; Brasília Belt; Araxá Group; Provenance

3.1 Introduction

The term mélange is used to describe a mapable "chaotic" assemblage of rocks, composed of blocks of rock assemblages of different types and degrees of metamorphism, bound together in a matrix of highly sheared shale or serpentinite (Hsu, 1968; Festa et al., 2010; Shervais et al., 2011; Wakabayashi and Dilek, 2011). Together with ophiolites, mélanges can commonly be found in orogenic belts and are characteristic in identifying ancient sutures zones (Coleman and Irwin, 1974). They are considered to represent the remains of an oceanic basin that no longer exists and contain a record of the evolution and destruction of oceanic lithosphere and are important for our understanding of the evolution of orogenic belts (Gansser, 1974; Dilek, 2006).

Mélanges can be formed by tectonic and/or sedimentary processes. The most classical example of a tectonic mélange forming environment is the accretionary wedge within a subduction zone (Cowen, 1985), however other tectonic environments may also form mélanges, such as strike-slip shear zones and collisional zones (Festa et al., 2010). Sedimentary processes, such as gravity mass movements, including block slides, debris avalanches and debris flows (Lucente and Pini 2003; Festa et al., 2010), are the dominant mechanism for mélange formation and include extensional environments and passive margins, where mass wasting processes can occur.

Several different environments for mélange formation can be created and subsequently destroyed during a collisional event by the several different accompanying tectonic and sedimentary processes. Turbidites accumulated in the trench and/or on the trench slope of the active margin (Okada, 1989; Underwood and Moore, 1995), or on the continental rise of the passive margin along the opposite side of the subducting ocean crust (An et al., 2017), can be involved in mélange formation found in suture zones. Dismembered remnants of syn-collisional sedimentary basins are rare, but where present they can elucidate the short-lived and dynamic interplay of these processes as oceanic subduction complexes give way to arc-continent collision (Bayona et al., 2011; Duffy et al., 2017; Guo et al., 2012; Ryan, 2008; Tate et al., 2014; Zhu et al., 2005). Analysis of these basins from a young orogen might be expected to provide a unique archive

of the rates at which processes of early orogenesis can occur, including the timing and drivers of various tectonic phases (De Smet et al., 1990), the lithological characteristics of the source areas (Floyd et al., 1990), and the relatively undocumented importance of reworking of the shale-dominated mélanges that are a ubiquitous and persistent component of collisional oogenesis (Barber, 2013; Festa et al., 2010).

The Brasília Belt is a Neoproterozoic orogenic belt, which formed during the agglomeration of West Gondwana. The Goiás-Pharusian Ocean was a large ocean which was closed during this process, consumed by the formation of the Goiás Magmatic Arc, which was active almost continuously from 930 to 630 Ma (Pimentel et al., 1999, 2016; Laux et al., 2005; Marques et al., 2017; Fuck et al., 2008, 2017). An ophiolitic mélange is located in the Brasília Belt, and contains mafic and ultramafic, quartzite and mylonitic granite blocks, within a matrix of garnet-mica schists known regionally as Araxá Group. The mélange is poorly understood, due to the lack of geochemical and isotopic data, together with a lack of a definitive and complete stratigraphy.

The collisional events which led to the formation of the Brasília Belt, involved the accreation of island-arcs (Pimentel and Fuck, 1992), but also involved the formation and dissemination of small localized basins. Previous studies of the Araxá Group indicate that it has a bimodal distribution of isotopic Nd (Pimentel et al., 2001, 2011; Piuzana et al., 2003b; Navarro et al., 2013; Falci et al., 2018), which indicates mixing of sediments from different sources. While most attention is focused at ophiolite related blocks, the provenance of quartzite and granite blocks found in the mélange is poorly constrained. While these metasedimentary rocks may represent pre-, syn- and post-collisional sediments, nappe-stacking and thrusting during the formation of the Brasília Belt superimposed and dismembered these deposits.

Examination of several samples of mica schist matrix of the mélange and their basement is conducted in this study, with the goal of determining the age and provenance and tectonic setting of sediment sources present in the ophiolite mélange. In order to do this, LA-ICP-MS U-Pb and Lu-Hf isotopic analyses were conducted on single zircon grains, recovered from samples of rock assemblages, and Sm-Nd isotopic analyses were also conducted on whole rock samples. These

results will be combined with the data from the ophiolite assemblage, in order to develop a model, explaining the evolution of the mélange in the context of the development of the Brasília Belt.

3.2 Geological Background

The Brasília Belt is a Neoproterozoic fold-and-trust belt, located in central Brazil (Fig. 3.1). It was created during the Brasiliano/Pan-African orogeny, by the collision of the São Francisco, Amazonian and Paranapanema cratons. Main features of the belt include a large sedimentary pile, a high-temperature metamorphic belt, an allochthonous block of Archean and Paleoproterozoic rocks and the Neoproterozoic Goiás Magmatic Arc. A Paleoproterozoic block exposed at the northern limit of the Brasília Belt, is considered to represent the basement of the orogenic belt (Fuck et al., 2014, 2017, and references therein). Other examples of these rock assemblages can be found in the Brasília Belt, with the best examples being the Silvânia Sequence and the Jurubatuba Granite, which were described by Fischel et al. (2001).

The sedimentary units of the Brasília Belt are located on the eastern side of the belt, on the western margin of the São Francisco Craton. These sedimentary rocks are interpreted to represent different depositional environments, beginning with passive margin sequences, to fore-arc or back-arc basin, to foreland basin (Pimentel et al., 2001).

The passive margin sequences are composed of the Paranoá, Canastra and Vazante groups. The main evidences are the provenience studies that suggest that these three groups have similar Nd T_{DM} model age values, 2.3 to 0.9 Ga. The Paranoá and Canastra groups are older, with a maximum and minimum age of 1.54 and 1.04 Ga for the deposition of the Paranoá Group (Pimentel et al., 2001, 2011; Matteini et al., 2012). The Vazante Group, on the other hand, has an upper age limit of 0.94 Ga (Rodrigues et al., 2010).

Syn-orogenic basin sequences include the Araxá and Ibiá groups (Pimentel et al., 2001). The Araxá Group is a large metasedimentary rock group composed of various types of mica schists and micaceous quartzites, thought to have been derived from pelitic and other deep

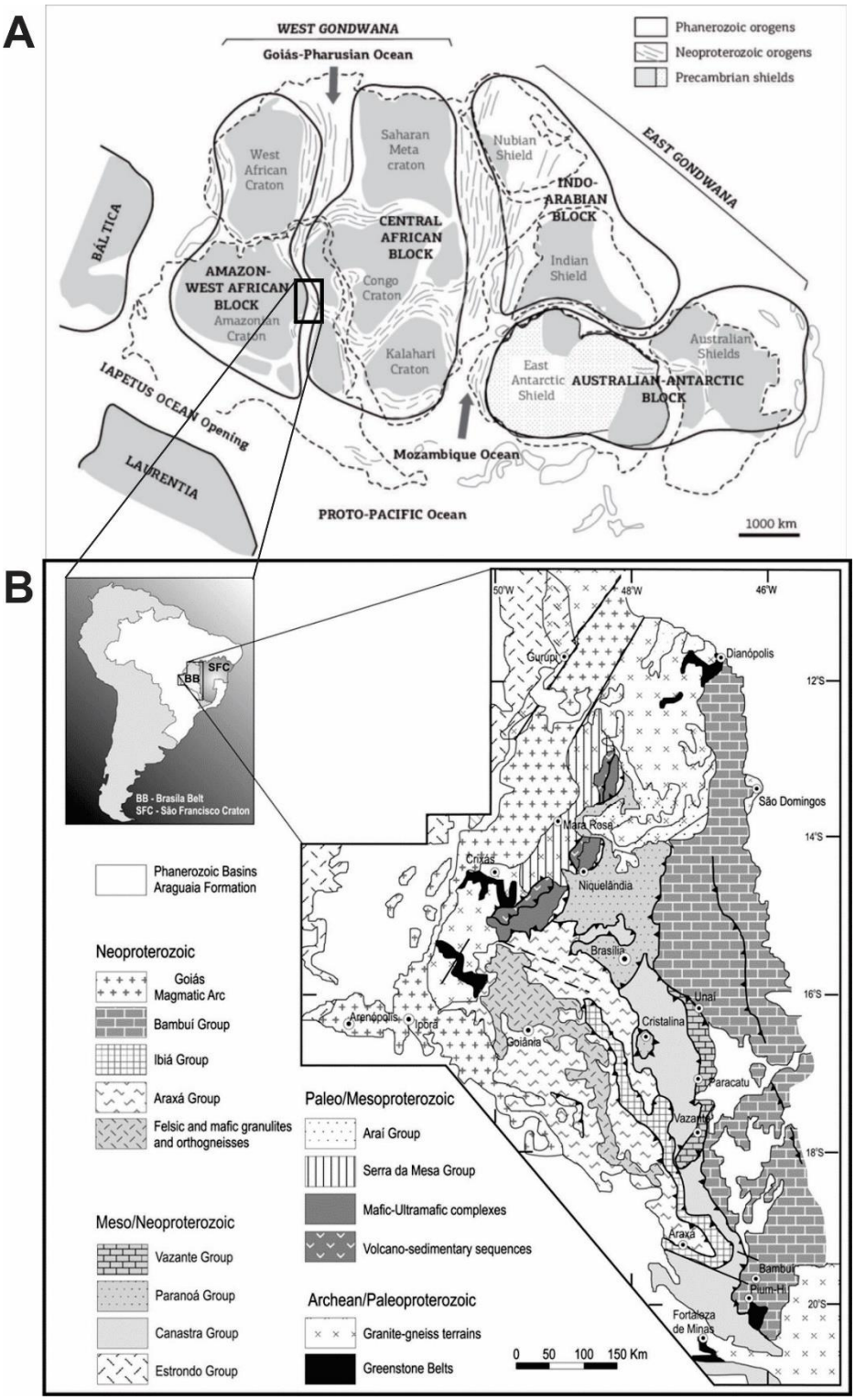

Figure 3.1. A. Crustal building blocks for the amalgamation of Gondwana, after the closing of the Goiás-Pharusian and Mozambique oceans (Cordani et al., 2013). B. Simplified geological map of the Brasília Belt (modified from Dardenne, 2000).

marine sediments deposited in a fore-arc or back-arc basin in a marine environment. The maximum age of deposition for these groups is considered to be about 790 Ma, which was determined by U-Pb analysis of zircon grains collected from the volcanic-sedimentary Maratá unit (Pimentel et al., 1992). Nd T_{DM} ages for these groups are bimodal, ranging from 2.23 to 1.00 Ga for the Araxá Group (Pimentel et al., 2001, 2011; Piuzana et al., 2003b; Rodrigues et al., 2010), which indicate different sedimentary sources, with one coming from the Goiás Magmatic Arc and the other possibly from the São Francisco Craton (Pimentel et al., 2011; Fuck et al., 2017). Thus, in the southern portion of the Brasília Belt, the Araxá Group is considered to have been deposited in a passive margin environment with an upper limit age of sedimentation between 1.0 and 0.9 Ga (Valeriano et al., 2004). This idea was applied to the southern portion of the Araxá Group by Falci et al. (2018), in which the group was described as a tectonic mixture of sedimentary units deposited in different tectonic environments and during different time periods, which were later tectonically juxtaposed through nappe stacking.

The Bambuí Group is considered to be the final sedimentary depositional basin in the Brasília Belt and is thought to have been deposited in a foreland basin, after the collisional processes that formed the orogenic belt (Fuck et al., 2017).

The Goiás Magmatic Arc is a Neoproterozoic juvenile arc, which is located on the western side of the Brasília Belt. This arc was active almost continuously from c. 930 to c. 600 Ma, however, studies have revealed three principal episodes of activity. The first episode occurred between c. 930 and c. 770 Ma and is related to intra-oceanic arcs, the second period displays a continental arc affinity and occurred from 670 to c. 600 Ma, and the final period of volcanism is related to late- to post-collisional granite intrusions, which occurred from c. 560 to 520 Ma (Pimentel et al., 1999, 2016; Laux et al., 2005; Marques et al., 2017). The final suturing of the magmatic arc with the Brasilia Belt was dated at c. 540 (Frasca et al., 2015), which was related to adakitic magmatic rocks in the magmatic arc, interpreted as evidence of arc delamination.

Araxá Group Mélange

The association of mafic and ultramafic assemblages, and discontinuous bodies of marble, disseminated in metasedimentary rocks was interpreted as an ophiolitic mélange by Drake Jr. (1980), in the sense of Gansser (1974), "The ophiolitic mélange is defined as an olistostromal and tectonic mixture of ophiolitic material and sediments of oceanic origin with exotic blocks." Mafic bodies composed of amphibole schist, have a Fe-enriched tholeiitic nature and show mid-ocean ridge tholeiitic or island-arc basalt affinity (Brod et al., 1992; Strieder and Nilson, 1992c; Valeriano and Simões, 1997; Seer et al., 2001; Klein et al., 2008). Piuzana et al. (2003b) dated an amphibolite, located to the east of Goiânia, at ca. 838 Ma. The ultramafic assemblages are composed principally of serpentinite, with smaller amounts of chlorite and talc schist. The serpentinites were formed from residual harzburgite, as indicated by the highly aluminous nature of associated chromite (Strieder & Nilson, 1992a, b). Metamorphism has affected the Araxá Group, increasing westward from greenschist facies to high-T amphibolite facies, and locally reaching as high as granulite facies. Some immature sequences have flyschoid characteristics (Drake Jr., 1980; Lacerda Filho et al., 1989). There are series of low angle faults and nappes, causing tectonic overlapping of the Araxá Group, verging to the east, in direction of the São Francisco Craton (Ferreira, 1972).

Three periods of igneous activity have affected the Araxá Group, similar to the Goiás Magmatic Arc, which are marked by numerous felsic igneous rock bodies. The first episode occurred around 833 Ma, dated on granite in the southern portion of the Araxá Group, and is thought to be related to oceanic arc magmatism (Seer and Moraes, 2013). The second episode occurred between 798 and 720 Ma (Klein et al., 2008; Pimentel et al., 2011; Seer and Moraes, 2013). The last episode occurred between 660 and 630 Ma (Pimentel et al., 2011; Klein et al., 2008; Seer and Moraes, 2013), and is regarded as associated to the collision between the Amazonian and São Francisco cratons. Klein et al. (2008) hypothesized that an extensional event occurred during this time interval, which commenced at roughly 800 Ma and lasted until about 760 Ma. Evidence of this event was the association of amphibolites with E-MORB signature, together with granites and metarhyolites of the Maratá sequence, in south Goiás. Metamafic rock assemblages have recently been identified to have N-MORB to E-MORB signature in other parts of the Araxá Group (Brown, 2019; Piaulino et al., 2019).

What has been presented in past works makes understanding the nature of the Araxá Group unclear, such as if there is only one Araxá Group or several? Figure 3.2 shows a portion of the Araxá Group with the distribution of T_{DM} model ages and U-Pb ages from earlier works. The presence of an ophiolitic mélange may indicate that part of the Araxá Group may have been under the influence of subduction. Different environments for its deposition have also been

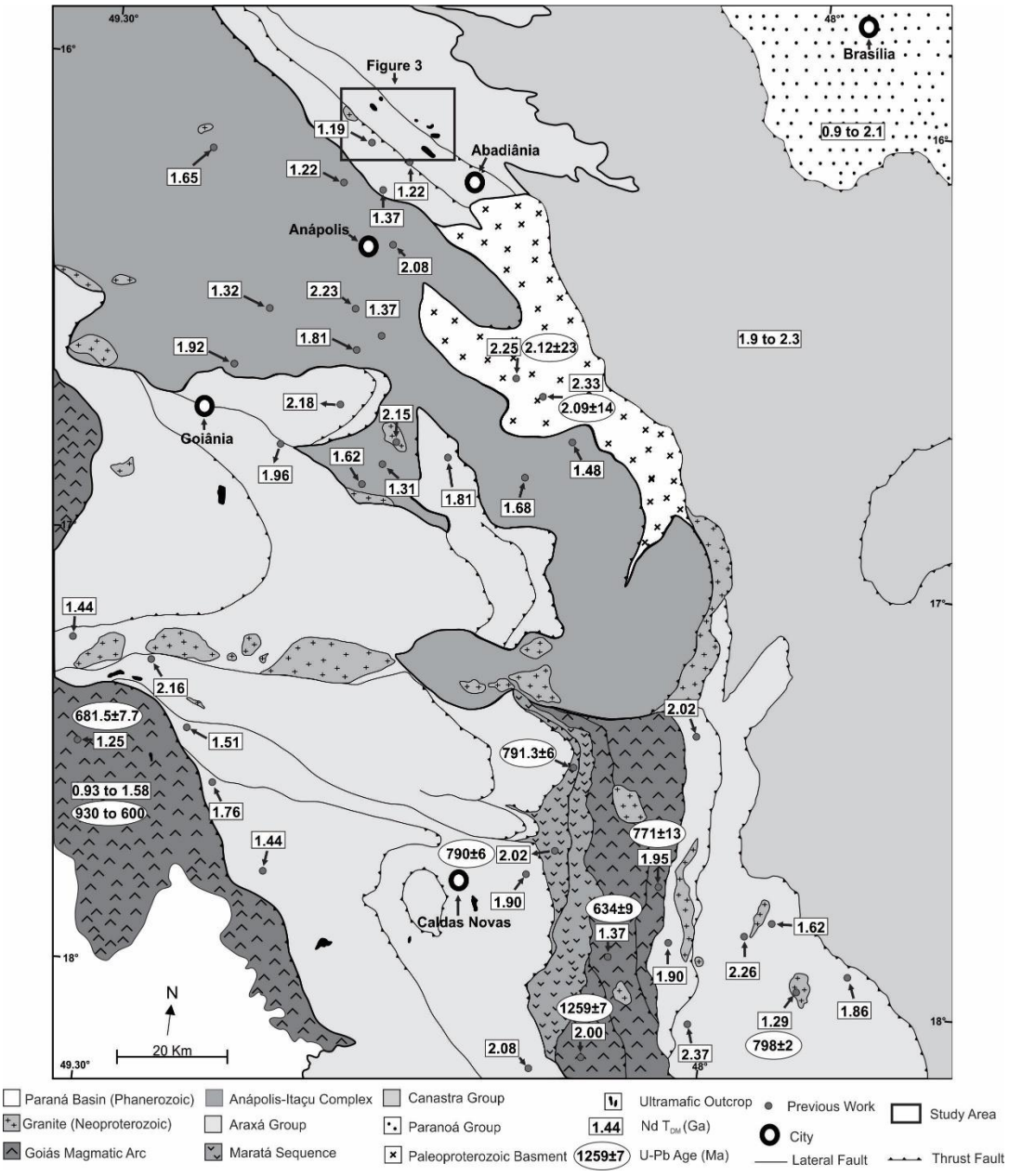

Figure 3.2. Generalized geological map, demonstrating past works in the Araxá Group, and the distribution of TDM model ages and some U-Pb ages. Values taken from Pimentel et al. (2001), Piuzana et al. (2003a and b), Navarro et al. (2005), Klien et al. (2008), Lilian (2017), Piaulino et al. (2019).

proposed, such as a fore- or back-arc basin (Pimentel et al., 2001), or a passive margin (Valeriano et al., 2004).

The presence of an ophiolitic mélange indicates that part of the Araxá Group may be related to subduction, or it could have been formed by other tectonic and sedimentary processes. The presence of a gravitational anomaly in central Brazil was interpreted as a suture zone (Hasui and Haralyi, 1985), which lead to the suggestion that the ophiolitic mélange may represent subduction related deposits (Strieder and Nilson, 1992). However, no other evidence has been documented to support this.

Past provenance studies in the Araxá Group (Pimentel et al., 2001; Piuzana et al., 2003b; Valeriano et al., 2004a; Klein, 2008; Navarro et al., 2013; Falci et al., 2018), suggest the deposition in different basins. Since the evolution of the Brasília Belt evolved from a passive margin, to a fore-arc setting, to a collisional setting (Pimentel et al., 2011), the opening and closing of different basins in different tectonic environments can be responsible for variations in detrital zircon ages and Nd T_{DM} model ages. There are several possible sources of sediments, which formed the Araxá Group such as sediments from the São Francisco Craton, volcanic arc derived sediments and the recycling of older basin sediments.

Study Area

The area of Abadiânia was selected for this study due to the presence of what Strieder (1989) described as an ophiolite mélange. The study area is located roughly 80 miles to the west of Brasília (Fig 3.3). Locally this part of the Araxá Group contains mostly metasedimentary rocks, consisting of muscovite-quartz schists and garnet-muscovite-biotite-quartz schists. Strieder (1989) considered that a gradation existed between these two different schist units that was marked by a thin graphite schist layer. Ophiolite assemblages are present within the metasedimentary package, consisting of four amphibole schist bodies and nine small ultramafic bodies. Brown (2019) determined that the amphibole schists have an N-MORB signature and may have formed in a back-arc environment c. 800 Ma. Also, present in the study area is a unit of mylonitic granite, which was considered by Berbert et al. (1970) to be part of a basement

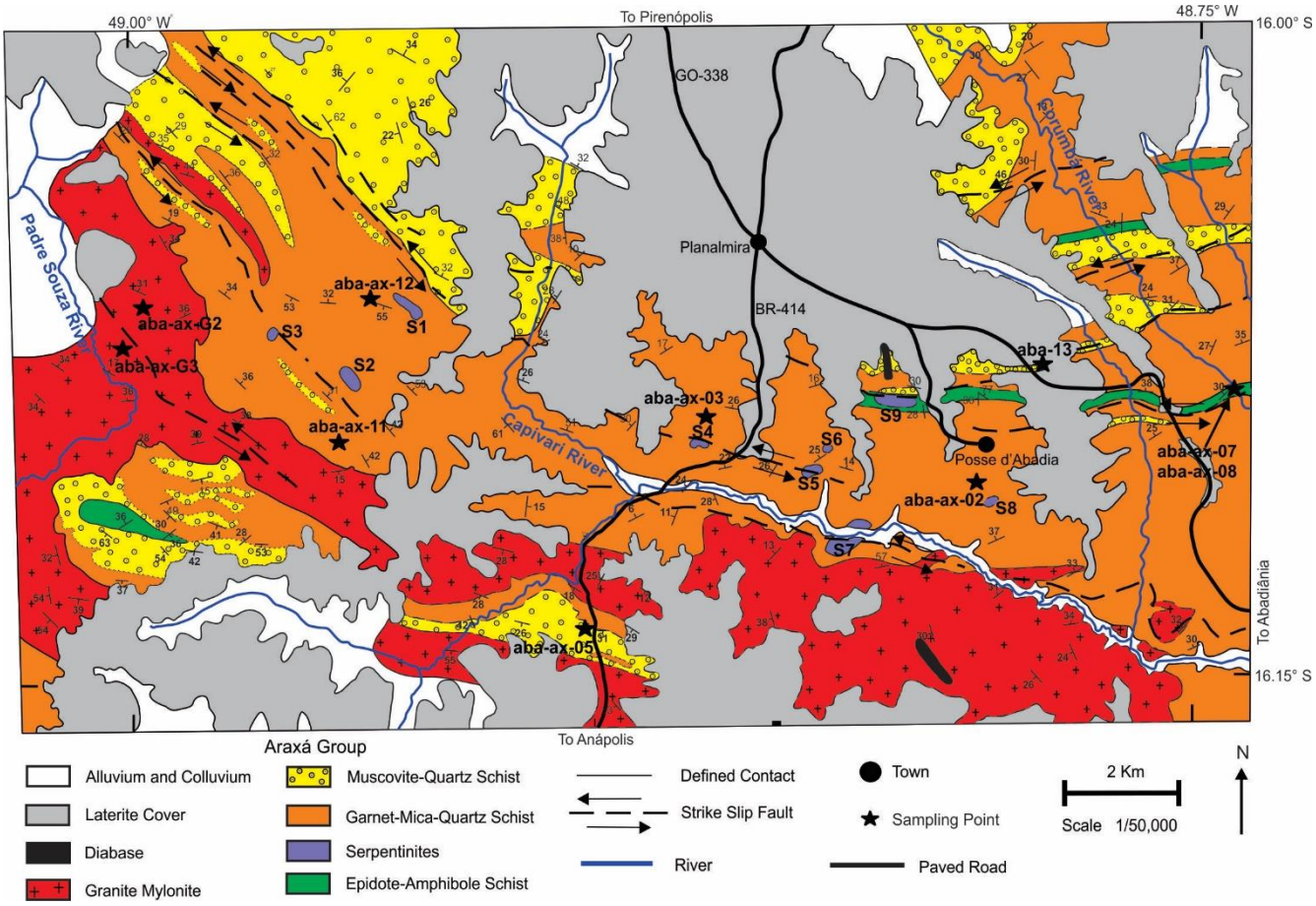

Figure 3.3. Geological map of the study area and sample locations (modified from Strieder 1989).

complex on which the metasedimentary rocks were deposited. A report by the Brazilian Geological Survey (CPRM, Justo and Scislewski, 1998) characterized the granite as a Neoproterozoic aged intrusion, related to the Goiás Magmatic Arc. Fresh outcrops are scarce in the study area, with most outcrops being highly altered, and higher elevations capped with laterite.

3.3 Methods

3.3.1 Samples

In order to study the mélange aspect of the study area a number of metasedimentary samples were collected. These included four samples of garnet-mica-quartz schist and two

samples of muscovite-quartz schist. The locations of the sample sites are shown in figure 3.3. Two samples representing the mylonitic granite were also collected from an area near the Padre Souza Creek. The distribution of the samples collected was selected in the hopes of being able to identify the individual assemblages of the mélange.

3.3.2 U-Pb

To extract zircon grains, samples were first processed in a rock crusher, producing chips roughly 3–5 cm in size. A Selfrag high voltage laboratory equipment, with a voltage of 130 kV and a frequency of 3 Hz, was used to defragment the samples liberating zircon grains. Zircon grains were concentrated using a pan to separate the heavy mineral fraction and a Franz was then used to remove the magnetic fraction. Zircon grains were handpicked using a binocular microscope. Grains were mounted in epoxy mounts and polished to create a smooth surface. HNO3 (ca. 2%) was used to clean the surface of the mounts. Backscatter electron images of the zircon grains were taken with an FEI-Quanta 450 scanning electron microscope, working at 20–25 kV, at the University of Brasília, in order to characterize grain zonation.

All zircon grain analyses followed the analytical procedure described by Bühn et al. (2009) and were conducted at the Geochronology Laboratory at the University of Brasília. U-Pb La-ICP-MS method was conducted on a Thermo Finnigan Neptune MC-ICP-MS, coupled with a New Wave UP213 Nd: YAG laser ($\lambda = 213$ nm). Measurements consisted of point analyses. The U-Pb analyses on zircon grains were carried out using the standard-sample bracketing method (Albarède et al., 2004); the GJ-1 standard zircon (Jackson et al., 2004) was used as the primary standard, for mass bias and drift correction.

The tuned masses were Uranium 238, Lead 207, 206 and 204 and Mercury 202. The integration time was 1 second and the ablation time was 40 seconds for all isotopes. A 30 µm spot size was used and the laser setting had an energy of 4-5 mJ/cm2 and a frequency of 10 Hz. Two to four unknown grains were analyzed between GJ-1 analyses. $^{206}Pb/^{207}Pb$ and $^{206}Pb/^{238}U$ ratios were time corrected. On smaller grains of zircon (~50 µm), single-spot laser-induced fractionation of the $^{206}Pb/^{238}U$ ratio was corrected using the linear regression method (Kosler et al. 2002). Results were checked against an unknown reference material, which during these

analyses was zircon standard 91500 (Wiedenbecket al. 1995, 2004), with an average value of 1068±18 (MSWD=0.95). Raw data were processed using and Excel sheet with the aid of "Chronus" software (Oliveira, 2015). Zircon ages were calculated using ISOPLOT v.3 (Ludwig, 2003), with isotopic ratio errors presented at the 1σ level.

3.3.3 Lu-Hf

The Lu-Hf isotope method on single zircon grains is compared to results attained on crystals previously analyzed by the U-Pb method. A Thermo Finnigan Neptune MC-ICP-MS was utilized for these analyses, conducted at the Geochronology Laboratory at the University of Brasília, using the method described by Matteini et al. (2010). The laser ablation analyses were conducted using a New Wave UP213 Nd: YAG laser (λ = 213 nm), utilizing a spot of 40 μm and a frequency of 10 Hz. The measured spots were analyzed in areas of the same age of individual zircon grains.

The εHf (T) values are calculated using the decay constant λ = 1.865 × 10−11, proposed by Scherer et al. (2001). The values of $^{176}Lu/^{177}Hf = 0.0384$ and $^{176}Hf/^{177}Hf = 0.282772$ were used for the depleted mantle (Chauvel and Blichert-Toft, 2001), and $^{176}Lu/^{177}Hf = 0.0113$ for average crust (Taylor and McLennan, 1985; Wedepohl, 1995). Before analyzing the zircon grains, the mass spectrometer is calibrated using a solution made from the SRM reference material JMC475. During analyses, various measurements of the GJ-1 zircon standard, were conducted.

3.3.4 Sm-Nd

Sm-Nd analyses were conducted at the Geochronology Laboratory at the University of Brasília, using the method described by Gioia & Pimentel (2000). Preparation for the Sm-Nd method analyses begins with whole rock samples being pulverized in a shatter box. 50 mg of sample were mixed with a $^{149}Sm/^{150}Nd$ spike solution and dissolved in Savillex capsules. Conventional cation exchange techniques were used to separate Sm and Nd from whole rock samples. Samples were evaporated onto Re filaments. Analyses were conducted on a Finnigan TRITON multi-collector mass spectrometer running in static mode. Uncertainties for the Sm/Nd

and $^{143}Sm/^{144}Nd$ ratios are better than ±0.5% (2σ) and ±0.005%(2σ), respectively, and were based upon repeated analyses of international rock standards BHVO-2, with $^{147}Sm/^{144}Nd$: = 0.1491 and $^{143}Nd/^{144}Nd$: = 0.512993±6?. $^{143}Sm/^{144}Nd$ ratios were normalized to $^{146}Nd/^{144}Nd$ ratio of 0.7219 and the decay constant of 6.54 x 10^{-12} was used. The T_{DM} model values were calculated using the method described by DePaolo (1981).

3.4 Results

Of the collected samples, two samples of garnet-mica schist (aba-ax-02 and aba-ax-12), two samples of quartzite (aba-13 and aba-ax05) and two mylonitic granites (aba-ax-G2 and aba-ax-G3) were analyzed for U-Pb. All of these samples, excluding aba-ax-G2, had zircon grains selected for Lu-Hf analysis. Results for all U-Pb and Lu-Hf analyses are shown in appendix 3.1 and 3.2. For whole rock Sm/Nd analysis, four samples of garnet-mica schist were selected, two samples of quartzite and one sample of mylonitic granite.

3.4.1 Petrography and U-Pb LA-ICP-MS

Garnet-Muscovite-Biotite-Quartz Schist

A total of four samples of garnet-muscovite-garnet-quartz schist (aba-ax-02, aba-ax-03, aba-ax-11 and aba-ax-12), were collected and thin sections made in order to study their mineral compositions. All four samples were very similar in their mineral assemblages, which consisted of garnet, muscovite, biotite and quartz, with some samples containing small amounts of tourmaline and others with carbonate minerals (Fig.3.4 A, B). Alternating quartz and muscovite and biotite bands define the foliation. Garnet grains have a characteristic “snow ball” appearance, and recrystallized quartz was observed in garnet pressure shadows. Chlorite is also present in small amounts, replacing biotite.

Two samples of garnet-mica-quartz schist (aba-ax-02 and aba-ax-12) were selected for U-Pb dating, in order to determine their sedimentary provenance. Sample aba-ax-02 has a zircon population of subhedral grains and magmatic zonation; there is another population of more rounded grains. Some of these grains have magmatic zonation, while others have well defined

cores with metamorphic overgrowths. Grain size varies from about 20 to over 200 µm. Sample aba-ax-02 had a total of 62 zircon grains analyzed, 58 of which were concordant, with ages

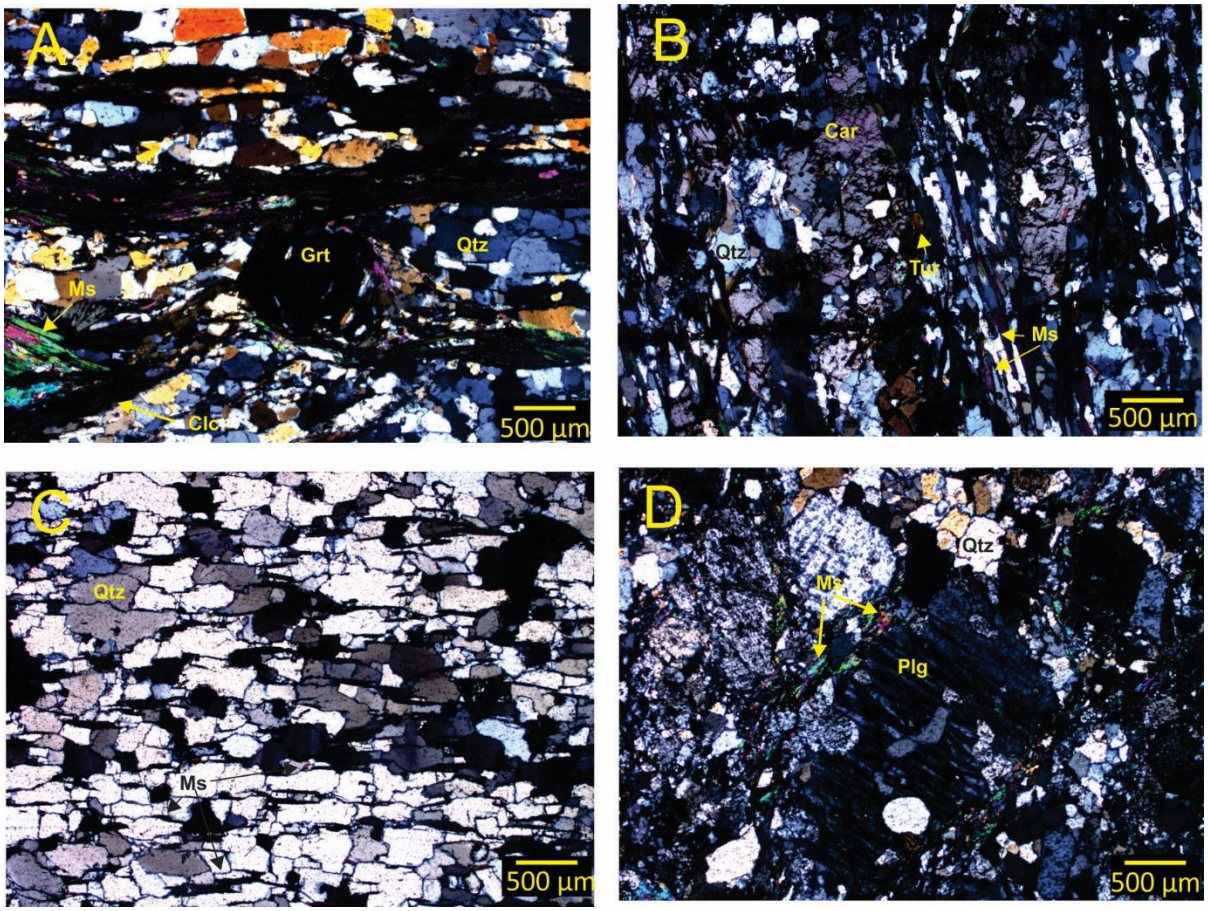

Figure 3.4. A. Sample aba-ax-012, showing a typical "snow ball" garnet. B. Carbonate mineral and tourmaline grains within schist sample aba-ax-02; foliation is defined by muscovite lamellae. C. Example of quartz schist, sample aba-ax-05. D. Typical example of granite "basement" aba-ax-G3. Car-carbonate, Clc-chlorite, Grt-garnet, Ms-muscovite, Plg-plagioclase, Tur-tourmaline, Qtz-quartz.

ranging from 672 to 3331 Ma. The population density graph shows that this sample is polimodal in age distribution, with several peaks ranging from 700 to 2100 Ma (Fig. 3.5). The maximum age of deposition for this sample is 672 Ma.

The zircon grains from sample aba-ax-12 are similar in size and morphology as sample aba-ax-02. Sample aba-ax-12 had a total of 62 grains analyzed, of which 54 grains were

concordant, with ages ranging from 615 to 3023 Ma. The density population graph has a bimodal distribution, with a major population centered around 664 to 800 Ma, and another centered around 1976 Ma (fig 3.5). The maximum age for sample aba-ax-12 is 615 Ma.

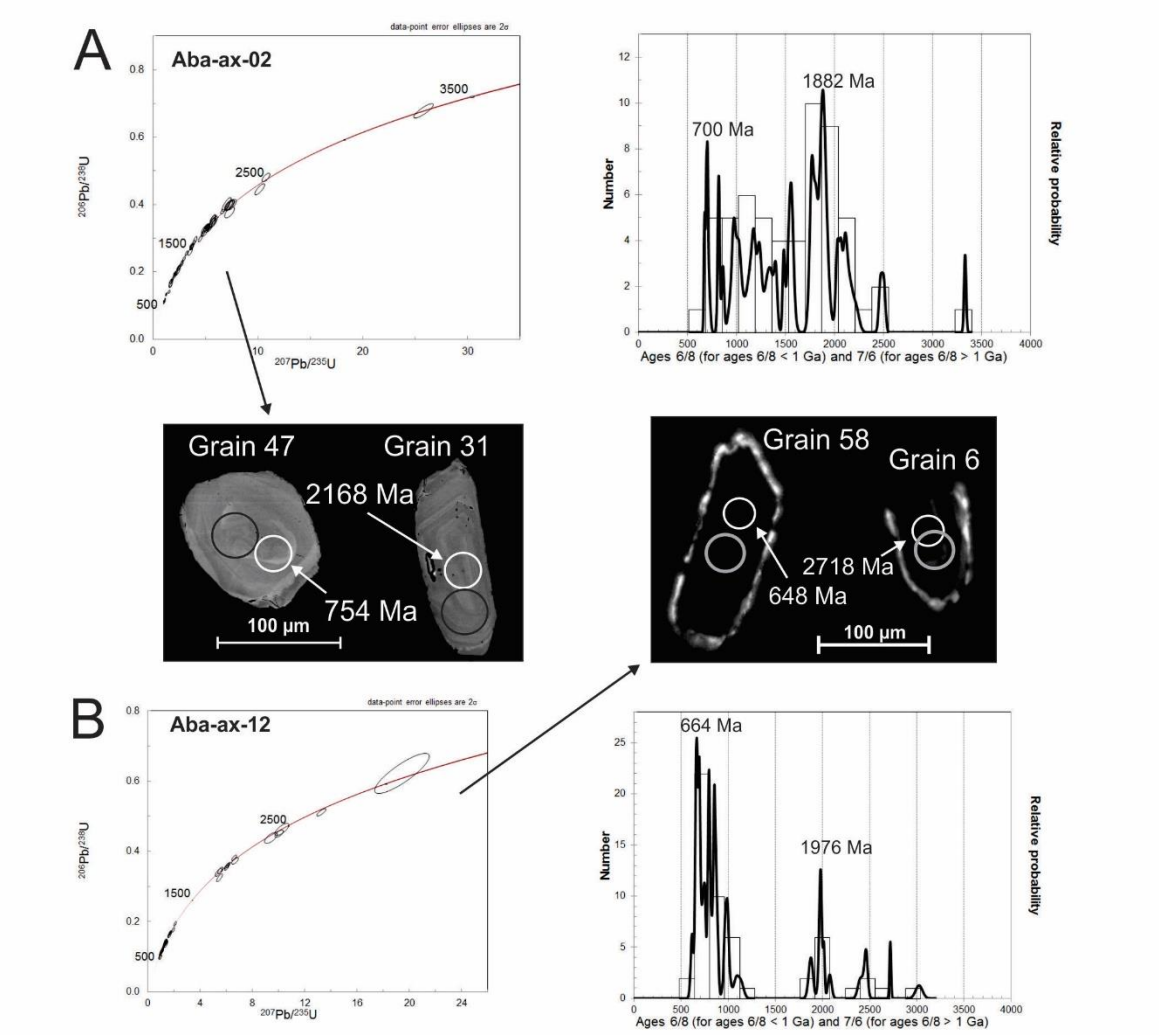

Figure 3.5. Examples of zircon grains in electron back scatter images or cathode luminescence, with concordia diagrams and population density diagrams for samples of garnet-mica schists: A. aba-ax-02 and B. aba-ax-12. White circles indicate the spot area for U-Pb analysis with the measured age for each spot. Black circles represent the spot where Lu-Hf analysis was conducted.

Quartzite

Two samples of quartzite were collected and made into thin sections. Sample aba-ax-05 is composed of about 90% quartz with 10% muscovite. Muscovite occurs in thin parallel bands,

which define the rock foliation (Fig. 3.4C). Sample aba-13 is composed almost entirely of quartz, with some magnetite grains present. This sample was also highly altered and no muscovite or internal structure was observed.

Zircon grains collected from two samples of muscovite-quartz schist (aba-13 and aba-ax-05) were analyzed by the U-Pb method. Zircon grains from these two samples are sub rounded to rounded. Grain size ranges from about 20 to 250 µm. The majority of the grain interiors have magmatic zonation with others showing a homogeneous appearance (fig 3.6). Some grains exhibit textures related to metamorphic regrowth and some metamorphic rims. Sample aba-13 had 61 zircon grains analyzed, with 50 grains having concordant ages ranging from 931 to 2981 Ma and a maximum age of sedimentation at 931 Ma. The population density graph has a polimodal distribution, with several peaks between 950 and 2150 Ma. Sample aba-ax-05 had 62 grains analyzed, 52 grains of which have concordant ages ranging from 926 to 2159 Ma. The population density curve also has a polimodal distribution, with peaks varying between 925 to 2125 Ma (fig 3.6) and a maximum age of deposition at 926 Ma.

Mylonitic Granite

Two samples were collected (aba-ax-G2 and aba-ax-G3), representing the mylonitic granite. According to Berbert et al. (1970), these samples were considered a quartz-feldspar gneiss. One of these represents a well-preserved granite sample (aba-ax-G2), while the other underwent mylonitization (aba-ax-G3). Sample aba-ax-G2 is composed of roughly 40% plagioclase, 20% orthoclase, 35% quartz and 5% biotite, with small amounts of muscovite (Fig. 3.4 D). Sample aba-ax-G3 contained bands composed of alternating layers of muscovite and biotite with zones of quartz and feldspar. Aba-ax-G3 contained about 10% biotite, 5% muscovite, 30% plagioclase, 25% orthoclase and 30% quartz.

Both samples had zircon grains separated for U-Pb analyses. Sample aba-ax-G2 had 13 zircon grains collected. Grains are subhedral and range in size from 50 to 200 µm. Cathode luminescence shows that the majority of the grains have defined cores, with metamorphic regrowth on the borders (Fig. 3.7). Sample aba-ax-G3 had 26 grains analyzed. Grains are subhedral and range in size from 50 to 400 µm. Cathode luminescence shows that some zircon

grains exhibit magmatic zonation, while others have defined cores and metamorphic borders; other still appear to have undergone recrystallization. U-Pb dating revealed that these two samples have similar calculated Discordia ages, with lower and upper intercepts at 404±49 Ma and 2103±11 Ma (MSWD = 0.68) for aba-ax-G2 and intercepts at 541±38 Ma and 2117.5±5.9

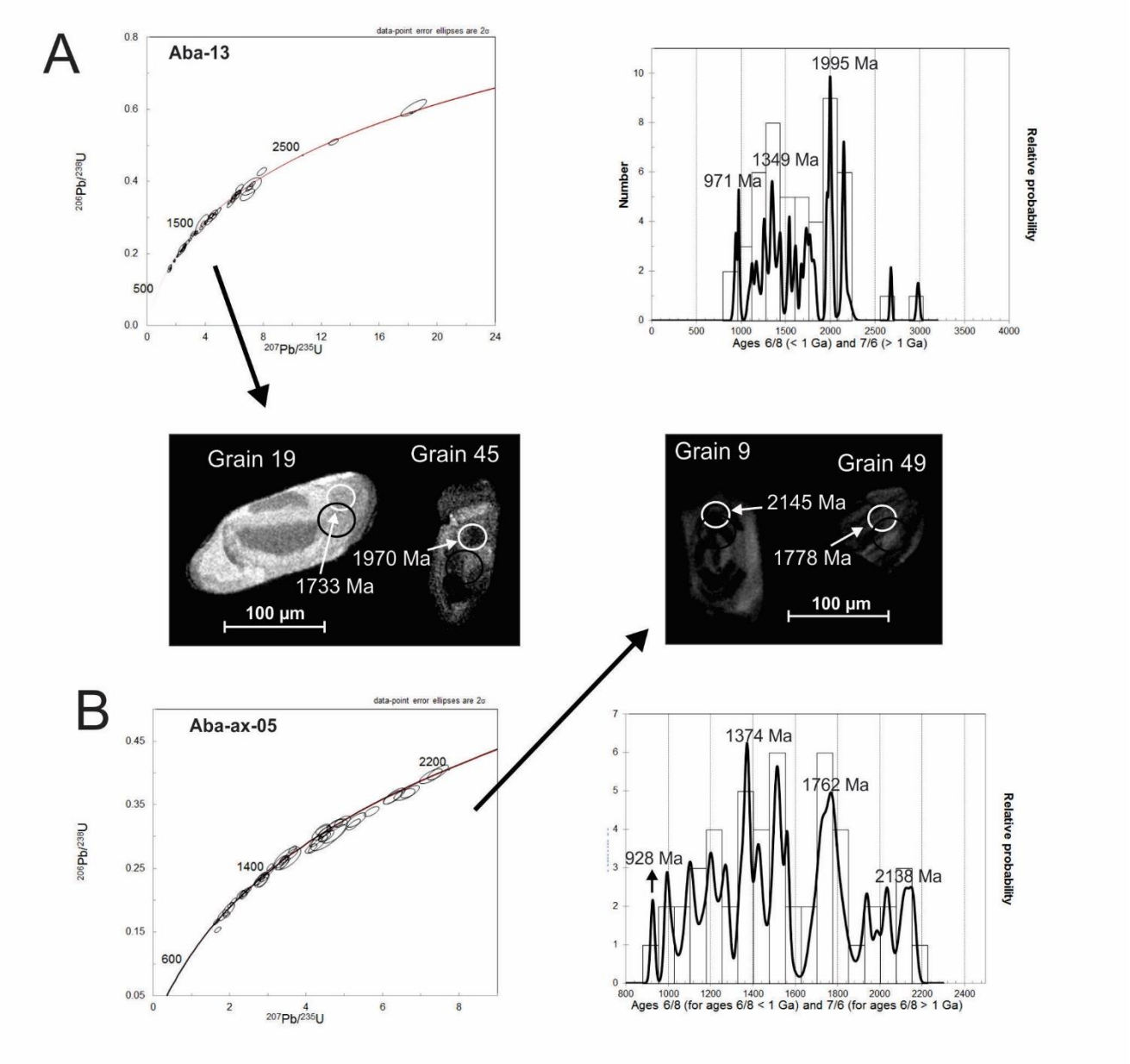

Figure 3.6. Examples of zircon grains in cathode luminescence, with concordia diagrams and population density diagrams for samples of mica-quartz schist: A. aba-13 and B. aba-ax-05. White circles indicate the spot area for U-Pb analysis with the measured age for each spot. Black circles represent the spot where Lu-Hf analysis was conducted.

Ma (MSWD=1.12) for aba-ax-G3. The upper intercepts are considered the age of crystallization of these samples.

3.4.2 Lu-Hf

Lu-Hf analysis was conducted on selected zircon grains from 5 samples. Results are shown in appendix 3.2. The samples of metasedimentary rocks aba-ax-02, aba-ax-05, aba-ax-12 and aba-13, all have a wide range of $\varepsilon_{Hf}(T)$, going from -23.5 to +16, indicating various sources for the zircon populations. The T_{DM} for the zircon grains of samples aba-ax-02, aba-ax-05 and aba-13, all fall in the range of 1.45 to 3.23 Ga. Sample aba-ax-12 has a set of younger T_{DM} values, which range from 0.58 to 2.76 Ga. Sample aba-ax-G3 has $\varepsilon_{Hf}(T)$ ranging from -0.97 to +2.18, and T_{DM} model age values of 2.38 to 2.52 Ga. Figure 3.8 shows the distribution of $\varepsilon_{Hf}(T)$ with its calculated U-Pb age.

3.4.3 Sm-Nd

A total of seven samples underwent whole rock analyses of Sm-Nd, four garnet-mica-quartz schists, two quartzites and one granite sample. Results are shown in table 3.1. In order to calculate the value of $\varepsilon_{Nd}(T)$ for the metasedimentary rock samples, an age of 638 Ma was used for "T", since this was the age given by Piuzana et al. (2003b) as the minimum age of deposition of the sediments, which compose the Araxá Group. The values for $\varepsilon_{Nd}(638\ Ma)$ for the garnet-mica schists range from -9.51 to 0.22. T_{DM} model age values for these four samples vary from 1.16 to 1.88 Ga. The muscovite-quartz schists have $\varepsilon_{Nd}(638)$ value of -7.78 and -11.57, and a T_{DM} age of 1.70 and 2.07 Ga. For the two granite samples the age of 2103 Ma was used for "T", giving a value of $\varepsilon_{Nd}(T)$ of 2.59. The distribution of $\varepsilon_{Nd}(T)$ values for the samples is shown in figure 9.

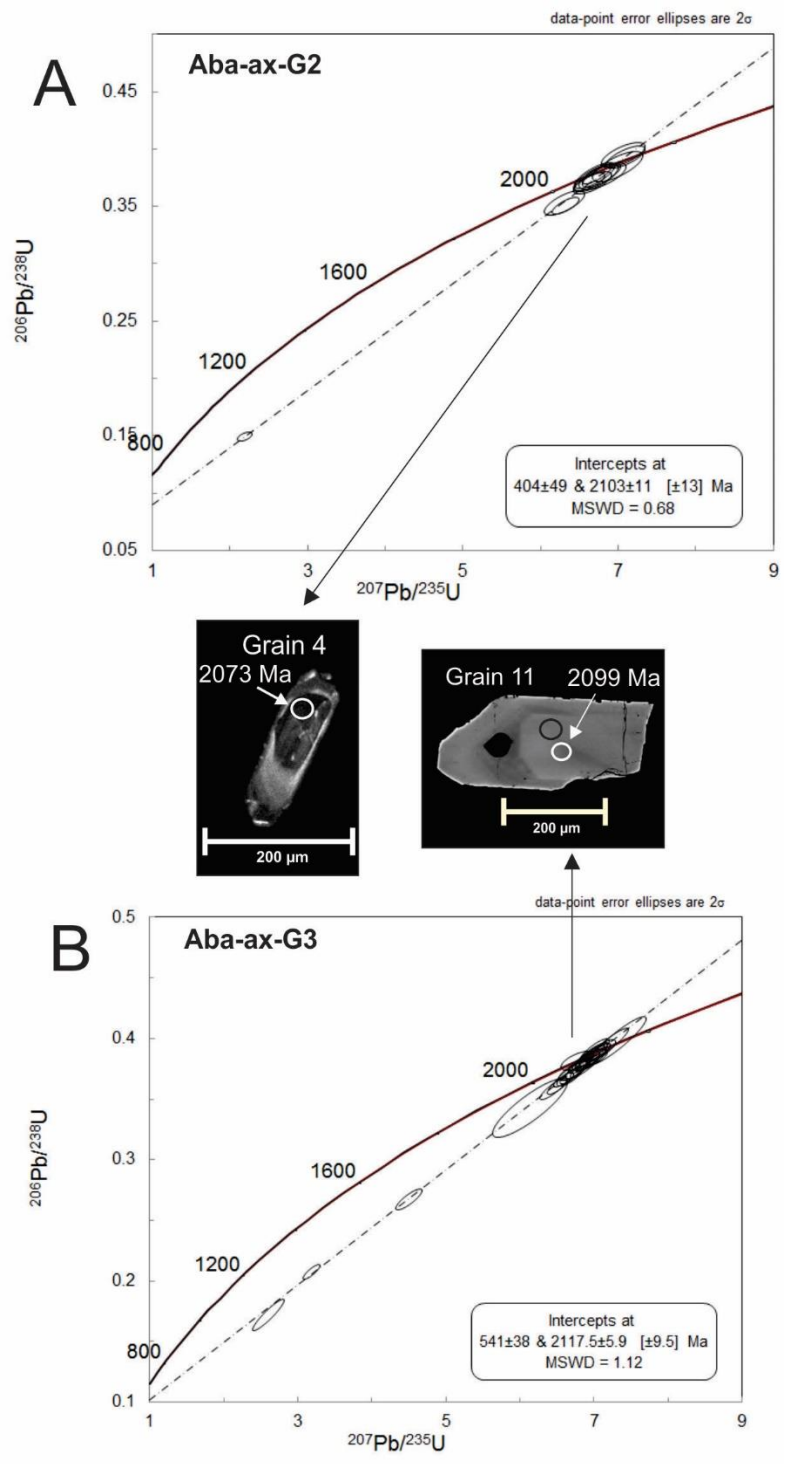

Figure 3.7. Examples of zircon grains in electron back scatter images and cathode luminescence, with discordia diagrams samples of basement granites: A. aba-ax-G2 and B. aba-ax-G3. White circles indicate the spot area for U-Pb analysis with the measured age for each spot. Black circles represent the spot where Lu-Hf analysis was conducted.

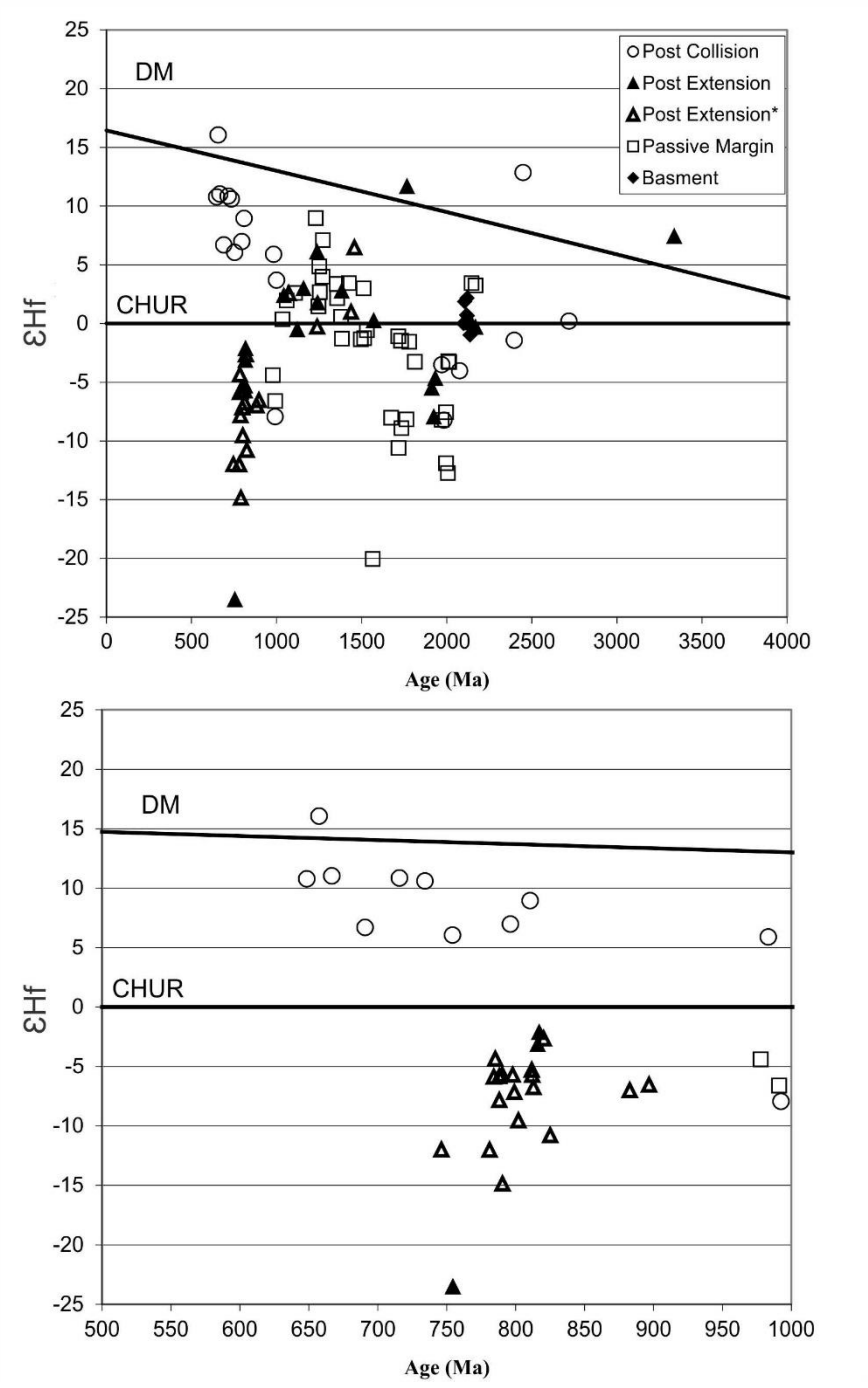

Figure 3.8. A. ƐHf of zircon grains, over their calculated U-Pb age. B. Close up view of the younger zircon grain populations. *- ƐHf values from Brown et al. (2019), metasedimentary rock samples aba-ax-07 and aba-ax-08.

3.5 Discussion

Mélanges are constructed and controlled through sedimentary and tectonic processes (Festa et al., 2010). The purpose of this study was to determine the provenance of the main metasedimentary and mylonitic granitic rock assemblages of the Araxá Group mélange in the area north of Abadiânia, and to relate them to the context of their depositional and tectonic environments. U-Pb and Lu-Hf analyses on zircon grains and Sm-Nd on whole rock samples were able to reveal several similarities and differences between the different units. Surprisingly some rock assemblages, which appear to be similar, in fact have different depositional histories. Eventually, mélange forming processes mixed and emplaced the different studied rock assemblages in their current arrangement, along with the ophiolite assemblages of metamafic and ultramafic rocks. At least three different tectonic/depositional environments can be described from the rock assemblages present in the mélange: passive margin, which is represented by the basement mylonite granites and quartzites; extensional, which is represented by the ophiolite sequence as described by Brown (2019); and collisional, which is represented by the garnet-mica schists, where one has a maximum age of deposition older than the collision of the Goiás Magmatic Arc with the São Francisco craton, and the other has a maximum age of deposition younger than the collision. These different environments are capable of producing different types of sedimentary controls and mélange types, but also, later tectonic events can modify previously formed mélanges (Festa et al., 2010).

Table 3.1. Summary of whole rock Sm/Nd data.

Sample	Sm(ppm)	Nd(ppm)	$^{147}Sm/^{144}Nd$	$^{143}Nd/^{144}Nd$	T (Ma)	ε_{Nd} (T)	T_{DM}
Aba-013	1.230	6.780	0.1097	0.511876+/-7	638	-7.78	1.70
ABA-AX-02	8.846	44.754	0.1195	0.511911+/-8	638	-7.90	1.82
ABA-AX-03	4.847	23.052	0.1271	0.512378+/-13	638	0.61	1.16
ABA-AX-05	2.136	11.134	0.1159	0.511708+/-14	638	-11.57	2.07
ABA-AX-11	6.699	32.096	0.1262	0.511953+/-3	638	-7.62	1.88
ABA-AX-12	7.392	33.008	0.1354	0.512393+/-5	638	0.22	1.25
ABA-AX-G3	8.724	52.084	0.1013	0.511449+/-6	2103	2.77	2.15

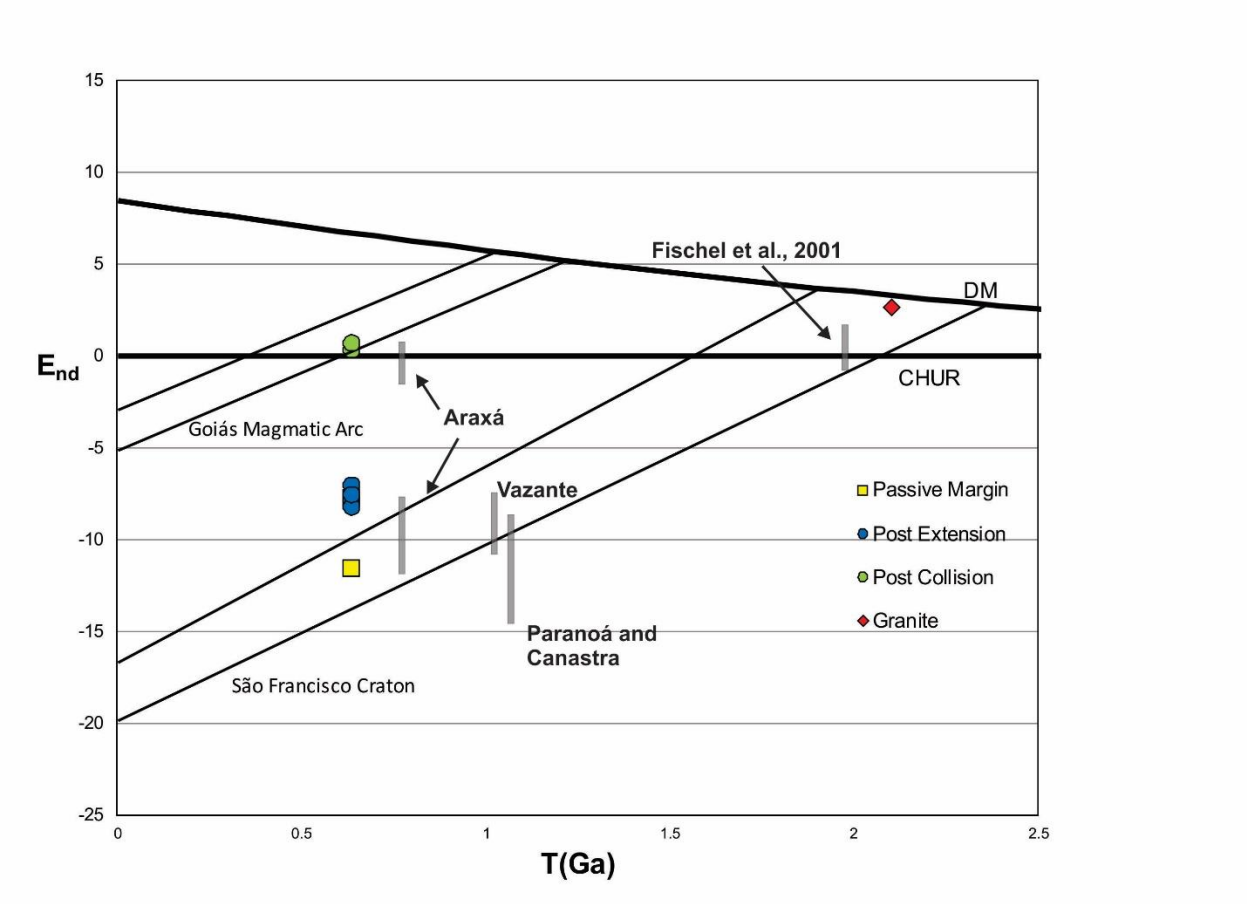

Figure 3.9. Graph showing the values of ε_{Nd} over time (T), of the different mélange components: passive margin (quartz schists), post extension and collision (garnet-mica schists) and granites. Shaded regions representing ε_{Nd} values for the Araxá, Vazante, Paranoá and Canastra groups, and the Goiás Magmatic Arc and São Francisco Craton are from Pimentel et al., (2001).

The garnet-mica schists are considered metapelitic in nature and constitute the matrix of the mélange in the study area. While petrographically similar, ε_{Nd} values indicate two different groups of schists. One group is represented by samples aba-ax-02 and aba-ax-11 with $\varepsilon_{Nd}(638)$ values of -7.90 and -7.62, and T_{DM} of 1.82 and 1.88 Ga, respectively. A second group is represented by aba-ax-03 and aba-ax-12, with $\varepsilon_{Nd}(638)$ values of 0.61 and 0.22, and T_{DM} of 1.16 and 1.25 Ga, respectively. These results mirror those reported by Pimentel et al. (2001) and Piuzana (2003b). The quartzites and the mylonitic granite, together with the ophiolitic assemblage, constitute blocks which entered into the mélange during its evolution.

3.5.1 Passive Margin

The passive margin environment is represented in the Brasília Belt by three principal metasedimentary units, the Paranoá, Canastra and Vazante groups. This environment and type of sedimentation was occurring through at least 1.2 to 0.93 Ga ago. The two muscovite-quartz schist samples have similar results and are most likely related to the same rock units. The ages of detrital zircon grains range from 931 Ma to Archean, and most likely were derived from the São Francisco Craton. This assumption is also supported by the results obtained by Sm-Nd whole rock analyses of aba-13 and aba-ax-05, with ε_{Nd} (T) of -7.78 and -11.57, and T_{DM} of 1.70 Ga 2.07, respectively. These values for Sm-Nd are similar to those reported from the Paranoá, Canastra and Vazante groups, which are considered to have been deposited in a passive margin environment (Dardenne, 2000; Pimentel et al. 2001, 2011; Rodrigues et al., 2010; Matteini et al., 2012).

U–Pb data from detrital zircon grains of the Paranoá Group indicate a maximum depositional age of 1.54 Ga, while a minimum depositional age of 1.04 Ga was calculated from U–Pb analysis of diagenetic xenotime overgrowth on detrital zircon (Matteini et al., 2012). The Canastra Group is considered to be an equivalent of the Paranoá Group (Fuck et al., 2017). The Vazante Group on the other hand has a younger zircon population than the Paranoá Group, with a major peak at 1.2 Ga and a smaller one at c. 0.95 Ga (Rodrigues et al., 2010; Matteini et al., 2012). The maximum age of deposition for the Vazante Group was established at 930 Ma (Rodrigues et al., 2010), which is the same as the studied muscovite-quartz schist. The similarities are interpreted to mean that the muscovite-quartz schist could be cogenetic with the Vazante Group. The Vazante Group is a narrow strip of pelite-carbonate rock assemblages, including phyllite, slate, quartzite, metasiltstone and algal dolomite (Rodrigues et al., 2010). While some successions of the Vazante Group do appear older, some of the assemblages have similar ε_{Nd} and T_{DM}, and the distributions of zircon populations for sample ROC-1 (Rodrigues et al., 2010), is very similar to aba-ax-05 and aba-ax-13.

The granite mylonite is the oldest rock unit dated from the mélange and is considered a piece of basement. Results showed that this unit is similar to the Natividade-Cavalcante crustal block and to the Silvânia Sequence and Jurubatuba Granite. It is possible that blocks of the granite mylonite could have entered the mélange by means of mass wasting, but it is likely that

tectonic processes could have been the cause. While not observed in this study, previous studies reported heavily mylonitic granite outcrops (Berbert, 1970; Strieder, 1989). This could indicate that tectonic processes (strike-slip movement) could have helped to introducing the Paleoproterozoic granites into the mélange. More evidence of this could the studied granite location in between the Natividade-Cavalcante crustal block and the Silvânia Sequence and Jurubatuba Granite. It is thought that the Silvânia Sequence and Jurubatuba Granite were accreted to the western border of the São Francisco Craton, sometime during the Neoproterozoic (Fischel et al., 1999). Because of the similarities between the Natividade-Cavalcante crustal block and the Silvânia Sequence and Jurubatuba Granite, it is possible that they were once connected and the latter was sheared off. The granite from this study is geographically in between these other two terrains and may represent a small isolated piece of the Natividade-Cavalcante crustal block.

While the blocks of granite could have been introduced into the mélange, as a basement complex, it could have been a possible source of sediment delivered to different basins. As stated above, what is considered to be the basement complex of the northern Brasília Belt outcrops as the Natividade-Cavalcante crustal block (Fuck et al., 2017) and consists of three rock forming events that are recorded in the calc-alkaline, metaluminous basement gneisses of this terrain, at 2.3 to 2.4 Ga, 2.2 Ga and 2144±21 Ma, and at 2042±12 Ma, age of a tonalite sample (Fuck et al., 2014; 2017). T_{DM} model ages range from 2.24 to 3.11 Ga, with $\varepsilon_{Nd}(T)$ values of +2 to 0, indicating a juvenile source for these rock assemblages (Fuck et al., 2014; 2017). Previous studies on the provenance of the passive margin sequences demonstrate that the basement complex was one of the sources of sedimentation on the passive margin of the São Francisco Craton (Rodrigues et al., 2010, 2012; Matteini et al., 2012).

3.5.2 Active Margin

One of the most important components of the mélange is its ophiolite assemblage. Identifying the environment in which the ophiolite formed is important in understanding what possible mélange could have formed. Brown et al. (2019) determined that the ophiolite assemblage may have formed in a back-arc environment, around 800 Ma ago. This extensional

event could have lasted for approximately 40 Ma, and would have created a large depositional basin. Mass-transport deposits, related to olistoliths and debris flows, would be common in this environment. The Maratá sequence was also formed during this time interval and could be related to an extensional event, or maybe was an active arc (Pimentel et al., 1996; Klein, 2008; Sabaraense, 2017). These tectonic features would have created basins which would have been situated between the Goiás Magmatic Arc and the passive margin of the São Francisco Craton, suggesting that they would be the principal sources for the sedimentary assemblages deposited in these basins.

3.5.2.1 Fore-Arc/Back-Arc – Extension

The first group of garnet-mica schists is represented by samples aba-ax-02 and 11. U-Pb results show sample aba-ax-02 has a variation in detrital zircon grains with major peaks at 700, 820 and 1880 Ma, with a maximum age of deposition of 672 Ma. The ε_{Hf} values for sample aba-ax-02 vary from positive to negative and together with their T_{DM} values, similar to the values recorded from the passive margin sequences (aba-ax-05 and aba-13). The younger zircon populations in sample aba-ax-02 have negative ε_{Hf} values. The negative ε_{Hf} values are an important distinguishing feature of sample aba-ax-02, since its younger zircon populations are similar to values recorded from the Maratá Sequence (Sabaraense, 2017). The combination of very negative $\varepsilon_{Nd}(T)$, ε_{Hf} values, and zircon populations derived from the continent, indicates that the major component in these sediments was derived from the continent (passive margin sequences), with a smaller amount delivered from the magmatic activity which created the Maratá Sequence. U-Pb and Lu-Hf results also point to populations that were derived from the Paleoproterozoic Natividade-Cavalcante crustal block.

The first period of sedimentation and mélange formation, represented by these garnet-mica schists, occurred between ca. 799 to 650 Ma, which coincides with the magmatic activity that formed the Maratá Sequence and the high-grade metamorphic event that formed the Anápolis-Itauçu complex, respectively. This first period of sedimentation received sediments from the Maratá Sequence, which probably represents a dismembered volcanic arc, and from the passive margin sequences of the Brasília Belt. Pimentel et al. (2011) suggested that some of these sediments may represent a deep marine equivalent of the passive margin sequences, however since they have younger zircon populations similar to those from the Maratá Sequence,

they were probably deposited in a fore or back-arc basin. Sedimentation continued during this phase until ca. 650 Ma, which is marked by the high-grade metamorphic event of the Anápolis-Itauçu complex.

Samples aba-ax-07 and 08 from Brown (2019) are also good candidates for sedimentary assemblages deposited during the extensional event. While all four of these schists have similar ε_{Nd} (T), samples aba-ax-07 and 08 have one large zircon population derived from the magmatic arc, and very few other grains from continentally derived sediments. The maximum age of deposition for these two schists is 712 Ma for aba-ax-07 and 685 Ma for aba-ax-08, which is very close to the maximum age for aba-ax-02 (672 Ma). Another thing that is similar with these rock samples is that the younger peaks all have negative ε_{Hf} values, indicating a reworking of older crust.

One of the differences between schists aba-ax-02, aba-ax-07 and aba-ax-08 is their distribution of zircon populations. Aba-ax-02 is polimodal with a large input from older cratonic sources. Aba-ax-07 and aba-ax-08 are both bimodal, with one main peak centered around 790 Ma, with a small input of older craton derived zircon grains. The difference between these schists could be caused by a change in deposition, for example aba-ax-02 could have been deposited by a large mass wasting event, which introduced a large amount of continental derived material in the back-arc basin, in a localized event. It is also possible that samples aba-ax-07 and 08 were deposited co-genetically with aba-ax-02, but in different basin.

Another possibility is that they could have been deposited at different points within the basin, with aba-ax-07 and 08 closer to the magmatic arc, and aba-ax-02 closer to the continental margin, a similar scenario presented by Ketly et al. (2008). Sediments of the Hentey basin have a similar distribution of zircon populations, with onset of sediments receiving more material from a volcanic arc, and the other receiving more from a Neoproterozoic source. Ketly et al. (2008) suggested that this difference in distribution is more related to the location of the source of the sediments, with sediments showing a large peak in volcanic arc related zircon grains, being sourced in the south near the Southern Mongolian arc, and the other group of sediments coming from the northern end of the basin, where there was a Neoproterozoic basement.

3.5.2.2 Collision – Post-Collision

The second type of garnet-mica schist is marked by a change in Nd T_{DM} model values, which represents a change in sediments being deposited. This change in sedimentation seems to coincide with the high temperature metamorphic event which formed the Anápolis-Itauçu metamorphic complex (AIC), which took place c. 670 to 650 Ma (Baldwin et al., 2005; Della Giustina et al., 2011), and which is thought to represent the metamorphic core of the Brasília Belt (Pimentel, 2016).

U-Pb results of sample aba-ax-12 show that it has a younger zircon population, with major peaks at 664, 795 and 1976 Ma and a maximum age of deposition of 615 Ma. ε_{Hf} values of the younger zircon populations (810 to 648 Ma) are all positive. Sample aba-ax-12 is similar to the schist analyzed by Piuzana et al. (2003b), and younger in age than the intrusive tonalite of c. 638 Ma (Piuzana et al., 2003b). The older zircon populations indicate that aba-ax-12, and aba-ax-03, have some input from an older source, such as passive margin sediments and the basement complex, which is also supported by ε_{Hf} values. However, while the youngest zircon grains dated from the first garnet-mica schist group all have negative ε_{Hf} values, the zircon grains in the same time interval for the second group all have positive values, indicating sediments derived from a juvenile source, such as the Goiás Magmatic Arc. A comparison of the presented data with results obtained by Matteini et al. (2010) from the Mara Rosa Arc demonstrates similar positive ε_{Hf} values. As suggested by Pimentel et al. (2001), these sediments may have been deposited in a fore- or back-arc environment.

While the two groups of garnet-mica schists are very similar, the Lu-Hf results can explain the variation in Nd values. While the two schist groups have overlapping zircon populations, the youngest populations from the first group have all negative ε_{Hf} values in contrast to the second group, which has only positive values. This indicates that the second period of sedimentation did not receive sediments from the Maratá Sequence and related rock units. These results are interpreted to mean that the two garnet-mica schist groups formed in different depositional centers, isolated from one another. It is this difference that can be accredited with the variation of Nd T_{DM} model ages found in the literature (Pimentel et al., 2001; Piuzana et al., 2003b). The implication is that later nappe stacking and dismemberment brought these two sedimentary rock units together after their deposition.

The second period of sedimentation takes place in the time interval between the Anápolis-Itauçu event and the final collision of the Amazonian Craton with the São Francisco Craton c. 600 Ma. The collisional events can create nappes, which later can be eroded and undergo mass wasting, becoming a source of sediment and blocks within a mélange. This kind of tectonic activity can cause the recycling of older mélanges and incorporate them into new ones (Festa et al., 2010). The presented results demonstrate that this did not happen with the available rock units, since the two different garnet-schist groups have distinct time intervals and arc materials. It is possible that another depositional center can be characterized by rock assemblages from the Araxá Group. Sample ANA 18 in Piuzana et al. (2003b) has Nd T_{DM} model age similar to the first group of garnet-mica schists, however it has zircon populations similar to the second group. It is possible that this schist sample may represent a mixture of arc derived sedimentary material that originated from the Maratá Sequence and the Goiás Magmatic Arc. If so, it could represent another distinct basin, which was not observed in this study. Figure 3.10 shows the variation of zircon population of the different metasedimentary rocks form this study and from the other passive margin sedimentary groups, plotted alongside the distribution of their T_{DM} model ages.

3.5.3 Shear Zone displacement – thrusting to Strike slip tectonics

While it is undetermined when it occurred, at some point large blocks of passive margin material, represented by aba-ax-05 and aba-ax-11, and granite samples aba-ax-G2 and G3

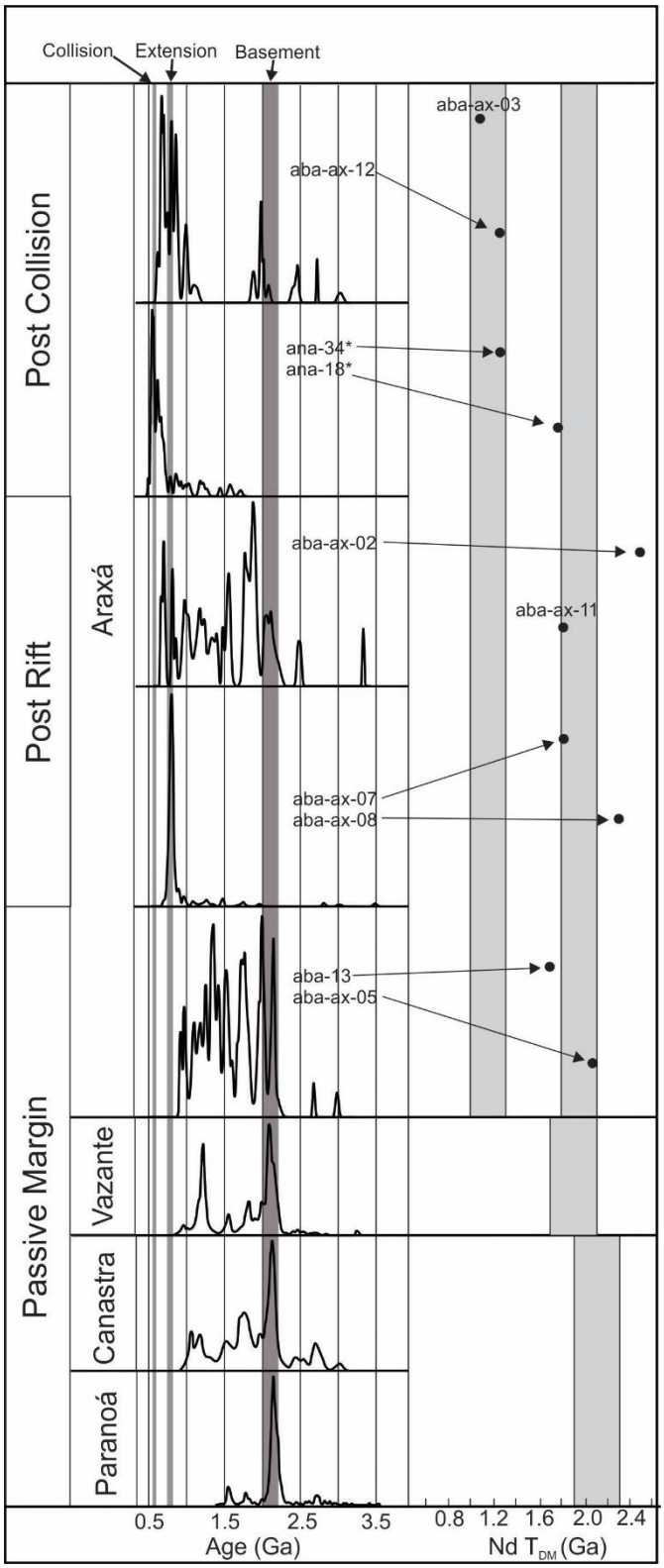

Figure 3.10. Diagram demonstrating the change in zircon population and ε_{Nd} in relation to the tectonic evolution of the study area.

entered into the mélange. The interpretation of the presence of the schist samples aba-ax-07 and 08 in contact with a metamafic outcrop is that the ophiolite assemblage entered into the mélange during the deposition of the first group of garnet-mica schists. It is possible that platform instability caused a mass wasting event, which carried these blocks into the depositional environment, which can happen in a back-arc/extensional environment. This deposition of material can also be caused by dismemberment of stacked nappes, as suggested by Falci et al. (2018). Alternatively, however, a large amount of material may have been transported into the mélange, via strike-slip faults.

Strike-slip deformation can dismember previously coherent stratigraphic successions, producing a tectonically disrupted unit (Festa et al., 2010). Evidence in supporting strike-slip tectonics begins with the studied granite. If it was part of the Natividade-Cavalcante crustal block, the granite was transported hundreds of km to the south, together with the Silvânia Sequence and Jurubatuba Granite. This can also hold true for the passive margin sequences, represented by samples aba-ax-05 and aba-13. If a shear zone formed in the back-arc rift zone, it could be responsible for the entrainment of large blocks of passive margin sequences, Paleoproterozoic granites and ophiolite assemblages, mixing these components with sediments already deposited within the back-arc basin. Reactivation during different periods of collisional tectonics could reactivate the shear zone and continue to recycling the pre-existing mélange. The Central Franciscan Belt contains a mélange composed of blocks of diverse lithologies and metamorphic grades embedded in a shale matrix, and with the presence of strike-slip activity, this mélange is a product of tectonic recycling (McLaughlin et al., 1988; Festa et al., 2010). While this model can explain some of the transport and sequence disruption which has occurred, to date no extensive shear zone has been identified, but the possibility that more Paleoproterozoic granitic bodies are located within the Araxá is high.

3.5.4 Regional Implications

This study indicates that there were at least two different time periods of sedimentation or mélange formation, as determined by the results of the garnet-mica schists. The time periods for mélange formation fall in between 790 and 650 Ma and 650 and 600 Ma. Later dismemberment

mixed these two units making their relationship in the field almost impossible to determine. The contacts between the different rock units are difficult to observe in the field, but it does appear that the ophiolite assemblage was incorporated into the mélange during the first period of mélange formation or sedimentation. It could not be determined when the passive margin blocks and the granite mylonite block entered into the mélange, but it might have been caused my strike-slip movement and other tectonic related processes. The contact between the two different garnet-mica schists is unknown, but more detailed sampling and Sm-Nd analysis will provide the easiest method at determining the limits of these two rock units. However, Lu-Hf analysis on zircon grain populations might demonstrate the presence of other depositional centers.

3.6 Conclusions

This study demonstrates that the rock assemblages of the Araxá Group represent different metasedimentary rocks, which were deposited at different times and in different and changing environments. Metamorphic overprinting has made it challenging to determine which rock assemblage is associated with what event, as demonstrated with the results of Sm-Nd, U-Pb and Lu-Hf isotopic analyses on the garnet-mica-quartz schists. The different schist samples appear to be similar in thin section, but yield very different isotopic results, which indicate the difference in time during which they were deposited and the provenance of the original sediments. This study also demonstrates the importance of identifying different tectonic environments. When individual environments can be determined in a mélange setting, it becomes easier to understand what mechanisms where involved in mélange formation.

- The blocks of quartzite and granite mylonite examined from the mélange are distinct rock units. The quartzite sample displays zircon populations and Sm-Nd model age and ε_{Nd} (T) values similar to the Vazante Group and was probably formed in a similar passive margin setting. Granitic mylonite rocks are Paleoproterozoic in age, and may represent basement assemblages, which crop out in the northern section of the Brasília Belt.

- Garnet-mica-quartz schists analyzed in this study are petrographicaly similar, but are isotopically different and represent at least two different periods of sedimentation, as defined by

the differences in zircon population and Sm-Nd model age and ε_{Nd} (T) values. The two groups of garnet-mica schists appear to have been formed apart from one another and were later superimposed tectonically on each other.

- Schist samples aba-ax-02 and 11 represent a period of sedimentation which occurred between c. 800 and 650 Ma and was deposited in a fore- to back-arc basin. Negative ε_{Hf} and ε_{Nd} values indicate that these schists incorporated reworked crustal material, which is probably related to the Maratá Sequence.

- Schist samples aba-ax-03 and 12 represent the second period of sedimentation, which took place between c. 650 and 600 Ma, and also was deposited in a fore- to back-arc basin. Positive ε_{Hf} and ε_{Nd} values indicate that sediments derived from the juvenile Goiás Magmatic arc were incorporated in these samples.

- Blocks of quartzite were probably introduced by mass wasting and strike-slip tectonics could have introduced the granite mylonite into the mélange. Dismemberment and nappe stacking caused by collisional events could have mixed the different sedimentary sequences, superimposing them on one another.

Acknowledgements

The author would like to acknowledge the Brazilian National Council for Scientific and Technological Development (CNPq) for the doctoral scholarship. The author also acknowledges the Instituto Nacional de Ciência e Tecnologia Estudos Tectônicos and CAPES for financial support. Reinhardt A. Fuck and Elton L. Dantas acknowledge CNPq research fellowships.

3.7 Appendix

Appendix 3.1. Summary of results of U/Pb LA-ICPMS data.

aba-ax-02											Apparent Ages						
	Th/U	$^{206}Pb/^{204}Pb$	1σ%	$^{207}Pb/^{206}Pb$	1σ %	$^{207}Pb/^{235}U$	1σ %	$^{206}Pb/^{238}U$	1σ %	Rho	$^{207}Pb/^{206}Pb$	2σ abs	$^{206}Pb/^{238}U$	2σ abs	$^{207}Pb/^{235}U$	2σ abs	% U-Pb disc[4]
006-ZR3	0.499	151673	16.50	0.27437	0.68	25.711	1.50	0.6796	1.28	0.86	3331	21	3343	67	3336	29	-0.35
053-ZR40	0.432	121225	21.42	0.16111	0.99	10.703	1.50	0.4818	1.06	0.71	2467	33	2535	44	2498	28	-2.75
065-ZR50	0.475	71626	14.67	0.16432	0.99	10.110	1.83	0.4462	1.50	0.82	2501	33	2378	59	2445	34	4.89
048-ZR37	0.491	47094	12.18	0.12549	1.40	6.960	2.52	0.4022	2.06	0.82	2036	49	2179	76	2106	44	-7.05
040-ZR31	0.434	60120	13.78	0.13477	1.57	7.458	2.30	0.4013	1.64	0.71	2161	54	2175	60	2168	41	-0.66
016-ZR11	0.864	46790	13.87	0.13126	1.47	7.251	2.13	0.4006	1.50	0.70	2115	51	2172	55	2143	38	-2.69
059-ZR46	0.220	36677	13.05	0.13106	2.09	7.224	2.75	0.3997	1.75	0.64	2112	72	2168	64	2139	48	-2.63
037-ZR28	0.343	347805	13.54	0.12739	0.85	6.990	1.45	0.3979	1.12	0.77	2062	30	2159	41	2110	26	-4.71
017-ZR12	0.368	74053	27.74	0.13041	1.13	7.149	1.95	0.3976	1.55	0.79	2103	39	2158	57	2130	34	-2.59
055-ZR42	0.518	136227	12.32	0.12488	0.86	6.554	1.19	0.3806	0.75	0.62	2027	30	2079	26	2053	21	-2.57
043-ZR32	0.356	29788	12.80	0.13901	1.92	7.259	2.61	0.3787	1.74	0.66	2215	66	2070	61	2144	46	6.52
018-ZR13	0.446	51815	12.18	0.11496	1.34	5.694	1.98	0.3592	1.42	0.71	1879	48	1978	48	1930	34	-5.27
007-ZR4	0.556	60279	14.82	0.11414	1.09	5.641	1.79	0.3584	1.37	0.77	1866	39	1975	47	1922	31	-5.80
066-ZR51	0.586	34696	11.09	0.11788	1.92	5.706	2.81	0.3510	2.02	0.72	1924	68	1940	67	1932	48	-0.79
056-ZR43	0.396	45444	17.46	0.11585	1.38	5.569	2.16	0.3486	1.62	0.75	1893	49	1928	54	1911	37	-1.83
028-ZR21	0.575	44190	11.65	0.11775	1.59	5.650	2.39	0.3480	1.75	0.73	1922	56	1925	58	1924	41	-0.14
019-ZR14	0.262	154409	12.80	0.11510	1.04	5.443	1.64	0.3430	1.21	0.74	1881	37	1901	40	1892	28	-1.03
073-ZR56	0.859	78309	12.20	0.11535	1.31	5.338	1.95	0.3356	1.40	0.72	1885	47	1865	45	1875	33	1.06
027-ZR20	0.480	78776	16.43	0.11066	0.99	5.120	1.55	0.3355	1.13	0.73	1810	36	1865	36	1839	26	-3.03
060-ZR47	0.466	99124	10.62	0.11252	1.26	5.195	1.66	0.3349	1.01	0.61	1840	45	1862	33	1852	28	-1.17
078-ZR61	0.749	60685	24.92	0.10911	1.43	5.013	2.06	0.3332	1.43	0.70	1785	52	1854	46	1821	35	-3.87
023-ZR16	0.562	70296	21.80	0.10972	1.26	5.040	1.76	0.3331	1.18	0.67	1795	45	1853	38	1826	30	-3.26
035-ZR26	0.875	76221	21.52	0.11661	1.24	5.340	1.87	0.3321	1.35	0.72	1905	44	1848	43	1875	32	2.97
036-ZR27	0.347	92145	13.27	0.11346	1.10	5.134	1.55	0.3281	1.02	0.66	1856	39	1829	32	1842	26	1.41
069-ZR54	0.363	76227	11.99	0.10729	1.33	4.835	1.94	0.3268	1.36	0.70	1754	48	1823	43	1791	32	-3.93
057-ZR44	0.796	42136	11.64	0.11077	1.64	4.930	2.62	0.3228	2.01	0.77	1812	59	1803	63	1807	44	0.49
039-ZR30	0.404	92003	13.76	0.10766	1.18	4.693	1.68	0.3161	1.14	0.68	1760	43	1771	35	1766	28	-0.60
067-ZR52	0.806	274711	42.67	0.10802	0.80	4.460	1.53	0.2994	1.26	0.82	1766	29	1688	37	1723	25	4.41
029-ZR22	0.226	87668	16.38	0.09684	1.30	3.949	2.09	0.2958	1.59	0.76	1564	48	1670	47	1624	34	-6.79
013-ZR8	0.194	123008	20.23	0.09578	1.21	3.705	2.49	0.2806	2.15	0.86	1543	45	1594	60	1573	39	-3.30
004-ZR1	0.297	483776	16.13	0.09259	0.59	3.578	1.13	0.2803	0.89	0.79	1480	22	1593	25	1545	18	-7.65
033-ZR24	0.151	223640	19.78	0.09660	0.98	3.697	1.64	0.2775	1.27	0.77	1560	36	1579	36	1571	26	-1.24
014-ZR9	0.622	71837	11.36	0.09485	1.39	3.612	1.94	0.2762	1.30	0.67	1525	52	1572	36	1552	31	-3.07
058-ZR45	0.491	29484	10.64	0.09636	1.69	3.478	2.47	0.2617	1.76	0.71	1555	63	1499	47	1522	39	3.61
075-ZR58	0.184	98900	13.81	0.08879	0.84	3.146	1.51	0.2569	1.21	0.80	1400	32	1474	32	1444	23	-5.31
050-ZR39	0.405	103654	21.62	0.08746	1.27	2.902	1.72	0.2406	1.10	0.64	1371	49	1390	28	1382	26	-1.39
049-ZR38	0.149	65994	11.71	0.08452	1.26	2.672	1.94	0.2293	1.44	0.74	1305	48	1331	34	1321	29	-2.01
034-ZR25	0.087	60998	16.57	0.08599	1.17	2.672	1.84	0.2253	1.37	0.74	1338	45	1310	32	1321	27	2.11
046-ZR35	0.183	73451	23.01	0.08141	1.03	2.396	1.57	0.2134	1.12	0.72	1231	40	1247	25	1241	22	-1.26
010-ZR7	0.310	55012	12.80	0.08140	1.50	2.384	2.16	0.2124	1.51	0.70	1231	58	1242	34	1238	31	-0.87
024-ZR17	0.218	132944	14.40	0.07912	0.93	2.311	1.54	0.2118	1.17	0.76	1175	37	1238	26	1216	22	-5.39
047-ZR36	0.243	15259	15.75	0.08147	2.60	2.346	4.03	0.2088	3.06	0.76	1233	100	1222	68	1226	57	0.83
044-ZR33	0.214	39372	9.56	0.07790	1.72	2.128	2.38	0.1981	1.61	0.68	1144	67	1165	34	1158	33	-1.82
074-ZR57	0.293	47220	12.33	0.07859	1.69	2.142	2.51	0.1977	1.81	0.72	1162	66	1163	39	1163	34	-0.10
070-ZR55	0.477	38614	9.98	0.07412	1.67	1.982	2.42	0.1940	1.71	0.71	1045	67	1143	36	1110	32	-9.40
045-ZR34	0.422	26252	16.31	0.07674	1.92	2.016	2.73	0.1905	1.90	0.70	1114	76	1124	39	1121	37	-0.90
077-ZR60	0.185	35988	18.23	0.07182	1.68	1.782	2.42	0.1799	1.69	0.70	981	68	1067	33	1039	31	-8.74
063-ZR48	0.186	106478	14.78	0.07339	1.10	1.789	1.57	0.1768	1.06	0.68	1025	44	1050	21	1042	20	-2.44
079-ZR62	0.287	38139	15.19	0.07059	1.50	1.679	2.18	0.1725	1.55	0.71	946	61	1026	29	1001	28	-8.51
030-ZR23	0.655	22411	19.69	0.06993	3.83	1.616	4.84	0.1676	2.93	0.61	926	153	999	54	976	60	-7.82
009-ZR6	0.438	38524	28.71	0.07281	1.94	1.629	2.68	0.1623	1.82	0.68	1009	78	969	33	982	33	3.88
038-ZR29	0.225	52529	16.07	0.07509	2.15	1.476	2.68	0.1426	1.56	0.58	1071	85	859	25	921	32	19.77
068-ZR53	0.039	94433	11.81	0.06613	1.12	1.233	1.69	0.1352	1.20	0.71	811	47	817	18	815	19	-0.82
054-ZR41	0.562	43330	11.22	0.06513	1.79	1.212	2.41	0.1349	1.57	0.65	779	75	816	24	806	27	-4.77
026-ZR19	0.317	14119	18.30	0.06562	2.31	1.059	3.17	0.1171	2.13	0.67	794	95	714	29	734	33	10.17
005-ZR2	0.615	216107	20.75	0.06161	0.77	0.978	1.28	0.1152	0.96	0.75	661	33	703	13	693	13	-6.36
008-ZR5	0.311	4073	20.07	0.06576	1.06	1.024	1.47	0.1130	0.95	0.65	799	44	690	12	716	15	13.61
025-ZR18	1.371	8009	11.38	0.06424	0.99	0.974	1.53	0.1099	1.10	0.72	750	42	672	14	690	15	10.32

aba-ax-05											Apparent Ages						
	Th/U	$^{206}Pb/^{204}Pb$	1σ%	$^{207}Pb/^{206}Pb$	1σ %	$^{207}Pb/^{235}U$	1σ %	$^{206}Pb/^{238}U$	1σ %	Rho	$^{207}Pb/^{206}Pb$	2σ abs	$^{206}Pb/^{238}U$	2σ abs	$^{207}Pb/^{235}U$	2σ abs	% U-Pb disc[4]
014-ZR8	0.360	185084	13.31	0.13461	0.86	7.459	1.49	0.4018	1.16	0.78	2159	30	2178	43	2168	27	-0.86
015-ZR9	0.239	64702	13.04	0.13319	1.09	7.272	1.69	0.3959	1.24	0.73	2141	38	2150	45	2145	30	-0.46
036-ZR25	0.430	85312	11.66	0.13145	1.01	6.730	1.51	0.3713	1.06	0.70	2117	35	2036	37	2077	26	3.87
050-ZR36	0.085	62726	14.42	0.12995	1.31	6.580	1.72	0.3672	1.06	0.61	2097	46	2016	37	2057	30	3.86
073-ZR53	0.933	138382	12.38	0.12540	1.08	6.310	1.81	0.3650	1.41	0.78	2034	38	2006	49	2020	32	1.41
028-ZR19	0.261	143085	18.60	0.12530	0.93	6.269	1.59	0.3628	1.24	0.78	2033	33	1996	42	2014	28	1.84
048-ZR34	0.351	145255	13.26	0.12197	0.95	5.725	1.41	0.3404	0.97	0.69	1985	34	1889	32	1935	24	4.87
009-ZR5	0.501	138654	44.66	0.11789	1.29	5.323	1.95	0.3274	1.42	0.73	1924	46	1826	45	1873	33	5.12
075-ZR55	0.124	461956	13.61	0.11083	1.23	4.957	1.70	0.3244	1.12	0.66	1813	44	1811	35	1812	29	0.12
033-ZR22	0.218	131387	27.87	0.11894	0.79	5.245	1.41	0.3198	1.11	0.79	1940	28	1789	35	1860	24	7.81
067-ZR49	0.364	76467	8.96	0.10820	1.23	4.759	1.81	0.3189	1.28	0.71	1769	45	1785	40	1778	30	-0.86
054-ZR38	0.434	74707	11.94	0.10323	1.24	4.444	1.68	0.3122	1.07	0.64	1683	45	1752	33	1721	28	-4.07
023-ZR14	0.506	254422	10.91	0.10565	1.08	4.499	1.60	0.3088	1.12	0.70	1726	39	1735	34	1731	26	-0.53
079-ZR59	0.335	67421	11.42	0.10409	1.62	4.410	2.25	0.3073	1.52	0.68	1698	59	1727	46	1714	37	-1.71
030-ZR21	0.654	28786	11.28	0.11264	1.76	4.741	2.70	0.3052	2.02	0.75	1842	63	1717	61	1774	45	6.79
039-ZR28	0.444	19285	11.83	0.10992	2.59	4.608	4.24	0.3041	3.34	0.79	1798	93	1711	100	1751	70	4.82
053-ZR37	0.660	86164	11.04	0.10901	1.26	4.537	1.80	0.3019	1.22	0.68	1783	46	1701	37	1738	30	4.62
040-ZR29	0.689	92494	10.15	0.10821	1.12	4.488	1.51	0.3008	0.94	0.62	1769	41	1695	28	1729	25	4.20
069-ZR51	0.243	46252	34.35	0.10533	0.95	4.262	1.59	0.2934	1.23	0.77	1720	35	1659	36	1686	26	3.57
063-ZR45	0.261	89602	26.11	0.10825	1.12	4.315	2.36	0.2891	2.04	0.87	1770	41	1637	59	1696	38	7.53
024-ZR15	0.365	50300	21.89	0.10656	1.03	4.142	1.53	0.2819	1.07	0.70	1741	37	1601	30	1663	25	8.06
004-ZR1	0.576	102024	13.09	0.09440	0.70	3.652	1.19	0.2805	0.89	0.75	1516	26	1594	25	1561	19	-5.14
070-ZR52	0.560	88454	13.01	0.09612	1.23	3.618	1.85	0.2729	1.34	0.72	1550	46	1556	37	1553	29	-0.36
058-ZR42	0.360	24414	11.15	0.09525	3.13	3.507	4.18	0.2670	2.75	0.66	1533	116	1526	75	1529	65	0.48
026-ZR17	0.376	133641	9.35	0.09385	0.91	3.442	1.40	0.2660	0.99	0.71	1505	34	1520	27	1514	22	-1.01
047-ZR33	0.220	90074	15.52	0.09427	0.99	3.423	1.48	0.2634	1.04	0.70	1514	37	1507	28	1510	23	0.44
078-ZR58	0.368	84109	11.49	0.09303	1.45	3.353	2.16	0.2614	1.56	0.72	1489	54	1497	42	1494	34	-0.56
077-ZR57	0.241	57180	11.43	0.09526	1.28	3.401	2.11	0.2589	1.63	0.78	1533	48	1484	43	1505	33	3.20
005-ZR2	0.478	3958	5.23	0.09676	0.50	3.435	1.23	0.2575	1.06	0.86	1563	19	1477	28	1512	19	5.48
007-ZR3B	0.360	20401	66.69	0.08751	0.60	3.051	1.10	0.2528	0.84	0.77	1372	23	1453	22	1420	17	-5.92
066-ZR48	0.175	134254	20.98	0.09005	0.75	3.062	1.29	0.2466	0.98	0.76	1427	29	1421	25	1423	20	0.41
006-ZR3N	0.355	158385	16.62	0.08762	0.61	2.888	1.28	0.2390	1.06	0.83	1374	23	1382	26	1379	19	-0.56
056-ZR40	0.327	92758	17.57	0.08709	1.04	2.859	1.53	0.2381	1.07	0.69	1362	40	1377	26	1371	23	-1.04
049-ZR35	0.357	105741	15.94	0.08911	1.32	2.904	1.80	0.2363	1.16	0.65	1407	50	1367	29	1383	27	2.79
010-ZR6	0.649	42790	14.15	0.08680	1.38	2.792	2.08	0.2333	1.51	0.73	1356	53	1352	37	1353	31	0.33
046-ZR32	0.250	29359	17.58	0.08893	1.83	2.849	2.69	0.2324	1.94	0.72	1403	69	1347	47	1369	40	3.97
038-ZR27	0.572	154549	9.97	0.08606	0.78	2.724	1.28	0.2295	0.95	0.74	1340	30	1332	23	1335	19	0.56
060-ZR44	0.174	74238	16.84	0.09050	1.23	2.858	1.87	0.2290	1.36	0.73	1436	47	1329	33	1371	28	7.43
008-ZR4	0.283	42584	33.33	0.08328	0.77	2.495	1.31	0.2173	1.00	0.76	1276	30	1267	23	1271	19	0.65
076-ZR56	0.265	80046	12.65	0.08181	1.18	2.411	1.80	0.2138	1.31	0.73	1241	46	1249	30	1246	26	-0.63
016-ZR10	0.151	233682	14.26	0.08018	0.70	2.344	1.16	0.2120	0.85	0.73	1201	28	1239	19	1226	17	-3.17
017-ZR11	0.239	58990	13.88	0.08113	1.29	2.354	1.85	0.2104	1.28	0.69	1225	50	1231	29	1229	26	-0.52
055-ZR39	0.253	86687	23.32	0.07948	1.20	2.300	1.74	0.2099	1.20	0.69	1184	47	1228	27	1212	24	-3.71
034-ZR23	0.178	75446	11.87	0.08302	0.97	2.387	1.53	0.2085	1.13	0.74	1270	38	1221	25	1239	22	3.83
074-ZR54	0.067	317935	29.46	0.07642	0.89	2.097	1.53	0.1991	1.19	0.78	1106	35	1170	25	1148	21	-5.81
018-ZR12	0.075	213463	12.13	0.07610	0.95	2.027	1.39	0.1932	0.94	0.68	1098	38	1139	20	1125	19	-3.72
080-ZR60	0.423	53983	35.68	0.07681	2.33	1.978	3.22	0.1867	2.19	0.68	1116	92	1104	44	1108	43	1.14
019-ZR13N	0.238	22572	26.35	0.07861	1.37	1.928	1.77	0.1778	1.05	0.59	1162	54	1055	20	1091	23	9.22
045-ZR31	0.360	36636	16.70	0.07499	2.27	1.834	3.05	0.1773	2.00	0.66	1068	90	1052	39	1058	40	1.49
057-ZR41	0.019	166024	13.17	0.07283	0.86	1.688	1.29	0.1681	0.90	0.69	1009	34	1002	17	1004	16	0.76
013-ZR7	0.571	101608	13.48	0.07150	1.01	1.639	1.60	0.1662	1.18	0.74	972	41	991	22	985	20	-2.01
020-ZR13B	0.402	3132	5.96	0.07945	1.33	1.692	1.80	0.1545	1.15	0.64	1183	52	926	20	1006	23	21.76

aba-ax-12												Apparent Ages						
	Th/U	$^{206}Pb/^{204}Pb$	1σ%	$^{207}Pb/^{206}Pb$	1σ %	$^{207}Pb/^{235}U$	1σ %	$^{206}Pb/^{238}U$	1σ %	Rho	$^{207}Pb/^{206}Pb$	2σ abs	$^{206}Pb/^{238}U$	2σ abs	$^{207}Pb/^{235}U$	2σ abs	% U-Pb disc[4]
058-ZR45	0.028	18065	49.59	0.22590	2.29	19.436	4.40	0.6240	3.74	0.85	3023	72	3126	184	3064	83	-3.39
009-ZR6	0.542	86392	22.10	0.18727	0.51	13.237	1.08	0.5126	0.88	0.81	2718	17	2668	38	2697	20	1.86
044-ZR33	0.596	61569	13.75	0.15942	1.41	10.194	2.14	0.4637	1.57	0.73	2450	47	2456	64	2452	39	-0.26
025-ZR18	0.185	147546	13.22	0.16070	0.91	10.018	1.33	0.4521	0.90	0.67	2463	31	2405	36	2436	24	2.37
040-ZR31	0.475	88783	11.11	0.15464	1.54	9.386	2.15	0.4402	1.46	0.68	2398	52	2351	57	2376	39	1.94
007-ZR4	0.186	165968	14.28	0.12393	0.52	6.555	1.08	0.3836	0.88	0.81	2014	18	2093	31	2053	19	-3.94
024-ZR17	0.365	159767	35.37	0.12840	1.14	6.634	1.60	0.3747	1.07	0.67	2076	40	2052	38	2064	28	1.18
004-ZR1	0.259	133873	12.09	0.12187	0.55	6.103	1.08	0.3632	0.86	0.79	1984	19	1997	29	1991	19	-0.68
015-ZR10	0.518	182637	13.13	0.12101	0.56	6.013	1.23	0.3604	1.03	0.84	1971	20	1984	35	1978	21	-0.65
017-ZR12	0.557	121527	13.71	0.12199	0.76	5.969	1.14	0.3548	0.76	0.67	1986	27	1958	26	1971	20	1.41
019-ZR14	0.733	96067	19.22	0.11521	1.13	5.510	1.62	0.3469	1.10	0.68	1883	41	1920	36	1902	28	-1.93
073-ZR56	0.460	70205	13.01	0.11409	1.24	5.369	1.90	0.3413	1.40	0.73	1866	44	1893	46	1880	32	-1.47
066-ZR51	0.793	90447	16.32	0.12063	0.95	5.436	1.75	0.3268	1.43	0.81	1966	34	1823	45	1890	30	7.27
077-ZR60	0.731	63814	18.69	0.07550	1.30	2.033	1.94	0.1953	1.39	0.72	1082	52	1150	29	1127	26	-6.28
054-ZR41	0.354	33900	13.57	0.07745	1.47	1.897	2.12	0.1776	1.48	0.70	1133	58	1054	29	1080	28	6.98
065-ZR50	0.269	117779	34.99	0.07131	1.12	1.679	1.84	0.1708	1.41	0.77	966	45	1016	26	1001	23	-5.20
005-ZR2	0.214	182935	11.77	0.07224	0.54	1.701	1.06	0.1708	0.83	0.79	993	22	1016	16	1009	14	-2.40
008-ZR5	0.614	57582	14.11	0.07254	1.23	1.680	1.77	0.1679	1.22	0.69	1001	49	1001	23	1001	22	0.04
029-ZR22	0.337	27559	13.94	0.07251	2.46	1.648	3.48	0.1648	2.42	0.70	1000	98	983	44	989	43	1.69
063-ZR48	0.886	99701	11.82	0.06939	1.13	1.551	1.81	0.1621	1.37	0.76	910	46	968	25	951	22	-6.34
068-ZR53	0.308	91811	33.60	0.06815	1.17	1.387	1.78	0.1476	1.29	0.72	873	48	888	21	884	21	-1.69
055-ZR42	0.423	69362	10.53	0.06700	0.96	1.330	1.65	0.1439	1.29	0.78	838	40	867	21	859	19	-3.44
049-ZR38	0.250	41783	27.35	0.07025	1.33	1.382	2.11	0.1427	1.60	0.76	936	54	860	26	881	25	8.11
057-ZR44	0.411	25645	35.96	0.06742	2.86	1.325	3.71	0.1425	2.34	0.63	851	117	859	38	857	43	-0.93
067-ZR52	0.339	28891	24.47	0.06499	3.05	1.274	4.19	0.1422	2.84	0.68	774	126	857	46	834	47	-10.70
014-ZR9	0.348	316192	14.31	0.06630	0.48	1.289	1.08	0.1410	0.89	0.83	816	20	850	14	841	12	-4.23
036-ZR27	0.986	43975	46.16	0.06845	2.41	1.322	3.26	0.1401	2.17	0.66	882	98	845	34	855	37	4.22
035-ZR26	0.488	23952	12.25	0.06683	2.60	1.284	3.60	0.1393	2.46	0.68	832	107	841	39	839	41	-1.00
047-ZR36	0.378	21024	12.77	0.07103	3.05	1.346	4.39	0.1374	3.13	0.71	958	122	830	49	866	50	13.38
028-ZR21	0.371	66326	14.97	0.06675	0.99	1.233	1.60	0.1340	1.20	0.75	830	41	811	18	816	18	2.32
013-ZR8	0.407	95379	13.97	0.06493	0.70	1.177	1.14	0.1315	0.82	0.72	772	29	796	12	790	13	-3.13
056-ZR43	0.342	32713	9.14	0.06619	1.92	1.194	2.80	0.1308	2.00	0.71	812	79	793	30	798	31	2.42
030-ZR23	0.502	38348	12.29	0.06642	1.63	1.197	2.26	0.1307	1.52	0.67	820	67	792	23	799	25	3.37
069-ZR54	0.117	50136	8.60	0.06429	1.73	1.154	2.46	0.1302	1.72	0.70	751	72	789	25	779	27	-5.02
023-ZR16	0.143	54176	11.54	0.06551	1.38	1.170	1.96	0.1295	1.34	0.68	791	58	785	20	787	21	0.70
038-ZR29	0.300	28626	16.20	0.06386	1.54	1.093	2.14	0.1241	1.44	0.67	737	65	754	20	750	23	-2.33
034-ZR25	0.373	82445	12.87	0.06348	1.17	1.079	1.86	0.1233	1.40	0.75	724	49	750	20	743	20	-3.50
043-ZR32	0.249	110128	12.62	0.06305	1.24	1.049	1.91	0.1206	1.41	0.74	710	52	734	20	728	20	-3.41
033-ZR24	0.451	17313	14.04	0.06527	2.53	1.060	3.37	0.1178	2.20	0.65	783	104	718	30	734	35	8.34
074-ZR57	0.202	18822	13.80	0.06318	3.05	1.023	4.28	0.1175	2.98	0.70	714	127	716	40	716	44	-0.22
027-ZR20	0.362	21230	14.31	0.06203	2.93	0.990	3.80	0.1158	2.39	0.63	675	123	706	32	699	38	-4.63
006-ZR3	0.379	82948	12.34	0.06168	0.94	0.970	1.62	0.1140	1.27	0.78	663	40	696	17	688	16	-5.00
076-ZR59	0.268	47511	15.70	0.06190	1.36	0.966	2.03	0.1131	1.45	0.72	671	58	691	19	686	20	-3.01
059-ZR46	0.195	134686	15.59	0.06204	0.89	0.966	1.61	0.1130	1.29	0.80	675	38	690	17	687	16	-2.16
064-ZR49	0.302	25312	13.95	0.06214	2.10	0.960	2.94	0.1120	2.03	0.69	679	89	685	26	683	29	-0.83
053-ZR40	0.178	35638	15.05	0.06183	1.81	0.939	2.72	0.1102	2.00	0.74	668	76	674	26	672	27	-0.82
060-ZR47	0.202	62775	12.41	0.06259	1.10	0.945	1.82	0.1095	1.40	0.77	694	47	670	18	676	18	3.48
016-ZR11	0.277	35843	14.71	0.06117	1.89	0.919	2.55	0.1090	1.66	0.65	645	80	667	21	662	25	-3.37
045-ZR34	0.405	75575	13.40	0.06220	1.24	0.934	1.91	0.1089	1.40	0.74	681	52	666	18	670	19	2.19
026-ZR19	0.283	60561	10.63	0.06137	1.28	0.909	1.89	0.1074	1.34	0.71	652	55	658	17	656	18	-0.81
046-ZR35	0.303	45853	9.29	0.06175	1.84	0.911	2.55	0.1070	1.71	0.67	665	78	655	21	657	24	1.56
075-ZR58	0.268	89633	14.33	0.06125	1.21	0.894	1.84	0.1058	1.33	0.72	648	52	649	16	649	18	-0.08
039-ZR30	0.270	28344	12.52	0.06122	2.16	0.846	3.07	0.1002	2.15	0.70	647	91	616	25	622	28	4.81
010-ZR7	0.402	16346	14.37	0.06730	2.65	0.929	3.98	0.1001	2.95	0.74	847	108	615	35	667	39	27.40

aba-13												Apparent Ages						
	Th/U	$^{206}Pb/^{204}Pb$	1σ%	$^{207}Pb/^{206}Pb$	1σ %	$^{207}Pb/^{235}U$	1σ %	$^{206}Pb/^{238}U$	1σ %	Rho	$^{207}Pb/^{206}Pb$	2σ abs	$^{206}Pb/^{238}U$	2σ abs	$^{207}Pb/^{235}U$	2σ abs	% U-Pb disc[4]
076-Zir56	0.388	414930	0.02	0.22009	1.03	18.371	10.53	0.6053	263.50	0.82	2981	33	3051	77	3009	37	-2.34
040-Zir29	0.094	109726	0.02	0.18273	0.71	12.870	8.10	0.5108	131.46	0.64	2678	23	2660	29	2670	20	0.66
079-Zir59	0.802	79155	0.02	0.13377	1.11	7.913	20.20	0.4290	252.86	0.68	2148	39	2301	42	2221	29	-7.13
077-Zir57	0.293	127025	0.02	0.13406	0.70	7.287	14.87	0.3942	188.14	0.68	2152	24	2142	27	2147	19	0.45
008-Zir4	0.309	20214	0.07	0.13444	3.16	7.186	57.11	0.3877	668.57	0.63	2157	108	2112	93	2135	72	2.08
019-Zir12	0.305	118217	0.01	0.13324	0.89	7.065	20.51	0.3845	280.52	0.74	2141	31	2097	39	2120	26	2.05
029-Zir20	0.253	112047	0.02	0.13399	0.80	7.090	15.75	0.3838	179.10	0.62	2151	28	2094	25	2123	20	2.65
007-Zir3	0.442	57178	0.04	0.12107	1.26	6.394	27.28	0.3830	298.46	0.66	1972	45	2090	41	2031	30	-6.00
055-Zir39	0.219	195391	0.01	0.12345	0.56	6.310	16.63	0.3707	217.75	0.77	2007	20	2032	28	2020	18	-1.28
015-Zir9N	0.514	232198	0.01	0.12260	0.60	6.243	19.50	0.3693	269.25	0.82	1994	21	2026	35	2010	21	-1.58
070-Zir52	0.690	18434	0.13	0.13778	2.16	6.929	40.96	0.3647	494.46	0.64	2199	74	2005	62	2102	50	8.86
063-Zir45	0.706	105003	0.01	0.12091	0.80	6.047	22.79	0.3627	292.25	0.77	1970	28	1995	36	1983	24	-1.29
053-Zir37	0.304	356912	0.00	0.12495	0.64	6.216	17.17	0.3608	214.04	0.72	2028	22	1986	26	2007	19	2.08
004-Zir1	0.276	104008	0.02	0.12355	1.20	6.133	37.79	0.3600	540.54	0.84	2008	42	1982	66	1995	40	1.29
014-Zir8	0.515	160675	0.02	0.12263	0.54	5.996	19.71	0.3546	277.56	0.83	1995	19	1957	33	1975	20	1.91
047-Zir33	0.305	169736	0.01	0.12014	0.56	5.699	18.16	0.3440	228.29	0.76	1958	20	1906	26	1931	18	2.69
016-Zir9B	0.199	120598	0.01	0.12287	0.95	5.784	31.41	0.3414	440.47	0.83	1998	34	1893	49	1944	31	5.25
013-Zir7	0.178	93377	0.01	0.11183	0.93	4.919	33.52	0.3190	411.25	0.80	1829	33	1785	41	1806	28	2.43
034-Zir23	0.501	99844	0.02	0.10834	0.67	4.641	21.47	0.3107	206.89	0.64	1772	24	1744	20	1757	17	1.57
066-Zir48	1.082	23847	0.06	0.10780	2.21	4.553	68.30	0.3063	704.00	0.69	1762	80	1723	65	1741	51	2.26
005-Zir2	0.371	85881	0.02	0.10630	0.92	4.490	30.48	0.3063	306.47	0.69	1737	34	1722	28	1729	23	0.83
006-Zir2N	0.517	66499	0.02	0.10506	1.01	4.420	35.89	0.3051	382.79	0.74	1715	37	1716	35	1716	26	-0.07
048-Zir34	0.721	78981	0.02	0.11017	0.91	4.626	28.80	0.3045	294.08	0.67	1802	33	1714	27	1754	22	4.92
028-Zir19	0.789	26585	0.14	0.10606	1.48	4.254	50.67	0.2909	523.83	0.71	1733	54	1646	44	1685	35	5.01
044-Zir30	0.902	54601	0.03	0.10266	0.68	4.073	29.22	0.2878	313.08	0.76	1673	25	1630	26	1649	19	2.54
074-Zir54	0.275	53327	0.03	0.09837	1.09	3.867	42.34	0.2851	406.79	0.71	1593	41	1617	33	1607	26	-1.47
010-Zir6	0.235	27028	0.16	0.09683	3.13	3.785	130.78	0.2835	1347.18	0.77	1564	115	1609	108	1590	78	-2.88
025-Zir16	0.129	60166	0.06	0.09940	0.72	3.728	30.31	0.2720	288.97	0.70	1613	27	1551	22	1577	18	3.85
037-Zir26	0.084	155544	0.04	0.09569	0.54	3.423	30.25	0.2594	310.12	0.78	1542	20	1487	21	1510	16	3.57
054-Zir38	0.279	85049	0.02	0.09512	0.85	3.378	38.39	0.2576	352.65	0.70	1530	32	1477	24	1499	20	3.47
069-Zir51	0.235	43933	0.03	0.08991	1.53	3.142	68.47	0.2535	578.29	0.68	1424	58	1456	38	1443	33	-2.29
064-Zir46	0.135	289399	0.01	0.09079	0.66	3.173	32.10	0.2535	268.37	0.67	1442	25	1456	18	1451	16	-0.97
060-Zir44	0.319	109786	0.02	0.08971	0.93	2.969	41.98	0.2400	311.43	0.60	1419	35	1387	19	1400	19	2.30
059-Zir43	0.292	26209	0.06	0.08781	1.24	2.836	63.29	0.2342	532.85	0.70	1378	47	1356	30	1365	27	1.59
075-Zir55	0.227	49005	0.06	0.08359	1.19	2.584	74.86	0.2242	658.10	0.76	1283	46	1304	35	1296	28	-1.62
035-Zir24	0.163	95071	0.02	0.08677	0.88	2.674	45.28	0.2235	334.66	0.62	1355	34	1300	18	1321	18	4.08
056-Zir40	0.215	76601	0.02	0.08664	1.02	2.639	63.46	0.2209	576.40	0.76	1352	39	1287	30	1312	25	4.87
017-Zir10	0.280	14060	0.16	0.08616	0.75	2.558	45.76	0.2153	379.33	0.70	1342	29	1257	19	1289	17	6.30
009-Zir5	0.279	19578	0.08	0.08223	3.28	2.423	183.19	0.2137	1389.79	0.67	1251	126	1248	67	1249	63	0.21
027-Zir18	0.226	28743	0.07	0.08566	1.15	2.514	68.92	0.2129	585.16	0.72	1330	44	1244	28	1276	25	6.50
039-Zir28	0.173	142671	0.01	0.08232	0.62	2.387	40.63	0.2103	305.79	0.66	1253	24	1230	14	1239	14	1.83
057-Zir41	0.119	132344	0.01	0.08300	0.93	2.401	61.18	0.2098	511.72	0.73	1269	36	1228	24	1243	21	3.25
018-Zir11	0.381	13098	0.34	0.07992	1.36	2.212	96.62	0.2007	801.53	0.75	1195	53	1179	35	1185	30	1.31
038-Zir27	0.255	50775	0.04	0.07881	0.78	2.121	57.22	0.1951	438.98	0.71	1167	31	1149	18	1156	17	1.56
030-Zir21	0.383	110497	0.05	0.07588	1.08	1.910	75.76	0.1825	484.36	0.61	1092	43	1081	18	1084	19	1.04
026-Zir17	0.389	92352	0.02	0.07713	0.69	1.909	56.90	0.1795	418.09	0.69	1125	27	1064	15	1084	14	5.36
078-Zir58	0.222	40982	0.03	0.07019	1.72	1.585	153.72	0.1638	1032.18	0.69	934	70	978	31	964	30	-4.68
045-Zir31	0.332	145575	0.01	0.07373	0.63	1.657	64.03	0.1630	470.66	0.72	1034	25	974	14	992	13	5.85
050-Zir36	0.134	23265	0.20	0.07581	0.82	1.649	93.35	0.1578	791.65	0.81	1090	33	944	22	989	19	13.37
058-Zir42	0.640	42653	0.05	0.07220	2.36	1.547	198.73	0.1553	1242.34	0.63	992	95	931	33	949	38	6.14

aba-ax-G2											Apparent Ages						
	Th/U	$^{206}Pb/^{204}Pb$	1σ%	$^{207}Pb/^{206}Pb$	1σ %	$^{207}Pb/^{235}U$	1σ %	$^{206}Pb/^{238}U$	1σ %	Rho	$^{207}Pb/^{206}Pb$	2σ abs	$^{206}Pb/^{238}U$	2σ abs	$^{207}Pb/^{235}U$	2σ abs	% U-Pb disc[4]
008-ZR4N	0.249	162466	24.38	0.12871	0.96	6.702	1.58	0.3776	1.20	0.76	2080	34	2065	42	2073	28	0.73
009-ZR4B	0.345	115164	11.29	0.12958	1.13	7.070	1.63	0.3957	1.13	0.69	2092	39	2149	41	2120	29	-2.71
004-ZR1	0.270	222643	17.00	0.12893	0.61	6.737	1.17	0.3789	0.93	0.79	2083	21	2071	33	2077	21	0.58
024-ZR11	0.325	152997	15.76	0.12933	0.79	6.644	1.20	0.3726	0.83	0.69	2089	28	2041	29	2065	21	2.27
025-ZR12	0.754	70939	9.73	0.12973	1.11	6.726	1.75	0.3760	1.31	0.75	2094	39	2057	46	2076	31	1.76
014-ZR6	0.347	176145	12.10	0.13063	0.93	7.101	1.44	0.3942	1.03	0.72	2106	32	2142	37	2124	25	-1.71
015-ZR7	0.375	73028	16.31	0.13051	0.89	6.796	1.46	0.3777	1.10	0.75	2105	31	2065	39	2085	26	1.87
026-ZR13	0.914	107452	15.69	0.13026	0.98	6.675	1.50	0.3716	1.07	0.72	2101	34	2037	37	2069	26	3.06
020-ZR10N	0.938	117850	16.02	0.12946	1.13	6.320	1.70	0.3541	1.21	0.72	2091	39	1954	41	2021	30	6.54
010-ZR5N	0.353	94309	14.74	0.13069	1.26	6.802	1.81	0.3774	1.25	0.69	2107	44	2064	44	2086	32	2.03
013-ZR5B	0.287	77737	12.18	0.13159	1.26	7.003	1.90	0.3860	1.38	0.72	2119	44	2104	49	2112	34	0.72
005-ZR2	1.987	7110	12.37	0.13059	0.63	6.327	1.12	0.3513	0.85	0.76	2106	22	1941	28	2022	19	7.83
017-ZR8B	0.471	1750	9.79	0.10608	1.43	2.191	1.78	0.1498	1.00	0.56	1733	52	900	17	1178	25	48.08
aba-ax-G3											Apparent Ages						
	Th/U	$^{206}Pb/^{204}Pb$	1σ%	$^{207}Pb/^{206}Pb$	1σ %	$^{207}Pb/^{235}U$	1σ %	$^{206}Pb/^{238}U$	1σ %	Rho	$^{207}Pb/^{206}Pb$	2σ abs	$^{206}Pb/^{238}U$	2σ abs	$^{207}Pb/^{235}U$	2σ abs	% U-Pb disc[4]
037-ZR25	0.456	174916	20.35	0.12838	0.93	6.771	1.31	0.3825	0.84	0.64	2076	33	2088	30	2082	23	-0.59
024-ZR15	0.271	37701	40.29	0.11103	0.65	3.181	1.43	0.2078	1.21	0.85	1816	24	1217	27	1453	22	33.00
026-ZR17	0.454	72227	27.43	0.12988	0.54	7.005	1.20	0.3911	1.01	0.84	2096	19	2128	36	2112	21	-1.51
029-ZR20	0.550	155059	21.64	0.13052	0.54	6.964	1.25	0.3870	1.07	0.85	2105	19	2109	38	2107	22	-0.18
027-ZR18	0.365	145719	22.26	0.13056	0.66	6.890	1.12	0.3827	0.83	0.74	2106	23	2089	30	2097	20	0.78
014-ZR08	0.386	293586	15.70	0.13099	0.49	7.041	1.01	0.3898	0.80	0.79	2111	17	2122	29	2117	18	-0.51
028-ZR19	0.357	115578	25.48	0.13079	0.63	6.950	1.21	0.3854	0.97	0.80	2109	22	2101	35	2105	21	0.35
030-ZR21	0.477	6693	9.88	0.12161	0.77	4.494	1.61	0.2680	1.37	0.85	1980	27	1531	37	1730	27	22.69
015-ZR09	0.380	206212	15.86	0.13053	0.53	6.807	0.96	0.3782	0.71	0.74	2105	18	2068	25	2087	17	1.76
019-ZR13	0.334	264214	26.35	0.13024	0.49	6.684	1.39	0.3722	1.25	0.90	2101	17	2040	44	2070	24	2.93
010-ZR07	0.418	138384	16.12	0.13035	0.68	6.714	1.15	0.3736	0.85	0.74	2103	24	2046	30	2074	20	2.69
016-ZR10	0.342	288814	63.48	0.13167	0.45	7.194	1.49	0.3962	1.37	0.92	2120	16	2152	50	2136	26	-1.47
040-ZR28	0.461	189008	19.11	0.13152	0.59	7.079	1.19	0.3904	0.96	0.81	2118	20	2125	35	2121	21	-0.29
006-ZR03	0.351	471759	15.30	0.13076	0.42	6.788	1.08	0.3765	0.92	0.85	2108	15	2060	32	2084	19	2.30
018-ZR12	0.478	238134	25.86	0.13150	0.42	7.057	0.92	0.3892	0.72	0.79	2118	15	2119	26	2119	16	-0.05
038-ZR26	0.525	190337	15.01	0.13151	0.82	6.984	1.16	0.3851	0.73	0.63	2118	29	2100	26	2109	21	0.85
009-ZR06	0.502	105236	21.76	0.13149	0.64	6.945	1.27	0.3830	1.03	0.81	2118	22	2090	37	2104	22	1.30
005-ZR02	0.346	262148	17.08	0.13039	0.45	6.543	1.15	0.3639	0.99	0.86	2103	16	2001	34	2052	20	4.88
034-ZR22	0.474	235748	18.55	0.13025	0.45	6.456	1.18	0.3595	1.02	0.87	2101	16	1980	35	2040	21	5.79
017-ZR11	0.468	270226	15.07	0.13162	0.42	6.905	0.87	0.3805	0.67	0.76	2120	15	2079	24	2099	15	1.94
008-ZR05	0.361	144854	22.26	0.13096	0.52	6.657	1.01	0.3686	0.78	0.77	2111	18	2023	27	2067	18	4.17
035-ZR23	0.322	259020	17.55	0.13110	0.36	6.699	0.96	0.3706	0.81	0.84	2113	13	2032	28	2073	17	3.81
007-ZR04	0.602	129352	37.15	0.12948	1.70	6.133	3.39	0.3435	2.91	0.86	2091	59	1903	96	1995	58	8.97
036-ZR24	0.557	40051	51.14	0.13301	0.79	7.315	2.19	0.3988	2.01	0.92	2138	27	2164	74	2151	39	-1.20
025-ZR16	0.282	84150	32.81	0.13200	0.40	6.874	1.17	0.3777	1.03	0.88	2125	14	2066	36	2095	21	2.79
020-ZR14	0.109	3835	8.13	0.10952	1.19	2.600	3.33	0.1721	3.09	0.93	1792	43	1024	58	1301	48	42.85

Appendix 3.2. Summary of in situ Lu/Hf data.

		Age					$^{176}Hf/^{177}Hf$		εHf	T_{DM}
	sample	(Ma)	$^{176}Hf/^{177}Hf$	±2SE	$^{176}Lu/^{177}Hf$	±2SE	(t)	±2SE	(t)	(Ga)
aba-13	zir 1	2008.12	0.281427	0.000029	0.000421	0.000000	0.281411	0.07	-3.20	2.49
	zir 2N	1715.30	0.281408	0.000026	0.000448	0.000005	0.281393	0.34	-10.59	2.51
	zir 5	1250.99	0.282136	0.000025	0.000334	0.000009	0.282129	0.62	4.88	1.53
	zir 6	1563.90	0.281250	0.000035	0.000851	0.000041	0.281225	2.45	-20.05	2.75
	zir 8	1994.81	0.281339	0.000035	0.001084	0.000091	0.281297	0.71	-7.55	2.65
	zir 9N	1994.43	0.281217	0.000034	0.001075	0.000015	0.281176	0.30	-11.88	2.81
	zir 19	1732.75	0.281450	0.000041	0.000638	0.000041	0.281430	0.84	-8.90	2.47
	zir 24	1355.44	0.281993	0.000029	0.000311	0.000008	0.281985	0.11	2.17	1.72
	zir 51	1423.62	0.282010	0.000035	0.001214	0.000039	0.281977	0.25	3.45	1.74
	zir 48	1762.49	0.281455	0.000035	0.000711	0.000014	0.281432	0.52	-8.15	2.47
	zir 28	1253.23	0.282093	0.000032	0.001144	0.000048	0.282065	0.16	2.69	1.62
	zir 30	1672.80	0.281516	0.000043	0.000705	0.000013	0.281493	0.27	-8.01	2.38
	zir 31	1033.97	0.282163	0.000035	0.001158	0.000022	0.282141	0.02	0.37	1.52
	zir 38	1530.48	0.281817	0.000033	0.000750	0.000008	0.281795	0.02	-0.57	1.98
	zir 39	2006.71	0.281196	0.000036	0.001352	0.000016	0.281144	0.27	-12.72	2.86
	zir 41	1269.11	0.282119	0.000036	0.001121	0.000118	0.282092	0.54	4.01	1.58
	zir 45	1969.64	0.281321	0.000032	0.000678	0.000007	0.281296	0.20	-8.18	2.64
	zir 58	977.63	0.282050	0.000038	0.000421	0.000004	0.282042	0.18	-4.39	1.65
aba-ax-05	zir 3N	1379.00	0.281956	0.000037	0.001176	0.000011	0.281925	0.01	0.58	1.81
	zir 4	1271.00	0.282235	0.000045	0.002355	0.000165	0.282179	0.60	7.12	1.47
	zir 6	1353.00	0.282045	0.002803	0.000973	0.000020	0.282020	0.18	3.37	1.68
	zir 7	991.00	0.281992	0.000047	0.001089	0.000004	0.281972	0.16	-6.59	1.76
	zir 8	2168.05	0.281525	0.000034	0.000877	0.000030	0.281489	0.15	3.26	2.38
	zir 9	2145.39	0.281559	0.000041	0.001213	0.000009	0.281509	0.07	3.46	2.36
	zir 11	1229.00	0.282291	0.000035	0.001381	0.000051	0.282259	0.52	8.99	1.36
	zir 14	1731.00	0.281693	0.000028	0.001616	0.000003	0.281640	0.02	-1.46	2.20
	zir 19	2014.00	0.281431	0.000031	0.000674	0.000007	0.281405	0.08	-3.27	2.50
	zir 17	1514.00	0.281809	0.000036	0.000776	0.000001	0.281787	0.02	-1.25	1.99
	zir 60	1108.00	0.282175	0.000031	0.000898	0.000004	0.282156	0.11	2.61	1.50
	zir 59	1714.00	0.281690	0.000036	0.000868	0.000024	0.281662	0.05	-1.08	2.16
	zir 58	1494.00	0.281821	0.000028	0.000844	0.000012	0.281797	0.05	-1.33	1.98
	zir 56	1246.00	0.282059	0.000040	0.000969	0.000010	0.282036	0.05	1.49	1.66
	zir 55	1812.00	0.281592	0.000059	0.001596	0.000081	0.281538	0.22	-3.24	2.33
	zir 31	1058.00	0.282189	0.000041	0.000937	0.000010	0.282171	0.10	1.98	1.48
	zir 33	1510.00	0.281944	0.000045	0.001236	0.000017	0.281909	0.09	3.00	1.83
	zir 35	1383.00	0.281896	0.000039	0.001001	0.000004	0.281870	0.03	-1.28	1.88
	zir 49	1778.00	0.281650	0.000026	0.001253	0.000020	0.281607	0.05	-1.55	2.24

aba-ax-02	zir 3	3336.00	0.280941	0.000084	0.001658	0.000091	0.280834	0.47	7.43	3.23
	zir 11	2143.00	0.281459	0.000054	0.001066	0.000009	0.281415	0.00	0.07	2.48
	zir 7	1238.00	0.282227	0.000148	0.002367	0.000119	0.282172	0.46	6.12	1.48
	zir 24	1571.00	0.281839	0.000059	0.001568	0.000059	0.281792	0.01	0.26	1.99
	zir 21	1924.00	0.281373	0.000039	0.001116	0.000002	0.281332	0.19	-7.95	2.60
	zir 43	1911.00	0.281450	0.000048	0.001108	0.000103	0.281410	0.62	-5.49	2.50
	zir 53	817.00	0.282239	0.000227	0.001932	0.000015	0.282209	0.07	-2.12	1.45
	zir 51	1932.00	0.281447	0.000038	0.000745	0.000008	0.281420	0.16	-4.66	2.48
	zir 47	754.41	0.281676	0.000036	0.002220	0.000022	0.281645	0.61	-23.50	2.26
	zir 48	1042.00	0.282241	0.000047	0.002436	0.000034	0.282193	0.08	2.40	1.47
	zir 41	816.00	0.282190	0.000049	0.000564	0.000009	0.282181	0.14	-3.12	1.46
	zir 39	1382.00	0.282020	0.000053	0.001333	0.000040	0.281985	0.14	2.78	1.73
	zir 35	1241.00	0.282065	0.000037	0.000746	0.000017	0.282047	0.07	1.77	1.64
	zir 34	1121.00	0.282081	0.000045	0.000992	0.000013	0.282060	0.02	-0.51	1.63
	zir 33	1158.00	0.282147	0.000049	0.000558	0.000018	0.282135	0.18	3.00	1.52
	zir 31	2168.00	0.281413	0.000047	0.000592	0.000003	0.281388	0.01	-0.31	2.52
	zir 30	1766.00	0.282018	0.000031	0.000895	0.000013	0.281988	0.35	11.69	1.71
aba-ax-12	zir 1	1983.79	0.281311	0.000043	0.000696	0.000001	0.281285	0.10	-8.24	2.66
	zir 2	992.61	0.281956	0.000031	0.001284	0.000039	0.281932	0.42	-7.95	1.82
	zir 8	796.33	0.282488	0.000040	0.000663	0.000005	0.282478	0.16	6.97	1.06
	zir 10	1971.16	0.281511	0.000049	0.002264	0.000008	0.281427	0.05	-3.51	2.49
	zir 11	666.83	0.282690	0.000045	0.001161	0.000010	0.282675	0.44	11.02	0.79
	zir 6	2718.33	0.281117	0.000038	0.001459	0.000028	0.281041	0.01	0.20	2.97
	zir 5	1001.19	0.282279	0.000039	0.001282	0.000003	0.282255	0.19	3.69	1.37
	zir 17	2076.16	0.281357	0.000031	0.000350	0.000006	0.281343	0.15	-4.04	2.57
	zir 19	657.51	0.282858	0.000042	0.002835	0.000077	0.282823	0.84	16.04	0.58
	zir 21	810.57	0.282544	0.000029	0.001275	0.000019	0.282525	0.33	8.93	1.00
	zir 22	983.42	0.282365	0.000053	0.001959	0.000007	0.282329	0.29	5.89	1.27
	zir 29	754.27	0.282493	0.000040	0.000999	0.000013	0.282479	0.24	6.05	1.06
	zir 32	734.30	0.282656	0.000050	0.002562	0.000039	0.282620	0.44	10.59	0.87
	zir 31	2397.87	0.281252	0.000032	0.001004	0.000004	0.281206	0.04	-1.44	2.76
	zir 33	2449.54	0.281659	0.000056	0.001818	0.000031	0.281574	0.47	12.85	2.26
	zir 57	715.88	0.282682	0.000066	0.003198	0.000105	0.282639	0.97	10.85	0.85
	zir 58	648.60	0.282697	0.000033	0.001465	0.000002	0.282680	0.29	10.76	0.79
	zir 59	690.88	0.282555	0.000040	0.001379	0.000013	0.282537	0.25	6.68	0.99
aba-ax-G3	zir 10	2136.00	0.281447	0.000033	0.001376	0.000093	0.281391	0.08	-0.97	2.52
	zir 8	2117.00	0.281469	0.000028	0.000440	0.000009	0.281451	0.02	0.73	2.43
	zir 11	2099.00	0.281467	0.000027	0.000629	0.000009	0.281442	0.00	-0.01	2.45
	zir 12	2119.00	0.281507	0.000051	0.000422	0.000002	0.281490	0.03	2.18	2.38
	zir 6	2104.00	0.281515	0.000039	0.000589	0.000005	0.281492	0.04	1.87	2.38
	zir 28	2121.00	0.281470	0.000052	0.000578	0.000023	0.281447	0.03	0.67	2.44

4. Conclusions

While the basic principal behind the formation of the Neoproterozoic Brasília Belt is straight forward, a collision between three crustal cratons (Amazonian, Paranapampaian and the São Francisco), the evolutionary history of some of the belts different rock groups is not so straight forward. The Araxá Group is a very enigmatic rock group, with various types of schists and blocks of igneous rock. The combination of blocks of metamafic rocks together with ultramafic assemblages has led to parts of the Araxá Group to be called an ophiolitic mélange. The study of ophiolites can yeild information regarding the enviornment in which they formed. Mélanges are mixtures of different rock units which can form in a variety of different tectonic and sedimentary enviornments. The presented study approched the problems with the evolutionary history of the Araxá Group, by conducting isotopoc geochronological studies on selected components of the ophiolitic mélange, and in the case of metamafic assemblages, geochmistry as well.

The geochronological and geochemical approach applied to the rock assemblages of the Araxá Group ophiolitic assemblage in the area of Abadiânia proved successful in unraveling part of its evolutionary history. The combination of U-Pb and Lu-Hf methods on zircon grains collected from the ophiolitic components, combined with the geochemical finger print of associated mafic assemblages, revealed information on the formational history of the ophiolites. A provenance study of the mélanges other assemblages would yield further insight on the evolution of the mélange in regards to the evolutionary history of the Brasília Belt.

The mafic assemblage of the study area is an epidote-amphibole schist. Six samples were collected for geochemical analysis, Sm-Nd whole rock analysis, and U-Pb and Lu-Hf on any collected zircon grains. Geochemical results indicate that the mafic rocks were formed in a back-arc environment. Sm-Nd results demonstrated the mantle origin of the mafic rocks. Of the six samples collected, one yielded a significant amount of zircon grains. Together with some inherited grains, a Discordia revealed an age of 800 Ma, interpreted as the age of crystallization.

Ultramafic body S9 is in contact with the sampled mafic body, and formed a large metasomatic border zone between the two bodies. Fluids formed during serpentinization reacted

with surrounding host rock to form these metasomatic zones. At the contact with the mafic body, a rodingite-like rock is present, while closer to the contact with the serpentinite, is a course-grained chlorite schist (black-wall). The contact between these two extremes is disrupted, but collected samples indicate that there exists a gradation in mineral assemblages between the two end members. Zircon grains were recovered from the metasomatic assemblages, and a range of ages were calculated, from 800 to 760 Ma. This 40 Ma interval delineates the period of metasomatism, but is interpreted as the period of back-arc rifting, which was indicated by the mafic rock assemblages.

These results summarize the key points of the first article, and indicate that, at least in the area of Abadiânia, the Araxá Group began its deposition in a back-arc environment. This environment also represents the beginning point of mélange activity. The ophiolitic mélange of the Araxá Group was probably formed mostly by sedimentary processes, related to mass wasting. The majority of the rocks found in the Araxá Group are represented by garnet-mica schists, however there are exotic blocks, such as granites and quartzite, which accompany the ophiolitic blocks.

The garnet-mica schists of the Araxá Group appear to be petrographically similar, but provenance studies demonstrate that there are at least two different rock units present. The first group represents rocks interpreted to have been deposited into the newly formed back-arc basin. These rocks have a negative whole rock ε_{Nd}, indicating that a large portion of detrital material forming these rocks came from the São Francisco craton. Zircon analyses demonstrate that zircon grains originated from the craton, but there are also younger populations, which came from the magmatic arc. This first period of deposition has a maximum age of deposition at roughly 740 Ma, as indicated by the youngest dated zircon grain, but generally speaking it can be said that deposition occurred before the high grade metamorphic event which formed the Anápolis-Itauçu metamorphic complex at 670-650 Ma. The second garnet-mica schist group marks sedimentation after the metamorphic event. It is characterized by positive ε_{Nd} values and younger zircon populations, with a maximum age of deposition at c. 615 Ma.

These data support the fact that these two seemingly similar schists are two different rock units. However, there are no textures or formations that indicate a mélange setting, except for the exotic blocks. Results from the second article indicate that the quartzite/quartz schist, is similar

to some of the passive margin units of the Brasília Belt, while the granite is a Paleoproterozoic rock similar to those found within the Natividade Block (Fuck et al., 2014). As stated, there are no mélange related textures in the schist, which could help in understanding when the exotic blocks where introduced into the mélange. One idea is that they could have been introduced during mass wasting along the back-arc basin, during the first period of deposition. It is also possible that they could have been introduced during the second period of deposition and/or tectonically by means of strike-slip movement, which could explain the presence of the granite block.

One of the things demonstrated in this study is the complexity of the evolutionary history of the Brasília Belt, there was more than just a collision of island arcs followed by a continental collision and the closing of the Goiás Ocean. This complexity is similar in style to that of the southwestern Pacific Ocean, an idea expressed also by Stern (1994) about the Mozambique Ocean. The Goiás Massif best represents a continent which could have been in a similar situation as one of the islands in present day Indonesia. Movements of this fragment within the Goiás Ocean, and whether it facilitated the formation of the back-arc rifting and the ultramafic complexes of Niquelândia, Barro Alto and Cana Brava, are beyond the scope of this study, but the fact that rifting coincided with the formation of the ultramafic complexes, and tectonic movements which could be related to the Goiás Massif would help to explain how the Araxá Group evolved in the way that it did.

Future studies in this area should address the variation of the two described periods of sedimentary deposition in the Araxá Group, the variation in the types of mafic rock assemblages and their formation environment, and U-Pb studies on metosomatic zircon grains related to ultramafic rock assemblages. Using whole rock Sm-Nd analysis, it may be possible to map the distribution of the two schists groups (pre-650 and post-650 Ma). Together with the distribution of older granitic bodies and passive margin metasedimentary rocks, it may be possible to determine crustal movements within the Araxá Group. Geochemical studies on metamafic rock assemblages would be able to demonstrate the variation and distribution of the back-arc basin, or may indicate another ophiolitic environment, such as a fore-arc environment on the eastern side of the Araxá Group. The dating of metasomatic zircon grains from the ultramafic assemblages can be a powerful tool in relating the different ultramafic sequences and determining the exact

sequence of events of ophiolite formation and relating periods of ophiolite formation to the evolution of the Brasília Belt.

5. References

Albarède, F., Telouk, P., Blichert-Toft, J., Boyet, M., Agranier, A., Nelson, B., 2004. Precise and accurate isotopic measurements using multiple-collector ICPMS. Geochim Cosmochim Acta 68: 2725-2744.

Ali, K.A., Stern, R.J., Manton, W.I., Kimura, J.-I., Khamees, H.A., 2009. Geochemistry, Nd isotopes and U–Pb SHRIMP zircon dating of Neoproterozoic volcanic rocks from the Central Eastern Desert of Egypt: new insights into the 750 Ma crust-forming event. Precambrian Research 171, 1–22.

An, W., Hu, X., Garzanti, E., 2017. Sandstone provenance and tectonic evolution of the Xiukang Mélange from Neotethyan subduction to India–Asia collision (Yarlung-Zangbo suture, south Tibet). Gondwana Research 41, 222–234.

Angeli, N., Navarro, G. R. B., Zanardo, A., Vlach, S. R. F., 2010, Caracterização Química de Cromitas nos Maciços de Cromínia e Mairipotaba, Goiás, Brasil. Geol. USP, Sér. cient., São Paulo, v. 10, n. 1, p. 87-99.

Arena, K.R., Hartmann, L.A., Lana, C., 2016. Evolution of Neoproterozoic ophiolites from the southern Brasiliano Orogen revealed by zircon U-Pb-Hf isotopes and geochemistry. Precambrian Research 285, 299–314.

Arena, K.R., Hartmann, L.A., Lana, C., 2017. Tonian emplacement of ophiolites in the southern Brasiliano Orogen delimited by U-Pb-Hf isotopes of zircon from metasomatites. Gondwana Research 49, 296-332.

Bailey, E.B., and McCallien, W.J., 1950, The Ankara mélange and the Anatolian thrust: Nature, v. 166, p. 938–943.

Bailey, E.B., and McCallien, W.J., 1953, Serpentinite lavas, the Ankara mélange and the Anatolian thrust: Philosophical Transaction of the Royal Society of Edinburgh, v. 62, no. 11, p. 403–442.

Baldwin, J. A., Brown, M., 2008, Age and duration of ultrahigh-temperature metamorphism in the Anápolis–Itauçu Complex, Southern Brasília Belt, central Brazil – constraints from U–Pb geochronology, mineral rare earth element chemistry and trace-element thermometry

Barber, A.J., 2013. The origin of mélanges: cautionary tales from Indonesia. J. Asian Earth Sci. 76, 428–438.

Barbosa O. 1955. Guia de Excursões. In: Congr. Brás. Geol., 9, 1955. São Paulo SBG. Noticiário 3:3-5.

Barbosa, O. Braun O.P.G., Dyer R.C., Cunha C.A.B.R., 1970a. Geologia da Região do Triângulo Mineiro, Bol. Div. de Fom. da Prod. Min., Rio de Janeiro (136): p. 1-140.

Barnes, I., and O'Neal, J.R., 1966. The relationship between fluids in some fresh Alpine-type ultramafics and possible modern serpentinization, western United States: Bulletin Geological Society of America, v. 80, p. 1947–1960.

Barnes, J.D., Beltrando, M., Lee, C.-T.A., Cisneros, M., Loewy, S., Chin, E., 2014. Geochemistry of alpine serpentinites from rifting to subduction: a view across paleogeographic domains and metamorphic grade. Chemical Geology 389, 29–47.

Bayona, G., Montes, C., Cardona, A., Jaramillo, C., Ojeda, G., Valencia, V., Ayala-Calvo, C., 2011. Intraplate subsidence and basin filling adjacent to an oceanic arc–continent collision: a case from the southern Caribbean-South America plate margin. Basin Res. 23, 403–422.

Belousova, E. A., Jiménez, J. M. G., Graham, I., Griffin, W. L., O'Reilly, S. Y., Pearson, N., Martin, L., Craven, S., Talavera, C., 2015, The enigma of crustal zircons in upper-mantle rocks: Clues from the Tumut ophiolite, southeast Australia. GEOLOGY, v. 43; no. 2; p. 119–122.

Berrocal, J., Marangoni, Y., Côgo de Sá, N., Fuck, R. A., Soares, J. E. P., Dantas, E., Perosi, F., Fernandes, C., 2004. Deep seismic refraction and gravity crustal model and tectonic deformation in Tocantins Province, Central Brazil, Tectonophysics, 388, 187– 199.

Berbert, C.O.; Corrêa, J.A.; Mello, J.C.R. 1970. Geologia da área de Interlândia-Abadiânia. Goiás. Rio de Janeiro, DNPM. 59 p. (Boletim 135).

Berbert C.O. 1970. Geologia geral dos complexos básicos-ultrabásicos de Goiás. In: SBG, Congr. Bras. Geol., 24, Anais, p. 41-50.

Bogdanova, S.V., Pisarevsky, S.A., Li, Z.X., 2009. Assembly and breakup of Rodinia (someresults of IGCP project 440). Stratigraphy and Geological Correlation 17, 259–274.

Brod J.A., Leonardos, O.H., Meneses P.R., Albuquerque M.A.C., Almeida R., Blanco S.B., Cardoso F.B.F, Romão P.A., Tallarico F.H.B.,Thomsen F.P.R. 1992. Geoquímica da Sequência Vulcano Sedimentar de Abadia dos Dourados e Complexo Chapada das Perdizes, Triângulo Mineiro – MG. Revista Escola de Minas, 45(1-2):164-166.

Bühn, B., Pimentel, M.M., Matteini, M., Dantas, E.L., 2009. High spatial resolution analysis of Pb and U isotopes for geochronology by laser ablation multi-collector inductively coupled plasma mass spectrometry (LA-MC-ICPMS). Anais Academia Brasileira de Ciencias 81, 99–114.

Carlson, R.L., 2001. The abundance of ultramafic rocks in Atlantic Ocean crust. Geophys. J. Inter. 144, 37–48.

Caxito, F., Ulein, A., Stevenson, R., Uhlein, G.J., 2014. Neoproterozoic oceanic crust remnants in northeast Brazil. Geology, doi: 10.1130/G35479.1.

Chauvel, C., Blichert-Toft, J.E., 2001. A hafnium isotope and trace element perspective on melting of the depleted mantle. Earth Planet. Sci. Lett. 190, 137–151.

Chidester, A.H., 1962. Petrology and geochemistry of selected talc bearing ultramafic rocks and adjacent country rocks in a North Central Vermont - U. S. Geol. Prof., Paper 345 : 207 pp.

Coleman, R.G., 1967, Low-temperature reaction zones and alpine ultramafic rocks of California, Oregon, and Washington: U.S. Geological Survey Bulletin 1247, 49 p.

Coleman, R. G., Irwin, W. P., 1974, Ophiolites and ancient continental margins, In Burk, C. A., and Drake, C. L. (eds) The geology of continental margins: New York, Springer-Verlag, p. 921-931.

Cordani, U.G., Brito Neves, B.B.B., D'Agrella, M.S., 2003a. From Rodinia to Gondwana: a review of the available evidence from South America. Gondwana Research 6(2), 275–284.

Cordani, U. G., Pimentel, M. M., de Arau´ jo, C. E. G., and Fuck, R. A., 2013, The significance of the Tansbrasiliano-Kandi tectonic corridor for the amalgamation of West Gondwana: Brazilian Journal of Geology, v. 43, n. 3, p. 583–597, http://dx.doi.org/10.5327/Z2317-48892013000300012.

Correia C.T., Sinigoi S., Girardi V. A. V., Mazzucchelli M., Tassinari C. C. G., Giovanardi T., 2012. The growth of large mafic intrusions: comparing Niquelandia and Ivrea igneous complexes. Lithos 155:67–182

Cowan, D.S., 1982, Deformation of partly dewatered and consolidated Franciscan sediments near Piedras Blancas Point, California, in Leggett, J., ed., Trench-Forearc geology: Sedimentation and tectonics on modern and ancient active plate margins: Geological Society of London, Special Publication, v. 10, p. 429–457.

Cowan, D.S., 1985, Structural styles in Mesozoic and Cenozoic mélanges in the western Cordillera of North America: Geological Society of America Bullettin, v. 96, p. 451–462.

Dalziel, I.W.D., 1997. Neoproterozoic–Paleozoic geography and tectonics: review, hypothesis, environmental speculation. Geological Society of America Bulletin 109, 16–42.

Dangerfield, A., Harris, R., Sarıfakıoğlu, E., and Dilek, Y., 2011, Tectonic evolution of the Ankara Mélange and associated Eldivan ophiolite near Hançili, central Turkey, in Wakabayashi, J., and Dilek, Y., eds., Mélanges: Processes of Formation and Societal Significance: Geological Society of America Special Paper 480, p. 143–169, doi:10.1130/2011.2480(06).

Danni, J.C.M., Fuck, R.A., Leonardos Jr., O.H., 1982. Archean and lower Proterozoic Units in Central Brazil. Geological Rundsch 71, 291–317.

Dardenne, M.A., 2000. The Brasília fold belt. In: Cordani, U.G., Milani, E.J., Thomaz Filho, A., Campos, D.A. (Eds.), Tectonic Evolution of South America. 31st International Geological Congress, Rio de Janeiro, pp. 231e263.

Della Giustina, M. E. S.D., Pimentel, M.M., Ferreira Filho, C. F., Hollanda, M. H. B. M., 2011. Dating coeval mafic magmatism and ultrahigh temperature metamorphism in the Anapolis-Itaucu Complex, Central Brazil. Lithos, v. 124, 1–2, 82–102

DePaolo, D.J., 1981. A neodymium and strontium isotopic study of the Mesozoic calc-alkaline granitic batholiths of the Sierra Nevada and Peninsular Ranges. California Journal Geophysical Research 86, 10470–10488.

Deschamps, F., Godard, M., Guillot, S., Hattori, K., 2013. Geochemistry of subduction zone serpentinites: a review. Lithos 178, 96–127.

De Smet, M.E.M., Fortuin, A.R., Troelstra, S.R., Van Marle, L.J., Karmini, M., Tjokrosapoetro, S., Hadiwasastra, S., 1990. Detection of collision-related vertical movements in the Outer Banda Arc (Timor, Indonesia), using micropaleontological data. J. SE Asian Earth Sci. 4, 337–356.

Dharm Rao, C. V., Santosh, M., Wu, Y., 2011, Mesoproterozoic ophiolitic mélange from the SE periphery of the Indian plate: U–Pb zircon ages and tectonic implications. Gondwana Research 19: 384–401.

Dilek, Y., Ahmed, Z., 2003. Proterozoic ophiolites of the Arabian Shield and their significance in Precambrian tectonics. Ophiolites in Earth History: Journal of the Geological Society of London, Special Publications, 218, pp. 685–701.

Dilek, Y., Thy, P., 2006. Age and petrogenesis of plagiogranite intrusions in the Ankaramélange, central Turkey. Island Arc 15, 44–57.

Dilek, Y., Furnes, H., 2014, Ophiolites and their Origins Deep biosphere record of in situ oceanic lithosphere and ophiolites. Elements 10: 93-100.

Drake Jr. A.A. 1980. The Serra de Caldas window. Professional paper United States Geological Survey Washington (1119-AB):1B-19B.

Dubińska, E., Wiewióra, A., 1999. Layer silicates from a rodingite and its blackwall from Przemilow (Lower Silesia, Poland): mineralogical record of metasomatic processes during serpentinization and serpentinite recrystallization. Mineralogy and Petrology 67, 223–237.

Dubińska, E., Bylina, P., Kozłowski, A., Dörr,W., Nejbert, K., Schastokc, J., Kulickie, C., 2004. U-Pb dating of serpentinization-hydrothermal zircon from a metassomatic rodingite shell (Sudetic ophiolite, SW Poland). Chemical Geology 203, 183–203.

Duffy, B., Kalansky, J., Bassett, K., Harris, R., Quigley, M., van Hinsbergen, D. J. J., Strachan, L.S., Rosenthal, Y., 2017. Mélange versus forearc contributions to sedimentation and uplift,

during rapid denudation of a young Banda forearc-continent collisional belt. Journal of Asian Earth Sciences 138, 186–210.

El Hadi, H., Simancas, J.F., Martínez-Poyatos, D., Azor, A., Tahiri, A., Montero, P., Fanning, C.M., Bea, F., González-Lodeiro, F., 2010. Structural and geochronological constraints on the evolution of the Bou Azzer Neoproterozoic ophiolite (Anti-Atlas, Morocco). Precambrian Research 182, 1–14.

El-Rahman, Y. A., Polat, A., Dilek, Y., Fryer, B., El-Sharkawy, M., Sakran, S., 2009. Geochemistry and tectonic evolution of the Neoproterozoic Wadi Ghadir ophiolite, Eastern Desert, Egypt. Lithos 113, 158–178.

Elter, P., Trevisan, L., 1973. Olistostromes in the tectonic evolution of the Northern Apennines. In: De Jong, K.A., Scholten, R. (Eds.), Gravity and Tectonics. John Wiley and Sons, New York, pp. 175–188.

Evans, B.W., Hattori, K., Baronnet, A., 2013. Serpentinite: what, why, where? Elements 9, 99–106.

Falci, A., Caxito, F. A., Seer, H. J., Valeriano, C. M., Dias, P. H. A., Pedrosa-Soares, A. C., 2018. Provenance shift from a continental margin to a syn-orogenic basin in the Neoproterozoic Araxá nappe system, southern Brasília belt, Brazil. Precambrian Research 306, 209-219.

Ferreira Filho, C.F., Kamo, S., Fuck, R.A., Krogh, T., Naldrett, A. J. Zircon and rutile U-Pb geochronology of the Niquelândia layered mafic-ultramafic complex, Brazil. Precambrian Research 68, 241–255, 1994.

Ferreira Filho, C.F., Naldrett, A.J., Gorton, M.P. REE and pyroxene compositional variation across the Niquelândia mafic and ultramafic layered intrusion, Brazil: petrological and metallogenetic implications. Transaction of the Institution of Mining and Metallurgy 107, 1–22, 1998.

Ferreira Filho, C.F., Pimentel, M.M., Araujo, S.M., Laux, J.H. Layered intrusions and volcanic sequences in central Brazil: Geological and geochronological constraints for Mesoproterozoic (1.25 Ga) and Neoproterozoic (0.79 Ga) igneous associations. Precambrian Research 183, 617–634, 2010.

Festa, A., Pini, G. A., Dilek, Y., Codegone, G., 2010, 14 Mélanges and mélange-forming processes: a historical overview and new concepts. International Geology Review Vol. 52, Nos. 10–12, 1040–1105.

Fischel, D.P., Pimentel, M.M., Fuck, R.A., 1998. Idade do metamorfismo de alto grau no Complexo Anápolis–Itauçu, determinada pelo método Sm–Nd. Rev. Bras. Geociˆenc. 28 (4), 543–544.

Fischel, D.P., Pimentel, M.M., Fuck, R.A., Armstrong, R.A., 2001. U–Pb SHRIMP and Sm–Nd geochronology of the Silvânia Volcanics and Jurubatuba Granite: juvenile Paleoproterozoic crust

in the basement of the Neoproterozoic Brasília Belt, Goiás, Central Brazil. Ann. Acad. Bras. Cienc. 73 (3), 445–460.

Flores, G., 1955, Les résultats des études pour les recherches pétroliféres en Sicile: Discussion, in Proceedings of the 4th World Petroleum Congress: Rome, Casa Editrice Carlo Colombo, Section 1/A/2, p. 121–122.

Floyd, P.A., Winchester, J.A., 1975. Magma type and tectonic setting discrimination using immobile elements. Earth and Planetary Science Letters 27: 211-218

Floyd, P.A., Leveridge, B.E., Franke, W., Shail, R., Dörr, W., 1990. Provenance and depositional environment of Rhenohercynian synorogenic greywackes from the Giessen Nappe, Germany. Geol. Rundsch. 79, 611–626.

Folha SE-22-X-B (Goiánia) 1980, Instituto Brasileiro de Geografia e Estatistica (IBGE), www.ibge.gov.br.

Frasca, A. A. S., 2015. PhD Thesis, Instituto de Geociências, Universidade de Brasília. Amálgamas do W-Gondwana na Província Tocantins. N°123. 1-171.

Frei, R., Rosing, M., Waight, T.E., Krogstad, E.J., Storey, M., Ulfbeck, D.G., Albarède, F., 2002. Hydrothermal-metasomatic and tectonothermal processes in the Isua greenstone belt (West Greenland): a multi-isotopic investigation of their effects on the Earth's oldest oceanic crustal sequence. Geochim. Cosmochim. Acta 66, 467–486.

Frimmel, H.E., Zartman, R.E., Spath, A., 2001. The Richtersveld Igneous Complex South Africa: U–Pb zircon and geochemical evidence for the beginning of Neoproterozoic continental breakup. The Journal of Geology 109, 493–508.

Frost, B.R., 1975. Contact metamorphism of serpentinite, chloritic blackwall at Paddy-Go- Easy pass, central Cascades, Washington. J Petrol 16:272-313.

Früh-Green, G.L., Connolly, J.A.D., Plas, A., Kelley, D.S., Grobety, B., 2004. Serpentinization of oceanic peridotites: implications for geochemical cycles and biological activity. The subseafloor biosphere at mid-ocean ridges. Geophysical Monograph Series 144.

Fuck, R.A., Brito Neves, B.B., Schobbenhaus, C., 2008. Rodinia descendants in South America. Precambrian Res. 160, 108–126.

Fuck, R. A., Dantas, E. L., Pimentel, M. M., Botelho, N. F., Armstrong, R., Laux, J. H., Junges, S. L., Soares, J. E., Praxedes, I. F., 2014. Paleoproterozoic crust-formation and reworking events in the Tocantins Province, central Brazil: A contribution for Atlantica supercontinent reconstruction. Precambrian Research 224, pp. 53-74.

Fuck R. A., Pimentel, M. M., Alvarenga, C. J. S., Dantas, E. L., 2017. The Northern Brasilia Belt. Chapter 11, São Francisco Craton, Eastern Brazil, Tectonic Genealogy of a Miniature Continent. Heilbron, M., Cordani, U. G., Alkmin, F. F., Regional Geology Reviews, Springer.

Furnes, H., Dilek, Y., de Wit, M., 2015. Precambrian greenstone sequences represent different ophiolite types. Gondwana Research 27, 649-685

Gansser, A., 1959, Ausseralpine Ophiolithprobleme. Eclogae geol. Helv. 52/2, 659-680. Ausseralpine Ophiolithprobleme. Eclogae geol. Helv. 52/2, 659-680.

Gansser, A., 1974, The ophiolite mélange: A world-wide problem on Tethyan examples: Eclogae Geologicae Helvetiae, v. 67, p. 479–507.

Gioia, S. M.C. L., and Pimentel, M. M., 2000. The Sm-Nd isotopic method in the Geochronology Laboratory of the University of Brasília. An Acad Bras Cienc 72: 219-245.

Giovanardi T., Girardi V.A.V., Correia C.T., Sinigoi S., Tassinari C.C.G., Mazzucchelli M., 2015. U-Pb zircons SHRIMP data from the Cana Brava Layered Complex: New constraints for the mafic-ultramafic intrusions of Northern Goiás, Brazil. Open Geosci 7:197–206

Giovanardi T., Girardi V. A.V., Correia C.T., Tassinari C.olombo C.G., Sato K., Cipriani A., Mazzucchelli M. 2017. New U-Pb SHRIMP-II zircon intrusion ages of the Cana Brava and Barro Alto layered complexes, central Brazil: constraints on the genesis andevolution of the Tonian Goias Stratiform Complex. Lithos, v.282-283, p.339-357.

Greenly, E., 1919, The Geology of Anglesey, Vols I and II: Memoirs of Geological Survey: London, HM Stationary Office, p. 1–388, 390–980.

Gruau, G., Rosing, M., Bridgwater, D., Gill, R.C.O., 1996. Resetting of Sm–Nd systematics during metamorphism of > 3.7 Ga rocks: implications for isotopic models of early Earth differentiation. Chem. Geol. 133, 225–240.

Guo, Q., Xiao, W., Windley, B.F., Mao, Q., Han, C., Qu, J., Ao, S., Li, J., Song, D., Yong, Y., 2012. Provenance and tectonic settings of Permian turbidites from the Beishan Mountains, NW China: implications for the Late Paleozoic accretionary tectonics of the southern Altaids. J. Asian Earth Sci. 49, 54–68.

Hasui, Y. & Haralyi, N.L.E. 1985. A mega-estruturação de Goiás. In: SIMP. GEOL. CENTRO-OESTE, 2. Goiânia, 1985. Atas... Goiânia, SBG. p. 120-144.

Hay, D.C., Dempster, T. J., 2009. Zircon Behaviour during Low-temperature Metamorphism. Journal of Petrology 50, 571-589.

Hefferan, K.P., Admou, H., Karson, J.A., Saquaque, A., 2000. Anti-Atlas (Morocco) role in Neoproterozoic Western Gondwana reconstruction. Precambrian Research 103, 89–96.

Hefferan, K., Soulaimani, A., Samson, S.D., Admou, H., Inglis, J., Saquaque, A., Chaib,L., Heywood, N., 2014. A reconsideration of Pan African orogenic cycle in theAnti-Atlas Mountains, Morocco. J. Afr. Earth Sci. v.98, p. 34–46.

Honnorez, J., Kirst, P., 1975. Petrology of rodingites from the equatorial Mid-Atlantic fracture zones and their geotectonic significance. Contributions to Mineralogy and Petrology 49, 233–257.

Hsü, K.J., 1968, Principles of mélanges and their bearing on the Franciscan-Knoxville Paradox: Geological Society of America Bullettin, v. 79, p. 1063–1074.

Hyndman, R. D., Currie, C. A., Mazzotti, S. P., 2005. Subduction zone backarcs, mobile belts, and orogenic heat., GSA Today? V. 15, no 2.

Irvine, T.N., Baragar, W.R.A., 1971. A guide to the chemical classification of the common volcanic rocks. Canad. J. Earth Sci. 8, 523–548.

Jackson, S.E., Pearson, N.J., Griffin, W.L., Belousova, E.A., 2004. The application of laser ablation inductively coupled plasma mass spectrometry to in situ U-Pb zircon geochronology. Chem Geol 211: 47–69.

Johnson, S.P., Rivers, T., De Waele, B., 2005. A review of the Mesoproterozoic to early Palaeozoic magmatic and tectonothermal history of south-central Africa: implications for Rodinia and Gondwana. Journal of the Geological Society 162, 433–450.

Jost, H., Chemale Jr., F., Dussin, I.A., Martins, R. A U-Pb zircon Paleoproterozoic age for the metasedimentary host rocks and gold mineralization of the Crixás greenstone belt, Goiás, Central Brazil. Ore Geology Reviews 37, 127–139, 2010.

Jost, H., Chemale Jr., F., Fuck, R.A., Dussin, I.A. Uvá complex, the oldest orthogneisses of the Archean-Paleoproterozoic terrane of central Brazil. Journal of South American Earth Sciences 47, 201– 212, 2013.

Junges, S.L., Pimentel, M.M., Dantas, E.L., Laux, J.H., 2003. New ID-TIMS U-Pb ages in the western portion of the Mara Rosa Arc: two hundred million years of arc building. In: 4th South American Symposium on Isotope Geology, Salvador, 2003. Short Papers, Salvador, CBPM, IRD, v1:198-201.

Justoe, L. J. E. C., Scislewski, G., 1998. Programa Levantamentos Geológicos Básicos Do Brasil Projeto De Mapeamento Geológico/Metalogenético Sistemático. Executado pela CPRM – Serviço Geológico do Brasil, Superintendência Regional de Goiânia.

Karaoglan, F.G., Parlak, O., Klotzli, U., Thoni,M., Koller, F., 2013. U–Pb and Sm–Nd geochronology of the Kizildag (Hatay, Turkey) ophiolite: implications for the timing and duration of suprasubduction zone type oceanic crust formation in the southern Neotethys. Geological Magazine 150, 283–299.

Kaufmann, F.J., 1886, Emmen- und Schlierengegenden nebst Umgebungen bis zur Brünigstrasse und Linie Lungern-Grafenort: Beiträge zur Geologische Karte der Schweiz, v. 24, no. 1, 608 p.

Kelty T. K., Yin, A., Dash, B., Gehrels, G. E., Ribeiro, A. E., 2008. Detrital-zircon geochronology of Paleozoic sedimentary rocks in the Hangay-Hentey basin, north-central Mongolia:Implications for the tectonic evolution of the Mongol-Okhotsk Ocean in central Asia. Tectonophysics, 451, 290 – 311.

Klein, P.B.W. 2008. Geoquímica de Rocha Total, Geocronologia de U–Pb e Geologia Isotópica de Sm–Nd das Rochas Ortognáissicas e Unidades Litológicas Associadas da Região Ipameri — Catalão (Goiás). Unpublished PhD Thesis, University of Brasília, Brazil, 154 pp.

Košler, J., Fonneland, H., Sylvester, P., Tubrett, M., Pedersen, R.B., 2002. U-Pb dating of detrital zircons for sediment provenance studies, a comparison of laser ablation ICPMS and SIMS techniques. Chem. Geol. 182, 605–618.

Kröner, A., Todt, W., Hussein, I.M., Mansour, M., Rashwan, A.A., 1992. Dating of late Proterozoic ophiolites in Egypt and the Sudan using the single grain zircon evaporation technique. Precambrian Research 59, 15–32.

Kröner, A., Cordani, U.G., 2003. African, southern Indian and South American cratons were not part of the Rodinia supercontinent: evidence from field relationships and geochronology. Tectonophysics 375, 325–352.

Lacerda Filho, J.V., 1989. Programa de Leventamentos Geológicos Básicos do Brasil. Folha Caraíba, SE.22-X-B-VI. Goiânia: CPRM, DNPM, p. 149.

Laux, J.H., Pimentel, M.M., Dantas, E.L., Armstrong, R.A., Junges, S.L., 2005. Two Neoproterozoic crustal accretion events in the Brasília belt, central Brazil. Journal of South American Earth Sciences 18, 183-198.

Li, X.H., Faure, M., Lin, W., Manatschal, G., 2013. New isotopic constraints on age and magma genesis of an embryonic oceanic crust: the Chenaillet Ophiolite in the Western Alps. Lithos 160–161, 283–291.

Li, Z.X., Li, X.H., Kinny, P.D., Wang, J., 1999. The breakup of Rodinia: did it start with a mantle plume beneath South China? Earth and Planetary Science Letters 173, 171–181.

Li, Z.X., Bogdanova, S.V., Collins, A.S., Davidson, A., De Waele, B., Ernst, R.E., Fitzsi-mons, I.C.W., Fuck, R.A., Gladkochub, D.P., Jacobs, J., Karlstrom, K.E., Lu, S.,Natapov, L.M., Pease, V., Pisarevsky, S.A., Thrane, K., Vernikovsky, V., 2008a.Assembly, configuration, and break-up history of Rodinia: a synthesis. Precam-brian Research 160, 179–210.

Lindsay, J. F., Korsch, R. J., Wilford, J. R., 1987. Timeing the breakup of a Proterozoic supercontinent: evidence from Australian intracratonic basins. Geology, 15, 1061-1064.

Liu, C.Z., Chung, S.L.,Wu, F.Y., Zhang, C., Xu, Y.,Wang, J.G., Chen, Y., Guo, S., 2016. Tethyan suturing in Southeast Asia: zircon U-Pb and Hf-O isotopic constraints from Myanmar ophiolites. Geology 44, 311–314.

Lucente, C.C., and Pini, G.A., 2003, Anatomy and emplacement mechanism of a large submarine slide within the Miocene foredeep in the Northern Apennines, Italy: A field perspective: American Journal of Science, v. 303, p. 565–602.

Ludwig, K.R., 1993. ISOPLOT – A Plotting and Regression Program for RadiogenicIsotope Data, Version 2.70. U.S. Geological Survey Open/File Report 91-445, 42pp.

Maltman, A.J. 1978. Serpentine textures in Anglesey, North Wales, United Kingdom. Geol. Soc. Am. Bull., 89(7):972-980.

Marques, G. C., Oliveira, C. G., Pimentel, M. M., Dantas, E. L., 2017. PhD Thesis, Instituto de Geociências, Universidade de Brasília. Evolução tectônica e metalogenética no contexto do depósito aurífero de Fazenda Nova, Arco Magmático de Arenópolis, Goiás. N° 137. 1-169.

Matteini, M., Junges, S.L., Dantas, E.L., Pimentel, M.M., Bühn, B., 2010. In situ zircon U–Pb and Lu–Hf isotope systematic on magmatic rocks: insights on the crustal evolution of the Neoproterozoic Goiás Magmatic Arc, Brasília belt, Central Brazil. Gondwana Research 17, 1–12.

Matteini, M., Dantas, E.L., Pimentel, M.M., Alvarenga, C.J.S., Dardenne, M.A., 2012. U-Pb and Hf isotope study on detrital zircons from the Paranoá Group, Brasília Belt, Brazil: Constraints on depositional age at Mesoproterozoic-Neoproterozoic transition and tectono-magmatic events in the São Francisco Craton. Precambrian Research 206–207, 168–181.

McLaughlin, R.J., Blake, M.C., Jr., Griscom, A., Blome, C.D., and Murchey, B., 1988, Tectonics of formation, translation, and dispersal of the Coast Range ophiolite, California: Tectonics, v. 7, p. 1033–1056.

Mello, J.C.R. & Berbert, C.O. 1969. Investigação Geológico-Econômica da Área de Morro Feio-Hidrolâudia, Goiás. Brasília, Conv. DNPM/ CPRM/MME. 73 p. (Boletim 132).

Moores, E.M., and Twiss, R.J., 1995. Tectonics: W.H. Freeman and Company New York, Third printing 2000, VB.

Moraes, R., Fuck, R.A., 1994. Deformação e metamorfismo das sequências Juscelândia e Serra da Malacacheta, Complexo Barro Alto, Goiás. Revista Brasileira de Geociencias 24, 189–197.

Moraes, R., Fuck, R.A., 1999. Trajetória P–T Horária para oMetamorfismo da Sequência Juscelândia, Goiás: Condições do Metamorfismo e Implicações Tectônicas. Revista Brasileira de Geociencias 29, 603–612.

Moraes, R., Brown, M., Fuck, R. A., Camargo, M. A., Lima, T. M., 2002. Characterization and P-T evolution of melt-bearing ultrahigh-temperature granulites: an example from the Anápolis-Itauçu complex of the Brasília Fold Belt, Brazil. Journal of Petrology, 43(9), 1673-1705.

Mutti, E., Bernoulli, D., Ricci Lucchi, F., and Tinterri, R., 2009, Turbidites and turbidity currents from Alpine 'flysch' to the exploration of continental margins: Sedimentology, v. 56, p. 267–318.

Navarro, G. R. B.; Zanardo, A., 2005, Petrografia e geoquímica das rochas metaultramáficas da região de Mairipotaba, Cromínia e Pontalina, Goiás. Revista Brasileira de Geociências, v. 359, n. 4, 483-492.

Navarro, G. R. B.; Zanardo, A., da Conceição, F. T., 2013. The Araxá Group in the South-Southwest Region of the Goiás State. Revista do Instituto de Geociências – USP, v. 13, n. 2, p. 5-28.

Nie, J., Horton, B. K., Saylor, J. E., Mora, A., Mange, M., Garione, C. N.,Basu, A., Moreno, C. J., Caballero, V., Parra, M., 2012. Integrated provenance analysis of a convergent retroarc foreland system: U-Pb ages, heavy minerals, Nd isotopes, and sandstone compositions of the Middle Magdalena Valley basin, northern Andes, Colombia. Earth-Science Reviews 110, 111 – 126.

O'Hanley, D.S., 1996. Serpentinites: Records of Tectonic and Petrological History. Oxford University Press.

Ohara, Y., Stern, R.J., Ishii, T., Yurimoto, H., and Yamazaki, T., 2002, Peridotites from the Mariana Trough: First look at the mantle beneath an active back-arc basin: Contributions to Mineralogy and Petrology, v. 143, p. 1–18, doi:10.1007/s00410-001-0329-2.

Okada, H., 1989. Anatomy of trench-slope basins: examples from the Nankai Trough. Palaeogeography, Palaeoclimatology, Palaeoecology 71, 3–13.

Oliveira F.V. 2015. Chronus: Um novo suplemento para a redução de dados U-Pb obtidos por LAMC-ICPMS. Dissertacao de Mestrado, Instituto de Geociências, Universidade de Brasília. 240p.

Paixão, M.A., Nilson A.A., Dantas, E.L., 2008. The Neoproterozoic Quatipuru ophiolite and the Araguaia fold belt, central-northern Brazil, compared with correlatives in NW Africa, in Pankhurst, R.J, et al eds., West Gondwana: Pre-Cenozoic correlations across the South Atlantic region: Geological Society of London Special Publication 294, p. 297-318, doi:10.1016/j.lithos.2007.06.016.

Patchett, P. J., and Chase, C. G. 2002. Role of transform continental margins in major crustal growth episodes. Geology 30:39–42.

Pearce, J.A., 2008. Geochemical fingerprinting of oceanic basalts with applications to ophiolite classification and the search for Archean oceanic crust. Lithos 100, 14–48.

Pedrosa-Soares, A.C., Vidal, P., Leonardos, O.H., Brito-Neves, B.B., 1998. Neoproterozoic oceanic remnants in eastern Brazil: further evidence and refutation of an exclusively ensialic evolution for the Araçuaí–West Congo Orogen. Geology 26, 519–522.

Pelleter, E., Cheilletz, A., Gasquet, D., Mouttaqi, A., Annich, M., El Hakour, A., Deloule, E., Féraud, G., 2007. Hydrothermal zircons: A tool for ion microprobe U–Pb dating of gold mineralization (Tamlalt–Menhouhou gold deposit — Morocco). Chemical Geology 245, 135–161.

Piauilino, P.F., Hauser, N., Dantas, E.L., 2019. From passive margin to continental collision: Geochemical and isotopic constraints for E-MORB and OIB-like magmatism during the neoproterozoic evolution of the southeast Brasília Belt. Precambrian Research, https://doi.org/10.1016/j.precamres.2019.105345

Pimentel, M.M., Fuck, R.A., 1992. Neoproterozoic crustal accretion in central Brazil. Geology 20, 375e379.

Pimentel, M.M., Fuck, R.A., and Alvarenga, C.J.S., 1996. Post-Brasiliano (Pan-African) high-K granitic magmatism in central Brazil: the role of Late Precambrian/ early Paleozoic extension. Precambrian Research vol. 80, pp. 217-238.

Pimentel, M.M., Fuck, R.A., Botelho, N.F., 1999. Granites and the geodynamic history of the Neoproterozoic Brasília belt, Central Brazil: a review. Lithos 46, 463–483.

Pimentel, M.M., Dardenne, M.A., Fuck, R.A., Viana, M.G., Fischel, D.P., 2001. Nd isotopes and the provenance of sediments of the Neoproterozoic Brasília Belt. Jour. South Am. Earth Sci. 14, 571e585.

Pimentel, M.M., Dantas, E.L., Fuck, R.A., Armstrong, R.A., 2003. Shrimp and conventional U-Pb age, Sm-Nd isotopic characteristics and tectonic significance of the K-rich Itapuranga suite in Goiás, Central Brazil. Anais da Academia Brasileria de Ciências 75, 97-108.

Pimentel MM, Ferreira Filho CF, Amstrong RA (2004a) Shrimp U–Pb and Sm–Nd ages of the Niquelandia layered complex: Meso (1,25 Ga) and Neoproterozoic (0,79 Ga) extensional events in central Brasil. Precambrian Res 132:132–135.

PimentelMM, Ferreira Filho CF, Armele A (2006) Neoproterozoic age of the Niquelândia complex, Central Brazil: further ID-TIMS and Sm–Nd isotopic evidence. J S Am Earth Sci 21:228–238.

Pimentel, M.M., Rodrigues, J.B., DellaGiustina, M.E.S., Junges, S., Matteini, M., Armstrong, R., 2011. The tectonic evolution of the Neoproterozoic Brasília Belt, central Brazil, based on SHRIMP and LA-ICPMS U-Pb sedimentary provenance data: A review. Journal of South American Earth Sciences, vol. 31 pp.345-357.

Pimentel, M. M., 2016. The tectonic evolution of the Neoproterozoic Brasília Belt, central Brazil: a geochronological and isotopic approach. Brazilian Journal of Geology, 46. Pp. 67-82.

Piuzana, D., Pimentel, M.M., Fuck, R.A., Armstrong, R.A., 2003a. SHRIMP U-Pb and Sm-Nd data for the Araxá Group and associated magmatic rocks: constraints for the age of sedimentation and geodynamic context of the southern Brasília Belt, central Brazil. Precambrian Research, vol. 125, pp. 139-160.

Piuzana, D., Pimentel, M.M., Fuck, R.A., Armstrong, R.A., 2003b. Neoproterozoic granulite facies metamorphism and coeval granitic magmatism in the Brasilia Belt, Central Brazil: regional implications of new SHRIMP U-Pb and Sm-Nd data. Precambrian Research, vol. 125, pp. 245-273.

Polat, A., Hofmann, A.W., 2003. Alteration and geochemical patterns in the 3.7–3.8 Ga Isua greenstone belt, West Greenland. Precambrian Research, v. 126, p. 197–218.

Queiroga, G.N., Pedrosa-Soares, A.C., Noce, C.M., Alkmim, F.F., Pimentel, M.M., Dantas, E., Martins, M., Castañeda, C., Suita, M.T.F., Prichard, F., 2007. Age of the Ribeirão da Folha ophiolite, Araçuaí Orogen: the U-Pb zircon dating of a plagiogranite. Geonomos 15, 61–65.

Queiroz, C.L., Jost, H., Silva, L.C., McNaughton, N.J., 2008. U-Pb SHRIMP and Sm-Nd geochronology of granite-gneiss complexes and implications for the evolution of the central Brazil Archean terrain. Journal of South American Earth Sciences, 26: 100–124.

Ranero, C.R., Sallares, V., 2004. Geophysical evidence for hydration of the crust and mantle of the Nazca plate during bending at the north Chile trench. Geology 32, 549–552.

Raymond, L.A., 1984, Classification of mélanges, in Raymond, L.A., ed., Mélanges: Their nature, origin and significance. Boulder, Colorado, Geological Society of America Special Paper 198, p. 7–20.

Rezende A., Nilson A.A., Silva A. da, Alvarenga C.J.S. de, Gebrim E., Godoi H.O., Lacerda Filho J.V. de, Danni J.C.M., Campos J.E.G., Brilhante J.R., Dardenne M.A., Resende M., Pimentel M.M., Botelho N.F, Barbosa P.A.R., Boas P.F.V., Lima T.M., Filho W.R. 1999. Descrição das Unidades Litoestratigráficas. In: Lacerda Filho J.V. de, Rezende A., Silva A. da (coords). Programa de Levantamentos Geológicos Básicos do Brasil - Geologia e Recursos Minerais do Estado de Goiás e Distrito Federal. Goiânia: conv. CPRM/ METAGO S.A./UnB. p. 31-78.

Rioux, M., Bowring, S., Keleme, P., Gordon, S., Miller, R., Dudás, F., 2013. Tectonic development of the Semail ophiolite: high-precision U-Pb zircon geochronology and Sm-Nd isotopic constraints on crustal growth and emplacement. Journal of Geophysical Research: Solid Earth 118, 2085–2101.

Rivalenti G, Correia CT, Girardi VAV, Mazzuchelli M, Tassinari CC, Bertotto GW (2008) Sr–Nd isotopic evidence for crustal contamination in the Niquelandia complex, Goiàs, central Brasil. J S Am Earth Sci 25:298–312

Robinson, P.T., Trumbull, R.B., Schmitt, A., Yang, J.-S., Li, J.-W., Zhou, M.-F., Erzinger, J., Dare, S., and Xiong, F., 2015, The origin and significance of crustal minerals in ophiolitic chromitites and peridotites: Gondwana Research, v. 27 (2), 486-506

Rodrigues, J.B., Pimentel, M.M., Dardenne, M.A., Armstrong, R.A., 2010. Age, provenance and tectonic setting of the Canastra and Ibiá Groups (Brasília Belt, Brazil): Implications for the age of a Neoproterozoic glacial event in central Brazil. J. S. Am. Earth Sci. 29 (2), 512–521.

Rodrigues J.B., Pimentel M. M., Buhn B., Matteini M., Dardenne M.A., Alvarenga C.J.S., Armstrong R.A., 2012. Provenance of the Vazante Group: New U–Pb, Sm–Nd, Lu–Hf isotopic data and implications for the tectonic evolution of the Neoproterozoic Brasília Belt. Gondwana Research 21, 439–450.

Rose, N.M., Rosing, M.T., Bridgwater, D., 1996. The origin of metacarbonate rocks in the Isua Archean Supracrustal belt, West Greenland. Am. J. Sci. 296, 1004–1044.

Ryan, P.D., 2008. Preservation of forearc basins during island arc–continent collision: some insights from the Ordovician of western Ireland, In: Draut, A. E., Clift, P.D., Scholl, D.W. (Eds.), Formation and Applications of the Sedimentary Record in Arc Collision Zones. Geological Society of America Special Paper, pp. 1–9.

Sabaraense, L.D., 2016. Proveniência dos grupos Araxá e Ibiá na porção sul da Faixa Brasília. Unpublished PhD Thesis, University of Brasília, Brazil,100 p.

Saccocia, P.J., Ding, K., Berndt, M.E., Seewald, J.S., Seyfried Jr.,W.E., 1994. Experimental and theoretical perspectives on crustal alteration at mid-ocean ridges. In: Lentz, D.R. (Ed.), Alteration and Alteration Processes AssociatedWith Ore-forming Systems Geological Association of Canada. Waterloo, Canada, Short Course Notes Vol. 11, pp. 403–431.

Samson, S.D., Inglis, J.D., D'Lemos, R.S., Admou, H., Blichert-Toft, J., Hefferan, K., 2004. Geochronological, geochemical, and Nd–Hf isotopic constraints on the origin of Neoproterozoic plagiogranites in the Tasriwine ophiolite, Anti-Atlas orogen, Morocco. Precambrian Research 135, 133–147.

Santos R.V., Oliveira C.G., Souza V.H.V., Carvalho M.J., Andrade T.V., Souza H.G.A. 2008. Correlação isotópica baseada em isótopos de Carbono entre os greenstone belts de Goiás. In: SBG, Congr. Bras. Geol., 44, Curitiba, Volume de Resumos, pg. 52.

Scherer, E., Münker, C., Mezger, K., 2006. Calibration of the lutetium–hafnium clock. Science 293, 683–687.

Seer H.J. 1999. Evolução Tectônica dos Grupos Araxá, Ibiá e Canastra na sinforma de Araxá, Araxá, Minas Gerais. Tese de Doutorado, Instituto de Geociências, Universidade de Brasília, 267 p.

Seer H.J. & Dardenne M.A. 2000. Tectonostratigraphic terrane analysis on Neoproterozoic times: the case study of the Araxá Synform, Minas Gerais, Brazil - implications to the final collage of the Gondwanaland. Revista Brasileira de Geociências, 30(1):78-81.

Seer H.J., Brod J.A., Fuck R.A., Pimentel M.M., Boaventura G.R., Dardenne M.A. 2001. Grupo Araxá em sua área tipo: um fragmento de crosta oceânica Neoproterozóica na Faixa de Dobramentos Brasília. Revista Brasileira de Geociências, 31(3):385-396.

Seer, H. J., Moraes, L. C., 2013 Within plate, arc, and collisional Neoproterozoic granitic magmatism in the Araxá Group, Southern Brasília belt, Minas Gerais, Brazil. Brazilian Journal of Geology, 43(2): 333-354.

Shervais, J. W., 2006. The significance of subduction-related accretionary complexes in early Earth processes, in Reimold, W. U., and Gibson, R. L., Processes on the Early Earth: Geological Society of America Special Paper 405, p. 173 – 192, doi: 10.1130/2006.2405(10).

Shervais J.W., Choi S.H., Sharp W.D., Ross J., Zoglman-Schuman M., Mukasa S.B. 2011, Serpentinite matrix mélange: Implications of mixed provenance for mélange formation, inWakabayashi J., Dilek Y.eds., Mélanges: Processes of Formation and Societal Significance: Geological Society of America Special Paper 480, doi:10.1130/2011.2480(01).

Sinton, J. M., L. L. Ford, B. Chappell, and M. T. McCulloch (2003), Magma genesis and mantle heterogeneity in the Manus back-arc basin, Papua New Guinea, J. Petrol., 44, 159 – 195, doi:10.1093/petrology/ 44.1.159.

Stern, R.J., 1994. Arc assembly and continental collision in the Neoproterozoic East African orogen: implications for the consolidation of Gondwanaland. Annual Reviews of Earth and Planetary Sciences 22, 319–351.

Stern, R.J., Reagan, M., Ishizuka, O., Ohara, Y., Whattam, S., 2012. To understand subduction initiation, study forearc crust: To understand forearc crust, study ophiolites. Lithosphere, doi:10.1130/L183.1.

Strieder, A.J. 1989. Geologia, Petrologia e Tectônica dos Corpos de Serpentinitos de Abadiânia (GO). Brasília. 208 p. (Dissertação de Mestrado, IG/UnB).

Strieder, A. J., Nilson A. A., 1992. Melange ofiolítica nos metassedimentos Araxá de Abadiânia (GO) e implicações tectônicas regionais. Revista Brasileira de Geociências, v. 22, n. 2, pp. 204-215.

Strieder, A. J., Nilson A. A., 1992a. Estudo petrológico de alguns fragmentos tectônicos da mélange ofiolítica em Abadiânia (GO): l – O protolito dos corpos de serpentinito. Revista Brasileira de Geociências, v. 22, n. 3, pp. 338-352.

Strieder, A. J., Nilson A. A., 1992b. Estudo petrológico de alguns fragmentos tectônicos da mélange ofiolítica em Abadiânia (GO): II – Cromita primária e suas transformações metamórficas. Revista Brasileira de Geociências, v. 22, n. 3, pp. 353-362.

Strieder, A. J., Nilson A. A., 1992c. Estudo petrológico de alguns fragmentos tectônicos da mélange ofiolítica em Abadiânia (GO): III – Texturas e composição química dos corpos máficos. Revista Brasileira de Geociências, v. 22, n. 3, pp. 363-371.

Suita M. T. F., Kamo S., Krogh T.E., Fyfe W.S., Hartmann L.A., 1994. U–Pb ages from the high-grade Barro Alto mafic–ultramafic complex (Goiás, central Brazil): middle Proterozoic continental mafic magmatism and upper Proterozoic continental collision. In: International Conference on Geochronology Cosmochronology and Isotope Geology, Berkeley, USGS, ICOG, Abstracts 8:309.

Suita, M. T. F.,Soares, A. C. P., Leite, C. A. S., Nilson, A. A., Prichard, H. M, 2004. Complexos ofiolíticos do Brasil e a metalogenia comparada das faixas Araçuaí e Brasília. In: PEREIRA, E;

CASTROVIEJO, R.; ORTIZ, F. (eds). Complejos Ofiolíticos en Iberoamérica: guías de prospección para metales preciosos. Madrid, Rede CYTED, 379p. cap. 5, p. 101-132.

Sun, S.S., McDonough, W.F., 1989. Chemical and isotopic systematics of oceanic basalts: implications for mantle composition and processes. In: Saunders, A.D., Norry, M. (Eds.), Magmatism in Ocean Basins, Geological Society of London Special Publication. 42, pp. 313–345.

Tamura, A. and S. Arai, 2006. Harzburgite-dunite-orthopyroxenite suite as a record of supra-subduction zone setting for the Oman ophiolite mantle. Lithos, 90: 43-56.

Tassinari, C.C.G., Munhá, J.M.U., Ribeiro, A., Correia, C.T., 2001. Neoproterozoic oceans in the Ribeira Belt (southern Brazil): The Pirapora do Bom Jesus ophiolitic complex: Episoder, v. 24, p. 245 – 251.

Tassinari C.G., Jost H., Santos J., Nutman A, Bennell M.R. 2006. Pb and Nd isotope signatures and SHRIMP U-Pb geochronological evidence of Paleoproterozoic age for Mina III gold mineralization, Crixás District, Central Brazil. V SAGI CD-ROM, pp. 527-529.

Tate, G.W., McQuarrie, N., von Hinsbergen, D.J.J., Bakker, R.R., Harris, R., Willet, S., Reiners, P., Fellin, M.G., Ganerød, M., Zachariasse, J.W., 2014. Resolving spatial heterogeneities in exhumation and surface uplift in East Timor: constraints of deformation processes in young orogens. Tectonics.

Taylor, S.R., McLennan, S.M., 1985. The Continental Crust; Its composition and evolution; an examination of the geochemical record preserved in sedimentary rocks. Blackwell, Oxford, pp. 312.

Trümpy, R., 1960, Paleotectonic evolution of the Central and Western Alps: Geological Society of America Bulletin, v. 71, p. 843–908.

Underwood, M.B., Moore, G.F., 1995. Trenches and trench-slope basins. In: Busby, C.J., Ingersoll, R.V. (Eds.), Tectonics of Sedimentary Basins. Blackwell Science, Cambridge, pp. 179–220.

Valeriano C.M, 1992. Evolução tectônica da extremidade meridional da Faixa Brasília, região da represade Furnas, Sudoeste de Minas Gerais. Instituto de Geociências, Universidade de São Paulo, São Paulo, Tese de Doutoramento, 198p.

Valeriano, C.M., Simões, L.S.A., 1997. Geochemistry of Proterozoic mafic rocks from the Passos nappe (Minas Gerais, Brazil): tectonic implications to the evolution of the southern Brasília belt. Revista Brasileira de Geociências 27 (1), 99-110.

Valeriano C.M., Machado N., Simonetti A., Valladares C.S., Seer H.J., Simões L.S.A. 2004. U-Pb geochronology of the southern Brasília belt (SE-Brazil): sedimentary provenance, Neoproterozoic orogeny and assembly of West Gondwana. Precambrian Research, 130:27-55.

Valeriano, C.M., Pimentel, M.M., Heilbron, M., Almeida, J.C.H., Trouw, R.A.J., 2008. Tectonic evolution of the Brasília belt, central Brazil, and early assembly of Gondwana. In: Pankhurst, R.J., Trouw, R.A.J., Brito Neves, B.B., De Wit, M.J. (Eds.), West Gondwana: Pre-cenozoic Correlations across the South Atlantic Region. Geological Society, London, Special Publications, vol. 294, pp. 197-210.

Villaros, A., Buick, I.S., and Stevens, G., 2012, Isotopic variations in S-type granites: An inheritance from a heterogeneous source?: Contributions to Mineralogy and Petrology , v. 163, p. 243–257, https://doi.org/10.1007/s00410-011-0673-9.

Wakabayashi J, Dilek Y (2003) What constitutes 'emplacement' of an ophiolite?: Mechanisms and relationship to subduction initiation and formation of metamorphic soles. Geological Society of London Special Publication 217: 427-44.

Wakabayashi, J., and Dilek, Y., 2011, eds., Mélanges: Processes of Formation and Societal Signifi cance: Geological Society of America Special Paper 480, doi:10.1130/2011.2480 (05).

Wedepohl, K.H., 1995. The compositions of the continental crust. Geochim. Cosmoch. Acta 59, 1217–1232.

Wiedenbeck, M.P., Allé, P., Corfu, F., Griffin, W., Meier, M., Oberli, F., Von Quadt, A., Roddick, J., Spiegel, W., 1995. Three natural zircon standards for U-Th-Pb, Lu-Hf, trace element and REE analyses. Geostand. Newslett. 19, 1–23.

Wiedenbeck, M.P., Hanchar, J.M., Peck, W.H., Sylvester, P., Valley, J., Whitehouse, M., Kronz, A., Morishita, Y., Nasdala, L., Fiebig, J., Franchi, I., Girard, J.-P., Greenwood, R.C., Hinton, R., Kita, N., Mason, P.R.D., Norman, M., Ogasawara, M., Piccoli, P.M., Rhede, D., Satoh, H., Schulz-Dobrick, B., Skår, O., Spicuzza, M.J., Terada, K., Tindle, A., Togashi, S., Vennemann, T., Xie, Q., Zheng, Y.-F., 2004. Further characterisation of the 91500 zircon crystal. Geostand. Geoanal. Res. 28, 9–39.

Zhu, J., Du, Y.S., Liu, Z.X., Feng, Q.L., Tian, W.X., Li, J. Pl, Wang, C.P., 2005. Mesozoic radiolarian chert from the middle sector of the Yarlung Zangbo suture zone, Tibet and its tectonic implications. Science in China Series D: Earth Sciences 35 (12), 1131–1139.